Self-healing concrete: a novel nanobiotechnological approach to heal the concrete cracks

A thesis
submitted in fulfilment
of the requirements for the degree

of

Doctor of Philosophy in Engineering

at

The University of Waikato

by

MOSTAFA SEIFAN

THE UNIVERSITY OF
WAIKATO
Te Whare Wānanga o Waikato

2018

Abstract

Concrete is one of the world's most versatile and widely used construction materials due to its unique properties, including high compressive strength, versatility, availability, affordability, simple preparation, fire resistance, excellent thermal mass, compatibility with steel reinforcement bar and the possibility of casting in desired shapes. Despite these advantages, crack formation is the main issue associated with the concrete structures. Low tensile strength, coupled with internal and external stresses, are recognized as the key causes of crack formation in a structure. Although the embedment of reinforcement bars limits the rate of crack growth, it cannot prevent crack initiation in concrete. The initiated cracks accelerate the structure degradation by allowing aggressive fluids and gasses to seep into the matrix. This phenomenon brings about a reduction in concrete service life, increases maintenance costs and, in severe cases, leads to structural failure.

With the help of biotechnological pathway, concrete can be designed to have self-healing characteristics to address the above mentioned problems. In this novel approach, a bio-concrete is made by the addition of microorganisms and nutrients into the matrix during the concrete preparation. Once a crack occurs in the concrete structure, the healing agent is activated and the precipitated calcium carbonate ($CaCO_3$) fills the initiated crack. The resulted $CaCO_3$ is recognized as the most compatible material with the concrete composition which has efficient bonding capacity with the crack surface. The main goal of this research was, therefore, to design a new generation of viable self-healing mechanism for application in bio self-healing concrete structures.

Initially, an investigation was performed to screen the most effective factors, including bacteria, nutrients and operating conditions, on $CaCO_3$ precipitation and to maximize the production of $CaCO_3$. Considering the different mechanical and physical properties of $CaCO_3$ polymorph (calcite, vaterite and aragonite), a morphological qualification based on X-ray diffraction (XRD) was conducted.

Since the concrete has a high pH (~12), the capability of microorganisms to produce $CaCO_3$ in such a condition was investigated. To evaluate the ability of the preliminarily designed bio-agent to induce $CaCO_3$ in high pH, the concrete environment was simulated using a laboratory fermentor. The results indicate that the proposed bio-agent is able to withstand high pH while decreasing the microbial viability. It was also found that the proposed $CaCO_3$ production mechanism significantly depends on the presence of air and its effectiveness enhances at a higher level of aeration. This observation shows that the efficiency of the bio self-healing mechanism decreases in the oxygen-limiting areas such as deeper cracks and interior parts of the matrix. To address this issue, possible use of oxygen releasing compounds (ORCs) was investigated. The effects of different ORCs on the concentration and morphology of $CaCO_3$ were screened, and an optimization study using response surface methodology was performed to further enhance the efficiency of the designed bio-self-healing mechanism in oxygen-limiting conditions. The results demonstrate that the presence of key ORCs at their optimum level can increase $CaCO_3$ production.

Considering the pore size of the concrete matrix, there is a high risk for microorganisms to squeeze and damage upon cement hydration. Furthermore, the exerted shear stress on the bio-agent during the concrete preparation and drying shrinkage as well as the concrete pH can adversely affect the performance of the bio-concrete. Therefore the topic was further explored to minimize the negative effects of direct incorporation of bio-agent into the concrete matrix. It has been proven that the addition of proper nano scale-size metallic particles can improve the properties of the concrete. Considering the unique characteristics of nanoparticles, magnetic iron oxide nanoparticles (IONs) were proposed as a protective vehicle for the bio-agent. Naked and amine-modified IONs were successfully synthesized and characterized by different techniques, including XRD, transmission electron microscopy (TEM), scanning electron microscope (SEM) and Fourier transform infrared spectroscopy (FTIR). The results indicate that the presence of naked IONs has a positive contribution to the production of $CaCO_3$ and can serve as the carrier for the bio-agent.

In the final part of this work, the performance of the designed bio self-healing concrete was investigated using various laboratory tests, including compressive

strength, water absorption, drying shrinkage and crack healing observation. The results show that the presence of proposed bio-agents in concrete not only contributes to improving the compressive strength but also results in decreasing the water absorption. To evaluate the self-healing behavior of this technology, several cracks were created in the concrete specimens. The microscopic observation revealed that the bio-concrete possesses a superior crack healing characteristic. The bio-concrete could effectively sense the concrete cracks and the resulted $CaCO_3$ sealed the damages.

This study uncovered several limitations of using bio self-healing mechanism in concrete. Most importantly, it elucidated the potential of applying this novel technology to enhance the concrete durability and mechanical properties by addressing the uncovered issues.

Dedication

This thesis is dedicated with love:

To my wife for her love and ongoing support.

To my parents for their endless support and encouragement.

Acknowledgements

I wish to express my thanks and appreciation to the many people who have encouraged, helped and supported me throughout this research. Firstly, I would like to convey my sincere gratitude to my chief supervisor Dr. Aydin Berenjian for the continued guidance, support and advice through the duration of this project. His valuable advice has helped me overcome many hurdles faced throughout my PhD. Thank you for all the encouragement, ideas, and critiques along the way.

My sincere appreciation and gratitude to my co-supervisors Associate Professor Ajit Sarmah and Dr. Ali Khajeh Samani for all the guidance and encouragement they have given me during this project. I would like to express my appreciation to Professor Sinniah Ilanko for providing teaching opportunity and supporting me to be a member of Waikato University.

I would also like to express my sincere thanks to Dr. Rob Torrens, Professor Kim Pickering, and Professor Brian Gabbitas for providing marking and lab demonstration opportunities to supplement my income. I would like to acknowledge the entire technical staff of the School of Engineering for assisting me with my research: Dr. Lisa Li, Helen Turner, Dr. Barry O'Brien, Dr. Judith Burrows, Shannon McMurray, Renat Radosinsky, Dean Sandwell, Annette Rodgers and Ian Honey. Special thanks to Steve Hardy and Peter Jarman on instrument support. I would also like to convey my sincere gratitude to Mary Dalbeth (Department of Engineering Secretary) for the administrative help.

Finally, but most of all, I wish to express my deepest appreciation to my wife and parents for all their encouragement, support, and patience, as always, for which my mere expression of thanks likewise does not suffice. I would never have been able to accomplish my PhD without your unconditional support.

Contributing Publications

The following refereed publications were resulted of the work presented in this thesis:

Journal Articles

(1) **Seifan, M.**, Sarmah, A.K., Samani, A.K., Ebrahiminezhad, A., Ghasem, Y., and Berenjian, A. *Mechanical properties of bio self-healing concrete containing immobilized bacteria with iron oxide nanoparticles.* Applied Microbiology and Biotechnology, 2018, accepted.

(2) **Seifan, M.**, Sarmah, A.K., Ebrahiminezhad, A., Ghasem, Y., Samani,A.K., and Berenjian, A. *Bio-reinforced self-healing concrete using magnetic iron oxide nanoparticles.* Applied Microbiology and Biotechnology, 2018. 102(5): p. 2167-2178.

(3) **Seifan, M.**, Ebrahiminezhad, A., Ghasemi, Y., Samani,A.K., and Berenjian, A. *The role of magnetic iron oxide nanoparticles on bacterially induced calcium carbonate precipitation.* Applied Microbiology and Biotechnology, 2018. https://doi.org/10.1007/s00253-018-8860-5.

(4) **Seifan, M.**, Ebrahiminezhad, A., Ghasemi, Y., Samani,A.K., and Berenjian, A. *Amine-modified magnetic iron oxide nanoparticle as a promising carrier for application in bio self-healing concrete.* Applied Microbiology and Biotechnology, 2017. 102(1): p.175-184.

(5) **Seifan, M.,** Samani, A.K., Hewitt, S., and Berenjian, A. *The effect of cell immobilization by calcium alginate on bacterially induced calcium carbonate precipitation.* Fermentation, MDPI, 2017, 3 (4), 57.

(6) **Seifan, M.**, Samani, A.K., and Berenjian, A. *A novel approach to accelerate bacterially induced calcium carbonate precipitation using oxygen releasing compounds (ORCs).* Biocatalysis and Agricultural Biotechnology, 2017. 12: p. 299-307.

(7) **Seifan, M.**, Samani, A.K., and Berenjian, A. *New insights into the role of pH and aeration in the bacterial production of calcium carbonate ($CaCO_3$).* Applied Microbiology and Biotechnology, 2017. 101 (8): p. 3131–3142.

(8) **Seifan, M.**, Samani, A.K., and Berenjian, A. *Induced calcium carbonate precipitation using Bacillus species.* Applied Microbiology and Biotechnology, 2016. 100 (23): p. 9895-9906.

(9) **Seifan, M.**, Samani, A.K., and Berenjian, A. *Bioconcrete: next generation of self-healing concrete.* Applied Microbiology and Biotechnology 2016. 100 (6): p. 2591-2602.

Book Chapter

(10) **Seifan, M.**, Samani, A.K., Burgess, J.J. and Berenjian, A. *The Effectiveness of Microbial Crack Treatment in Self Healing Concrete* in *High Value Processing Technologies*, A. Berenjian, H. Jafarizadeh-Malmiri, and Y. Song, Editors. 2016, Nova Science, New York, USA. p. 97-124.

Conference Papers

(11) **Seifan, M.,** Samani, A.K., and Berenjian, A. *Healing the concrete cracks using a novel nanobiotechnological approach*, in *Waikato Young Research Engineers Symposium (WYRES)*. November 2017, Hamilton, New Zeland.

(12) **Seifan, M.,** Samani, A.K., Berenjian, A., and Eckersley, J. *The screening and morphological quantification of bacterial production of calcium carbonate*, in *Chemeca: Chemical Engineering - Regeneration, Recovery and Reinvention*. 2016, Adelaide, Australia.

Table of Contents

List of Figures

List of Tables

Chapter 1

Introduction

1.1 Background information

Concrete is one of the most used materials in the world due to its availability, high compressive strength and relatively low cost. Every year billions of tonnes of concrete are produced and consumed worldwide. Despite the concrete advantages, it is susceptible to cracking under internal and external stresses in both plastic and hardened stages.

Although the cracks may not endanger the concrete strength in early age, their formation and extension can be a serious risk to concrete integrity and lifespan in the long term. Cracks are one of the main causes of concrete deterioration and decrease in structure durability. Once a crack forms in the concrete, the aggressive substances penetrate into the crack due to capillary action. This phenomenon results in reinforcement bar corrosion and reduction in concrete integrity and durability. As a consequence, the concrete service life will be decreased. In addition, cracks are a serious threat when the tightness of the retaining structures need to be guaranteed. For instance, liquid or gas leakage from waste reservoirs, waste water treatment pods, container tanks, underground structures, aqueducts, and tunnels lead to decrease in concrete functionality. Therefore an urgent action is required to prevent the crack extension and deterioration of the structure.

To date, different techniques have been introduced to repair the concrete cracks. In this case, repairing compounds, such as chemical and polymer sealers, are applied on the concrete surface. However, the application of sealers is associated with several drawbacks. Firstly, it requires labour to monitor the structure to detect and seal the generated cracks. The size of induced cracks are in the range of a few micrometers and can be extended if an appropriate measurement is not taken. The microcracks cannot be detected by visual examination. Instead, non-destructive techniques, such as an ultrasonic testing method, can be used for crack detection. However, these techniques cannot be used for those parts of the structures which are not reachable. Furthermore, poor weathering and low heat resistance, sensitivity to moisture and temperature, poor bonding with concrete, and susceptibility to degradation and delamination with age are the other issues associated with external coating methods.

Alternatively, a self-healing approach is able to address the shortcomings associated with the external sealing techniques. In general, an ideal treatment should have quality, long shelf life, pervasiveness, and the ability to heal cracks repeatedly an unlimited number of times. One promising solution would be the incorporation of self-healing mechanisms, which are found in nature, into the concrete matrix. Specifically, a biotechnological approach offers a sustainable and viable self-healing mechanism to address the concrete cracking issue. Some microorganisms are capable of inducing $CaCO_3$ minerals through different pathways under specific conditions. $CaCO_3$ is one of the most compatible materials with the concrete matrix. A biotechnological approach to heal the concrete crack is hypothesized as a potential alternative to conventional methods. Once a crack occurs in concrete matrix, the bio-concrete intrinsically heals the crack with $CaCO_3$ through a green pathway.

1.2 Research objectives

Despite the utilization of chemical and polymer sealers to seal the concrete cracks, they are not sustainable and permanent and, more importantly, they cannot guarantee the concrete integrity. The biotechnological approach offers an alternative solution to address the concrete cracking phenomenon by providing a long-lasting compatible material with concrete compositions through a sustainable pathway. However, to be industrially applicable, this technology requires addressing the critical aspects. The main aim of this study is to design a viable nanobiotechnological pathway to intrinsically heal the concrete cracks upon their formation.

More specifically, the prime objectives of this thesis are:

- To screen the potent bacteria, nutrients, and operating condition for biomineralization of $CaCO_3$
- To optimize the biosynthesis of $CaCO_3$ using the significant factors on biomineralization of $CaCO_3$

- To characterize and quantify the morphology of the precipitated $CaCO_3$ crystals
- To investigate the effects of pH and aeration on biomineralization of $CaCO_3$
- To identify the significant ORCs on the biosynthesis of $CaCO_3$ for enhancing the biomineralization process in oxygen-limiting areas
- To optimize the oxygen releasing capacity using the effective ORCs to maximize oxygen liberation in deepest parts of concrete cracks and pores
- To synthesize and characterize two types of magnetic IONs as the vehicles to protect bacteria from the concrete harsh environment
- To immobilize the selected bacteria on fabricated IONs
- To determine the effect of naked and functionalized IONs on biomineralization of $CaCO_3$ and identify the optimum concentrations of nanoparticles
- To investigate the effects of the designed bio self-healing agent on mechanical properties and durability of concrete

1.3 Thesis outline

The objectives of the current study are addressed in nine chapters as outlined below.

Chapter 2 presents the critical review of the current study. In this chapter an overview of the concrete properties and its drawbacks is provided. The possible approaches and their disadvantages to address the shortcomings with the concrete matrix are discussed. Specifically, a comprehensive overview of the microbial pathways to induce $CaCO_3$ as an alternative sustainable approach to conventional techniques for sealing the concrete cracks is given. Moreover, prospective challenges in microbial crack treatment are discussed.

Chapter 3 provides details on the materials, equipment, methodology, and experimental procedures used throughout this research.

Chapter 4 evaluates the potential nutrients, microorganisms, and operating conditions to induce $CaCO_3$ precipitation. Since the performance of a bio self-healing concrete highly depends on the efficiency of the crack sealing, an optimization study is performed to achieve the highest concentration of $CaCO_3$. The morphology of $CaCO_3$ can also affect the performance of the bio self-healing concrete. Therefore a morphological quantification is proposed based on XRD analysis, and the effective parameters on $CaCO_3$ morphologies are identified.

Chapter 5 studies the effect of alkalinity on bacterially induced $CaCO_3$ precipitation. The influence of aeration on the biosynthesis of $CaCO_3$ is also investigated and the optimum level of aeration is proposed. This chapter determines the possibility of using selected microorganisms and nutrients in the concrete matrix.

Chapter 6 evaluates the effect of ORCs on biomineralization of $CaCO_3$. The optimization study is subsequently conducted to maximize the concentration of $CaCO_3$. The optimum concentrations of significant ORCs are determined using response surface methodology to enhance the bio self-healing capability to seal the entire cracks.

Chapter 7 presents the effect of nanomaterials on the biomineralization process and mechanical properties of concrete. Since some of the nanoparticle materials have a positive influence on concrete properties, magnetic IONs are proposed as (i) an improving agent for concrete characteristics, and (ii) a protective vehicle for bacterial viability in the concrete environment. In this sense, two types of IONs are successfully synthesized and characterized. The effect of bacterial immobilization on the biosynthesis of $CaCO_3$ is also investigated and the optimum concentrations of IONs are proposed.

Chapter 8 evaluates the effect of the designed bio self-healing agents on concrete properties. The concrete crack sealing efficiency was determined through crack healing observation and the precipitated crystals inside the concrete are characterized. Compressive strength, water absorption, sorptivity, and drying shrinkage tests are performed to determine the influence of the bio self-healing agent on mechanical properties and durability of the concrete.

Chapter 9 provides overall conclusions for this research and recommendations for areas of further investigation.

Chapter 2

Literature review [1]

[1] This chapter forms the basis of a journal article published in the Journal of Applied Microbiology and Biotechnology and a book chapter published in Nova Science (USA), as referenced below.

[1] **Seifan, M.**, Samani, A.K., and Berenjian, A. *Bioconcrete: next generation of self-healing concrete.* Applied Microbiology and Biotechnology 2016. 100 (6): p. 2591–2602.

[2] **Seifan, M.**, Samani, A.K., Burgess, J.J., and Berenjian, A. *The Effectiveness of Microbial Crack Treatment in Self Healing Concrete.* In High Value Processing Technologies, A. Berenjian, H. Jafarizadeh-Malmiri, and Y. Song, Editors. 2016, Nova Science. p. 97–124.

2.1 Concrete

Concrete is one of the most commonly used construction materials which plays an indispensable role in many fields. It is widely used in the construction of buildings, underground structures, dams, storage tanks, seaports, roads, bridges, tunnels, subways, and other infrastructures. High compressive strength, availability, durability, versatility, simple preparation, compatibility with reinforcement bars, fire-resistance, excellent thermal mass, low price, and the possibility of casting in desired shapes and sizes are the unique characteristics of the concrete.

Concrete is primarily composed of cement, water and aggregate (fine and coarse). Cement characteristics depend on the relative amount of its composition. Typical composition limits for Portland cement can be defined in Table 2-1, which consists of additional minor compounds. Based on required purposes, different types of cement, such as ordinary, modified, rapid-hardening, low-heat, sulphate resisting, high slag blast-furnace, white, and Pozzolana Portland are produced. To enhance its mechanical properties and modify characteristics, admixtures, such as plasticizers, superplasticizers, accelerators, set-retarders, water-reducing, and air entraining admixtures, often mix with other compositions. Cement is the most important constituent of the concrete mixture. Cement binds the aggregates and fills the micro voids between coarse and fine particles as it reacts with water. This phenomenon is called hydration and has a crucial role in the strength of concrete.

Table 2-1 Approximate composition limits of Portland cement (weight %) [3].

Oxide	Content percent
CaO	60-67
SiO_2	17-25
Al_2O_3	3-8
Fe_2O_3	0.5-6.0
MgO	0.1-4.0
Alkalis	0.2-1.3
SO_3	1-3

2.2 Cracking as the main concrete issue

Strength and durability are two significant characteristics which have a direct impact on concrete service life. Although concrete has a high compressive strength capacity, it has low tensile strength and is susceptible to cracking. Cracking is one of the main causes of concrete deterioration and decrease in the concrete's integrity, durability and serviceability. Cracks can be formed in both plastic and hardened stages. In general, there are two types of cracks in respect to their width, namely structural and non-structural cracks (surface cracks). Non-structural and surface cracks are less likely to cause structural failure; therefore they can be repaired by applying sealants or grouts. However, those cracks, which have the potential of becoming destructive, are mostly repaired by stitching, doweling and, in some cases, replacement of the structure [4].

Concrete cracks can be initiated due to many factors. Concrete structures experience flexural stresses during their life time. In this sense, cracks are generated if the tensile stress exceeds the concrete tensile strength. Therefore concrete is reinforced with steel bars, typically in the form of steel rods lain throughout the structure. The reinforced concrete resists not only compression but also bending and other exerted tensile stresses. Therefore an intelligent design will result in concrete resists in both compression and tensile stresses. Reinforcement bars have a positive effect on crack's width restriction by controlling the plastic shrinkage; however, they cannot prevent crack formation. Other reasons which result in cracking are formwork movement, shrinkage on drying fresh concrete, thermal stress during cement hydration, external loading, internal stresses (mostly caused by uneven settlement), expansion and contract upon wetting and drying cycles, poor construction, and error in design and detailing. Furthermore, in cold regions, frozen water trapped in a matrix causes increased fluid pressure and therefore cracks occurred when induced stress exceeded the concrete tensile strength [5].

By increasing the size of capillary pores and cracks, the flow rate of fluids or gasses into concrete is increased. Crack development and consequently concrete corrosion through the reaction of destructive substances with concrete composition and reinforcement bars results in a significant reduction in the structure service life. Since the bar corrodes, the rust occupies more space within the concrete matrix,

exceeding the volume occupied by the reinforcement bar. This not only decreases the concrete tensile strength but also results in further crack development. Although cracks may not endanger the concrete strength in early age, undoubtedly, their formation can be a serious risk to concrete lifespan in the long term. Annually, a considerable budget is allocated for repair of existing cementitious structures in many countries worldwide [6, 7]. The direct cost of crack repair and maintenance has been estimated at \$147 per m^3 of concrete, despite the fact that concrete production costs range between \$65 to \$80 per m^3 [8].

Cement production is another issue arising from the replacement of concrete structures when they become deteriorated by devastating cracks. As illustrated in Figure 2-1, cement production results in significant environmental and sustainability issues through its manufacturing and delivery processes. The cement industry is attributed to one-tenth of carbon dioxide emissions as the main cause of increasing greenhouse gas emissions [9]. Therefore preventive approaches to restrain and terminate crack formation at the early stage are crucial.

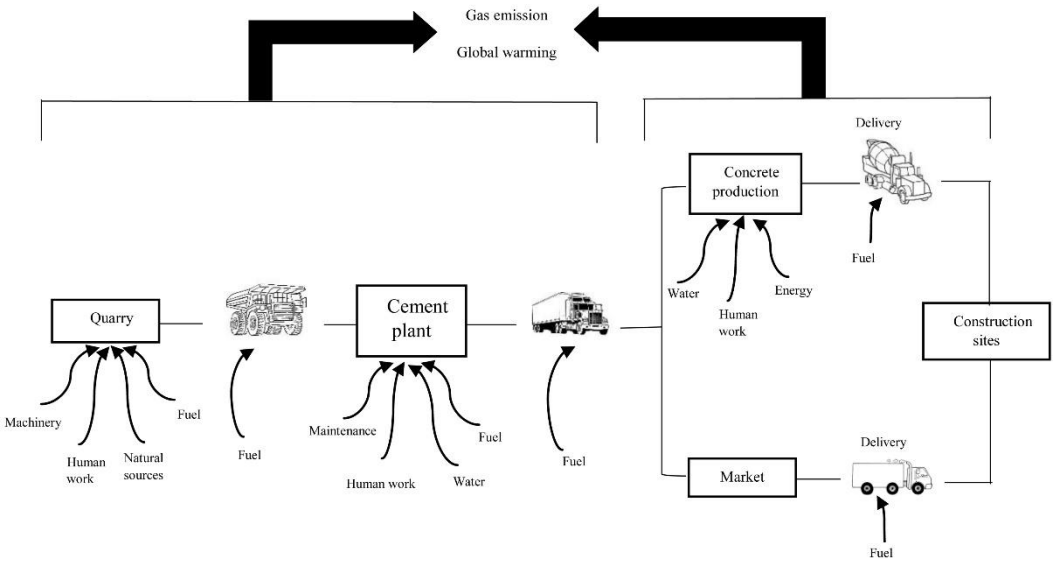

Figure 2-1 Energy consumption and gas emission in cement production cycle [2].

2.3 Concrete crack treatments

Concrete crack and pore treatments are generally divided into passive and active approaches. In the passive form of treatments, sealing agents are applied externally

and only seal the surface defects. When a crack is detected, chemical mixtures and polymers, such as the sealants, will be either injected or sprayed into the cracks [10, 11]. These sealers usually comprise chemical materials, such as epoxy resins, chlorinated rubbers, waxes, polyurethane, acrylics, and siloxane. Passive treatments are applicable to many existing concrete structures due to their availability, while they have many limitations which hinder their usage. Some of the limitations in the use of chemical sealers are poor weather resistance, moisture sensitivity, low heat resistance, unsustainability, poor bonding with concrete, susceptibility to degradation and delamination with age, and different thermal expansion coefficient between concrete and sealers [12-15]. Since the passive treatments are not permanent, they require labor to detect cracks, examine the concrete integrity, and repeat the repair as required. These result in a high maintenance cost. More importantly, the passive techniques are limited to the exterior sides and reachable parts of the structures.

On the other hand, active crack treatment methods involve the incorporation of a healing agent into a matrix during concrete preparation. Active treatment techniques, which are also known as self-healing methods, can operate independently in different conditions regardless of the crack position. The self-healing mechanisms must be activated naturally without the need for human intervention. To date, different self-healing approaches for concrete crack sealing have been proposed. Some of these phenomena occur naturally without the addition of a healing agent, while others can be achieved by incorporation of the healing agent into the concrete matrix during casting. De Rooij et al. [16] proposed an overview of natural causes (physical, chemical, and mechanical) of self-healing mechanisms in concrete. As shown in Figure 2-2, the physical cause, specifically swelling of hydrated cement particles, results in a minor crack blockage. The crack can also be partially healed upon chemical processes. The hydration of unhydrated cement particles is a chemical process that contributes to sealing micro cracks. However, its success highly depends on the availability of unhydrated cement and it can be effective in a young concrete when the crack's widths are small. Another chemical process likely to occur is the formation of $CaCO_3$ on the crack face. This phenomenon is the most effective mechanism contributing to autogenous healing concrete [17, 18]. It has been reported that the clogging of the crack passage by fine

particles existing in the surrounding, or by particles broken off from the fracture surface, may contribute to a minor natural self-healing mechanism [19].

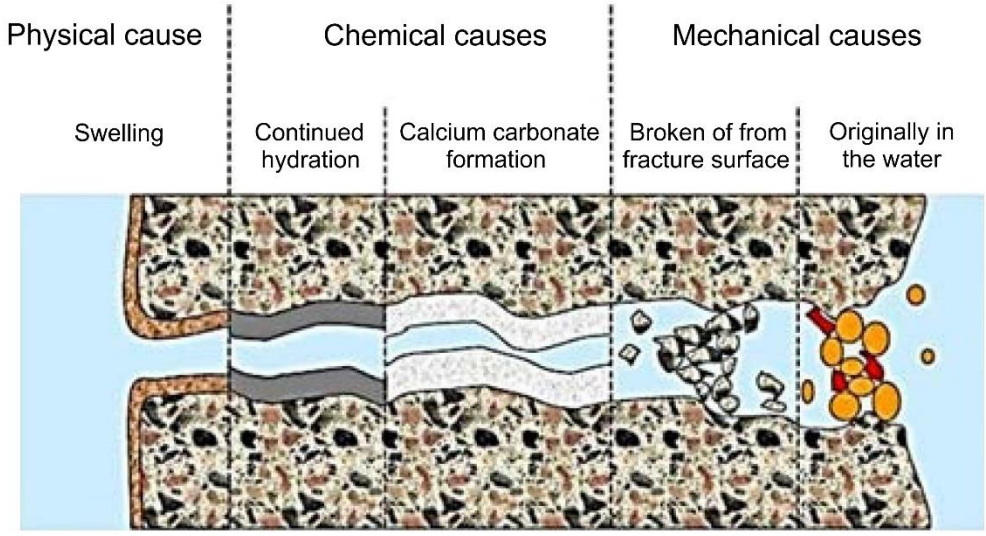

Figure 2-2 Possible causes of self-healing concrete: swelling of the cement matrix, continued hydration, formation of $CaCO_3$ or calcium hydroxide and sedimentation of particles [16].

Cementitious materials, such as concrete, can be designed to have self-healing characteristics [20]. Unlike the natural self-healing mechanisms, this type of self-healing approach requires the addition of healing materials during concrete preparation. As depicted in Figure 2-3 to Figure 2-5, a self-healing mechanism in concrete can be established through three main strategies: (i) autogenous healing, (ii) capsule based healing, and (iii) vascular healing [21].

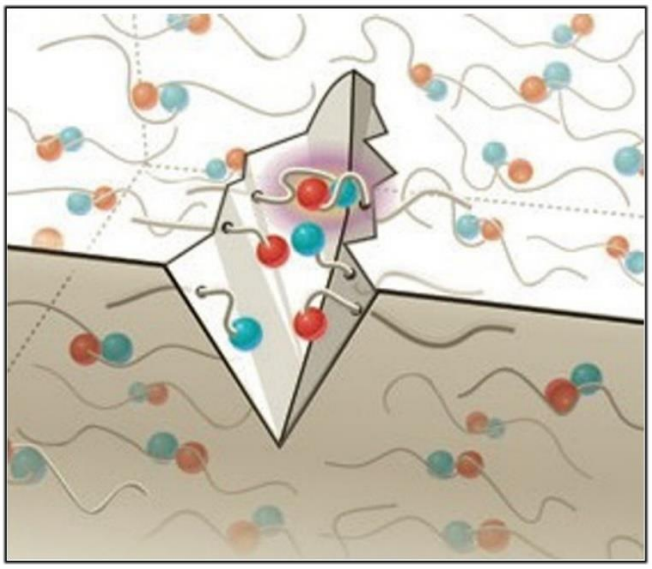

Figure 2-3 Autogenous (intrinsic) self-healing concrete strategy [21].

Self-healing treatments have been inspired by the intrinsic healing behavior of concrete, which is known as autogenous healing and occurs due to the composition of the concrete mixture [2]. It has been reported that the concrete has the ability to fill cracks by producing $CaCO_3$ through the hydration of un-hydrated cement particles, and the dissolution and subsequent carbonation of $Ca(OH)_2$ [22, 23]. Younger concrete tends to experience the hydration of unhydrated cement particles that still exist in the matrix. As shown in Eq. 2-1, calcium hydroxide is produced by the reaction of water and calcium oxide present in the concrete constituent. The reaction of calcium hydroxide and atmospheric carbon dioxide results in $CaCO_3$ production (Eq. 2-2) [18].

$$CaO + H_2O \rightarrow Ca(OH)_2 \quad (2\text{-}1)$$

$$Ca(OH)_2 + CO_2 \rightarrow CaCO_3 + H_2O \quad (2\text{-}2)$$

Due to the abundance in nature and compatibility with cementitious compositions, $CaCO_3$ is one of the most useful and versatile fillers to plug the voids, porosities, and cracks in concrete. The success of autogenous healing strongly depends on the position and quantity of unhydrated cement, the age of the concrete, and presence of water [24-26]. Mostly, unhydrated cement particles are located away from the

surface of the concrete where most of the cracking occurs. Moreover, it has been noted that autogenous healing tends to favor narrow cracks [27-30]. A practical way to improve autogenous healing is to reduce water to cement (w/c) ratio. However, increasing cement portion to reduce w/c ratio has an adverse effect on shrinkage and workability, and demands more cement production. In addition, the hydration of unhydrated cement in a large volume placement during autogenous healing may result in the formation of new cracks. Exothermic chemical reaction between unhydrated cement and water generates significant heat and the temperature gradient raises the likelihood of cracking.

Encapsulation of chemical or polymeric materials into concrete is another type of self-healing method (Figure 2-4). In this approach, a self-healing agent is incorporated inside discrete capsules (spherical or cylindrical shape) and mixed with other constituents during concrete mixing. Released healing agent upon capsule rupture caused by cracking reacts with water, moisture, concrete compositions or secondary component embedded in concrete. Although the releasing of the healing agent into a damaged area due to gravitational and capillary forces results in sealing crack [24], it does not behave the same as concrete compositions in many conditions and, in some cases, it leads to extending the existing cracks. Moreover, the incorporated capsules and the remaining space after activation have an adverse influence on the concrete integrity. Low viability under some environmental conditions and not being repetitive over concrete lifespan are the other limitations in using a capsule based self-healing strategy. In addition, a capsule preparation and encapsulation process are expensive, and it cannot be guaranteed that the capsules and healing agent remain intact during the concrete mixing process. These requirements make encapsulation method a difficult practice for commercial self-healing concrete application.

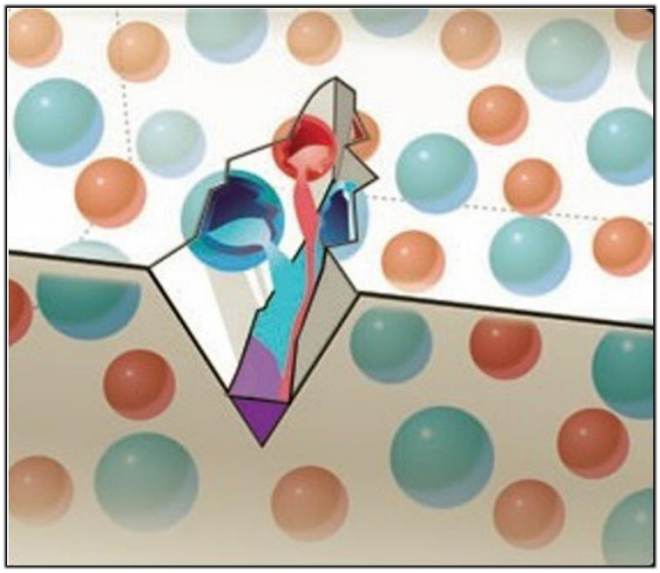

Figure 2-4 Capsule based self-healing concrete strategy [21].

The healing agent can also be inserted in the concrete matrix through vascular network. As shown in Figure 2-5, vascular technique supplies the healing agent from the outside of the structure through distributed vascular networks which have been already embedded in the matrix during concrete preparation. The mechanism of activation in the vascular healing technique is the same as capsule based. As cracking occurs, the healing agent, which is kept in a reservoir, runs through embedded veins due to a pressure gradient. The vascular healing approach has also many limitations. If the healing agent released more than crack capacity, it not only causes aesthetic issues but also increases the maintenance cost to compensate the healing agent lost. Embedment of vascular networks inside the concrete matrix is complex and the veins may rupture during the vibrating process. Moreover, the presence of long vascular networks in the concrete matrix decreases the structural integrity and a blockage in veins prevents the transfer of the healing agent to other parts. These shortcomings result in a significant reduction in the healing capacity.

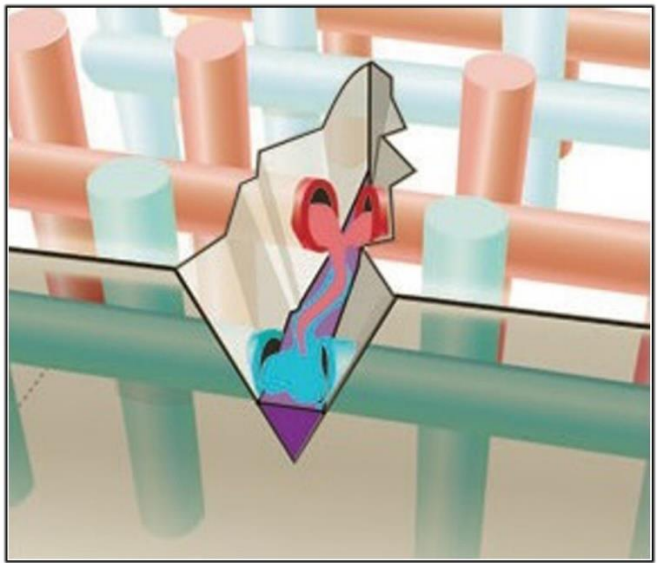

Figure 2-5 Vascular based self-healing concrete strategy [21].

2.4 Biotechnological approach

Due to the drawbacks of existing treatments, alternative innovative active treatment methods are in high demand. An ideal treatment should have quality, long shelf life, pervasiveness, and the ability to heal cracks repeatedly an unlimited number of times [31]. Recently, the biotechnological approach has attracted researchers' attention as a promising way to address the issues associated with active and passive crack treatments. Biotechnological discipline is defined as scientific and practical knowledge of microorganisms' behavior and their products under different conditions. It offers an alternative, sustainable and environmentally friendly approach for many industrial applications. Over the last decade, the application of biotechnological products (bio admixture) has emerged for constructional purposes to provide additional properties. For instance, the addition of industrially produced microbial polysaccharides has been reported to enhance water retention, set retarding, and flowability of dry-mix mortars, wall plasters, self-leveling underlayers, and injection grouts [32, 33].

The bio products can also be used as the self-healing agent for constructional materials. It is widely known that microorganisms contribute to the precipitation of a wide diversity of minerals, such as carbonates, phosphates, sulfides, and silicates. Among all bio-precipitate minerals, the production of $CaCO_3$ has drawn much

attention due to its role in environmental and industrial applications. The precipitation of carbonate minerals by microorganisms broadly occurs in different geological environments, such as fresh and marine water [34], soil [35], cave [36, 37] and hot spring [38]. Apart from the role of biomineralization in nature, a large number of applications involving the microbial $CaCO_3$ precipitation with important scientific and technological implications have been reported. The main applications of $CaCO_3$ biomineralization are protection of limestone monuments [39], removal of Ca^{2+} ions from wastewaters [40], surface treatment of construction materials [12, 41], improvement of brick properties [42, 43], removal of contaminants and heavy metals from groundwater [44], plugging the pores of oil reservoirs [45], strengthening of sand columns [46], soil consolidation [47, 48], and atmospheric CO_2 sequestration [49]. Since $CaCO_3$ is one of the most compatible materials to concrete and mortar, its green precipitation through a biological approach will address the shortcomings associated with construction materials. Successful implementation of this innovative treatment method will also result in a longer lifespan of concrete structures as well as significant reduction in cement production and structural replacement. Therefore to design a bio-concrete mixture, a comprehensive understanding of biological approaches to induce $CaCO_3$ precipitation is needed.

2.5 Approaches to induce $CaCO_3$ precipitation

This part covers the generic and fundamental principles to design a self-healing concrete through the sustainable biotechnological approach. Biomineralization refers to the process of mineral formation by living organisms which is a widespread phenomenon in nature [50]. Biomineralization can be accomplished through biologically controlled mineralization (BCM) and biologically induced mineralization (BIM) processes. In BCM mineral particles are deposited intracellularly in a specific location within or on the cell, and the process is independent of environmental conditions [51, 52]. This process is a highly regulated mechanism which produces more uniform particle size and shape as well as consistent mineral morphologies [52]. Well-defined composition and structure minerals are produced through the BCM process.

In contrast to BCM, the BIM process occurs in an open environment as an uncontrolled consequence of microbial metabolic activity [34]. In this process biominerals are formed through the reaction of metabolic products generated by microorganisms with the surrounding environment. Bacterial structure and a schematic diagram of $CaCO_3$ production are shown in

Figure **2-6**. Mineral precipitation occurs by successful attachment of the positively charged ions to the negatively charged microbial cell walls. The BIM process usually occurs in an anaerobic environment or at oxic–anoxic boundary. Its effectiveness highly depends on the concentration of dissolved inorganic carbon, nucleation site, pH, temperature, and Hartree energy (E_h) [53, 54].

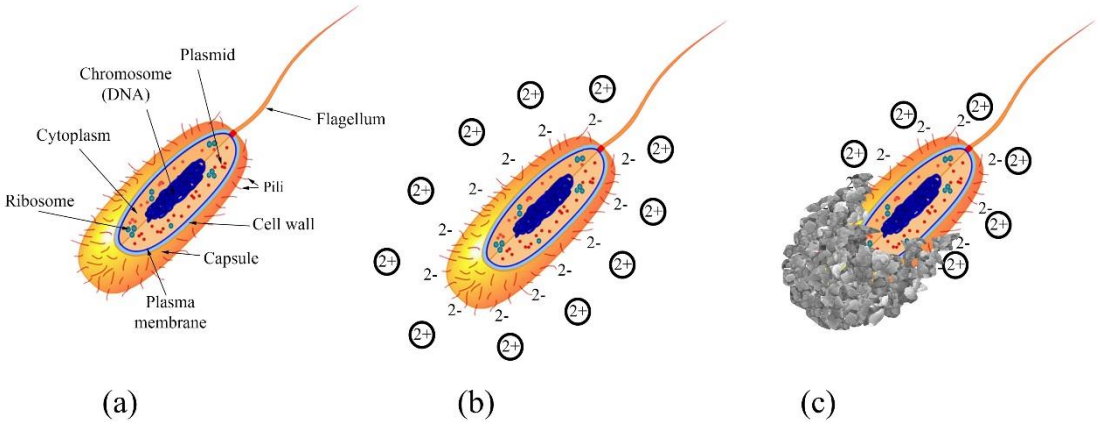

Figure 2-6 (a) Bacterial cell structure, (b) negative charged cell wall and presence of positive charged ions and (c) bio mineral precipitation [1].

Microbially induced $CaCO_3$ precipitation (MICP) can be achieved through two metabolic pathways, namely autotrophic and heterotrophic.

2.5.1 Autotrophic pathway

Autotrophic pathway happens in the presence of carbon dioxide for which microbes convert carbon dioxide to carbonate through three distinct ways, namely (i) non-methylotrophic methanogenesis (by Methanogenic archaea); (ii) oxygenic

photosynthesis (by *Cyanobacteria*); and (iii) anoxygenic photosynthesis (by Purple bacteria) [55].

Non-methylotrophic methanogenesis pathway converts carbon dioxide and hydrogen to methane (Eq. 2-3). Accordingly, anaerobic oxidation of methane by electron acceptors, such as sulfate (shown in Eq. 2-4), results in the production of bicarbonate [56]. The produced carbonate will then result in $CaCO_3$ precipitation in the presence of calcium ions as it is shown in Eq. 2-5. This pathway is more common in marine sediments.

$$CO_2 + 4H_2 \rightarrow CH_4 + 2H_2O \quad (2\text{-}3)$$

$$CH_4 + SO_4^{2-} \rightarrow HCO_3^- + HS^- + H_2O \quad (2\text{-}4)$$

$$Ca^{2+} + 2HCO_3^- \leftrightarrow CaCO_3 + CO_2 + H_2O \quad (2\text{-}5)$$

The photosynthesis process is also an autotrophic pathway to produce $CaCO_3$ in the presence of calcium ions. There are two groups of photosynthetic bacteria, namely oxygenic and anoxygenic photosynthetic bacteria. Oxygenic and anoxygenic photosynthesizing organisms utilize different types of electron donors to produce methanal. As shown in Eq. 2-6, water acts as an electron donor in oxygenic photosynthesis. In anoxygenic photosynthesis, however, hydrogen sulphide (H_2S) acts as an electron donor in the redox reaction (Eq. 2-7), and therefore oxygen is not generated [57, 58]. Removal of carbon dioxide during microbial photosynthesis from bicarbonate solutions results in carbonate production [52]. This phenomenon leads to a localized increase in pH and finally $CaCO_3$ precipitation in the presence of calcium ions [54]. Summary of photosynthesis chemical reactions for $CaCO_3$ production are listed from Eq. 2-6 to Eq. 2-9.

$$CO_2 + H_2O \xrightarrow{Oxygenic\ Photosynthesis} (CH_2O) + O_2 \quad (2\text{-}6)$$

$$CO_2 + 2H_2S + H_2O \xrightarrow{Anoxygenic\ Photosynthesis} (CH_2O) + 2S + 2H_2O \quad (2\text{-}7)$$

$$2HCO_3^- \leftrightarrow CO_2 + CO_3^{2-} + H_2O \quad (2\text{-}8)$$

$$CO_3^{2-} + H_2O \leftrightarrow HCO_3^- + OH^- \quad (2\text{-}9)$$

Despite the possibility of calcium precipitation through photosynthesis, this method is only feasible in the presence of carbon dioxide in the surrounding environment. This indicates that the photosynthesis pathway can only be used in the areas that the concrete structure is exposed to carbon dioxide and light.

2.5.2 Heterotrophic pathway

Microbial communities may precipitate crystals as a result of their growth in different natural habitats. Crystal formation is attributed to the medium composition used to grow heterotrophic bacteria and is a common phenomenon in nature. Heterotrophic growth of different genera of bacteria such as *Bacillus*, *Arthrobacter*, and *Rhodococcus* species on organic acid salts (acetate, lactate, citrate, succinate, oxalate, malate, and glyoxylate) results in the production of carbonate minerals. These bacteria use organic compounds as a source of energy. Based on the salts and carbon sources present in the medium, these bacteria are able to produce various crystals, such as $CaCO_3$ and magnesium carbonate. Chemical reactions to form $CaCO_3$ in the presence of calcium acetate as a source of low molecular weight acid and calcium ion are listed in Eq. 2-10 to Eq. 2-12 [59].

$$CH_3COO^- + 2O_2 \xrightarrow{Heterotrophic\ bacteria} 2CO_2 + H_2O + OH^- \quad (2\text{-}10)$$

$$2CO_2 + OH^- \rightarrow CO_2 + HCO_3^- \quad (2\text{-}11)$$

$$2HCO_3^- + Ca^{2+} \rightarrow CaCO_3 + CO_2 + H_2O \quad (2\text{-}12)$$

$CaCO_3$ precipitation through utilization of organic acid has been widely documented in different substrate environments, including caves (walls, ceilings, and speleothems), marines, lakes, and soils. It was noted that utilization of heterotrophic bacterial communities (*Arthrobacter* and *Rhodococcus*) isolated from stalactite in the cave can produce $CaCO_3$ in the presence of calcium acetate [37, 60]. Moreover, the contribution of *Arthrobacter* and *Rhodococcus* species isolated from

polar environments on precipitation of $CaCO_3$ crystal with calcium citrate and calcium acetate as carbon source has been extensively investigated [35]. Cacchio et al. [61] did another conceptual research and it was found that *Bacillus* and *Arthrobacter* species are capable of precipitating $CaCO_3$ under alkaline carbonate medium. The presence of the organic acid as the sole source of carbon and energy is the most significant advantage of this pathway.

2.5.2.1 Sulfur cycle

The sulfur cycle is another mechanism of producing $CaCO_3$. The sulfur cycle follows by dissimilatory reduction of sulphate. In this process $CaCO_3$ is produced if the calcium source, organic matter, and sulphate are present in the medium. The increase in pH as a result of degasification of hydrogen sulfide shifts the reaction towards precipitation of $CaCO_3$ [55]. Production of $CaCO_3$ through reducing calcium sulfate ($CaSO_4$) to calcium sulfide (CaS) by sulfate reducing bacteria is shown in Eq. 2-13 to Eq. 2-16 [62].

$$CaSO_4 + 2(CH_2O) \rightarrow CaS + 2CO_2 + 2H_2O \quad (2\text{-}13)$$

$$CaS + 2H_2O \rightarrow Ca(OH)_2 + H_2S \quad (2\text{-}14)$$

$$CO_2 + H_2O \rightarrow H_2CO_3 \quad (2\text{-}15)$$

$$Ca(OH)_2 + H_2CO_3 \rightarrow CaCO_3 + 2H_2O \quad (2\text{-}16)$$

2.5.2.2 Nitrogen cycle

Production of carbonate or bicarbonate through the nitrogen cycle can be established through three main pathways, namely (i) urea or uric acid degradation (ureolysis), (ii) ammonification of amino acids, and (iii) dissimilatory nitrate reduction [56, 63]. As a result of the nitrogen cycle, $CaCO_3$ is precipitated upon the presence of sufficient calcium ion in the medium. These urease positive microorganisms are involved in the nitrogen cycle and can produce $CaCO_3$ through urea hydrolysis [64-66]. Microorganisms such as *Bacillus spharecus* and *Bacillus peusturii* are able to produce biominerals through metabolic reaction in the presence

of a calcium source. Fundamental reactions to induce $CaCO_3$ precipitation are shown in Eq. 2-17 and Eq. 2-18 [67].

$$Ca^{2+} + CO_3^{2-} \leftrightarrow CaCO_3 \quad (2\text{-}17)$$

$$Ca^{2+} + 2HCO_3^- \leftrightarrow CaCO_3 + CO_2 + H_2O \quad (2\text{-}18)$$

Microbial metabolic activities lead to an increase in carbonate concentration and pH [11, 15, 68]. Increase in pH facilitates the transformation of carbon dioxide to carbonate [26]. These metabolic conversions promote $CaCO_3$ precipitation (mostly in the stable form of calcite that is abundant in nature) [67, 69]. Through urease activity in the presence of bacteria, one mole carbamic acid (NH_2COOH) and one mole ammonia (NH_3) are produced from urea hydrolysis (Eq. 2-19). As can be seen from Eq. 2-20, carbamic acid hydrolysis produces one mole carbonic acid (H_2CO_3) and one mole of extra ammonium simultaneously.

$$CO(NH_2)_2 + H_2O \xrightarrow{Microorganism} NH_2COOH + NH_3 \quad (2\text{-}19)$$

$$NH_2COOH + H_2O \rightarrow NH_3 + H_2CO_3 \quad (2\text{-}20)$$

According to Eq. 2-21 and Eq. 2-22, the reaction of hydroxide ion (which is already produced from the reaction of water and ammonia) and carbonic acid produces carbonate (CO_3^{2-}) [70]. As can be seen in Eq. 2-23, positively charged calcium ions can then bind to the negatively charged bacterial cell.

$$2NH_3 + 2H_2O \rightarrow 2NH_4^+ + 2OH^- \quad (2\text{-}21)$$

$$2OH^- + H_2CO_3 \rightarrow CO_3^{2-} + 2H_2O \quad (2\text{-}22)$$

$$Ca^{2+} + Cell \rightarrow Cell - Ca^{2+} \quad (2\text{-}23)$$

$$Cell - Ca^{2+} + CO_3^{2-} \rightarrow Cell - CaCO_3 \quad (2\text{-}24)$$

To complete the last reaction (Eq. 2-24), calcium ion can be provided either by internal sources that are available in the cement structure or by adding chemicals such as calcium chloride, calcium nitrate or calcium lactate to the concrete mixture.

Another pathway to produce minerals is known as dissimilatory nitrate reduction. Denitrification defines as a respiratory process that results in the reduction of nitrate (NO_3^-) to nitrite (NO_2^-), nitric oxide (NO), nitrous oxide (N_2O), and nitrogen gas (N_2) [1]. Minerals are precipitated through oxidation of organic compounds by the reduction of nitrate via denitrifying bacteria. The most significant attribute of this approach is its application in anaerobic zones. The microorganisms that are involved in the denitrification process are facultative anaerobes; mainly *Denitrobacillus*, *Thiobacillus*, *Alcaligenes*, *Pseuodomonas*, *Spirillum*, *Achromobacter*, and *Micrococcus* species [71]. As a consequence of organic compound denitrification, carbon dioxide, water and nitrogen are produced (Eq. 2-25). According to Eq. 2-26 an increase in pH due to consumption of H^+ during the denitrification process results in carbonate or bicarbonate production [72]. The final reaction of calcium source and carbonate results in precipitation of $CaCO_3$ (Eq. 2-27).

$$Organic\ compound + a\ NO_3^- + b\ H^+ \xrightarrow{Denitrification} c\ CO_2 + d\ H_2O + e\ N_2 \quad (2\text{-}25)$$

$$CO_2 + 2OH^- \rightarrow CO_3^{2-} + H_2O \quad (2\text{-}26)$$

$$Ca^{2+} + CO_3^{2-} \rightarrow CaCO_3 \quad (2\text{-}27)$$

Production of $CaCO_3$ via denitrification process in concrete is not well-developed and needs further research to elucidate. However, studies on soil improvement properties have illustrated that efficacy of ureolysis is higher than the denitrification approach in respect to the production of $CaCO_3$ [47, 73]. Urea hydrolysis occurs in a short period of time. Therefore $CaCO_3$ precipitation through the ureolysis pathway is the fastest approach among the $CaCO_3$ biomineralization processes [74].

2.6 Effective factors on MICP

2.6.1 The effects of nutrients on MICP

To implement MICP at different fields, the effect of nutritional compounds and environmental factors on the biomineralization process needs to be assessed. Until recently, the majority of conducted investigations have been focused on the possibility of $CaCO_3$ precipitation by various microbial strains and nutrients. The main step towards the MICP process is the selection of potent strains. Hammes et al. [75] isolated the urease bacterial strains from different environmental samples. They found that the selected isolates were closely related to the *Bacillus sphaericus* genes. Fujita et al. [40] reported that the isolated ureolytic subsurface bacteria from the Eastern Snake River Plain aquifer in Idaho are able to induce $CaCO_3$ precipitation. In another investigation, the *Bacillus* species isolated from calcareous sludge showed the possibility of $CaCO_3$ precipitation [67]. In this sense, the presence of a bacterial healing agent will not guarantee the filling of the entire cracks, voids, and porosities. Since the crack and pore size varies from the micro to macro ranges, the durability of the concrete structure will be further increased when the entire cracks and porosities are filled with $CaCO_3$. Therefore, to maximize the crystal precipitation, it requires determining the optimal concentrations of nutritional compounds.

2.6.2 The effects of aeration and pH on MICP

On the other hand, the variation of environmental parameters such as aeration and pH may have inhibitory or effect on biomineralization process. It is known that the availability of oxygen (aeration) is one of the critical factors affecting the fermentation process [76]. Although oxygen is essential for microbial growth and biosynthesis, a higher elevated oxygen than required by bacterial cells is toxic. Similar to other biosynthesis processes, the lack of oxygen may affect the biomineralization of $CaCO_3$. It has been reported that the precipitation of $CaCO_3$ is limited to the surface area of the concrete matrix where the sufficient oxygen is available for bacteria to initiate the biomineralization [77]. The decrease in $CaCO_3$ precipitation with the increase in crack depth was observed by Qian et al. [78]. They

noticed that the biomineralization of $CaCO_3$ was completely inhibited for the crack depth of greater than 10 mm, and the maximum bioprecipitation occurred at a depth of 1.5 mm. Wang et al. [79] employed high resolution X-ray computed microtomography analysis (X-ray μCT) to examine inside a bio-concrete specimen. Their results show that the $CaCO_3$ mostly deposited in the surface layer of the specimen and the precipitation rate decreased with the increase in crack depth. The literature demonstrates the bioprecipitation of $CaCO_3$ in the concrete specimen is a function of depth and highly dependent on the availability of oxygen. This major drawback results in a reduction in bio self-healing efficiency mechanism, and therefore it requires to address the limitation for enhancing the mineral precipitation inside the cracks and pores.

In many in situ conditions, the application of aerobic biodegradation processes is more likely to be limited due to the lack of oxygen required by microorganisms [80]. Oxygen releasing compounds (ORCs) are an engineered material proposed to enhance in situ aerobic bioremediation processes. They intend to release oxygen at a controlled rate to enhance the aerobic bioremediation processes. ORCs are cheaper and more reliable than the utilization of a oxygen bubbling system. They can be used in a pure form or in mixtures with other compounds [81]. The utilization of ORCs has been reported as a method to accelerate bioremediation of aerobically degradable compounds [82]. Despite the oxygen liberating process by solid ORCs being slower than liquid ORCs, the solid ORCs provide more stable and long-lasting oxygen generation [83]. Moreover, if the oxygen releasing process takes place rapidly, the resulted oxygen cannot be utilized by the microorganism and it may increase the cell toxicity. ORC decomposes in the presence of water or moisture to produce H_2O_2. When ORC hydrates, molecular oxygen needed for bacterial metabolic activity is liberated due to the natural decomposition of H_2O_2 [84]. This is hypothesized that when a concrete undergoes cracking, water penetrates into the deepest part of microcrack due to the capillary action and, consequently, an adequate amount of oxygen for bacterial germination is produced.

Another possibility of decreasing the bio self-healing efficiency would be the concrete pH. Alkaliphilic bacteria such as *Bacillus* species can tolerate the extreme concrete environment and therefore they are the most attractive species for bio self-

healing concrete. Studies illustrate that these thick membrane spore forming bacteria can survive without nutrients for hundreds of years [85]. Moreover, the dormant endospores are able to withstand environmental changes or chemicals as well as ultraviolet radiations and mechanical stresses [24, 86]. However, the concrete has a pH of ~12 and exposes many environmental conditions which may inhibit the bacterial metabolism. The direct incorporation of the microorganism into the concrete matrix can influence the microbial metabolic activity. Jonkers et al. [65] incorporated *B. cohnii* spores directly into the concrete matrix. The number of viable cells in the concrete specimen was investigated after curing ages of 9, 22, 42, and 153 days. Although the number of viable bacteria cells in the concrete matrix was approximately constant up to 9 days, it dramatically decreased after 22 and 42 days by 80% and 90%, respectively. Their results indicate that the bacterial cells could be viable for up to 4 months (135 days) in the concrete matrix.

2.6.3 Strategies to protect the bacterial cells

A possible strategy to address the viability loss is the protection of bacterial cell through encapsulation or immobilization in protective matrix prior to concrete mixing. Different encapsulation techniques have been tested for bacterial protection against the concrete environment. For instance, the immobilization of bacterial cells in hydrogel has been proposed to determine its effectiveness on bio self-healing efficiency [87]. According to their results, the immobilization of bacterial cells into hydrogel showed a superior crack sealing capacity and positive effect on water permeability as compared to the non-bacterial series. In another investigation, Van Tittelboom et al. [15] reported the positive effect of silica gels to protect bacteria in the concrete matrix. They found that the incorporation of bacterial cells into silica gel could completely seal the concrete crack compared to unprotected cells. The immobilization of bacterial cells into expanded clay particle was proposed by Wiktor and Jonkers [66]. After curing in water, a higher crack healing capacity was observed when the concrete specimen was supplemented with immobilized spores. Melamine formaldehyde based microcapsules [26] and diatomaceous earth [10], were also noted as the promising vehicles to protect the bacterial cells in the concrete environment.

Considering the pore size of the concrete and bacterial cell, there is a high risk for the cells to squeeze upon cement hydration. On the other hand, the shear force on bacterial cells during concrete mixing and casting as well as gradual shrinkage of the concrete may influence the bacterial cells and, consequently, the bio self-healing concrete performance will be affected. It is believed that the immobilization of bacteria in the protective matrix can prevent the cell damage. Another alternative solution to avoid the crushing of bacterial cells in the concrete matrix over time can be the addition of air-entraining agents [65]. The presence of air-entraining agents in the concrete mix results in the creation of isolated micropores where the bacterial cells can be protected. However, this technique is not effective because the resulted micropores cannot protect the bacterial cells from high pH and exerted shear force during concrete preparation and casting.

2.7 Effects of nanoparticles on concrete properties

Despite the positive effect of immobilization on bacterial viability, the majority of encapsulation materials adversely affect the mechanical properties (compressive strength) of concrete, specifically if their dosages are higher than 1% of cement weight [88]. Among the protective particles, the adsorption of bacterial cells onto diatomaceous earth shows an increase in concrete compressive strength. This increase in compressive strength is attributed to the protective matrix pozzolanicity rather than the effect of immobilized bacterial cells. Therefore it is required to immobilize the bacterial cells in a suitable matrix that increases or at least prevents a decline in the concrete compressive strength.

Conventionally, several mineral additives, such as silica fume and fly ash, have been tested in cementitious materials due to their ability for partial bonding and filling the micro and macro voids [89]. The concrete is a nanostructured, multiphase and composite material [90]. The use of nanotechnology would offer the possibility of great advances in concrete technology and is able to improve the concrete's bulk properties. More recent studies show that the implementation of nano-sized materials, such as nano-SiO_2, nano-Fe_2O_3 and nano-ZrO_2, in cement composites has a significant effect on the kinetics and hydration of cement [91-93].

The nano scale-size of particles are able to enhance the concrete properties from conventional grain-size materials of the same chemical composition. In general, nanotechnology refers to the understanding and controling of matter at dimensions smaller than 100 nanometers. The unique characteristics of nano-sized particles, including larger surface area and greater electrostatic force, result in a higher capability to fill in voids as compared to the conventional mineral additives. Many studies have reported the positive effect of the nano-sized particle on the cementitious materials properties. Oltulu and Sahin [89] investigated the effect of nano-SiO_2, nano-Al_2O_3 and nano-Fe_2O_3 powders on compressive strength and capillary absorption of mortar. They found that the addition of nano powders at 1.25% significantly increases (7–32%) the compressive strength of mortar specimen. The addition of selected nano powders also resulted in a 14% decrease in capillary absorption as compared to the control specimen. To increase the compressive and flexural strengths, Li et al. [94] suggested the addition of nano-SiO_2 or nano-Fe_2O_3 into the cement mortar mixture. In another investigation Jo et al. [95] experimentally tested the effect of nano-SiO_2 particles on compressive strength of mortar. It was found that the presence of nano-SiO_2 can enhance the compressive strength of mortar specimen as compared to the samples containing silica fume at 7 and 28 days. Apart from enhancing the compressive and flexural strengths, it has been found that nano-Fe_2O_3 has a smart self-diagnostic potential (temperature or strain sensing) [93, 94]. Considering the positive effects of nanoparticles on the concrete properties, the utilization of the innovative nanobiotechnological approach for immobilization purposes can be a promising achievement to significantly increase the efficiency of bio self-healing concrete.

2.7.1 Magnetic iron oxide nanoparticle immobilization

Magnetic iron oxide nanoparticles (IONs), mostly magnetite (Fe_3O_4) and maghemite (γ-Fe_2O_3), are known as an important form of half-metallic materials [96]. Nanoparticles have superior properties over the bulk materials. The unique physical and chemical properties of IONs, including superparamagnetism, the ease of synthesis and subsequent functionalization, high surface area to volume ratio, and more importantly the biocompatibility characteristics, make them into a highly

promising tool for biotechnological purposes [96, 97]. Due to these notable characteristics, IONs have been used in medical and biological applications, such as drug delivery [98], removal of heavy metals in water [99], and biomolecular separation or purification [100-102].

IONs can also be used as a carrier for the microorganism. It is known that the bacterial cell walls have a strain dependent net negative charge. The presence of carboxyl or phosphate groups in teichoic acids linked to either the peptidoglycan or the underlying plasma membrane in Gram positive strain results in the cell walls possess a negative charge [103], while the availability of phospholipids and lipopolysaccharides in Gram negative bacteria is the main reason to impart the negative charge. The interaction between magnetic IONs and bacterial cell walls due to electrostatic attraction or repulsion contribute to adsorption of nanoparticles onto the bacterial cells.

On the other hand, the applications of nanoparticles may have a toxicity effect depending on the nanoparticles' type and concentration volume superficial characteristics [104, 105]. It has been reported that IONs have contradictory effects on bacterial cells. Some studies demonstrate an inhibitory effect of IONs on bacterial cells [106, 107], while the other investigations show a satisfactory influence of IONs on bacterial cells [108, 109]. The cells' physiology and IONs concentration are the prime influential parameters which can stimulate or inhibit the bacterial growth [110].

Over recent years, extensive efforts have been devoted to stabilizing the fabricated nanoparticles by surface coating. In this case, the modified IONs consist of the following parts: (i) magnet core, (ii) surface coating, and (iii) functionalized outer coating [111]. The center of IONs are made of a superparamagnetic core and play an important role in the overall magnitude of magnetization force. As shown in Figure 2-7, the functionalized outer coating can be different types of biocompatible and hydrophilic polymeric materials, such as polyvinyl alcohol [112], dextran [113], polyethylene glycols [114], poly vinyl pyrrolidone, polyacrylic acid, polylactide–co-glycolide and polyethyleneimine [110]. IONs can also be coated by aminosilanes such as 3-aminopropyltriethosysilane (APTES) [115, 116], Lysine [117] and p-aminophenyltrimethoxysilane (APTS). Figure 2-8 displays an

illustration of the amino acid coated IONs. The functionalized coated IONs have a promising influence on colloidal stability as compared to the naked IONs. Considering the positive influence of nano-scaled particles on concrete properties, the immobilization of bacterial cells on IONs not only enhance the possibility of $CaCO_3$ precipitation in the concrete matrix but also address the shortcomings associated with the direct incorporation of the healing agent into the concrete mixture.

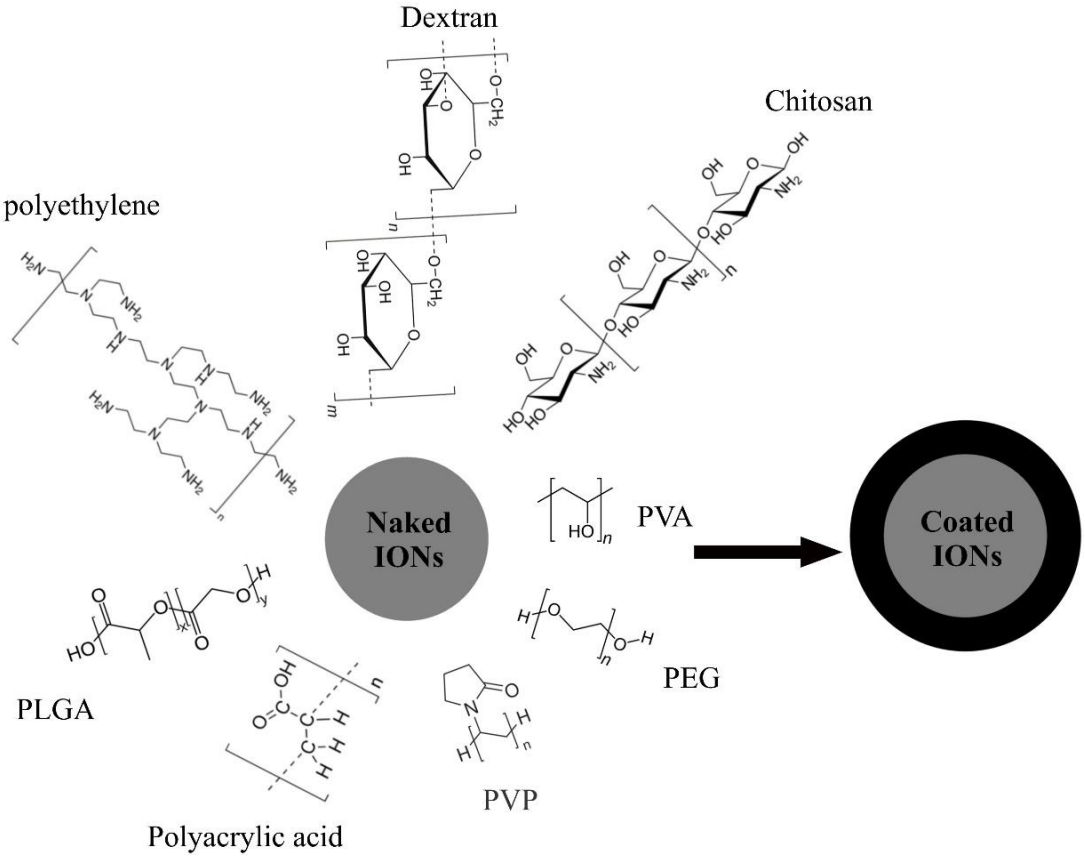

Figure 2-7 Functionalization of magnetic IONs with Chitosan, PEG, Dextran, PLGA, PVA, Polyacrylic acid.

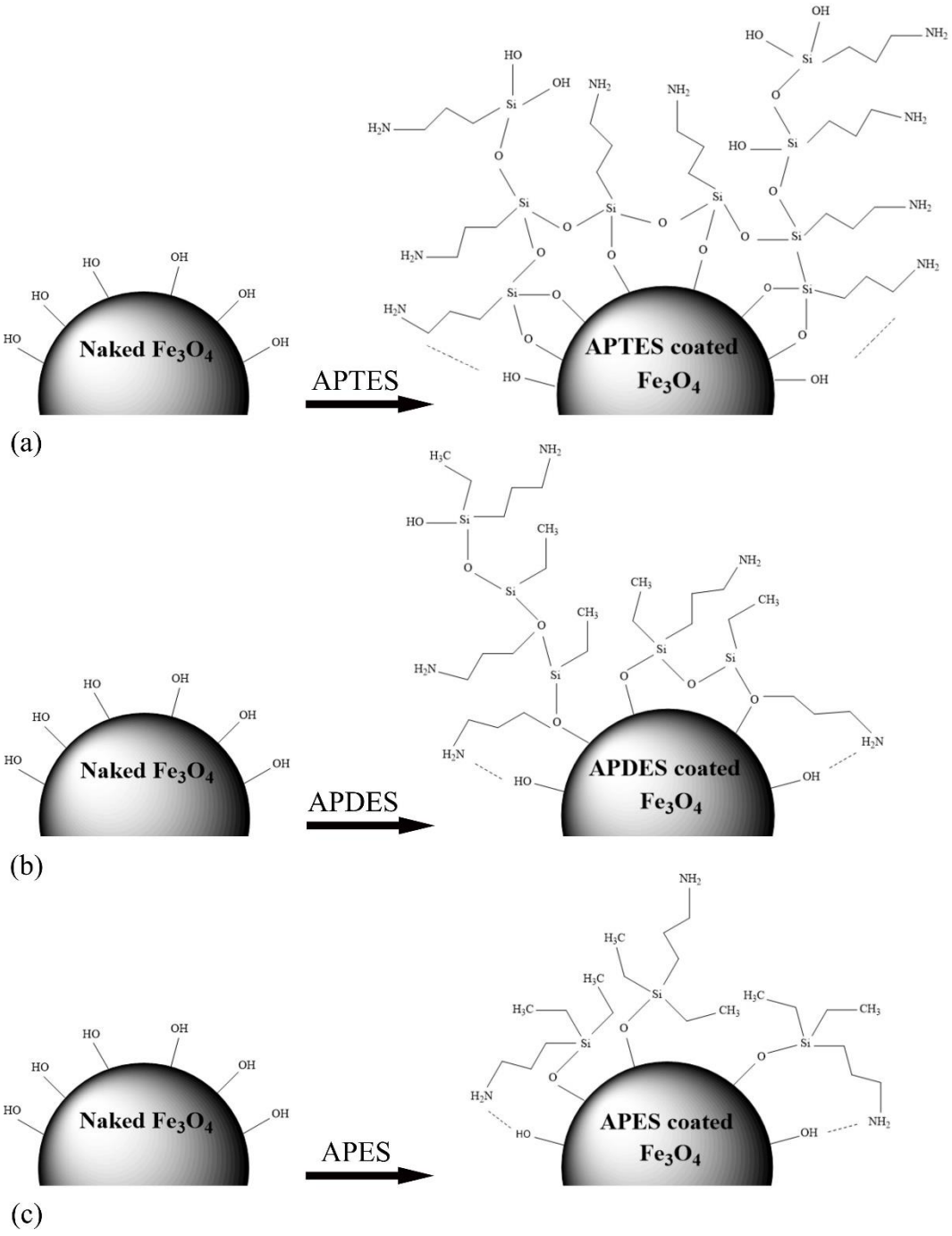

Figure 2-8 Functionalization of magnetic IONs with different amino-functional alkoxysilanes: a) APTES, b) APDES and c) APES.

2.7.2 Magnetic iron oxide nanoparticle synthesis

Over recent years, different protocols, such as thermal decomposition [118-120], sonochemical synthesis [121-123], sonochemical synthetic route [124], hydrothermal synthesis [125-127], microemulsion [128, 129], co-precipitation

[130], laser pyrolysis techniques [131], electrochemical synthesis [132], microorganism mediated synthesis (Magnetotactic bacteria and iron reducing bacteria) [133-135], have been proposed for the efficient synthesis of IONs. Among the possible techniques to produce IONs, the co-precipitation method offers an inexpensive and convenient way with a higher yield and ease of surface treatment.

However, the major challenge to fabricate IONs is the control of nanoparticle size and shape, stability, and dispersibility in a solvent [134]. Since the magnetism depends on the magnetic domain, the IONs' properties highly rely on the size of the nanoparticle. It has been observed that the precipitated nanoparticles' characteristics, such as size and shape, depends on the type of salts, the ratio of Fe(II)/Fe(III), the reaction temperature, the pH and ionic strength of the media, stirring speed, and the addition rate of the basic solution [136-138]. In term of dispersibility challenge, the high surface area/volume results in aggregation of IONs to minimize the surface energy. The addition of anionic surfactants as dispersing agents leads to stabilizing nanoparticle suspension. Moreover, it has been reported that the presence of surfactants in the solution can control the size of precipitated nanoparticles [134]. Another challenge associated with naked IONs is oxidization of nanoparticles upon air exposure. Oxidization of nanoparticles not only leads to losing the magnetization force but also decreases the dispersibility. Practically, one potential strategy to address this drawback would be the provision of a proper surface coating. However, the surface functionalization may negatively change the magnetization force, and therefore the bacterial adsorption can be affected.

2.8 Performance of the bio self-healing concrete

Since the self-healing concrete is still a relatively new technology, various types of methods and materials have been developed. A different research group studied the performance of a bio-self-healing concrete containing various genera of bacteria and nutrients. Among all possible pathways for MICP, ureaolysis and metabolic conversion of calcium lactate to $CaCO_3$ are the most used approaches to design the bio self-healing concrete.

Wang et al. [139] studied the influence of MICP on the permeability of concrete by incorporation of immobilized *Bacillus sphaericus* cells. It was found that the permeability of specimen with polyurethane immobilized bacteria decreases by six times as compared to the specimens without bacteria. In another investigation the effectiveness of immobilized *Bacillus sphaericus* in diatomaceous earth on the water absorption was investigated. The results indicated that the water absorption in the specimen with immobilized bacteria was 50% of those specimen without bacteria [10]. Bang et al. [5] studied the effect of *Sporosarcina pasteurii* on compressive strength of mortar specimen at 7 and 28 days. It was found that the highest concentration of immobilized *Sporosarcina pasteurii* on porous glass beads can substantially increase the compressive strength of the mortar specimen by 24%. Moreover, compressive strength improved with the increase of cell concentration from 6.1×10^{7} cells/cm^{3} to 3.1×10^{9} cells/cm^{3}. Chahal et al. [140] examined the influence of *Sporosarcina pasteurii* on fly ash concrete properties. They tested the compressive strength, water absorption and chloride permeability of a fly ash bio-concrete. They found that the inclusion of bio-agent contributes to an increase in the compressive strength (22%), and a positive effect on the rapid chloride permeability and water absorption was noticed. Erşan et al. [141] reported the effect of immobilized ureulytic and denitrifying bacteria into protective materials on compressive strength of concrete. Their study indicated that the application of *Bacillus sphaericus* in concrete resulted in a decrease in compressive strength at 7 and 28 days by 63% and 60%, respectively. Although utilization of denitrifying bacterium (*Diaphorobacter nitroreducens*) caused the reduction in compressive strength for both 7 and 28 days, immobilization of *Diaphorobacter nitroreducens* in expanded clay and granular activated carbon marginally enhanced compressive strength.

Metabolic conversion of an organic compound (organic acid salt) is another potential approach to design a bio self-healing concrete [65, 66, 86, 142]. In this approach, aerobic oxidation of organic acids leads to the production of carbon dioxide which results in carbonate production in an alkaline environment. The presence of a calcium source as cation results in the production of $CaCO_3$. Metabolic conversion of calcium lactate to $CaCO_3$ in the presence of oxygen is shown in Eq. 2-28.

$$CaC_6H_{10}O_6 + 6O_2 \xrightarrow{Metabolic\ conversion} CaCO_3 + 5CO_2 + 5H_2O \quad (2\text{-}28)$$

To investigate the effectiveness of this pathway, Jonkers et al. [65] tested the influence of *Bacillus cohnii*, *Bacillus pseudofirmus* and some organic compounds, such as calcium lactate and calcium acetate, on the compressive strength of mortar. It was found that the presence of bacteria in the samples contributes to a decrease in the compressive strength, while calcium lactate showed the highest compressive strength among the organic compounds. Likewise, Wiktor and Jonkers developed a two-component self-healing system using calcium lactate and encapsulated *Bacillus alkalinitrilicus* into the expanded clay particles to ensure the viability and functionality of the bacteria in high pH [66]. Their experimental results showed that the bio-concrete can fill the crack (up to 0.46 mm width) when the specimen's submerged in water for 100 days.

A review of the possible biotechnological pathways to induced $CaCO_3$ reveals that despite its potential application for designing a self-healing concrete, the mechanism is not efficient enough to fill the entire cracks. As described above, the majority of investigations have focused on using different genera of bacteria to induce $CaCO_3$ precipitation and evaluating their effects on mechanical properties of the concrete. However, the role of the effective factors on biomineralization of $CaCO_3$, such as the type and concentration of bacteria and nutrients, as well as operating conditions and surrounding pH, have received little attention. Furthermore, the literature study demonstrates the direct incorporation of bacterial cells into the concrete matrix significantly results in a decline in the cell viability and crack healing efficiency.

Accordingly, this research was performed to gain an insight into the role of significant parameters on the biosynthesis of $CaCO_3$ and to design an efficient bio self-healing agent to address the current issues associated with the application of bio-concrete technology.

Chapter 3

Materials and methods

This chapter describes the experimental and analytical methods used in the research chapters of the thesis.

3.1 Materials

3.1.1 Chemicals

A wide range of chemicals were used for bacterial growth, and solid- and liquid-state fermentations: calcium chloride anhydrous, calcium lactate pentahydrate, calcium nitrate tetrahydrate, calcium acetate hydrate, yeast extract, urea, calcium peroxide, zinc peroxide, magnesium peroxide, urea-hydrogen peroxide, ammonium hydroxide, $FeCl_3.6H_2O$, $FeSO_4.7H_2O$, 3-aminopropyl triethoxysilane (APTES), glutaraldehyde solution (25%), sodium cacodylate were purchased from Sigma-Aldrich (USA). Bacto^{TM} Peptone was obtained from Becton Dickinson (USA). Glucose and glycerol were purchased from Merck Millipore (Germany) and Ajax Finechem Pty Ltd (New Zealand), respectively. Active silicone antifoam agent, sodium hydrogen carbonate and nutrient agar plates were purchased from Fort Richard Laboratories (Auckland, New Zealand). Sodium hydroxide, sodium chloride, and hydrochloric acid (36%) were purchased from a domestic supplier.

3.1.2 Culture preparation

3.1.2.1 Microorganism

Among many organisms inhabiting the soil, bacteria are the most abundant microorganism. The soil is the host of various bacteria ranges from ten million to one billion cells per gram. They differ in shape, and their sizes vary from 0.2 to 3 µm. In this study four bacterial strains which have potential to induce different precipitants were chosen. All of the isolates were selected from *Bacillus* species because of producing endospores, which help them to tolerate extreme environmental conditions, such as hotness, coldness and radiation exposure, for a long period of time. Their properties enable them to be used in a wide range of applications, such as agricultural, pharmaceutical, medical and many other industrial processes [143]. *Bacillus licheniformis* ATCC 9789, *Lysinibacillus*

sphaericus ATCC 4525, *Bacillus subtilis* ATCC 6633 and *Bacillus sphaericus* SBL 04/203 were purchased from NZ culture collection and are illustrated in Figure 3-1.

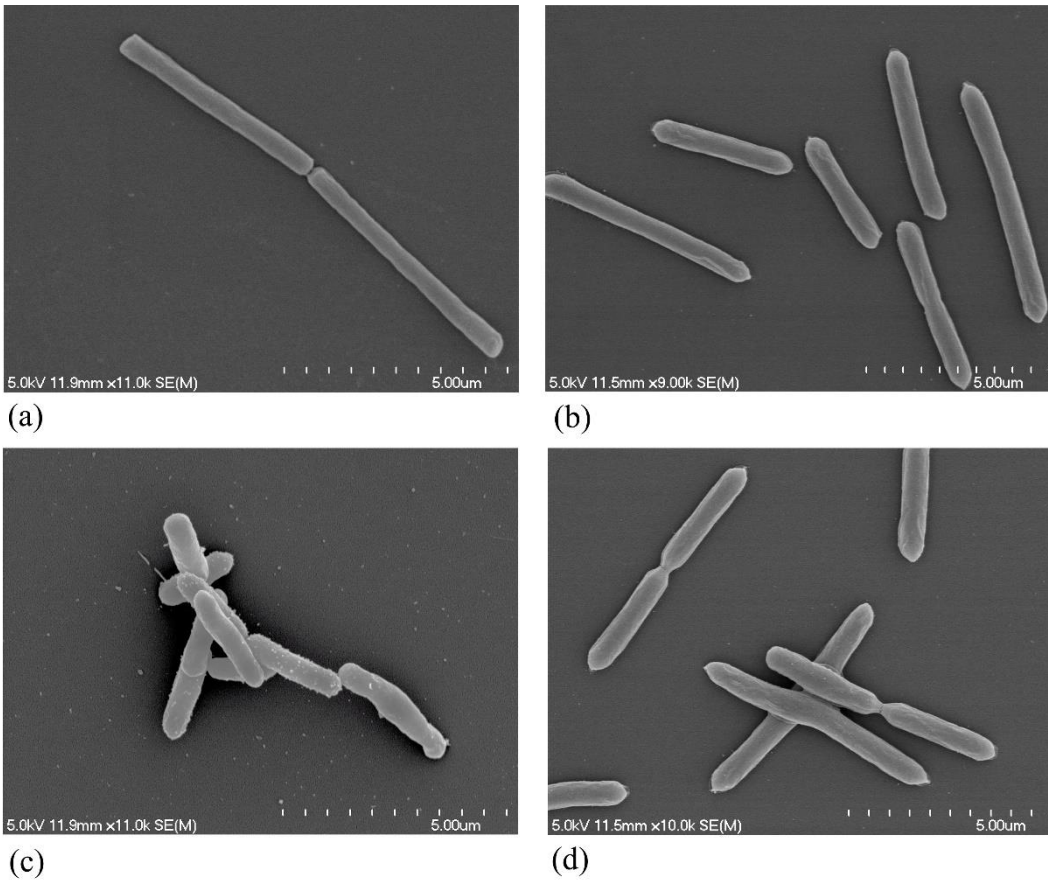

Figure 3-1 Bacterial strain morphology: a) *Bacillus licheniformis*, b) *Bacillus subtilis*, c) *Lysinibacillus sphaericus* and d) *Bacillus sphaericus.*

3.1.2.2 Microorganism revival and culture media

Bacteria are generally kept in two conditions: freeze-dried and frozen form. One of the best methods of preserving bacteria is freeze-drying due to the high stability of a dry powder and simple handling aspect. Therefore to cultivate and prepare a stock solution, the freeze-dried strains need to be revived. To rehydrate the bacteria, a cut was made in the middle of the vial containing bacterial pellet. Afterwards, 15 drops of optimum growth medium containing 0.5% (*w/v*) bacto™ peptone, 0.5% (*w/v*) glucose and 0.05% (*w/v*) yeast extract which was already sterilized by autoclaving (Tomy, SX 700, USA) at 121°C for 20 min, was added to each vial. As the

suspension mixed well, the bacteria were transferred to the 150 mL solution of growth medium. The cultures were incubated under shaking condition (120 rpm) at 37°C for two days.

Then, 500 µL of culture was transferred to the nutrient broth agar plates and spread across the whole surface. Agar plates were sealed with parafilm and incubated under the same condition for a couple of days. Bacterial growth was regularly monitored during incubation time. Consequently, the grown bacterial cells were scraped off from the plates and suspended in a sterilized saline solution (sodium chloride 0.9% *w/v*). To inactivate the vegetative cells and produce a pure suspension of spores, the bacteria suspension was mixed well and placed in a water bath (Clifton, UK) at 80°C for 10 min. The cell debris was then removed by centrifuging the solution at 1800 rpm for 10 min (Sigma laboratory centrifuge. 5-15, Germany). The obtained spore solutions were kept in a fridge for liquid and solid state fermentation experiments.

3.1.2.3 Stock solution preparation

Seed stock cultures can be used in the case of mutation, contamination or if loss of viability occurs. After the bacterial rehydration, two seed stock solutions for each strain were prepared from early growth cultures. For this purpose, 50 mL of fresh grown bacteria was centrifuged and the pellet was mixed with 10 mL autoclaved skim milk and 4 mL glycerol. The vials were sealed and put in a -18°C freezer for 20 min before storing in ultra-low temperature freezer (Arctiko DAI 1418, Denmark) at -80°C.

3.1.2.4 Colony counting and growth monitoring

The number of spores was counted by plate counting method. To make an accurate count of the spores, one milliliter aliquot of the medium was taken from the solution, appropriately diluted, then streaked on the nutrient plate, and incubated at 37°C for 24 h. The average was used for counting and the results were expressed as colony forming units per milliliter (CFU/mL). The growth rate of the bacteria was

calculated by measuring the absorbance at a wavelength of 600 nm (Shimadzu, UV-1700, Kyoto, Japan) during the fermentation process.

3.2 Experimental methods

3.2.1 Screening and optimization of bacterial strain, nutrients and operating conditions to enhance MICP process

In screening and optimization studies, two types of fermentation processes were performed. Solid state fermentation was used to determine the capability of the isolates to induce $CaCO_3$ precipitation. Screening of the effective parameters on biomineralization of $CaCO_3$ and also determination of the optimum levels of significant factors to maximize the $CaCO_3$ were carried out through liquid fermentation. Preparation of these two fermentation processes is described in the following sections.

3.2.1.1 Screening study at solid state fermentation (B4 medium)

To assess the possibility of producing $CaCO_3$ by bacterial strains, solid state fermentation was carried out using a standard B4 medium [144]. Briefly, 2.5 g calcium acetate, 4 g yeast extract and 10 g glucose were dissolved in 1L distilled water. To solidify, 15 g agar (Becton Dickinson, USA) was added to the medium and pH was adjusted to 8.0 using NaOH solution. The concentrated solution was sterilized by autoclaving for 20 min at 121°C, and as the temperature dropped to 50°C, the medium was poured into the Petri dishes. The dishes were kept inside laminar flow to reach ambient temperature and then the lids were put back on dishes to avoid any unintended contamination.

Fifty µL of each isolate was spread on the B4 plates and sealed with parafilm to avoid water evaporation and, subsequently, they incubated in a stationary condition at 37°C for two weeks. Autoclaved cell cultures were used as the control sets. Furthermore, a set of B4 medium without calcium acetate was prepared to observe the effect of organic calcium salts on bacterial growth. After precipitation, individual colonies were taken at different intervals to observe the formation of

crystals. The crystals were scraped off from the plate surface and washed repeatedly with distilled water to remove adhering medium and agar. Crystal aggregates were dried overnight at 70°C and then kept in a desiccator for further consideration.

3.2.1.2 Screening the significant variables on $CaCO_3$ precipitation

Liquid media were used to screen the significant parameters affecting biomineralization of $CaCO_3$. A single factor experimental design was used to screen the significant variables affecting the biomineralization process. A total of 13 variables were selected for screening the most significant factors on $CaCO_3$ biomineralization as follows: (1) *B. licheniformis* ATCC 9789, (2) *L. sphaericus* ATCC 4525, (3) *B. subtilis* ATCC 6633, (4) *B. sphaericus* NZRM 4381, (5) urea, (6) calcium chloride, (7) calcium lactate, (8) calcium nitrate, (9) calcium acetate, (10) yeast extract, (11) incubation period, (12) temperature and (13) agitation speed. The statistical importance of each factor was obtained at 0.1 probability level according to the analysis of variance (ANOVA) test and also R^2 was used to evaluate the goodness of fitted model.

All nutrients, including calcium sources and yeast extract besides urea, were separately dissolved in distilled water to prevent premature formation of $CaCO_3$ and then sterilized by autoclaving at 121°C for 20 min. Due to the fact that the heat may change the properties of urea, the solution was sterilized by passing through 0.2 µm membrane filter paper (Millipore, Ireland). Experimental samples were prepared in 200 mL Erlenmeyer flasks according to the chemical compositions noted in screening and optimization experimental design. Media were inoculated with different concentrations of isolates and incubated under various temperature, incubation time and agitation speed after fitting a sufficient amount of cotton wool plug on top of each flask. Figure 3-2 shows the prepared media for optimization purposes during liquid state fermentation. Sterility of pipettes, pipette tips, glass Petri dishes, shake flasks, fume hood, inoculation loops, culture media, and chemicals was ensured during chemical preparation and experiment.

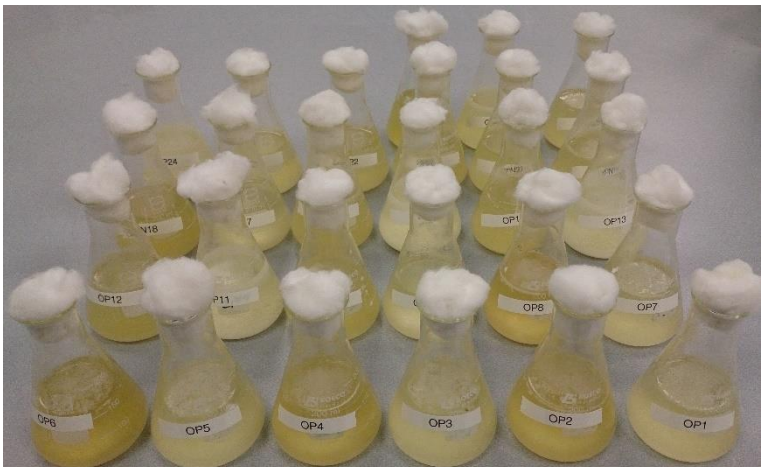

Figure 3-2 Media preparation for liquid state fermentation process.

3.2.1.3 Optimization of microbial $CaCO_3$ precipitation

In order to optimize the microbial $CaCO_3$ precipitation, the optimum levels of significant factors were determined using response surface methodology (RSM) with a central composite face-centered (CCF) design matrix. A total of 27 experiments runs with three replications at the central point were conducted to determine the optimum levels of the significant variables at three different normalized levels of -1, 0 and 1. In order to predict the production of $CaCO_3$, the second-order polynomial regression model was used to fit the experimental data according to the following equation:

$$Y = \beta_0 + \sum \beta_i X_i + \sum \beta_{ij} X_i X_j + \sum \beta_{ii} X_i^2 \quad (3\text{-}1)$$

where Y is $CaCO_3$ concentration (response), β_0 is the constant coefficient, β_i, β_{ii}, and β_{ij} are the coefficients of the linear, quadratic and synergic effects, respectively, and X_i and X_j are the coded values of variables.

3.2.2 Calcium carbonate extraction and measurement

To extract the precipitated $CaCO_3$, different types of techniques, including oven drying, freeze drying and filtration, were used. In the first technique, the liquid fermented medium was poured into an aluminum tray and dried at 50°C for 48 h

(Figure 3-3a). The remaining powder was collected from the tray and well grinded using a mortar and pestle. Due to the presence of salts in the obtained bioproduct, they quickly attract the surrounding moisture to saturate the surface liquid and become hygroscopic. The powder obtained using oven drying could not be used for evaluation of crystals, and therefore freeze drying was altered. In this process removal of the solvent from the frozen medium is done by a sublimation process. To preserve the structure of crystals, rapid cooling was applied. Liquid medium was poured into containers and frozen in a -80°C freezer for 8 hr. A piece of filter paper was put on top of the containers and they were placed in a freeze dryer equipped with a vacuum control system to regulate the pressure (Labconco 2.5 Liter, the US). After 48 h, the obtained powder was kept in a desiccator. The freeze dried powder had the same properties of oven dried powder and tend to become damp quickly during the examination.

To overcome this obstacle, vacuum filtration as an alternative approach was used. The fermented liquid culture was well mixed with a magnetic stirrer for 3 min. As shown in Figure 3-3b, the medium was subsequently vacuum filtered through 0.2 µm membrane filter paper (Advantec mixed cellulose ester, Japan), washed with plenty of distilled water and oven dried overnight at 70°C. The final pH and absorbance of each medium were just measured prior to filtration by standard pH Meter (Cyberscan 100, Eutech Instruments) and spectrophotometer (Shimadzu, UV-1700, Kyoto, Japan) at 600 nm, respectively.

(a) (b)

Figure 3-3 $CaCO_3$ extraction using: a) oven drying and b) filtration.

3.2.3 Cell fixation method

There are different types of bacterial fixation approaches using formaldehyde (FA), glutaraldehyde (GA), osmium tetroxide (OsO_4) and uranyl acetate (UrAc). In this study fixation using glutaraldehyde was performed for observing the morphology of bacterial cells. In order to fixate the bacteria, the suspension cells were washed twice with phosphate-buffered saline solution. All fixations were conducted at room temperature. A drop of the bacterium was placed on the microscope slide, and a circular motion was performed to achieve a thin smear on the glass slide. The heat fixation step was conducted by passing the bacterial smear through the flame of a Bunsen burner. Subsequently, the cells were fixed in 2.5% glutaraldehyde in the 0.1 M sodium of cacodylate buffer for 45 min. The slides were washed with the normal saline solution for 15 min and dehydration step was performed by placing the slide in a graded series of ethanol (30, 50, 70, 80, 90 and 95%) for 10 min. The glass slide was then kept in absolute ethanol for 20 min. Air drying of the bacterial cells can cause severe deformation and damage in the surface structure. Therefore, to preserve the cell surface structure, a critical point drying (Polaron) was performed. All fixation methods were performed in duplicates.

3.2.4 Morphological observation and crystal characterization

To observe and characterize the precipitated crystals during this study, the following methods were used.

3.2.4.1 Optical microscope

The formation of $CaCO_3$ crystals due to the heterotrophic growth of bacteria on the B4 medium was periodically observed using a BX51 polarized microscope (Olympus, USA). In this sense, the precipitates were separated from the media, washed with distilled water to remove impurities, oven dried, and placed onto a glass slide.

3.2.4.2 Morphological observation

The high-resolution images taken by scanning electron microscope (SEM) can provide topographical, morphological and compositional information. SEM analysis was performed by using Hitachi S-4700 (Japan) to observe the shape and the size of precipitated particles. Moreover, the bacterial morphology and surface structure of the concrete samples were analyzed by SEM.

In addition to morphological observation, analysis of quantitative elemental composition was performed by energy dispersive X-ray spectroscopy (EDS) which was equipped with SEM instrument. Prior to mounting the samples into the SEM chamber, the powder was finely ground and placed on a sticky carbon tape attached to aluminum stub. To prevent image disturbance caused by charge, specimens were covered with a thin layer of platinum using a sputter coater (Hitachi, E1030). Stub was attached to the sample holder and, subsequently, the height was adjusted according to the standard gauge. The specimen was mounted into the main chamber and high vacuum condition was applied. Morphological observation and elemental composition study were conducted at 5 and 15 KeV, respectively.

3.2.4.3 Crystal characterization

X-ray diffraction (XRD) was used as a non-destructive analytical technique to identify and quantify the morphology of precipitated $CaCO_3$. The mineralogy study on precipitates was performed at room temperature by a Panalytical Empyrean diffractometer (The Netherland), equipped with a 5 mm beam mask using the CuKα radiation. X-rays are emitted from high accelerating voltage generator and converted into voltage pulses in the detector. The well-ground powder was back-packed into a sample holder and positioned on a sample batch changer. The exploration range (2θ) was adjusted from 15° to 75° and data were collected for the step size, the voltage, and the current of 0.0530°, 45 kV, and 40 mA, respectively. The experimental results were then evaluated by Highscore plus V.4.0 software (PANalytical, The Netherland).

3.2.5 Morphological quantification approach

Physical properties of bacterially induced $CaCO_3$ precipitation strongly relies on the portion of each polymorph. To quantify the percentage of these polymorphs, the XRD internal standard method using three sets of calibration curves was used. A schematic diagram of preparing calibration curves to quantify $CaCO_3$ polymorphs is presented in Figure 3-4. Pure calcite was purchased from Sigma-Aldrich (USA) and the pure vaterite and aragonite were synthesized as it noted in following part.

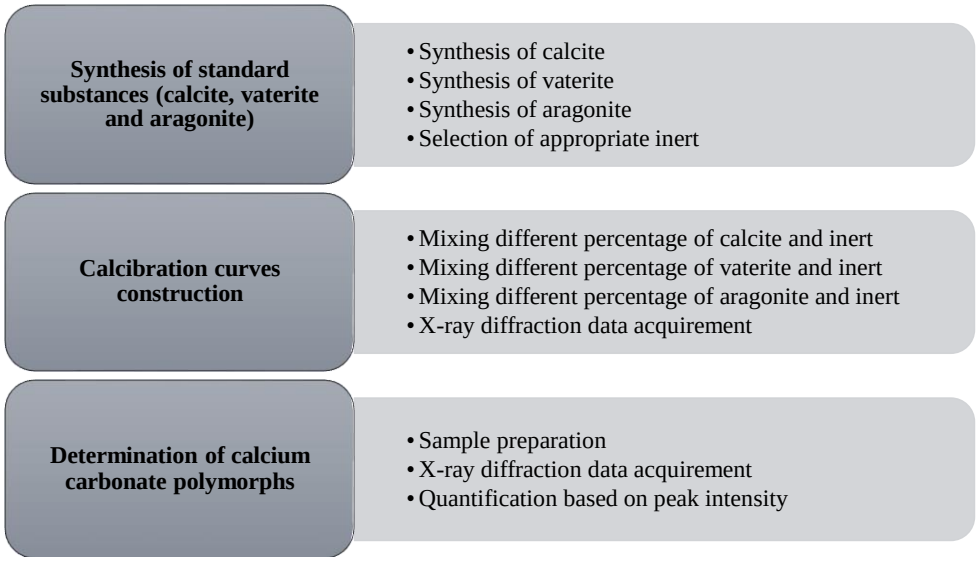

Figure 3-4 Schematic procedure showing the quantification of $CaCO_3$ polymorphs [145].

3.2.5.1 Aragonite synthesis

Aragonite synthesis can be performed via carbonation technique. CO_2 bubbling is the most industrial promising technique to produce $CaCO_3$ (calcite) from lime stone due to being a simple and cost effective method. However, the presence of appropriate salts using carbonation under specific operational conditions (sonication) increases the possibility of producing aragonite. Various combination of chemicals in different reactive conditions were considered to minimize the impurity of the precipitated powder.

Pure aragonite was synthesized according to the method presented by Zhou et al. [146]. Aragonite was prepared by CO_2 bubbling inside the solution of calcium

chloride dehydrate (Merckmillipore, Germany) and sodium hydrogen carbonate (Scientific Supplies Ltd, New Zealand). The schematic flow chart process of aragonite synthesis is shown in Figure 3-5. 250 mL of distilled water was heated by a water bath to 70°C and 0.01 M calcium chloride dehydrate and 0.02 M sodium hydrogen bicarbonate were dissolved into distilled water. Afterwards, CO_2 was bubbled at the rate of 2.5 cm^3/L for 10 min. The solution sonicated (Qsonica-Q800R, USA) in an ultrasonic amplitude of 75% (500 W) for 31 min (5 sec irradiation and 5 sec off). A 13 mm horn tip was inserted 2 cm from the top surface of the solution and the waves transmitted at a constant frequency of 24 kHz. After precipitation, the solution was filtered through 0.4 µm mixed cellulose membrane filter (MicroAnalytix Pty Ltd, Japan). The powder was rinsed three times with distilled water and finally washed with acetone. The filter was placed in an oven at 70°C for 24 h. To prevent morphological changes the powder was preserved in a container and kept in a desiccator for SEM observation and XRD analysis. This process was repeated 15 times to obtain enough aragonite for construction of calibration curve.

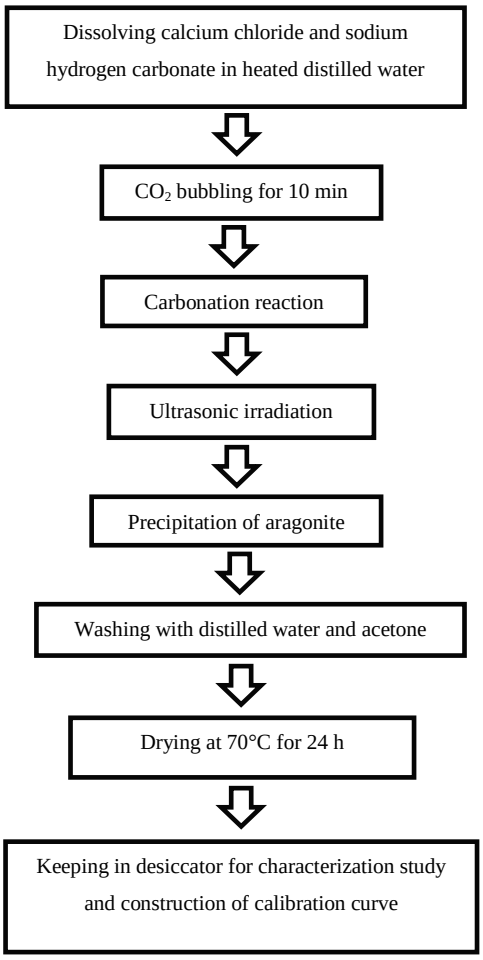

Figure 3-5 The schematic flow chart procedure for aragonite synthesis.

3.2.5.2 Vaterite synthesis

Pure vaterite particles were successfully synthesized by a combination of two salt solutions according to the approach presented by Mori et al. [147]. A solution of calcium chloride (1 M) quickly was poured in 1 M solution of potassium carbonate and an ultrasonic homogenizer (19.5 kHz, 300 W) was used to mix them homogeneously. Centrifugation (at 1600 rpm for 6 min) was employed to extract the vaterite particles which precipitated during 3 min ultrasonic irradiation. Three steps of washing were done to obtain a fine particle. In the first stage, the pellet was kept and mixed with distilled water. Centrifugation was repeated and the supernatant was removed. The next two washing steps were performed with absolute ethanol and acetone. The powder was removed from the centrifugal tubes, dried on the oven at 70°C for 12 h and kept in the desiccator for performing SEM

and XRD. The SEM images of prepared pure calcite, aragonite and vaterite particles are shown in Figure 3-6.

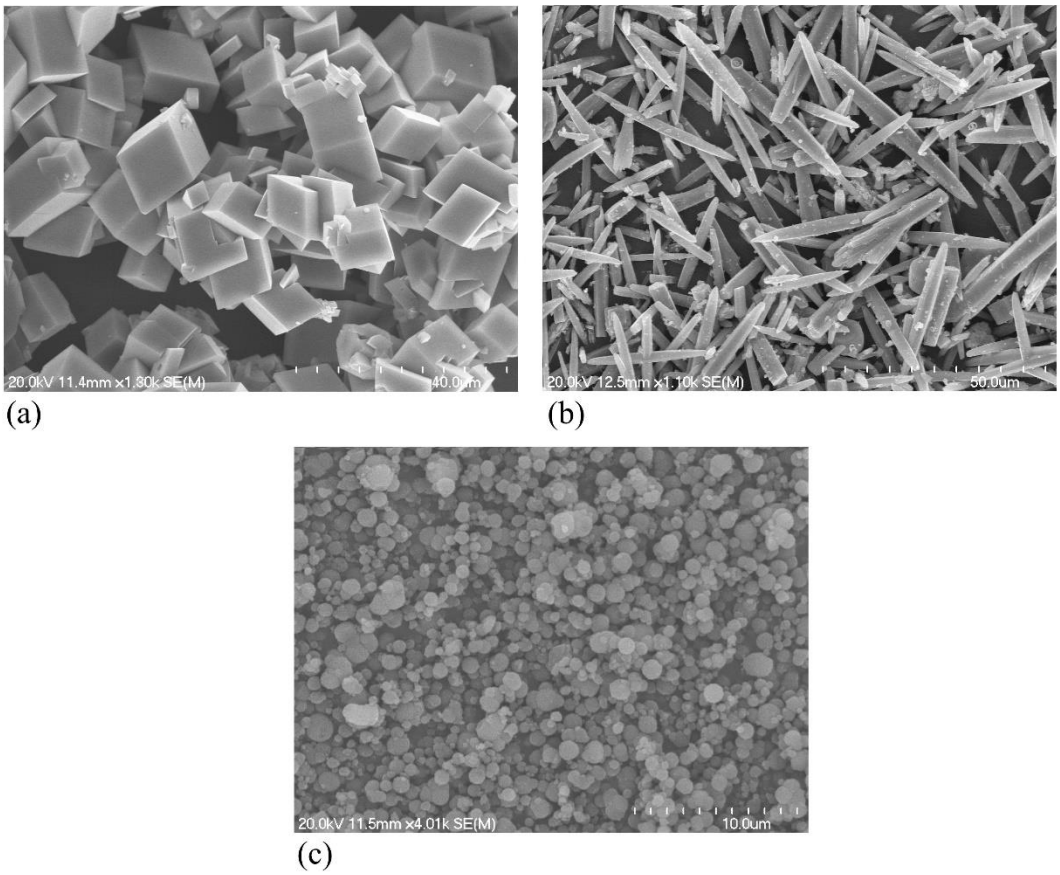

Figure 3-6 SEM micrographs of pure calcite, vaterite and aragonite [2].

3.2.5.3 Quantification approach

The crystal size, peak position and stability are the significant factors to determine a standard inert. Aluminum oxide (Sigma-Aldrich, USA) was selected as a standard inert due to having a uniform crystallite size and, more importantly, it does not have overlap with the $CaCO_3$ polymorphs peaks. Different percentages of pure calcite, aragonite and vaterite were mixed with a standard inert (0%, 20%, 40%, 60%, 80% and 100% *w/w*) and the powders were mixed by a vortex mixer for 30 min to obtain a homogenous mixture. The calibration curves were constructed with the average peak intensity of polymorphs. Figure 3-7a, b and c depict a 3D X-ray calibration curves of calcite, vaterite and aragonite, respectively. The maximum peak intensity of calcite (29.36°), vaterite (27.11°) and aragonite (26.26°) decreases with the

increase in inert portion. The quantitative determination of the polymorphs was determined via comparison of peaks mixture (homogeneous and well-grinded) with the calibration functions.

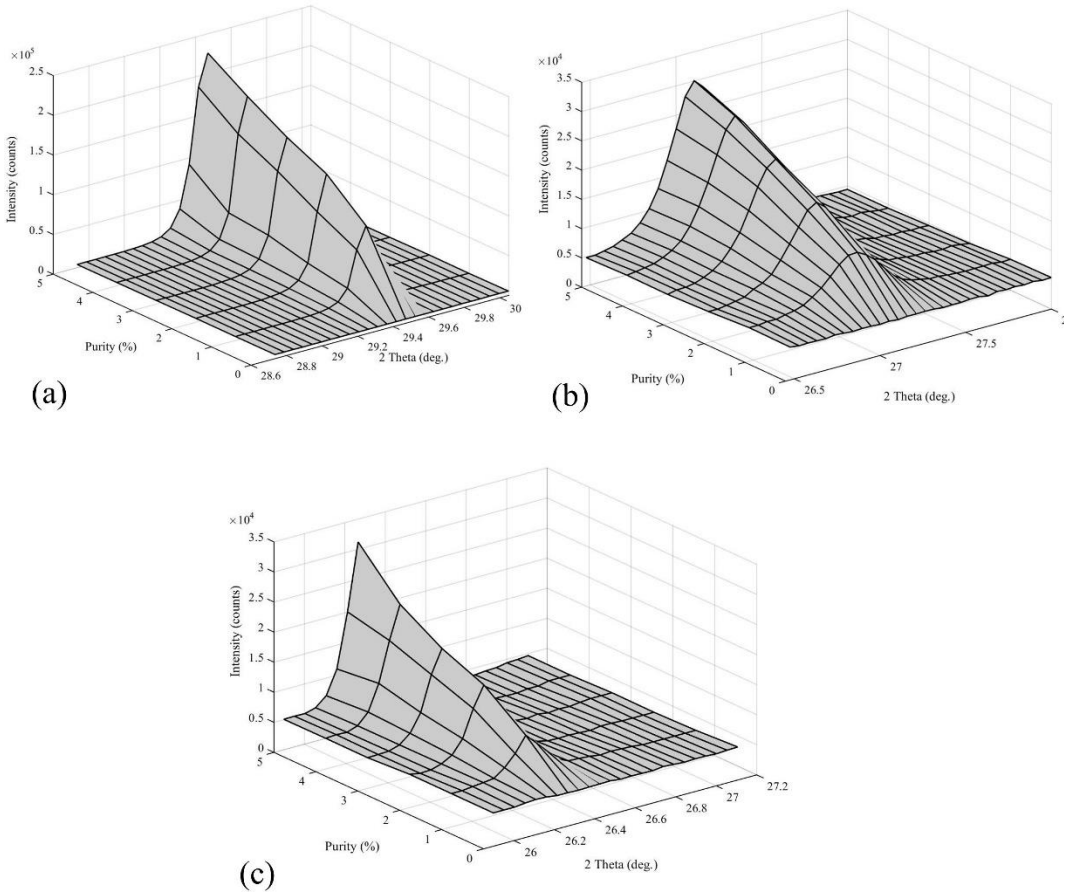

Figure 3-7 3D calibration curves of $CaCO_3$ polymorph: a) Calcite, b) Vaterite and C) Aragonite.

3.2.6 Bioreactor set up

A 3-L laboratory-scale fermentor (BioFlo/CelliGen 115, New Brunswick Scientific Co., MA, USA) was employed to simulate the concrete environment. AFS Biocommand (New Brunswick Scientific) was used for controlling the bioprocess and data acquisition. The bioreactor was equipped with a top-driven stirrer, and two six-blade Rushton impellers were placed on the agitation drive shaft (i.e., diameter 52 mm, width 16 mm, length 18 mm). To ensure gas bubble dispersion and provide a high rate of oxygen transfer, four stainless steel internal baffles (i.e., width 13 mm,

length 140 mm) were positioned inside the vessel. The maximum adjustable levels of stirrer and aeration rate were 1200 rpm and 5 standard liters per minute (SLPM), respectively.

A standard two-point calibration method (pH 7 and 12 buffer standards) was performed to calibrate the pH electrode. The pH of the medium was kept constant with a measurement error of 0.01 by automatic addition of base (2M NaOH) or acid (2M HCl). Dissolved oxygen (DO) was measured by DO probe, which was already calibrated using a standard two-point calibration method (0% and 100%). The 0% calibration was conducted by introducing nitrogen into the fermentor at a rate of 1 SLPM until the reading stabilized. The span calibration (100% air saturated condition) was achieved by the provision of 50 rpm agitation speed and vigorous sparge air into the bioreactor for 30 min. The DO values were recorded according to these calibration set points. The foam level was controlled during batch fermentation by addition of silicon-based defoamer agent into the vessel. To detect the formation of foam, a level probe, which is sensitive to wetness, was used. The diluted sterilized antifoam was pumped upon the formation of foam (wet contact) to alleviate the biofilm formation.

The external sparger tube attached to the controller was sterilized with the circulation of sodium hypochlorite solution at 1% for 1 h. The tube was subsequently rinsed with sterilized distilled water to eliminate the chlorine residues. Airflow was then introduced into the vessel through a 6 mm ring sparger and dispersed 10 mm below the impeller. To avoid batch spoilage and environmental contamination, filter-sterilized air (0.2 µm) was sparged into the bottom of the vessel.

3.2.7 Design of the batch experiments

The fermentation medium was prepared as previously described (Chapter 4). The bioreactor was sterilized using an autoclave at 121°C for 20 min, cooled and then inoculated according to the optimum condition (4.5% *v/v* of each isolate). During the fermentations, samples were taken from the fermentor at intervals to determine the concentration of soluble calcium and bacterial growth rate. The bioreactor was

thoroughly cleaned to avoid the clogging of the sparger and attachment of bioproduct to the pH, DO and foam probes at the end of each experiment.

In the first stage of the investigation in fermentor, the batch fermentations were carried out at various aeration rates and a constant mixing speed of 150 rpm at 35°C to determine the effect of aeration on the bacterial production of $CaCO_3$. It has been shown that the availability of a high level of CO_2 inhibits the bacterial metabolic activity and subsequently it leads to a decrease in the yields. Therefore, to minimize the inhibitory effects, and also increase the availability of oxygen in the media, the maximum aeration rate was set to 4.5 SLPM. The increase in airflow rate resulted in a massive foam formation during experiment runs. Hence a sterilized solution of antifoam agent was pumped into the vessel to alleviate the foam formation and provide a better oxygen transfer in the system. In the second stage, the batch fermentations were performed at different levels of pH with a constant air flow rate of 0.5 SLPM to explore the influence of alkalinity on the bacterial growth and $CaCO_3$ precipitation. The pH tended to decrease over experimental runs, and it was stabilized by the addition of base to the bioreactor.

3.2.8 Screening of significant ORCs affecting MICP process

Different concentrations of ORCs were placed in sterile watch glasses and sterilization was performed under a fume hood using ultraviolet light irradiation (UV) for an hour. The fermentations were carried out in 200-mL Erlenmeyer flasks containing the autoclaved optimum medium. To screen the effect of ORCs on bacterial precipitation of $CaCO_3$, a different concentration of ORCs were added to the fermentation medium. The media were then inoculated with bacterial strains and the anaerobic fermentation was performed accordingly.

3.2.9 Optimization of significant ORCs for MICP process

In order to enhance the microbial $CaCO_3$ precipitation, the optimum concentrations of significant ORCs from the screening stage were determined using the RSM with the CCF design matrix. MODDE package software was used for the experimental

design, statistical analysis of the data and building of the quadratic model. The data obtained from RSM were then fitted via the response surface regression procedure, using the second order polynomial equation described previously in Eq. 3-1.

3.2.10 Synthesis of naked magnetic iron oxide nanoparticles (IONs)

In this study a co-precipitation approach was used to synthesize high-quality magnetic IONs with an average particle size of 11 nm. As schematically shown in Figure 3-8, this technique consists of mixing ferric and ferrous ions with ammonium hydroxide under an inert atmosphere. Briefly, 0.74 g $FeSO_4.7H_2O$ and 1.17 g $FeCl_3.6H_2O$ with the molar ratio of 1:1.75 were dissolved in 50 mL distilled water. The solution was stirred at a temperature of 70°C and purged with N_2 to prevent oxidation of ferrous ions for 60 min. Afterwards, 5 mL ammonium hydroxide solution (32%) was quickly added to the reaction solution and the mixture maintained for another 60 min. Magnetic nanoparticle powders were precipitated due to the following reaction (Eq. 3-2):

$$Fe\ (\mathrm{II}) + 2Fe(\mathrm{III}) + 8OH \rightarrow Fe_3O_4 \downarrow + 4H_2O \qquad (3\text{-}2)$$

A permanent magnet was used to separate the magnetic particles from the non-magnetic particles, and then the black precipitates were washed with hot distilled water several times to remove impurities. The prepared IONs powder was achieved by drying overnight at 50°C and kept in the fridge under N_2 atmosphere until immobilization.

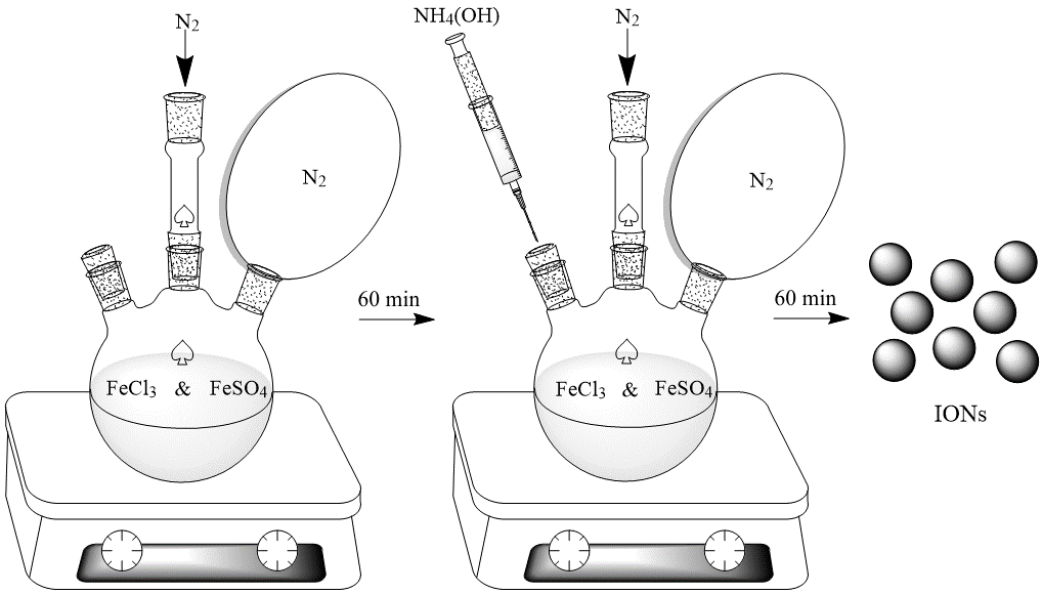

Figure 3-8 Schematic illustration of the steps involved in the synthesis of IONs using co-precipitation method.

3.2.11 Synthesis of 3-aminopropyl-triethoxysilane (APTES) coated IONs

In this study APTES-coated IONs were synthesized using a chemically modified procedure as illustrated in Figure 3-9. 0.7 g of naked IONs were dispersed into a mixture of 25 mL distilled water and absolute ethanol (ratio 1:1) by ultrasonic vibration (Qsonica- Q800R, USA) for 2 min. Then, 2.8 mL of APTES solution was added to the mixture under nitrogen atmosphere and the reaction was maintained with vigorous stirring at 40°C. After 2 h, the APTES coated precipitate was magnetically collected, washed with absolute ethanol and doubled-distilled water and, consequently, oven dried for 24 h at 50°C. The same as naked IONs, APTES-coated IONs were preserved under N_2 atmosphere until the characterization and the immobilization processes were performed.

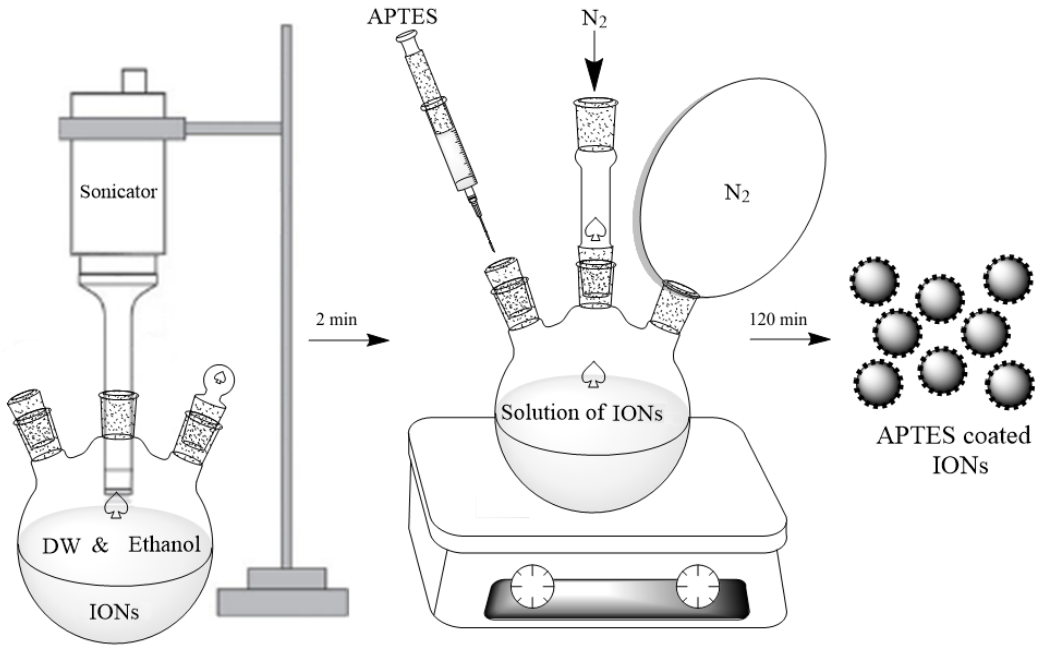

Figure 3-9 Schematic representation for APTES functionalization of naked IONs.

3.2.12 Nanoparticle characterization

Different analytical techniques were performed to characterize the synthesized nanoparticles. Transmission electron microscopy (TEM, Philips, CM10; HT 100 kV) and SEM were used to observe the morphology and size of the prepared nanoparticles. Fourier transform infrared (FTIR, PerkinElmer 100 spectrum) and XRD analysis were carried out to verify the fabrication of magnetic nanoparticles.

3.2.13 Immobilization of bacterial cells with IONs

Various concentrations of magnetic IONs were mixed with sterilized distilled water and sonicated at 500 W for 1 min. To attach the IONs to the cell surface, the bacteria were transferred to the mixture of either naked or APTES-coated IONs and then incubated in a shaker incubator at 180 rpm (35°C). Figure 3-10 illustrates the schematic decoration of bacterial cells with naked and APTES-coated IONs. After immobilization the mixture was transferred to the fermentation media for evaluating $CaCO_3$ precipitation biosynthesis. In case of bio self-healing concrete evaluation, the immobilized cells were directly added to the concrete ingredients and the mixture was mixed accordingly.

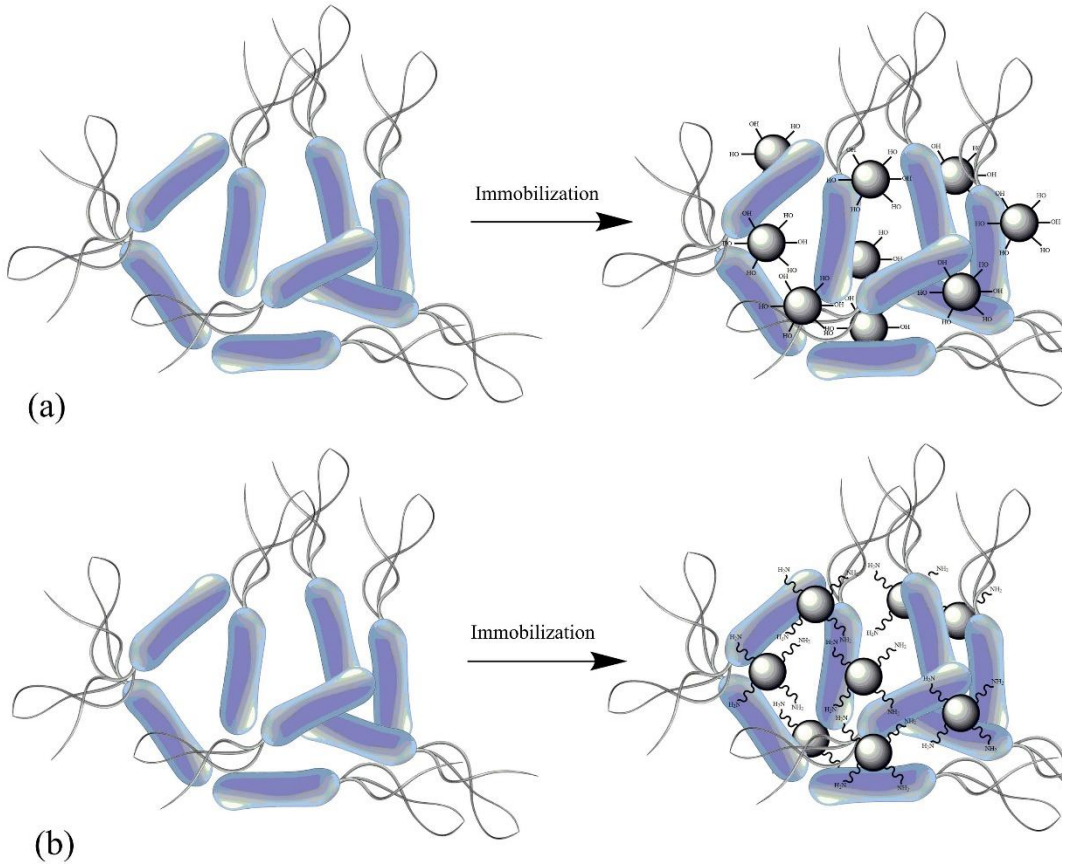

Figure 3-10 Bacterial cell decoration using: a) naked IONs and b) APTES-coated IONs.

3.3 Evaluation of bio self-healing concrete

3.3.1 Concrete mixture design and casting procedure

A series of concrete samples were prepared using ordinary Portland cement, coarse and fine aggregates and tap water. The mix proportions of the control concrete specimens are given in Table 3-1. The same ratio of sand-to-aggregate (S/A) was used for the control and bio-based specimens. Molds of different sizes and shapes were used to evaluate the performance of the designed bio-concrete in terms of compression capacity, water absorption, drying shrinkage, and crack sealing. The cylindrical molds with the dimension of 100 × 200 mm (ASTM C39 [148]) and 25 × 25 mm were used for compression test and crack sealing evaluation, respectively. The prism beam molds with the dimension of 75 × 75 × 285 mm (ASTM C157 [149]) were used for drying shrinkage test. A disc mold with dimensions of 100 × 50 mm was used for the water absorption test.

Table 3-1 Concrete mix proportions.

Material	Proportions (%)
Ordinary Portland cement	16
Sand	4
Aggregate	40
W/C	0.6

3.3.2 Compressive strength test

Figure 3-11 shows the schematic mold used for the compressive test. The molds were lightly coated with nonreactive release material and three equal layers of well-mixed concrete were poured into each mold. Concrete was consolidated with the rounded end of the tamping rod (16 × 600 mm) using 25 strokes. The rodding process was distributed uniformly over the cross section of the specimen, and for each layer, the rod passed through 25 mm of the layer being consolidated. The outside of the molds were tapped with a mallet to close the space left by rodding after consolidation of layers. When the consolidation was done, the surface of the concrete was struck off and flattened with the tamping rod and trowel, respectively. Wet burlap was used for covering the molds to prevent the evaporation of water over the curing period. The concrete specimens were removed from the molds 24 h after casting. The samples were stored in a vibration-free moist condition in accordance with the requirements of specification ASTM C511 [150] until the test was performed.

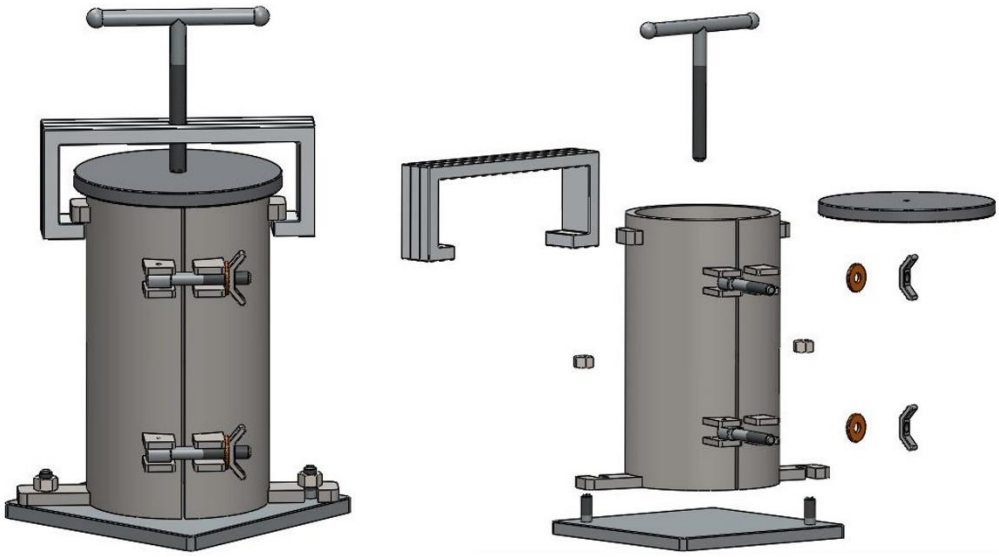

Figure 3-11 Cylindrical compressive strength mold: a) fully assembled view drawing and b) exploded view drawing.

The compression test was performed at ages 3, 7 and 28 days, and three replication specimens were prepared for each test age. The specimen's ends were capped conforming to ASTM C617 [151] before conducting the compression test. In the beginning, gypsum and water were weighed according to the recommended ratio and then a violent mixing was performed until no visible gypsum aggregation was in the mixture. To remove the gypsum from the contact plate, mineral oil was brushed on the plate contact and then a thin layer of gypsum plaster was poured on the top of the specimen. As depicted in Figure 3-12a, the specimen was positioned in the sample holder, gently pressed and kept perpendicular for an hour. A slight twisting motion was applied to remove the specimen from the contact plate (Figure 3-12b).

(a) (b)

Figure 3-12 Capping cylindrical concrete specimen procedure: a) support plate to keep the specimen perpendicular on contact plate and b) specimens after capping.

The compressive strength test for moist-cured specimens was carried out by a Contest compression machine (Bracknell, England) according to ASTM C39. As can be seen from Figure 3-13, the specimen was placed on the lower bearing block with its hardened face up. The load indicators were set to zero and rate of moving was adjusted to 1 mm/min. The loading was kept constant until the sample fails, and the maximum load carried by the sample was recorded as the failure load. All compressive strength values are presented as mean value ± standard error (SE).

Figure 3-13 Cylinder compression test machine configuration.

To prepare the bio-based concrete, the nutritional compounds were dissolved in required water. The solution was then inoculated with immobilized bacteria and the mixture was stirred for two min. The solution was then gradually added to the concrete ingredients and the concrete was mixed homogenously. To carry out the compressive strength, water absorption, drying shrinkage and crack sealing evaluation tests, the bio-based specimens were prepared in a similar way where the control samples were casted, cured, capped and tested.

3.3.3 Water absorption test

Capillary water absorption is a phenomenon where fluids move in porous materials. In this study water absorption rate assessment was performed using the method described by ASTM C1585 [152]. According to the specification, the rate of water absorption is expressed by determining the increase in the mass of the sample caused by penetration of water as a function of time. It is worth noting that in this approach, only one surface of the concrete discs is exposed to water. After demolding the specimens at 24 h, the samples were cured in water for 9 days at 35°C to activate the bacteria and initiate $CaCO_3$ precipitation. Thereafter, they were placed in an oven at a temperature of 50 ± 2°C, controlled relative humidity of 80 ± 3% for 3 days. After the drying process, the specimens were stored in a sealable container allowing free flow of air around the samples at 23°C for 15 days. Then the side of the samples was sealed using water proofed tape. A plastic sheet was loosely attached on top of the specimen to seal the top surface of the specimens and avoid water evaporation. The mass of sealed specimens was recorded as the initial mass. As can be seen from Figure 3-14, the sample was positioned on top of the support which was already placed in the container. Tap water was then poured in a container to reach 1-3 mm above the provided support rods and the water level was kept constant for the duration of the test. The mass of the specimen was recorded at the following intervals: 1, 5, 10, 20, 30, and 60 min. The measurement was continued every hour up to 6 h from the initial placing of the specimens on top of the support bars (exposure to water). After initial measurements the mass of sample was recorded every day up to 9 days from initial measurement. The water absorption rate is expressed as follows

$$\boldsymbol{I = \frac{m_t}{A \times D}} \quad (3\text{-}3)$$

where I is the absorption rate (mm), and m_t represents the change in specimen mass in grams at the time t. The terms of A and D are the exposed area of the specimen and the density of the water in g/mm^3, respectively.

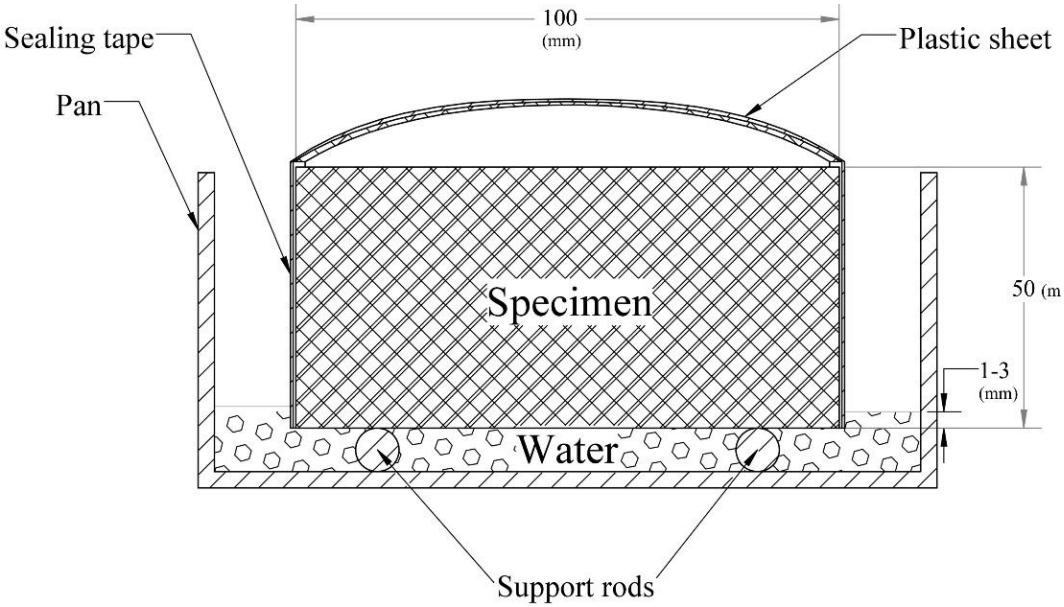

Figure 3-14 Schematic of the water absorption testing procedure.

3.3.4 Drying shrinkage test

The drying shrinkage test was performed in general accordance with ASTM C157 [149]. As is shown in Figure 3-15, prismatic beam molds were used for the drying shrinkage test. The gage studs were placed and adjusted in the center of the end plates and the molds were secured by screwing four bolts on holding plates. The molds were then prepared with an even coat of releasing oil prior to casting the concrete mixture in two equal layers. Each layer was consolidated by rodding and the concrete was entirely placed around each gage stud.

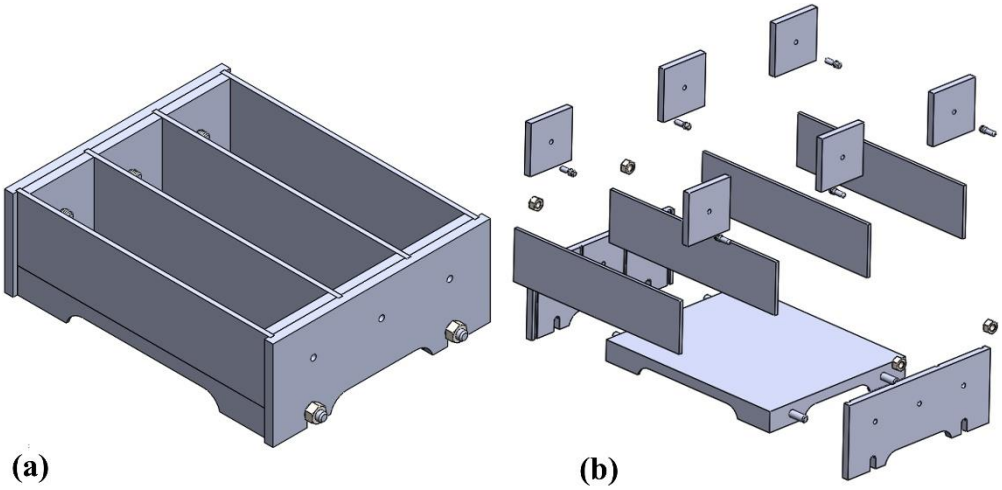

Figure 3-15 Three gang drying shrinkage beam mold: a) fully assembled view drawing and b) exploded view drawing.

The specimens were removed from the molds at age of 24 h and they were immediately placed in a lime-saturated solution for 30 min at 23°C. After removing the samples from the curing tank, initial length measurement was conducted using a length comparator (Alpa, Italy) in accordance with ASTM C490 [153]. As illustrated in Figure 3-16, the comparator apparatus was zero using a reference rod and the concrete specimen length was recorded. After initial length reading, the specimens were stored in the lime-saturated solution for 28 days at 23°C. The second reading was performed at the end of curing period in the same manner described above. The specimens were then removed from the lime-saturated water and left to undergo drying shrinkage in a drying room. The comparator readings of the drying shrinkage specimens were taken after curing of 4,7,14, 28 days, and after 8, 16, 32, and 64 weeks. The following equation was used to determine the drying shrinkage strain at a particular time

$$L = \frac{L_t - L_0}{L_g} \quad (3\text{-}4)$$

where L is the change in length at time t, and L_t and L_0 represent the comparator readings of the specimen at age t and initial time minus reference rod length at corresponding ages, respectively. L_g is nominal gage length in mm.

(a) (b)

Figure 3-16 Apparatus for measurement of length changes: a) without reference rod and b) set zero with reference rod.

3.3.5 Creation of crack in concrete samples

A realistic crack was created to investigate the effect of the designed bio-based agent on the concrete crack sealing. Since it is not possible to control the initial crack width over loading process, six cylindrical samples were cast in two different sizes. After casting, the molds were placed in moist conditions at 23°C for 24 h. The specimens were then demolded and the cured samples were obtained by storing the samples in moist conditions for 72 h. The realistic cracks were prepared by performing a simulated splitting test. To prevent collapse during crack formation under tensile stress, the specimens were wrapped with duct tape. As schematically illustrated in Figure 3-17, the sample was then placed in a vise and the realistic crack was induced by manually screwing the handle.

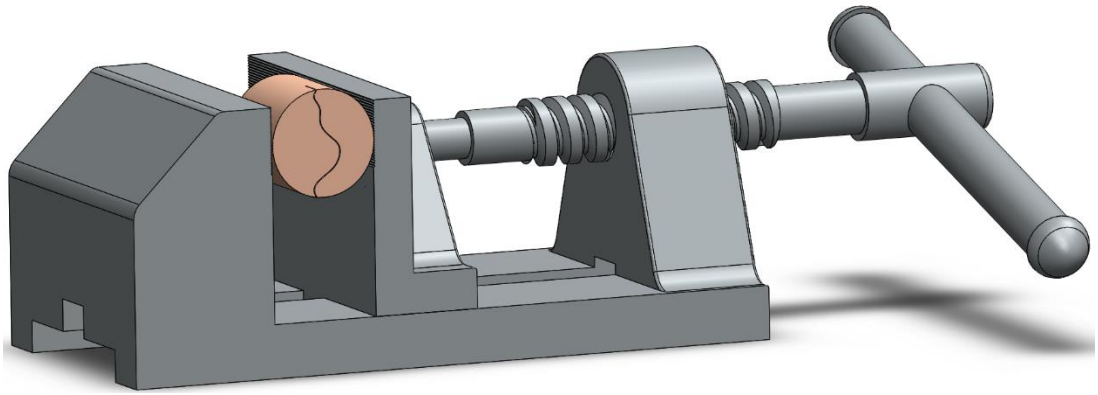

Figure 3-17 Manual crack creation in cylindrical concrete specimen using a press vice.

3.3.6 Crystal characterization

The treated samples were examined by SEM. A piece of a concrete specimen was placed on an aluminum stub and coated for SEM observation and EDS analysis. The bio-precipitate was also analyzed using XRD. At the end of the immersion period, the bio-precipitates were removed from the cracks, washed with distilled water and oven dried at 70°C for 24 h. The crystals were then checked with an XRD instrument.

3.3.7 Crack sealing evaluation

In addition to crystal observation, an optical microscope was used to monitor the crack closure and determine the efficiency of bio self-healing concrete. The specimens were examined by imaging with a light microscope (Leica MZ12, Switzerland) equipped with a camera (Carl Zeiss, AxioCam HRc, Germany) to check the initial crack width. After the initial examination, the specimens were submerged in water. The visual crack closure was assessed by imaging at age of 28 days from casting.

Chapter 4

Screening and optimization of bacterially induced $CaCO_3$ precipitation [2]

[2] This chapter forms the basis of a research paper published in the Journal of Applied Microbiology and Biotechnology, as referenced below.

[154] **Seifan, M.**, Samani, A.K., and Berenjian, A. *Induced calcium carbonate precipitation using Bacillus species.* Applied Microbiology and Biotechnology, 2016. 100 (23): p. 9895–9906.

4.1 Introduction

$CaCO_3$ is one of the cheapest inorganic compounds which has been found industrially applicable in many fields, including construction purposes, coating pigment, rubbers, plastics, paper, cosmetic, food, and horticulture [155]. In recent years, microbial production of $CaCO_3$ has emerged as one of the most attracting subjects due to its potentially wide range of applications. The precipitation of carbonate minerals by microorganisms broadly occurs in different geological environments, such as fresh and marine water [34], soil [35], cave [36, 37], and hot spring [38]. Apart from the role of biomineralization in nature, a large number of applications involving the microbially induced $CaCO_3$ precipitation with important scientific and technological implications have been reported. The main applications of $CaCO_3$ biomineralization are protection of limestone monuments [39], removal of Ca^{2+} ions from wastewaters [40], surface treatment of construction materials [12, 41], improvement of brick properties [42, 43], removal of contaminants and heavy metals from groundwater [44], plugging the pores of oil reservoirs [45], strengthening of sand columns [46], soil consolidation [47, 48], atmospheric CO_2 sequestration [49], and filling concrete cracks [26, 66, 156].

Although the feasibility of microbial $CaCO_3$ precipitation in different areas, such as microbiology, evolutionary biology and geology, has been reported, the literature is suffering from a comprehensive study for screening and optimization of the effective factors on $CaCO_3$ biosynthesis. To date, the majority of published works have focused on the possibility of $CaCO_3$ precipitation by various microbial strains and nutrients in restricted operational conditions. Since a high concentration of nutrients and calcium sources as well as different operating conditions may have an adverse impact on the biomineralization process, the effects of these variables need to be determined.

The objectives of this chapter are to investigate the effective factors on enhancing the biomineralization of $CaCO_3$. As the optimum level of significant factors can considerably improve the efficiency of the bioprocess, an optimization study is the primary importance. In the following sections, the effects of different variables on microbial production of $CaCO_3$ are discussed, and the optimum levels of significant factors are presented to achieve the highest concentration of $CaCO_3$. Moreover, the

mineralogy and morphology of precipitates are the other important parameters that need to be considered. $CaCO_3$ morphologies (calcite, vaterite and aragonite) have different physical properties, such as solubility, density and hardness that can significantly affect the final bio self-healing concrete performance. Therefore a morphological quantification is proposed to quantify the morphology of the produced $CaCO_3$.

4.2 Results

4.2.1 Screening of the effective factors on the MICP process

Bioprecipitation of $CaCO_3$ was explored in two phases of culture media, namely solid- and liquid-state fermentations. The first fermentation medium was used to identify the heterotrophic precipitation of $CaCO_3$ by the isolates. The latter medium was used for screening and optimization of effective factors on the MICP process to induce the highest concentration of $CaCO_3$.

4.2.1.1 Identification of potent $CaCO_3$ producing bacteria

In a preliminary evaluation, the possibility of microbial $CaCO_3$ precipitation via selected heterotrophic genera of bacteria isolated from New Zealand was studied. It has been reported that heterotrophic growth of microbial communities on organic acid salts, such as acetate, lactate, citrate, succinate, oxalate, malate and glyoxylate can promote mineral production [1]. The isolates were tested for $CaCO_3$ precipitation using a B4 solid medium [144]. B4 is composed of calcium acetate, yeast extract, glucose and agar. In this case, calcium acetate plays the role of the calcium and carbon source to initiate the biomineralization of $CaCO_3$.

A different range of crystal size and shape were identified from polarized microscope and SEM. The result obtained from the polarized microscope demonstrated the precipitation of crystals in the presence of bacteria at the end of incubation time. As shown in Figure 4-1, precipitated crystals at the end of the incubation period possessed strong polarized characteristics. This indicates the crystals were mainly composed of inorganic minerals [157]. Although *B.*

licheniformis, *L. sphaericus* and *B. subtilis* produced larger crystals, the number of colonies were remarkably lower than those produced by *B. sphaericus*. No crystallization was observed in the presence of dead cells. Furthermore, the absence of crystals in B4 media (without calcium acetate addition) confirmed that the presence of organic acid salt is essential for heterotrophic precipitation of $CaCO_3$.

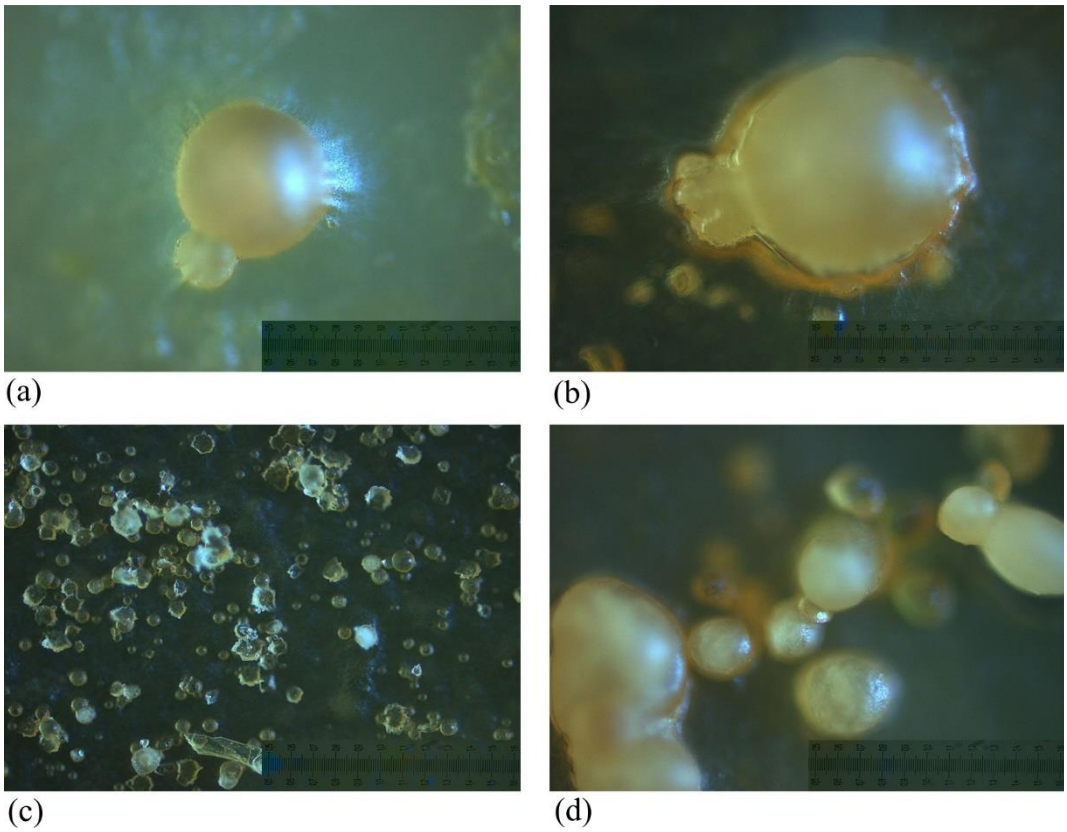

Figure 4-1 Precipitation of $CaCO_3$ by different microbial strains on B4 media: a) *B. licheniformis*, b) *L. sphaericus*, c) *B. sphaericus*, and d) *B. subtilis*.

4.2.1.2 Screening the significant variables on MICP

In the previous section, a constant composition of culture media (solid state media) was used to evaluate heterotrophic precipitation of $CaCO_3$ via the selected isolates. Despite the precipitation of $CaCO_3$ on B4 media, the effect of key parameters controlling bioprecipitation needs to be considered to maximize the production of $CaCO_3$. A higher bacterial cell surface in the fermentation process provides a favorable nucleation site for precipitation of $CaCO_3$. Therefore a liquid state

fermentation was chosen to address the limitation of solid state media for bacterial growth, distribution and precipitation.

There are many factors affecting the biomineralization process. Recognition of these variables ranges is one of the most significant steps in the screening study. In order to identify the significant factors on biomineralization of $CaCO_3$, different concentration of bacteria and nutritional components were grown under various operating conditions. Having a rough estimation of parameter ranges prior to the screening study, sets of preliminary experiments were carried out to identify the appropriate level of affecting factors. Thirteen potent variables enhancing the biomineralization of $CaCO_3$ along with their levels are listed in Table 4-1. To ensure the selected strains are capable of producing $CaCO_3$ in the liquid media, the lowest limit of cell concentration was adjusted to 0 % *v/v*. As presented in Table 4-1, different genera of bacteria with various concentration ranging 0–5 % *v/v* were used for the screening investigation. To determine the highest concentration of calcium salts, a set of identical media with two concentrations of calcium salts were prepared and incubated in the same conditions. The results disclose that the production of $CaCO_3$ was significantly higher in those media containing a lower concentration of calcium salt and the concentration of calcium source that exceeded 40 g/L resulted in a dramatic decline in $CaCO_3$ precipitation. This finding is in agreement with results reported in the literature [158, 159].

Table 4-1 Experimental variables and their level for microbial production of $CaCO_3$.

Variable number	Variable name	Value	
		Lowest level	Highest level
X_1	*Bacillus licheniformis* ATCC 9789 (% *v/v*)	0	5
X_2	*Lysinibacillus sphaericus* ATCC 4525 (% *v/v*)	0	5
X_3	*Bacillus sphaericus* NZRM 4381 (% *v/v)*	0	5
X_4	*Bacillus subtilis* ATCC 6633 (% *v/v*)	0	5
X_5	Urea (g/L)	0	65
X_6	Calcium chloride (g/L)	0	40
X_7	Calcium lactate (g/L)	0	40
X_8	Calcium nitrate (g/L)	0	40
X_9	Calcium acetate (g/L)	0	40
X_{10}	Yeast extract (g/L)	0	4
X_{11}	Incubation time (h)	72	336
X_{12}	Temperature (°C)	33	45
X_{13}	Agitation speed (rpm)	0	140

The results indicate that only six factors had a positive significant effect on $CaCO_3$ production (Table 4-2). Although the selected strains are capable of heterotrophic growth on B4 medium, the screening results indicate that *B. licheniformis* and *B. sphaericus* have a higher ability to produce $CaCO_3$ crystals in the liquid fermentation medium. In the biomineralization process, $CaCO_3$ is induced when calcium ions accumulate in extracellular in a certain condition. Although the presence of calcium source for MICP is crucial, the low and excessive concentration of Ca^{2+} might have an adverse impact on the biosynthesis process. The results show that calcium chloride is the most preferred calcium source to induce $CaCO_3$ precipitation, while the remained calcium sources have an adverse impact to the biomineralization process.

Urea plays an important role in the biosynthesis of $CaCO_3$ through a ureolytic pathway. In this approach hydrolysis of urea leads to the production of carbonate, and $CaCO_3$ crystals are precipitated when a suitable calcium source is present in the

surrounding. The screening results show that the presence of urea is required for biomineralization of $CaCO_3$; however, the excessive concentration of urea (greater than 65 g/L) inhibits the bioprecipitation of $CaCO_3$.

It is known that the presence of nitrogen sources is beneficial for bacterial growth. Generally, nutritional starvation contributes to a decrease or cessation of bacterial growth and effective metabolism. Therefore the presence of an appropriate concentrated nutrient is essential to increase the effectiveness of biomineralization. Among all common nutrients, yeast extract was tested due to its availability and high performance. It was shown that the presence of yeast extract has a positive influence on the $CaCO_3$ precipitation. Hence yeast extract was chosen as a variable for further investigation.

Incubation temperature is one of the most significant operating conditions which may affect the biomineralization processes. The results indicate that the bioprecipitation of $CaCO_3$ is independent of temperature (33–37°C), and therefore fermentation at a constant temperature of 35°C was used for the optimization study. Agitation is another important operating condition that enhances bacterial growth through the distribution of nutrients and oxygen in the fermentation medium. In contrast to temperature, agitation speed had a positive effect on biomineralization of $CaCO_3$. Hence agitation speed was used as a variable operating condition during optimization investigation.

Incubation time was another factor considered in the screening stage. The screening results indicate that the incubation time is not an efficient factor on the production of $CaCO_3$. It was observed that the maximum crystals are precipitated at the beginning of the fermentation process (<110 h) and the rate of $CaCO_3$ precipitation decreased with the time. Since $CaCO_3$ crystals are formed in the early stage of fermentation, 108 h was selected as the incubation time for optimization stage.

Table 4-2 The effects of variables in screening stage.

Terms	Variable name	Significance
Strains	*Bacillus licheniformis*	*p*-value < 0.1
	Lysinibacillus sphaericus	*p*-value > 0.1
	Bacillus sphaericus	*p*-value < 0.1
	Bacillus subtilis	*p*-value > 0.1
Nutrients	Urea	*p*-value < 0.1
	Calcium chloride	*p*-value < 0.1
	Calcium lactate	*p*-value > 0.1
	Calcium nitrate	*p*-value > 0.1
	Calcium acetate	*p*-value > 0.1
	Yeast extract	*p*-value < 0.1
Operating conditions	Incubation time	*p*-value > 0.1
	Temperature	*p*-value > 0.1
	Agitation speed	*p*-value < 0.1

4.2.2 Optimization of MICP process

In order to optimize the microbial $CaCO_3$ precipitation, the response surface methodology (RSM), using a central composite face-centered (CCF) design matrix, was used to determine the optimum levels of significant variables. For this purpose a total of 27 experiment runs were carried out, and experimental design with the actual level of variables are shown in Table 4-3. Four variables at three levels including *B. licheniformis*, *B. sphaericus*, yeast extract and agitation speed were used in the media containing a fixed amount of urea and calcium chloride under a controlled temperature. To determine the final concertation of calcium salt, a set of identical media with two concentrations of calcium chloride were prepared and incubated at the same conditions. The results show that the production of $CaCO_3$ is significantly increased in those media containing the lower concentration of calcium salt, and the concentration of calcium source exceeded than 40 g/L resulted in a dramatic decline of $CaCO_3$ precipitation. The finding is in good agreement with

results reported in the literature [158, 159]. Hence a constant amount of calcium chloride (40 g/L) was chosen for the optimization study.

Table 4-3 Level of variables examined in optimization using central composite face (CCF) design.

Run	Coded levels				Calcite (g/L)	Vaterite (g/L)
	Yeast extract (g/L) (X_{10})	***Bacillus licheniformis* % (*v/v*) (X_1)**	***Bacillus sphaericus* % (*v/v*) (X_3)**	**Agitation (rpm) (X_{13})**		
1	2 (-1)	3 (-1)	3 (-1)	60 (-1)	0.67	1.21
2	4 (1)	3 (-1)	3 (-1)	60 (-1)	0.12	1.18
3	2 (-1)	5 (1)	3 (-1)	60 (-1)	0.69	3.48
4	4 (1)	5 (1)	3 (-1)	60 (-1)	0.12	1.27
5	2 (-1)	3 (-1)	5 (1)	60 (-1)	1.49	2.09
6	4 (1)	3 (-1)	5 (1)	60 (-1)	0.30	1.08
7	2 (-1)	5 (1)	5 (1)	60 (-1)	0.49	2.09
8	4 (1)	5 (1)	5 (1)	60 (-1)	0.08	1.01
9	2 (-1)	3 (-1)	3 (-1)	100 (1)	0.12	0.56
10	4 (1)	3 (-1)	3 (-1)	100 (1)	0.10	1.26
11	2 (-1)	5 (1)	3 (-1)	100 (1)	11.89	18.08
12	4 (1)	5 (1)	3 (-1)	100 (1)	0.07	1.45
13	2 (-1)	3 (-1)	5 (1)	100 (1)	18.43	11.50
14	4 (1)	3 (-1)	5 (1)	100 (1)	0.08	1.39
15	2 (-1)	5 (1)	5 (1)	100 (1)	8.74	25.04
16	4 (1)	5 (1)	5 (1)	100 (1)	0.07	1.52
17	2 (-1)	4 (0)	4 (0)	80 (0)	0.21	0.53
18	4 (1)	4 (0)	4 (0)	80 (0)	0.14	1.27
19	3 (0)	3 (-1)	4 (0)	80 (0)	0.81	2.80
20	3 (0)	5 (1)	4 (0)	80 (0)	0.23	1.30
21	3 (0)	4 (0)	3 (-1)	80 (0)	0.19	3.33
22	3 (0)	4 (0)	5 (1)	80 (0)	0.30	1.04
23	3 (0)	4 (0)	4 (0)	60 (-1)	2.84	8.21
24	3 (0)	4 (0)	4 (0)	100 (1)	4.95	27.85
25	3 (0)	4 (0)	4 (0)	80 (0)	1.96	8.25
26	3 (0)	4 (0)	4 (0)	80 (0)	2.27	10.56
27	3 (0)	4 (0)	4 (0)	80 (0)	2.70	8.31

As noted earlier, the production of NH_4^+ through hydrolysis of urea results in an increase in pH, and this increase correlates with $CaCO_3$ precipitation. Figure 4-2 shows the increase in pH in the optimization study. The results obtained from the optimization study show that the pH increased in all fermentation media, and, interestingly, the maximum increases were observed in those samples which produced the higher concentration of $CaCO_3$. In contrast to screening samples, the optimization runs showed the higher increase in pH. The maximum increase in pH in screening step was 1.07, while in the optimization study, more than double of this value was noticed.

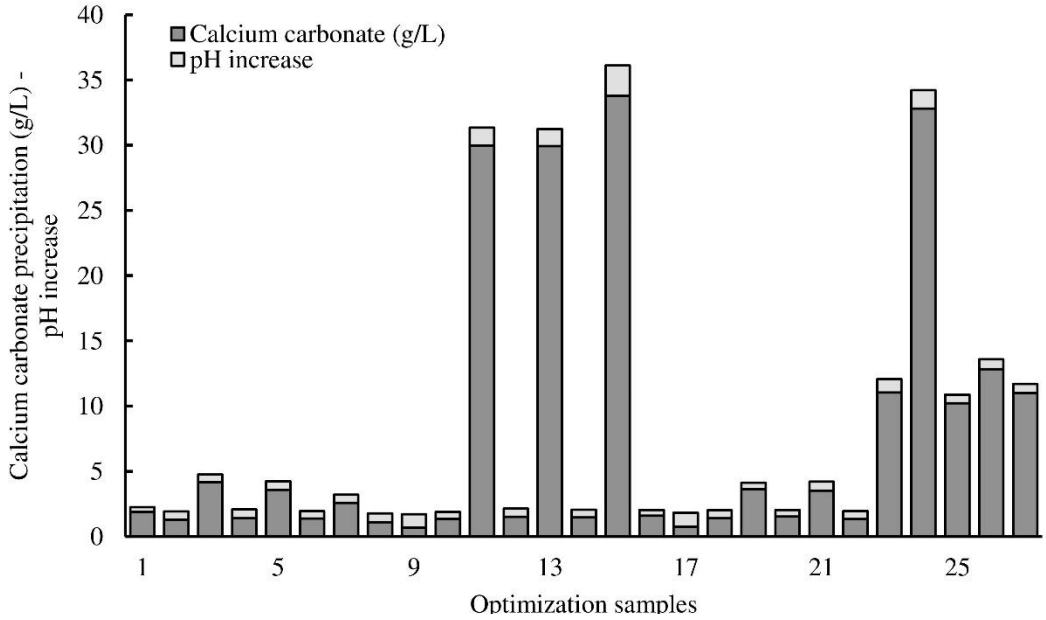

Figure 4-2 Variation of $CaCO_3$ precipitation and pH in the optimization study.

4.2.3 Experimental verification

In order to determine the optimal levels of variables, the regression equation, by remaining inside the region of experimental levels, was solved. The model predicted that the highest concentration of $CaCO_3$ is achieved when the fermentation media consists of 2 g/L yeast extract, 40 g/L calcium chloride, 65 g/L urea, 4.5% (*v/v*) *B. licheniformis* and 4.5% (*v/v*) *B. sphaericus* at agitation speed and temperature of 100 rpm and 35°C, respectively. To validate the model, replications were prepared based on the suggested concentrations. It was noted that

the observed and predicted results had a high degree of similarity in the production of $CaCO_3$ by only 5% of error.

4.2.4 Morphological observation

A microscale examination of purified crystals precipitated on B4 medium was carried out by using SEM to confirm the production and the crystal shape of $CaCO_3$ induced by different microbial strains. The SEM micrographs of precipitated crystals showed that different morphologies of $CaCO_3$ can be produced by selected isolates. Figure 4-3 depicts the $CaCO_3$ crystals produced on B4 media. The SEM micrographs of colonies revealed that calcite and vaterite were the most predominant morphologies induced by the strains.

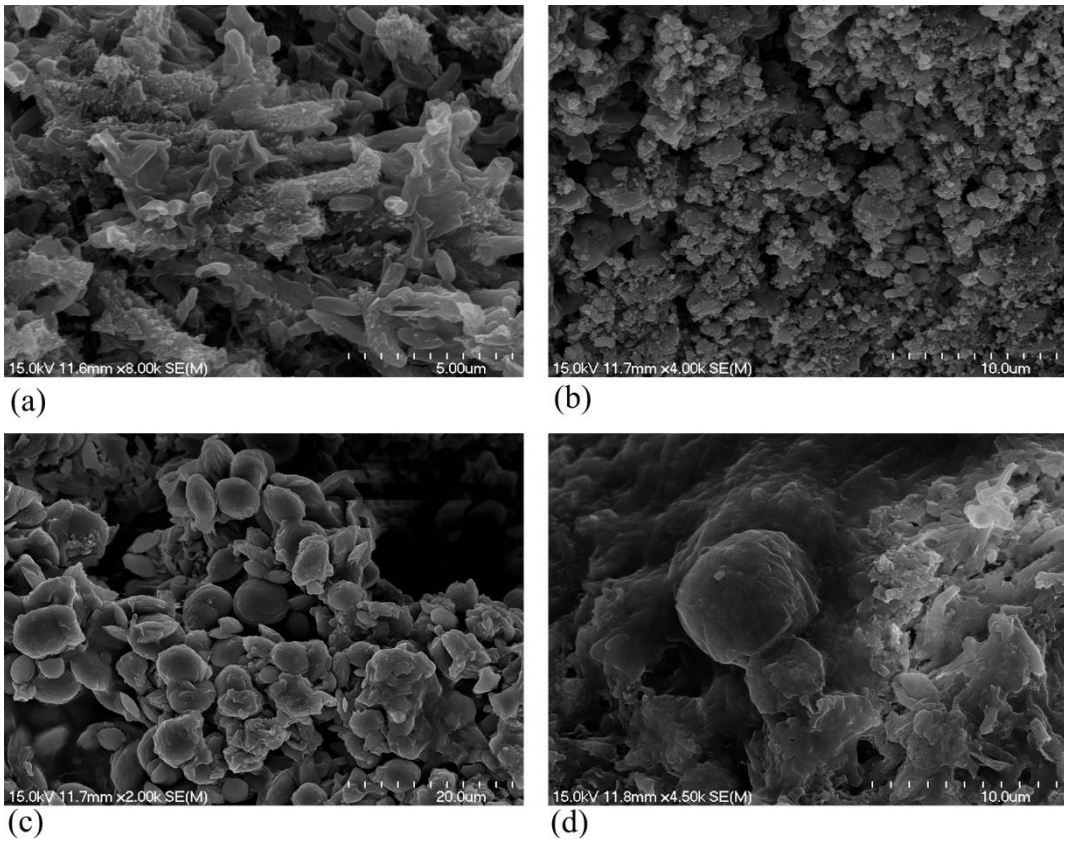

Figure 4-3 SEM micrographs of $CaCO_3$ crystals precipitated on B4 media containing microbial strain: a) *B. licheniformis*, b) *L. sphaericus*, c) *B. sphaericus*, and d) *B. subtilis*.

Precipitation of $CaCO_3$ in the screening stage was also studied by SEM analysis. Vaterite and calcite were the main two morphologies in the screening samples. Figure 4-4a and b show spherical particles predominantly precipitated in the media containing calcium chloride, *B. licheniformis*, *L. sphaericus,* and *B. sphaericus*. Conversely, the micrograph of calcite particles which produced in the media containing calcium lactate, *B. licheniformis,* and *B. subtilis* is depicted in Figure 4-4c. As expected, a combination of calcite and vaterite were formed in the center points runs which contained all isolates and nutrients (Figure 4-4d). A comparison between vaterite produced in solid and liquid state fermentation revealed that the crystals precipitated in solid media were smooth while the liquid media produced porous, rough and even broken crystals.

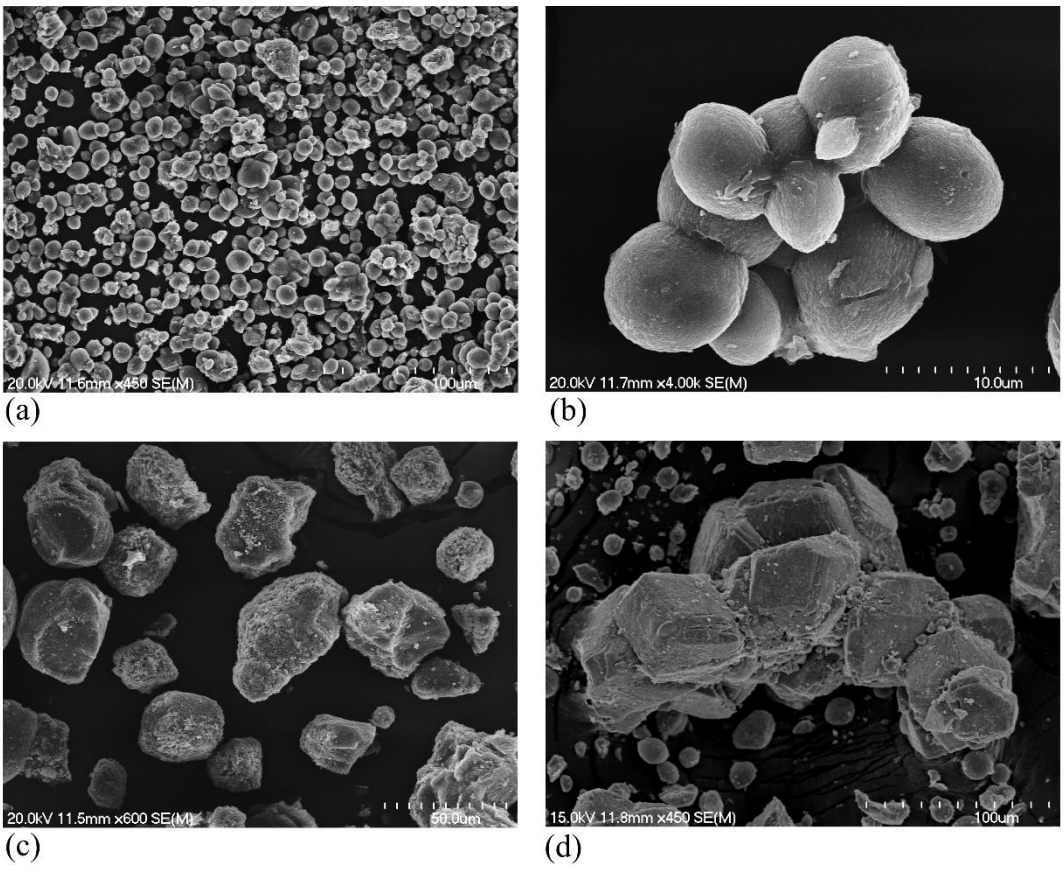

Figure 4-4 Scanning electron micrographs of $CaCO_3$ crystals precipitated in the screening study.

Calcite and vaterite particles can be also distinguished in the optimization samples. Figure 4-5 presents the SEM micrograph corresponding to the produced crystals in the optimization study and the optimum media. It was noticed that the size of produced crystals in the optimization study was slightly bigger than those precipitated in the screening study. As shown in Figure 4-5a and b, the average vaterite size of 20 µm was observed in the optimization samples which was approximately two times bigger than those produced in the screening stage. SEM was also performed for the optimized samples and the results are given in Figure 4-5 c–d. As expected, calcite and vaterite were precipitated for the samples containing the optimum concentration of nutrients and operating conditions.

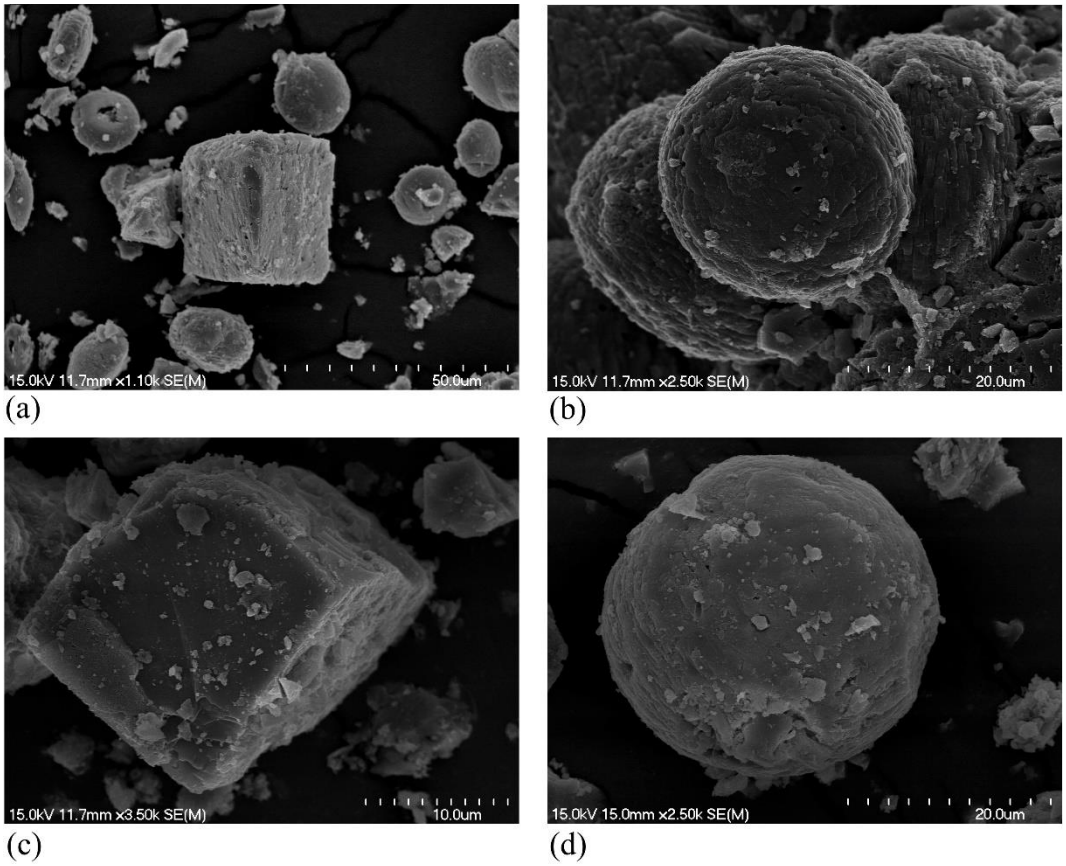

Figure 4-5 Scanning electron micrographs of $CaCO_3$ crystals precipitated in the: a–b) optimization runs and c–d) optimized samples.

Bio-precipitates were further characterized using EDS at 15.0 keV. EDS as an analytical method was employed to detect the elements presented in the newly

formed crystals. Elements existing in a sample are detected by atomic number, and the amount of them can be determined by the intensity of peaks. To determine the elemental ratio of pure $CaCO_3$, EDS was performed for pure calcite and the elemental spectrum is shown in Figure 4-6a. EDS was also performed for the produced bio-precipitates in the optimized sample to confirm that the precipitated crystals were $CaCO_3$ (Figure 4-6b). A high degree of similarity was observed between the EDS spectra of the pure $CaCO_3$ and the optimized sample. The results disclose that calcium, carbon and oxygen were the predominant elements in bio-precipitates. Considering the atomic ratio, it could be concluded that the precipitates were $CaCO_3$. Moreover, elemental mapping for the precipitated crystal was determined using EDS, and the uniform distributions of carbon, calcium and oxygen are shown in Figure 4-7.

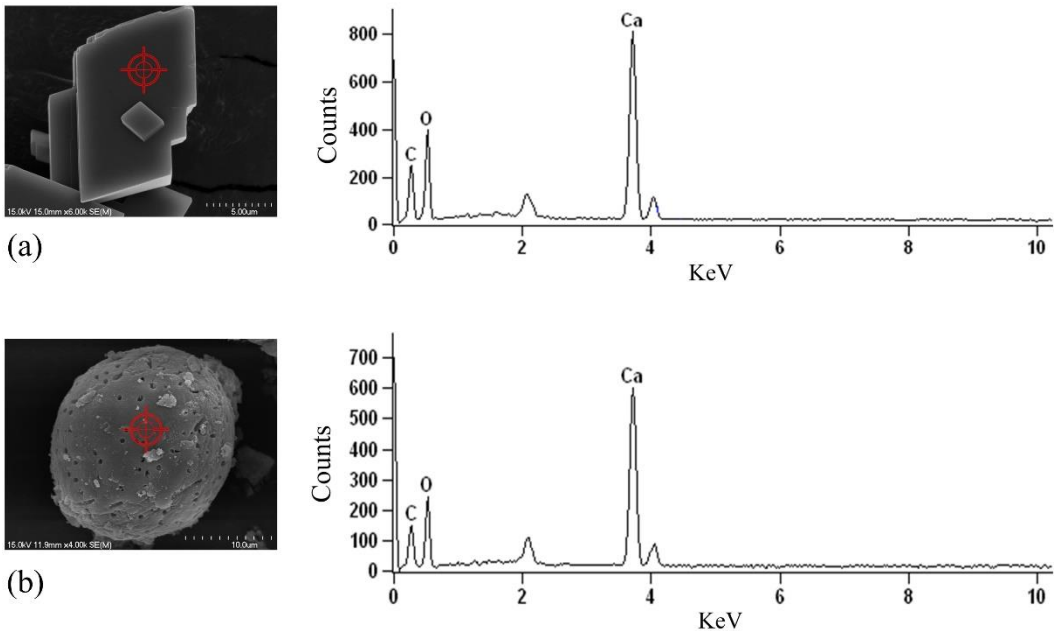

Figure 4-6 EDS spectra for: a) pure $CaCO_3$ crystal and b) precipitated crystal in the optimized sample.

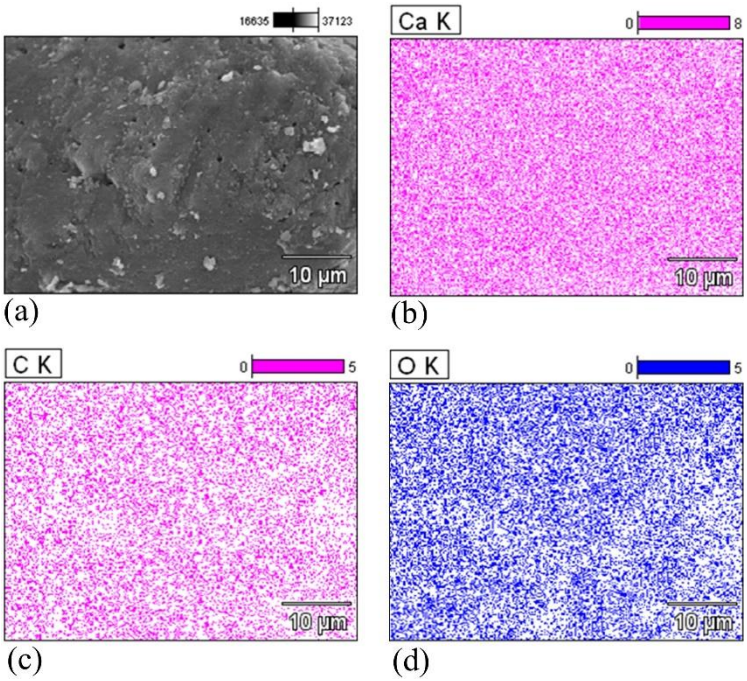

Figure 4-7 Corresponding EDS elemental mapping images of precipitated $CaCO_3$ crystals.

4.2.5 Structural characterization and morphological quantification of precipitated particles

XRD analysis was performed to analyze the morphology of the produced crystals during the biomineralization of $CaCO_3$. The production of two crystals (vaterite and calcite) on B4 media has been supported by XRD examination. As depicted in Figure 4-8, XRD spectra confirm the heterotrophic precipitation of $CaCO_3$ on the B4 media.

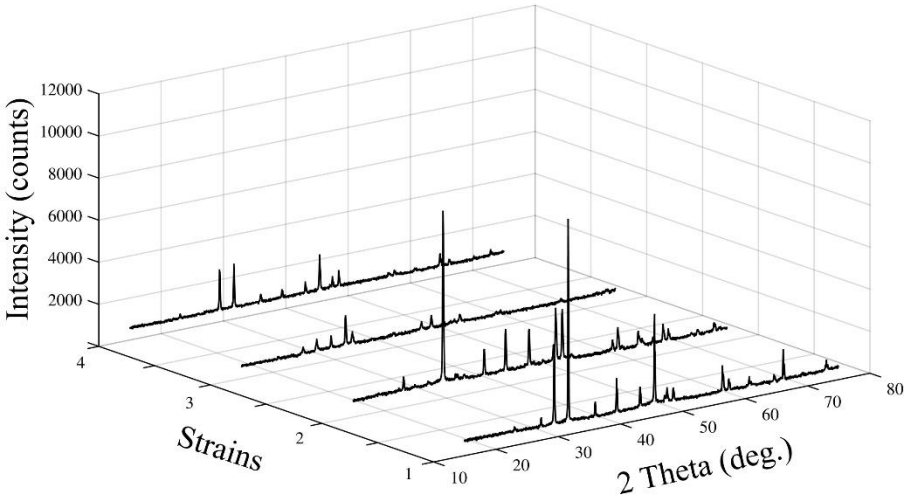

Figure 4-8 XRD patterns of $CaCO_3$ precipitated in the B4 media.

XRD spectra of the produced crystals in the optimization stage are presented in Figure 4-9 where the angle of 29.36° and 27.11° represent calcite and vaterite, respectively. Figure 4-10 depicts XRD spectrum for the optimized sample obtained in validation step where the lattice planes of 104 and 113 indicate the formation of calcite and vaterite, respectively [154].

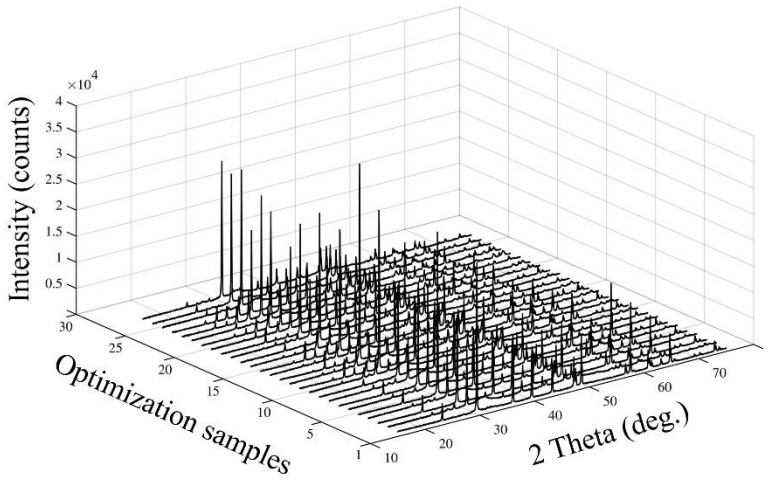

Figure 4-9 XRD patterns of $CaCO_3$ crystals precipitated in optimization study.

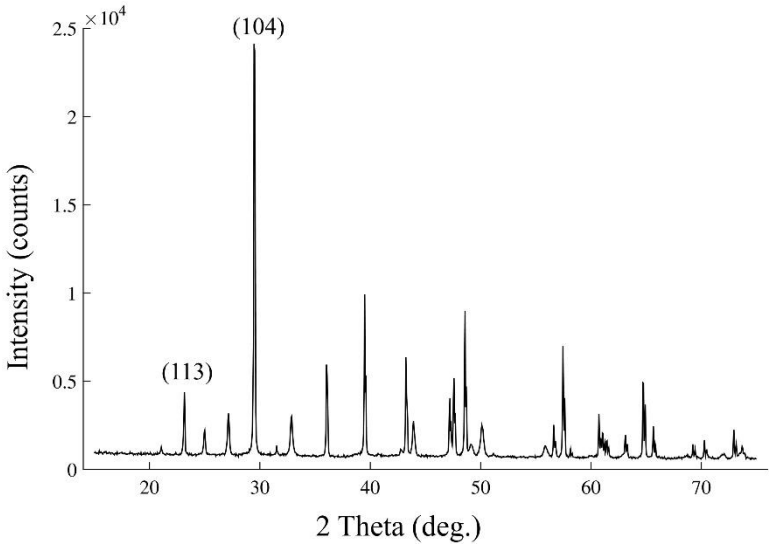

Figure 4-10 XRD spectra for $CaCO_3$ crystals precipitated in optimized sample.

Although calcite and vaterite were detected in all samples, this ratio was not consistent across the samples. However, no aragonite was precipitated in screening and optimization studies. Figure 4-11 illustrates the ratio of $CaCO_3$ polymorphs (calcite to vaterite) precipitated in the optimization study. It was noted that the media containing a low concentration of *B. licheniformis* and *B. sphaericus* under a lower level of agitation speed (60 rpm) produced maximum calcite. Whereas the increase of *B. licheniformis* and agitation speed (100 rpm) led to precipitate the least calcite. This variation was also observed in the screening stage.

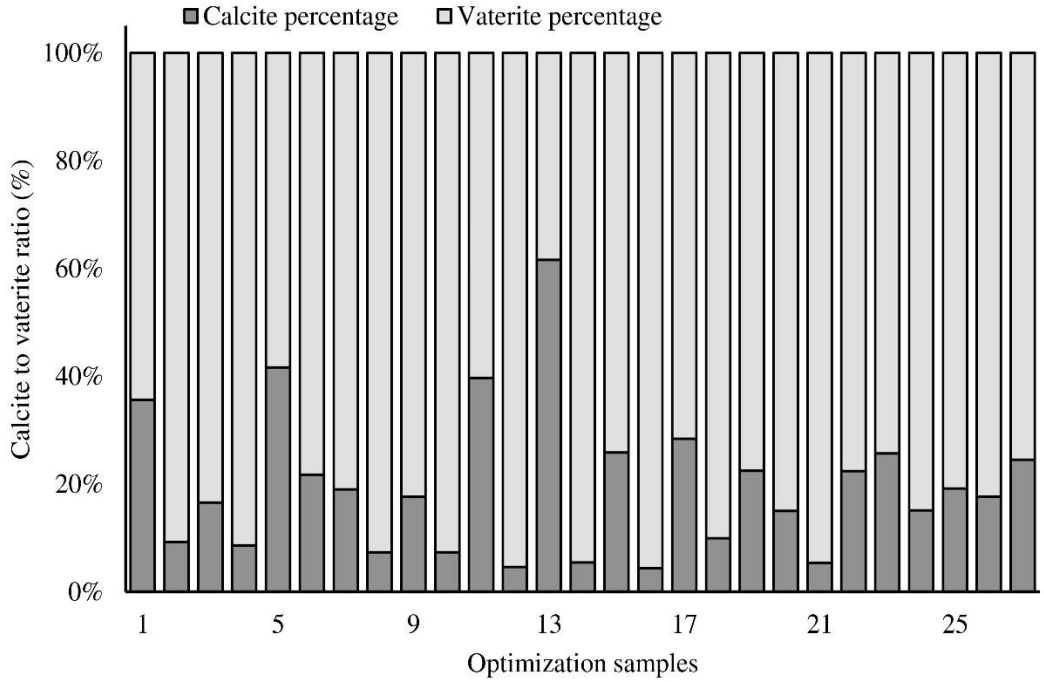

Figure 4-11 The ratio of $CaCO_3$ polymorphs (calcite to vaterite) precipitated in optimization study.

4.3 Discussion

4.3.1 Screening study

There are many factors, including nutrient, calcium source, reactant concentration, cell concentration, temperature, and agitation, which may inhibit or promote $CaCO_3$ precipitation. Therefore the screening study was carried out to identify the most significant factors on the MICP process. As the bacterial cells serve as nucleation sites for precipitation of $CaCO_3$, screening of potent isolates on the biomineralization process was performed. All of the isolates were selected from *Bacillus* species because of producing endospores which help bacteria to survive in harsh conditions such as heat, cold and radiations for long periods. Various concentrations of these bacteria were used for the screening step. Although heterotrophic growth of all strains showed that they are capable of producing $CaCO_3$ in the B4 media, the screening results indicate that only *B. licheniformis* and *B. sphaericus* have significant capability for $CaCO_3$ production.

In the biomineralization process, $CaCO_3$ is induced when calcium ions accumulate extracellularly in a certain condition. In the screening studies, the effect

of four types of calcium source, namely calcium chloride, calcium lactate, calcium nitrate and calcium acetate on biomineralization of $CaCO_3$ were investigated. Different concentrations of calcium sources were used in order to evaluate the effectiveness of calcium ions on biomineralization. The results show that calcium chloride is the most preferred calcium source to induce $CaCO_3$ crystals, while the addition of calcium nitrate, calcium acetate, and calcium lactate adversely affect the biomineralization. Although the presence of a calcium source for microbial $CaCO_3$ precipitation is crucial, the concentration of Ca^{2+} has a great influence on the resulted $CaCO_3$ concentration. In the screening stage, it was demonstrated that the presence of low and excessive amounts of Ca^{2+} have an adverse impact on microbial production of $CaCO_3$. The data show that a high concentration of Ca^{2+} may inhibit the activity of microbial strain and, consequently, the production of $CaCO_3$ is affected. This might be due to the presence of a high amount of metal ions which surround the bacterial cells, inhibit their growth and metabolism. Another explanation for the decrease in the enzymatic activity might be the increase in electrolyte concentration during the formation of minerals [160]. On the other hand, a few electron acceptors are involved in ionic reaction when a low concentration of Ca^{2+} is used. This result is in accordance with the literature. Gorospe et al. [161] studied the effect of different calcium sources on urease activity of *S. pasteurii*. It was reported that the presence of calcium sources has a negative effect on urease activity as compared to the control samples. It was found that the presence of calcium chloride results in 51% reduction in enzymatic activity. As a result, a constant concentration of calcium chloride (40 g/L) was chosen for optimization study.

Urea is an organic nitrogen compound, and urease activity as a widespread phenomenon in nature plays an important role in the metabolisms involved by bacteria, yeasts and filamentous fungi. Urea is one of the main components to produce carbonate ions in ureolysis pathway as shown in Eq. 4-1 to Eq. 4-4.

$$CO(NH_2)_2 + H_2O \xrightarrow{\text{Microorganism}} NH_2COOH + NH_3 \quad (4\text{-}1)$$

$$NH_2COOH + H_2O \rightarrow NH_3 + H_2CO_3 \quad (4\text{-}2)$$

$$2NH_3 + 2H_2O \rightarrow 2NH_4^+ + 2OH^- \quad (4\text{-}3)$$

$$2OH^- + H_2CO_3 \rightarrow CO_3^{2-} + 2H_2O \quad (4\text{-}4)$$

Hydrolysis of urea leads to producing ammonia and carbamic acid. As can be seen from Eq. 4-1, the reaction between ammonia and water produces NH_4^+ which results in an increase in local pH, and therefore it shifts in the bicarbonate equilibrium. This phenomenon results in an alkaline environment which facilitates the precipitation of $CaCO_3$. In ureolysis pathway, the increase in pH is a sign of urea hydrolysis and it might be an indication of crystal formation.

Generally, nutritional starvation may contribute to a decrease or cessation of bacterial growth and effective metabolism. Therefore the presence of appropriate concentrated nutrient is essential to increase the effectiveness of biomineralization. Yeast extract as a nitrogen source was tested due to its availability and high-performance. The results demonstrate that the presence of yeast extract has a positive influence on the $CaCO_3$ biosynthesis. However, a high concentration of yeast extract shows an inhibitory effect on the $CaCO_3$ production. The bacterial activity is inhibited when a high concentration of yeast extract is used which prevents electron transportation between existing calcium ions in the media and negatively charged cell walls. The screening results indicate that the utilization of yeast extract, more than 3 g/L, dramatically declines the microbial $CaCO_3$ precipitation.

Apart from nutritional compounds, operating conditions may have a great influence on the bioprecipitation of $CaCO_3$. Since the bacteria inhabit in a wide range of habitats, from polar marines to hot springs, the optimum temperature of bacterial growth varies, and this may affect the microbial effectiveness to initiate the biomineralization process. The results obtained in the screening stage show that the temperature is not an efficient factor on the biosynthesis of $CaCO_3$. This demonstrates that the selected microbial strains are not sensitive to the temperature range (33–37°C), and this is in agreement with the result reported earlier [158]. This also indicates that the biomineralization of $CaCO_3$ is applicable in a wide range of surroundings. Since the concrete structures are built in various environments, this finding demonstrates that the efficiency of a bio self-healing concrete is not affected by temperature variations. The incubation time is required for enzyme production

and formation of carbonate crystals by the bacterial cells. Okwadha et al. [159] reported that more than 95% of urea hydrolyzed by *S. pasteurii* during the first 100 h of fermentation. In another study Xu et al. [162] investigated the effect of fermentation time on biomineralization of $CaCO_3$. They observed a dramatic drop in concentration of soluble calcium ions during the first 30 h of fermentation, indicating the majority of crystals are formed in the first 30 h of fermentation. Our results also indicate the incubation time is not an efficient factor on the production of $CaCO_3$, and biomineralization of $CaCO_3$ decreased after 108 h. This reduction is due to the decrease in the number of viable cells and their urease activity. Mixing is another potential factor influencing the bioprocesses. Agitation is not only beneficial for bacterial growth but also provides more interactions between negatively charged bacterial cells and calcium ions. In contrast to temperature and incubation time, the results reveal that the agitation exerts a significant influence on the precipitation of $CaCO_3$ compared to the stationary state. It was observed that the variation of agitation speed has an effect to the extent of mixing in the shake flasks. Agitation not only affects oxygen availability but it also has a great effect on the availability of other nutritional compounds in the fermentation solution. Moreover, it has been reported that agitation mode can enhance bacterial enzymatic activity [163, 164], and it consequently contributes to decompose a higher concentration of urea. On the other hand, the bacterial enzymatic activity may be affected at the high agitation rates. The low enzyme activity at high agitation speeds is attributed to the effect of shear stress on bacterial cells and enzyme structure [165].

4.3.2 Optimization study

In the screening stage, the effects of multiple bioprocess parameters were investigated. To maximize the bacterially induced $CaCO_3$ precipitation, an optimization study using the CCF design was performed. To predict the production of $CaCO_3$, the experimental results were fitted with a second-order polynomial function. Considering the effective factors, the polynomial regression based model is presented as follows:

$$Y = 8.34 + 1.80X_1 + 1.72X_3 - 5.27X_{10} + 5.82X_{13} - 4.71X_1^2 - 4.85X_3^2 - 6.20{X_{10}}^2 + 14.65{X_{13}}^2 - 1.82X_1X_3 - 2.15X_1X_{10} + 2.02X_1X_{13} - 2.07X_3X_{10} + 2.08X_3X_{13} - 5.09X_{10}X_{13} \quad (4\text{-}5)$$

where Y is the response, X_1, X_3, X_{10}, and X_{13} are *B. licheniformis*, *B. sphaericus*, yeast extract and agitation speed, respectively. Analysis of variance (ANOVA) was used to check the adequacy of the model and the results are shown in Table 4-4. The results show that the Fischer's *F*-test is highly significant (*p*-value < 0.007) for the regression. The model was also evaluated for its suitability by examining the lack of fit. According to the ANOVA results, the lack of fit is not significant for the model (*p*-value > 0.1).

Table 4-4 Analysis of variance of the quadratic model for the central composite face-centered (CCF) design.

Source	DF	SS	MS (variance)	*F*-value	*p*-value	SD
Total	26	4490.41	172.708	-	-	-
Constant	1	1488.26	1488.26	-	-	-
Total corrected	25	3002.14	120.086	-	-	10.9584
Regression	14	2565.93	183.281	4.62175	0.007	13.5381
Residual	11	436.217	39.6561	-	-	6.29731
Lack of Fit	10	432.785	43.2785	12.6096	0.216	6.57864
Pure error	1	3.4322	3.4322	-	-	1.85262

DF: degree of freedom, *SS*: sum of squares, *MS*: mean sum of squares, *SD*: standard deviation

Figure 4-12 to Figure 4-14 present the response contour plots to visualize the influence of the effective variables on the production of $CaCO_3$. Each surface plot shows the effect of two variables on the response by keeping the other variables at their zero levels. As can be seen from Figure 4-12a, a relatively high concentration of *B. licheniformis* and *B. sphaericus* facilitate the precipitation of $CaCO_3$. Correlation between microbial growth rate and $CaCO_3$ production (response) shows

that an increase in the number of cells provides the higher nucleation sites and, consequently, more $CaCO_3$ crystals are precipitated.

Apart from the influence of bacteria and nutritional compounds, the effect of agitation speed requires further investigation. In this study agitation was used to increase the oxygen transfer and nutrient distribution for microbial cells. Various agitation speeds were considered to evaluate their effect on the biomineralization of $CaCO_3$. Agitation is not only beneficial for bacterial growth but also provides more interactions between negatively charged bacteria cells and electron acceptors present in media (Ca^{2+}). The interactive effects of agitation speed and yeast extract on biomineralization of $CaCO_3$ are depicted in Figure 4-12b. It was found that the increase of agitation speed has a positive effect on the response, while a lower concentration of yeast extract was found to be effective on the biosynthesis of $CaCO_3$.

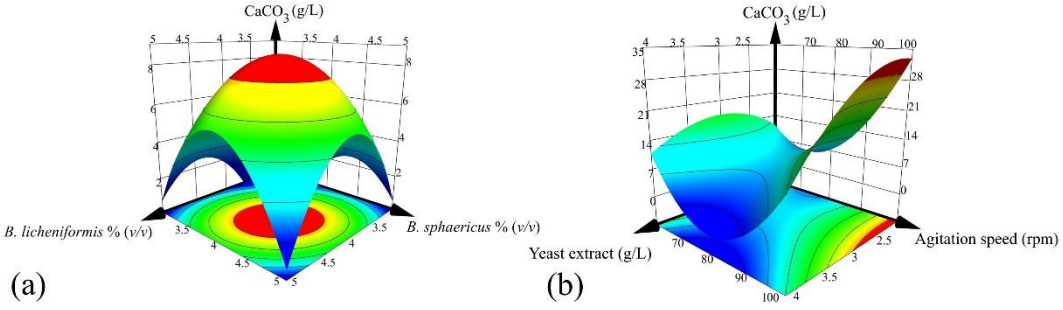

Figure 4-12 3D response surface plots for $CaCO_3$ production showing the interactive effects of: a) *B. licheniformis* and *B. sphaericus* and b) yeast extract and agitation speed.

Unlike the interaction between agitation speed and yeast extract, the increase in both inoculum sizes and agitation speed are favorable to induce a higher concentration of $CaCO_3$ precipitation (Figure 4-13a–b). The results show that the maximum amount of bio-precipitates can be achieved when the concentrations of *B. licheniformis*, *B. sphaericus* and shaking speed are adjusted at 4.5% (*v/v*), 4.5% (*v/v*) and 100 rpm, respectively.

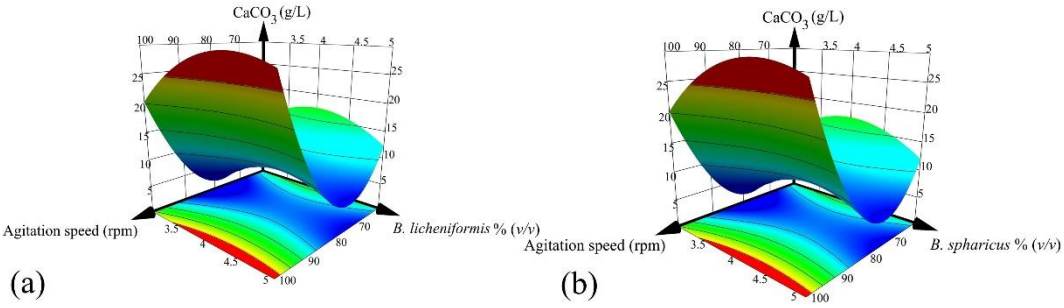

Figure 4-13 3D response surface plots for $CaCO_3$ production showing the interactive effects of: a) agitation speed and *B. licheniformis* and b) agitation speed and *B. sphaericus*.

Figure 4-14a–b demonstrates the interactive effects of yeast extract, *B. licheniformis*, and *B. sphaericus* on the production of $CaCO_3$. The plot shows that the response increased with the increase in *B. licheniformis* concentration from 3.6 to 4.8% (*v/v*); however, the production of $CaCO_3$ decreased as the concentration of yeast extract reached its upper level. A similar trend was observed when *B. sphaericus* and yeast extract were used.

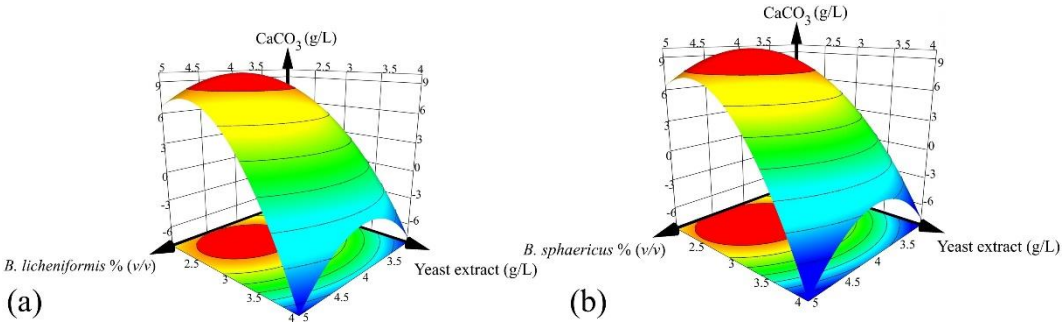

Figure 4-14 3D response surface plots for $CaCO_3$ production showing the interactive effects of: a) *B. licheniformis* and yeast extract and b) *B. sphaericus* and yeast extract.

4.3.3 Morphological observation and crystal characterization

$CaCO_3$ properties, including particle size, its distribution, morphology, specific surface area, brightness, and chemical purity, have a strong impact on its application in various industries [155]. Among these factors, the morphological aspect is one of the most significant characteristics. The diversity of $CaCO_3$ mineralization and various saturation levels result in the production of different polymorphs (calcite,

vaterite and aragonite). Physical properties of $CaCO_3$ polymorphs are given in Table 4-5. The reason for producing various polymorphs through biomineralization of $CaCO_3$ is not well understood. However, factors, including bacteria surface wall properties, bacteria metabolic activities, extracellular polymeric substance (EPS) content, and the composition of media, have an influence on the morphology and the size of produced crystals.

Table 4-5 Physical properties of calcite, vaterite and aragonite.

Properties	Calcite	Vaterite	Aragonite
Solubility product (K_{sp})	3.36×10^{-9}	1.66×10^{-8}	6×10^{-9}
Density (g/cm^3)	2.71	2.54	2.93
Hardness (Mohs scale)	3	3	3.5-4
Refractive index	1.58	1.55	1.63
Coordination number	6	6	9
Color	Usually white, but also colorless, gray, green, red, pink, yellow and brown	Colorless	Colorless, white, gray, yellowish, purple, green, red and reddish white

Physical properties of microbial $CaCO_3$ precipitation strongly rely on the portion of each polymorph. The crystalline structure of $CaCO_3$ polymorphs is illustrated in Table 4-6. The different morphology results in different peaks and intensities. The most intensive peaks occur at the angle (2θ) of 29.36°, 27.11° and 26.26° for calcite, vaterite and aragonite, respectively.

Table 4-6 Crystalline structure of $CaCO_3$ polymorphs.

Polymorphs	Highest peak position (2θ)	Miller Indices (hkl)	Crystal system
Calcite	29.36°	104	Hexagonal
Vaterite	27.11°	113	Hexagonal-Dihexagonal Dipyramidal
Aragonite	26.26°	111	Orthorhombic

In the biomineralization process, the bacterial cell wall provides a nucleation site, allowing the positive ions to attach a negatively charged bacterial cell surface to form minerals. The bacterial cell surface differences are mainly due to the amount of peptidoglycan, the amidation level of free carboxyl and the availability of mycolic and teichoic acids. For instance, the absence of mycolic acids in *Arthrobacter* sp. causes a hydrophilic cell wall, whereas the presence or production of mycolic acids in *Rhodococcus* sp. results in the hydrophobic cell wall and, consequently, it is likely to influence cell surface charge [37, 166]. The composition of medium and concentration of EPS also affects the formation of various morphologies. It was reported that the abundance of EPS and the type of amino acids in the medium have a certain influence on the mineralogy of bio-precipitates [167]. It should be pointed out that the crystal size may be affected by EPS and the composition of fermentation media. This study indicates that the type of electron acceptor also has an effective influence on morphology. It was found that calcite particles are mainly produced when bacteria utilize organic acid (calcium lactate), whereas vaterite crystals predominantly precipitate when calcium chloride is used as an electron acceptor. Apart from these factors, the viscosity of the medium also showed an impact on production of different morphologies. It was noted that the probability of calcite formation in a natural environment improves as the viscosity of the medium increases [168]. The precipitation of crystals revealed that the likelihood of producing vaterite by isolates increased when the water activity increased. This investigation shows that operating conditions have no influence on the $CaCO_3$ morphology.

4.4 Chapter summary

The effectiveness of a bio self-healing concrete relies on various factors, including the amount of bio-precipitates and the possibility of activation in diverse environments at a short period of time. The utilization of suitable microbial compounds at their optimum levels can significantly enhance the efficiency of bio self-healing concrete by filling the entire cracks and pores. In this chapter various parameters, including bacterial strains, media compositions and operating conditions, were investigated to determine the effective factors on

biomineralization of $CaCO_3$. The results indicate that *B. licheniformis*, *B. sphaericus*, yeast extract, urea, calcium chloride, and agitation speed have a significant influence on biomineralization efficiency. It was noticed that calcite and vaterite particles are predominantly produced by *B. licheniformis* and *B. sphaericus*. To determine the influential parameters on $CaCO_3$ morphologies, a novel morphological quantification using XRD was performed. The study demonstrates that the bacterial cell surface properties, EPS, the viscosity of the medium and the type of electron acceptor (Ca^{2+}) are the effective factors on the morphology of bio-precipitates.

Chapter 5

The effect of pH and aeration on the MICP process [3]

[3] This chapter forms the basis of a research paper published in the Journal of Applied Microbiology and Biotechnology, as referenced below.

[169] **Seifan, M.**, Samani, A.K., and Berenjian, A. *New insights into the role of pH and aeration in the bacterial production of calcium carbonate ($CaCO_3$).* Applied Microbiology and Biotechnology, 2017. 101 (8): p. 3131–3142.

5.1 Introduction

The effectiveness of a bio self-healing concrete depends on the extent of $CaCO_3$ precipitation. It has been reported that bacterial production of $CaCO_3$ is affected by the concentration of dissolved inorganic carbon and calcium, pH, nucleation site, and Hartree energy (E_h) [53, 54]. In the previous chapter, the effective factors on the MICP process were identified and their optimum concentrations were determined to maximize the biomineralization process in an uncontrolled pH condition.

During screening and optimization studies, the concentration of bioproduct showed a relationship with pH. Concrete has a pH of ~12 and exposes many environmental conditions which may inhibit the bacterial metabolism. Therefore the ability of bacteria to tolerate a high pH and also the capability of inducing $CaCO_3$ precipitation in such conditions are the main challenges to their application in concrete environment. Although the survivability of bacteria in a relatively harsh environment has been reported [170], the capability of producing minerals in such environments has remained a matter of debate. Kim et al. [170] examined the ability of isolated bacteria from concrete to tolerate an alkaline environment by growing them on alkaline nutrient broth. It was found that the isolates could grow on nutrient agar broth (pH 11) near their optimal growth temperature. In another study the influence of initial pH on the bacterial precipitation of $CaCO_3$ was investigated by Li et al. [171]. The authors performed fermentations with the initial pH of 6–8 and found that a higher initial pH of medium leads to induce $CaCO_3$ precipitation crystals in a shorter time.

Another issue which arises might be the presence of bacteria inside the concrete structures in which there is no sufficient oxygen for bacterial germination and metabolism and, consequently, $CaCO_3$ precipitation is limited on the surface area of the crack. In general, aerobic organisms utilize oxygen to facilitate efficient growth leading to produce bioproduct under certain conditions. However, the possibility of toxin formation, inhibitory effect on metabolism, and respiration in microorganisms may increase if a high supply of oxygen (more than its critical level) presents in the surrounding. The oxygen toxicity potentially occurs at the exponential growth phase rather than the stationary phase. Considering the

robustness of bacterial growth at the exponential growth phase, and its significant role in biomineralization of $CaCO_3$, it is vital to provide a condition to enhance the bacterial growth without elaborating a considerable amount of toxin.

The fermentation is a complex dynamic process that may be affected by many factors, including aeration and alkalinity levels. There is a scarcity of literature on the effect of oxygen and alkalinity on the bacterial production of $CaCO_3$. Therefore this chapter aims to investigate: (I) the effect of aeration on bacterial growth and $CaCO_3$ production, and (II) the performance of bacteria to induce $CaCO_3$ precipitation at the different ranges of pH.

5.2 Results

5.2.1 Monitoring parameters over uncontrolled-pH fermentation

In the preliminary study, the variations of cell growth, $CaCO_3$ precipitation, DO and pH were monitored during an uncontrolled-pH fermentation. In this sense, the bioreactor containing the optimum medium inoculated and the aeration and agitation speed were adjusted to 0.5 SLPM and 150 rpm, respectively. Figure 5-1 illustrates the variation of pH, DO, bacterial growth, and bacterial production of $CaCO_3$ throughout the fermentation process.

The bacterial growth rate can be distinguished into different phases. The cell concentration increased exponentially from 5 h to reach the maximum value at 40 h, followed by a slight decrease and remained constant until the end of fermentation. It was found that the highest concentration of bacterial cell was attained during the first 40 h of fermentation. Interestingly, a correlation was observed between bacterial cell growth and $CaCO_3$ precipitation which more than 60% of $CaCO_3$ crystals were precipitated over the exponential cell growth phase (40 h). This indicates the significant impact of cell number as a nucleation site for ionic exchange to induce $CaCO_3$ precipitation.

The variations in DO concentration and pH strategy were also monitored during the cultivation time. The concentration of DO decreased sharply and reached its lowest level (15%) at 30 h. However, an increase in DO concentration was observed

from 30 h to 60 h and then it stabilized until the end of fermentation. The same trend for DO and pH profiles was observed during the first 70 h of fermentation. pH started to drop suddenly at the exponential phase and fell to the lowest level (pH 7). Thereafter, the pH was increased to the highest level (8.2) and followed a slight decrease for the rest of the fermentation period.

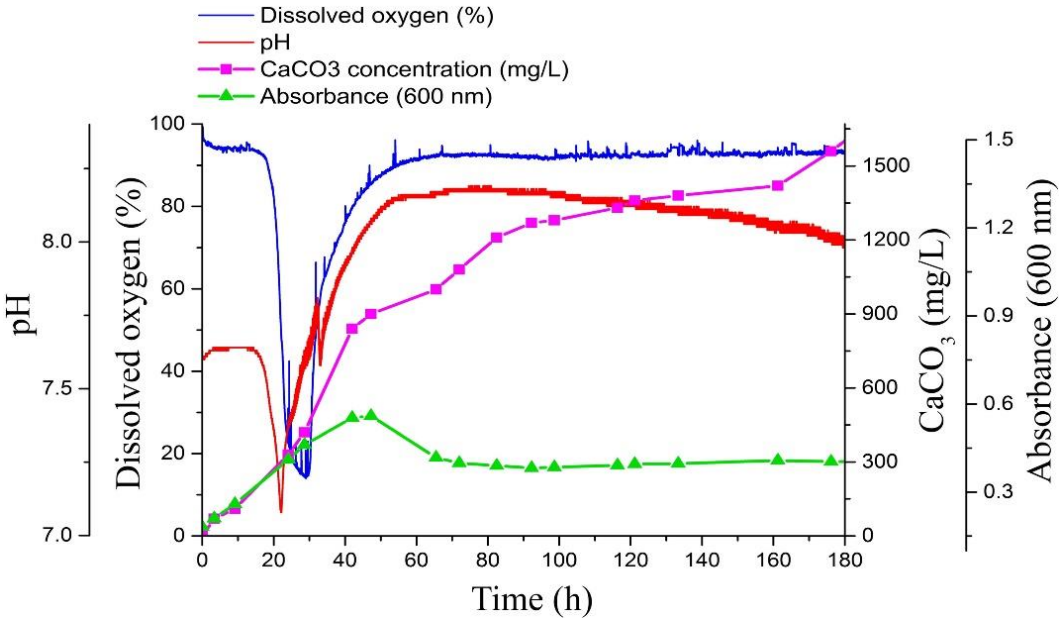

Figure 5-1 Variation in bacterial growth, DO, pH and $CaCO_3$ concentration over the course of uncontrolled-pH fermentation.

5.2.2 Aeration controlled batch fermentations

In the previous experiment, air flow rate was kept constant at 0.5 SLPM and the variations of DO, pH, bacterial growth, and $CaCO_3$ production were monitored. In this set of experiments, the effect of aeration on the bacterial cell growth and the production of $CaCO_3$ was investigated. It has been shown that the availability of a high level of CO_2 inhibits the bacterial metabolic activity and subsequently it leads to decrease the bio products' yield. Therefore to minimize the inhibitory effects and also increase the availability of oxygen in the media, the maximum aeration rate was set to 4.5 SLPM. The increase of airflow rate resulted in a massive foam formation during experiment runs. Therefore a sterilized solution of antifoam agent was pumped into the vessel to alleviate the foam.

The analysis of variance (ANOVA) with the confidence level of 95% was conducted to determine whether the aeration has a significant contribution on the yield. As shown in Table 5-1, fermentation runs were performed at four aeration rates of 0.5, 1.5, 2.5 and 4.5 SLPM. It was observed that the higher aeration rate was in favor of $CaCO_3$ precipitation. The *p*-value of 0.003 indicates the addition of oxygen during fermentation has a significant impact on the yield (Table 5-2).

Table 5-1 Experimental conditions and results for the aeration controlled batch fermentations.

Run	Aeration (SLPM)	$CaCO_3$ concentration (mg/L)	SD	Cell concentration (CFU/mL)	SD	Yield ($\times 10^{-8}$ mg $CaCO_3$ /cell)
1	0.5	1655.82	359.49	11.9×10^6	4.2×10^5	13.92
2	1.5	3194.40	289.57	21.8×10^6	1.8×10^6	14.63
3	2.5	5473.29	326.87	29.0×10^6	2.8×10^6	18.87
4	4.5	7099.14	336.41	32.0×10^6	1.4×10^6	22.19

SD: Standard deviation

As compared to the fermentation at 0.5 SLPM, the increase in aeration rate to 1.5-2.5 SLPM resulted in an increase in the $CaCO_3$ yield (*p*-value <0.05). Although the increase of airflow to its upper level (4.5 SLPM) had a positive effect on the $CaCO_3$ yield, its contribution was not significant as compared to 2.5 SLPM airflow. It should be pointed out that the similar profiles for DO were observed for all aeration rates over the course of fermentation. The DO concentration began to decrease at all aeration levels, followed by a gradual increase and reaching a plateau.

Table 5-2 Analysis of variance showing the significance of aeration on the bacterial production of $CaCO_3$ (yield).

Source of Variation	*SS*	*DF*	*MS*	*F-value*	*p-value*	*F crit.*
Between Groups	7.36448×10^{-15}	3	2.45483×10^{-15}	32.192	0.003	6.591
Within Groups	3.05017×10^{-16}	4	7.62542×10^{-17}	-	-	-
Total	7.6695×10^{-15}	7	-	-	-	-

DF: degree of freedom, *SS:* sum of squares, *MS*: mean sum of squares, *F crit.*: F critical value

Figure 5-2 shows the concentration of soluble Ca^{2+} during aeration controlled batch fermentations. The results indicate that the majority of insoluble Ca^{2+} was induced during 80 h of fermentation. The possibility of $CaCO_3$ precipitation was also tested in the absence of cells as negative control. In this case, the fermentor was inoculated with no bacteria and the result shows no precipitation took place during the fermentation.

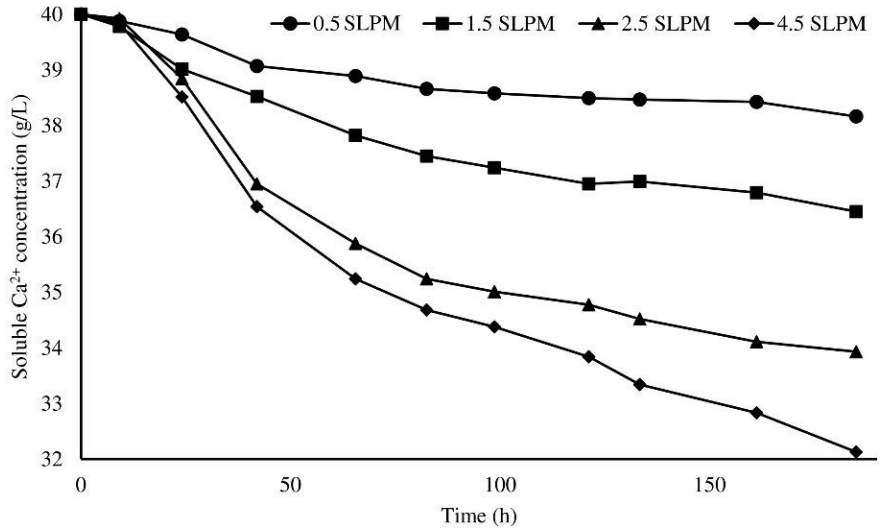

Figure 5-2 Soluble Ca^{2+} ion concentration as a function of time at aeration controlled fermentation runs.

5.2.3 Controlled-pH batch fermentations

The effect of pH on the bacterial production of $CaCO_3$ and the total cell concentration were investigated in the controlled-pH batch fermentations. The

preliminary testing disclosed that the increase of pH is in favor of microbial $CaCO_3$ production; however, the extent of that requirement is uncertain. In this case, fermentation runs were conducted at pH 9, 10, 11 and 12, and the responses (i.e., $CaCO_3$, cell concentration and yield) were determined at the end of fermentation. The experimental conditions and results for controlled- pH batches are summarized in Table 5-3.

Table 5-3 Experimental conditions and results for controlled-pH batch fermentations.

Run	pH	$CaCO_3$ concentration (mg/L)	SD	Cell concentration (CFU/mL)	SD	Yield ($\times 10^{-5}$ mg $CaCO_3$/cell)
1	9	5345.24	316.60	85.00×10^3	4.2×10^3	6.29
2	10	7315.33	347.59	33.15×10^3	1.2×10^3	22.06
3	11	8051.23	375.83	27.20×10^3	2.8×10^3	29.60
4	12	10511.92	324.91	6.80×10^3	5.6×10^2	154.59

SD: Standard deviation

It was found that the bacteria could tolerate in the highest pH; however, the cell viability decreased when the pH increased. The results indicate that the viability of bacteria in medium with the pH of 10 decreased by 2.5-fold as compared to pH 9. The least decline in the cell concentration was noticed when the pH of the medium increased from 10 to 11. Total cell concentration in the medium with the pH 11 was only 80% of the counterpart in the pH 10. The comparison of the cell concentration during various pH fermentations exhibited that the maximum drop in cell viability occurred at the pH of 12. Interestingly, the experimental results show the selected $CaCO_3$ producing bacteria are able to survive at pH 12 with the final cell concentration of 6.8×10^3 CFU/mL.

Table 5-4 Analysis of variance showing the significance of pH level on the bacterial production of $CaCO_3$ (yield).

Source of Variation	*SS*	*DF*	*MS*	*F-value*	*p-value*	*F crit.*
Between Groups	3.2527×10^{-6}	4	8.1353×10^{-7}	225862	<0.001	5.1921
Within Groups	1.8009×10^{-11}	5	3.6019×10^{-12}	-	-	-
Total	3.2541×10^{-6}	9	-	-	-	-

DF: degree of freedom, *SS:* sum of squares, *MS*: mean sum of squares, *F crit.*: F critical value

Apart from the viability of bacteria in alkaline conditions, the ability to produce $CaCO_3$ in different pH ranges was investigated. The concentration of precipitated $CaCO_3$ during different pH conditions is displayed in Table 5-3. The results show that the concentration of $CaCO_3$ increased when pH increased. The maximum concentration of $CaCO_3$ achieved at pH of 12, while the least $CaCO_3$ precipitation obtained when the pH was adjusted to 9. Moreover, it was found that the bacterial production of $CaCO_3$ in the medium with pH 9 was 3.2-times higher than the uncontrolled-pH. Similar observations were noticed when the pH of the medium was altered to 10, 11 and 12. The fermentation experiment under the pH of 10 led to induce 37% higher $CaCO_3$ precipitation than the pH of 9. However, only 10% increase in $CaCO_3$ precipitation was achieved when the pH of medium changed from 10 to 11. According to the controlled-pH runs, the highest increase in $CaCO_3$ concentration was obtained at pH 12. In this condition, a 6.4-fold increase in total induced $CaCO_3$ precipitation was achieved. The concentrations of soluble Ca^{2+} during controlled-pH fermentation experiments are shown in Figure 5-3. The results obtained by negative control indicate that no $CaCO_3$ precipitation was induced during the fermentation with no bacterial inoculation. Although a decline in the cell concentration was observed when the pH increased, the bacterial production of $CaCO_3$ was increased. As given in Table 5-4, the *p-value* of <0.001 indicates the higher pH value is favorable for the bacterial production of $CaCO_3$ yield. The ANOVA results also show a high value for *F* in comparison to the upper critical *F*-value at 5% significant level. This indicates the experimental results were in a high level of validity.

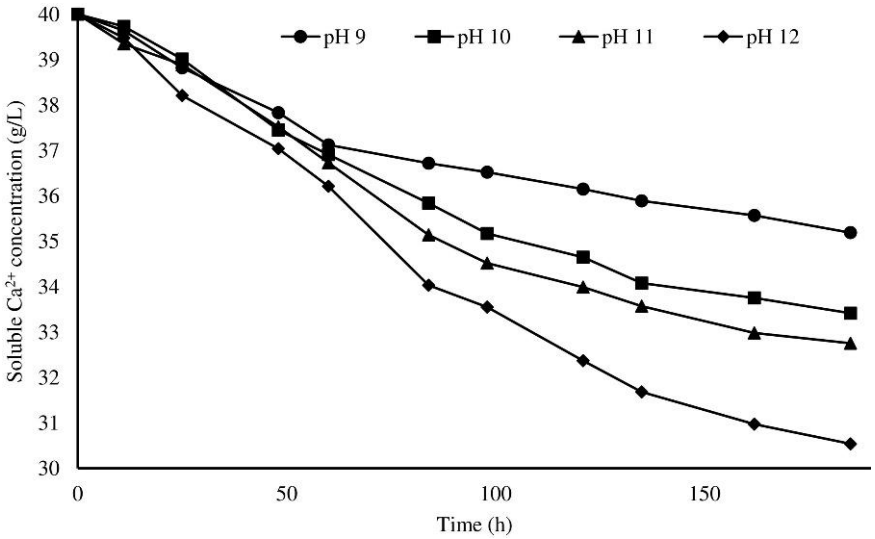

Figure 5-3 Soluble Ca^{2+} ion concentration as a function of time at controlled-pH fermentation runs.

5.2.4 Morphological analysis of produced $CaCO_3$ crystals

Image analysis was performed using SEM to study the morphological characteristics of produced biominerals. The SEM micrographs of bioprecipitates illustrate the variety of shapes and sizes that can be formed when the pH and aeration rate are changed. The SEM micrographs of biominerals produced at different aeration levels are depicted in Figure 5-4. Figure 5-4a–b show the presence of $CaCO_3$ polymorphs during fermentation at airflow rates of 0.5 SLPM and 1.5 SLPM, respectively. An assemblage of bio-precipitates induced at 2.5 SLPM airflow rate is displayed in Figure 5-4c. As shown in Figure 5-4d, similar morphology was observed for precipitated $CaCO_3$ by selected isolates at the highest aeration rate (4.5 SLPM).

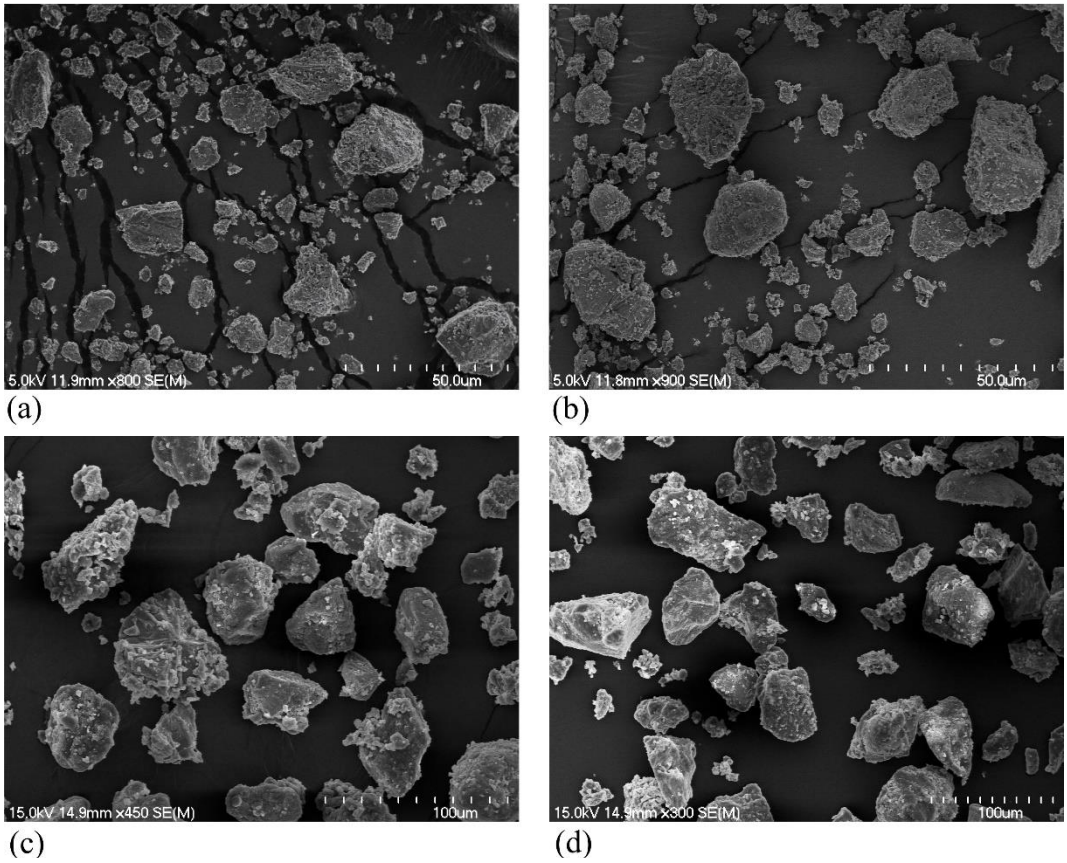

Figure 5-4 SEM micrographs of $CaCO_3$ produced during fermentation at: a) 0.5 SLPM, b) 1.5 SLPM, c) 2.5 SLPM and d) 4.5 SLPM.

Interestingly, Figure 5-5a–b depicts the imprints of bacterial cells on the surface of the biominerals. This indicates the attachment of Ca^{2+} ions to the negatively charged bacterial cell walls, and then bacterial escaping during biomineralization were accomplished to induce $CaCO_3$ crystals.

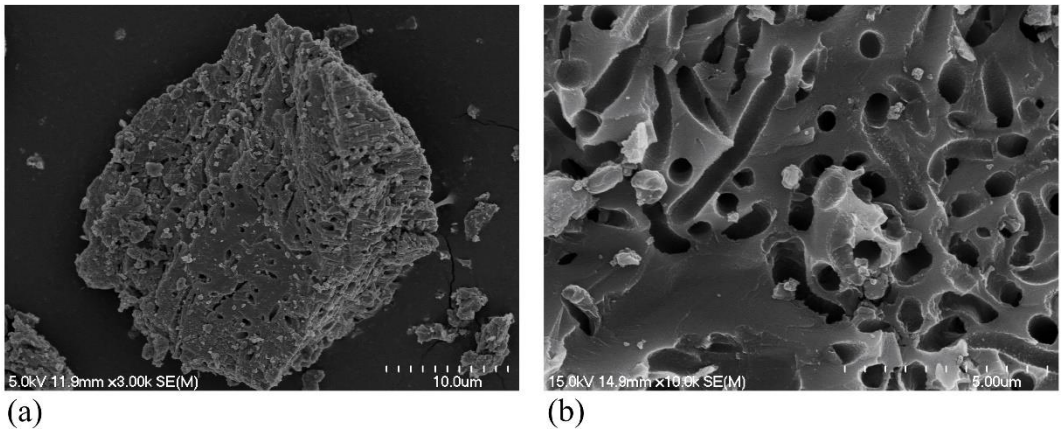

Figure 5-5 SEM micrographs showing the presence of bacterial imprints on the precipitated crystals at: a) 2.5 SLPM and b) 4.5 SLPM.

The morphological observation was also performed for the precipitated biominerals at the controlled-pH fermentation runs. Figure 5-6a–d demonstrates the effect of pH on the shape and size of bio-precipitates. The SEM images illustrate the precipitated minerals were mainly between 10 µm and 20 µm.

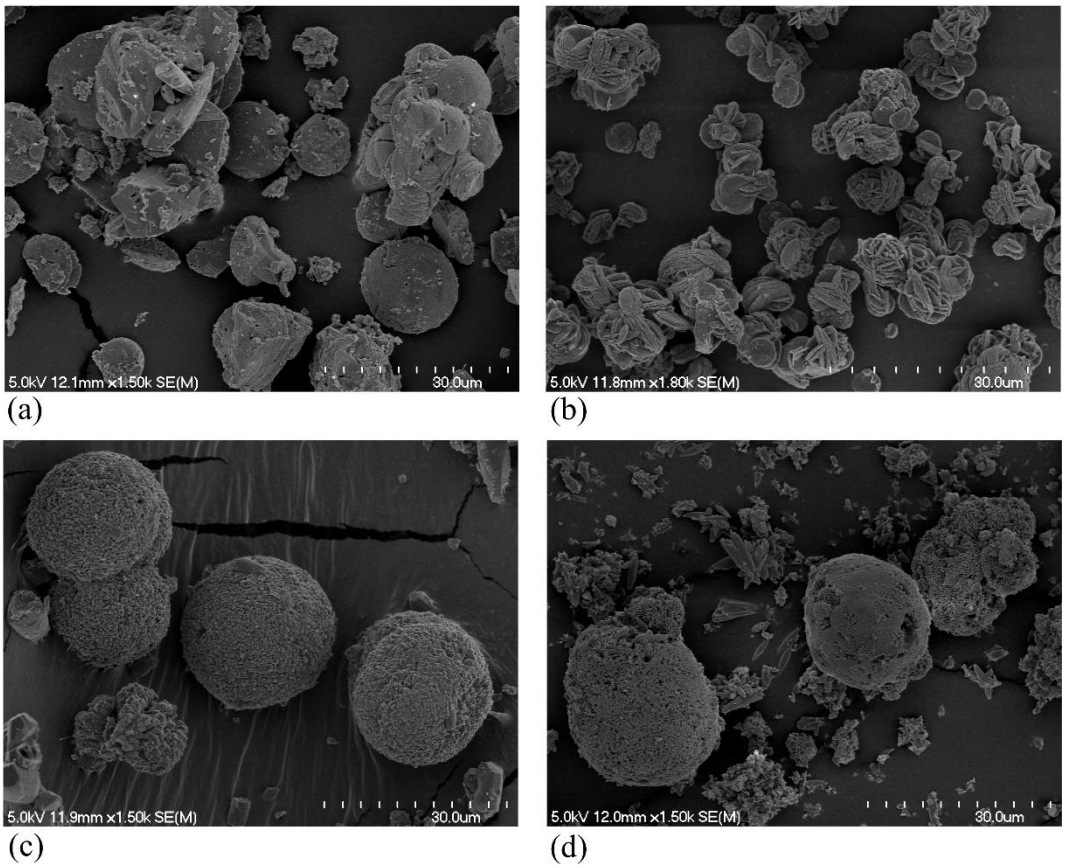

Figure 5-6 SEM micrographs of $CaCO_3$ produced during controlled-pH fermentations at pH of: a) 9, b) 10, c) 11 and d) 12.

Despite the similarity in the shape of precipitated $CaCO_3$ crystals in controlled-pH batches, different degrees of porosities and crystal surface textures were observed. In general, the bio-precipitates became rough and porous as the pH was increased. A distinct surface morphology was observed during the course of fermentation at a pH of more than 10. Figure 5-7a–b demonstrates the magnified polycrystal surfaces induced at pH 10 and 12, respectively. The fermentation process at pH 10 led to precipitate spherical particles composed of compact layers, while the crystal observation at pH 12 was completely different from those particles

observed at a lower pH. Most strikingly, the surface of the bio-precipitates deposited at pH 12 was highly rough and composed of randomly rhombohedral oriented particles with a size of 0.2–0.4 µm.

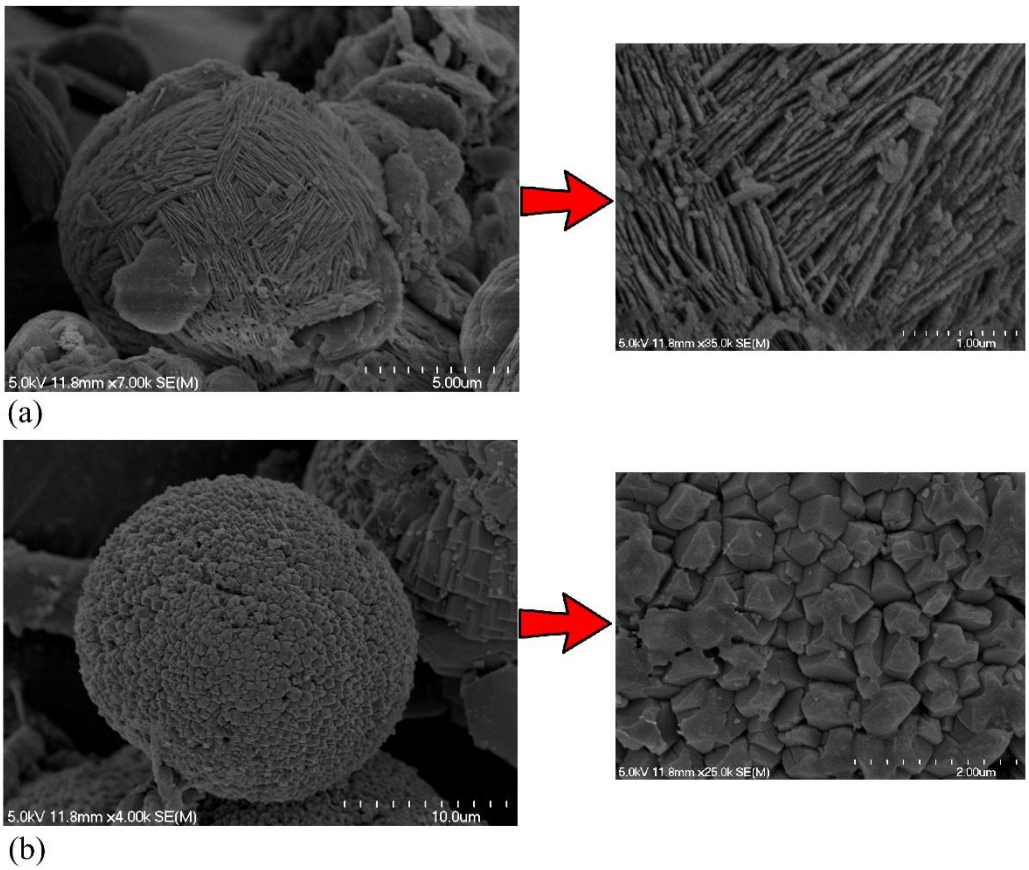

Figure 5-7 SEM micrographs showing the surface structure and texture of crystals precipitated at pH of: a) 10 and b) 12.

Elemental composition analysis was conducted using EDS at 15.0 keV to determine the elements presented in the bio-precipitates. The elements were detected and quantified based on the intensity of peaks. The EDS analysis was performed for the deposited crystals during aeration controlled and controlled-pH fermentation runs. As shown in Figure 5-8, EDS analysis was also conducted for pure $CaCO_3$ to compare with the spectra obtained during fermentations.

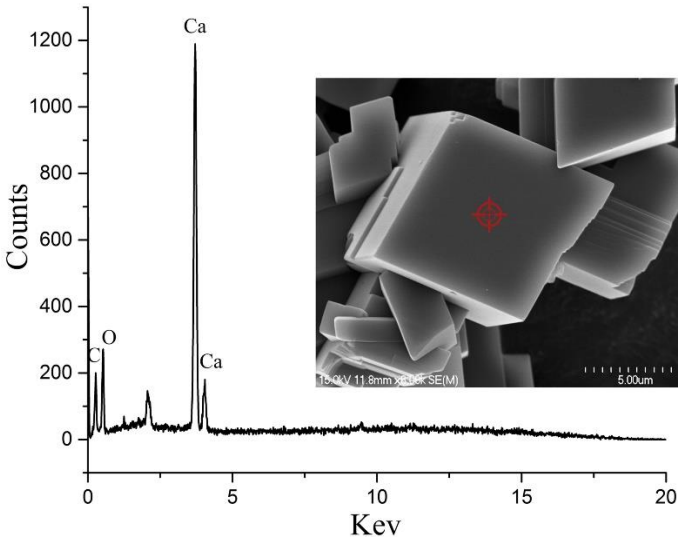

Figure 5-8 EDS spectra for the pure $CaCO_3$ crystal.

Figure 5-9 and Figure 5-10 represent the EDS spectra for the precipitated crystals during the fermentation at aeration controlled and controlled-pH, respectively. The EDS analysis indicated that calcium, carbon, and oxygen were the most abundant elements existing in bio-precipitates. The production of $CaCO_3$ by bacteria was also confirmed by the comparison between EDS spectra obtained from pure $CaCO_3$ and the crystals precipitated in batch fermentation runs. A high degree of similarity between pure $CaCO_3$ crystals spectrum and those precipitated in different pH media and aeration levels confirmed the biominerals were $CaCO_3$.

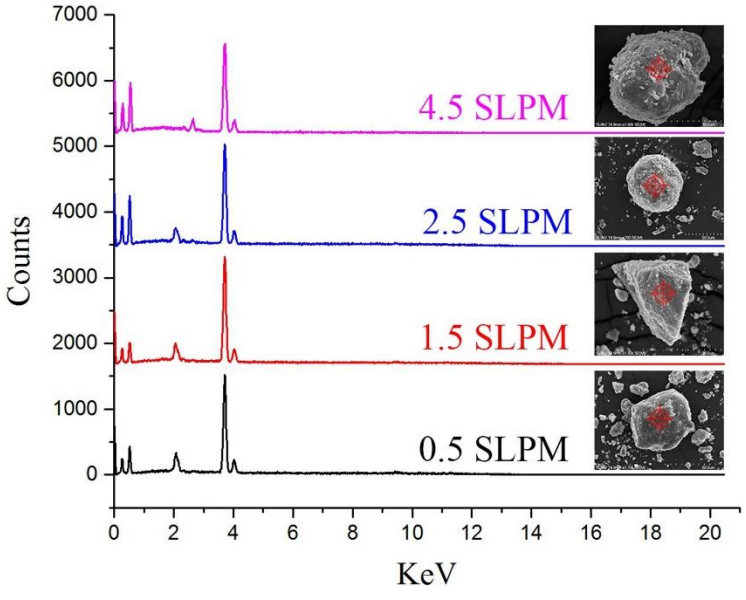

Figure 5-9 EDS spectra of precipitates over aeration controlled fermentations.

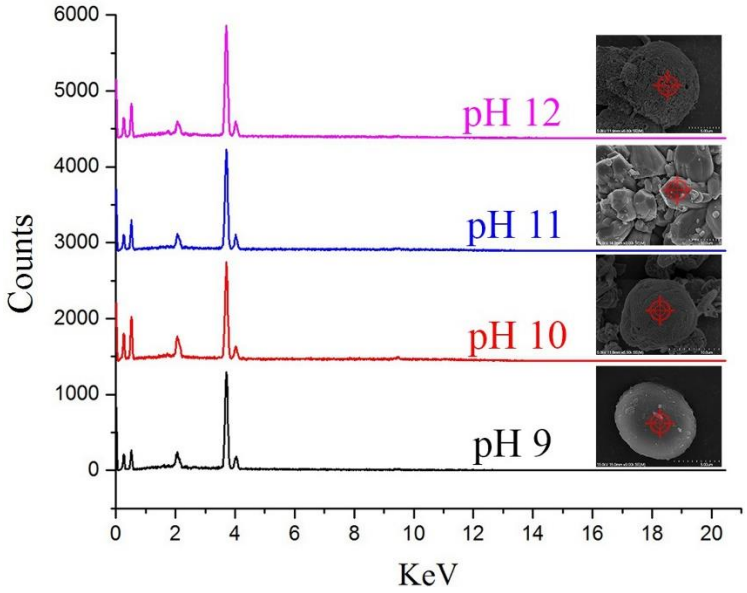

Figure 5-10 EDS spectra of precipitates over controlled-pH fermentations.

5.2.5 Structural characterization of produced $CaCO_3$ crystals

In all cases, precipitated biominerals were characterized by XRD to confirm the precipitation of $CaCO_3$ and determine the presence of polymorphs (calcite, vaterite, and aragonite) in the bio-precipitates. Figure 5-11 and Figure 5-12 demonstrate XRD spectra for induced $CaCO_3$ particles during aeration and controlled-pH fermentation experiments, respectively.

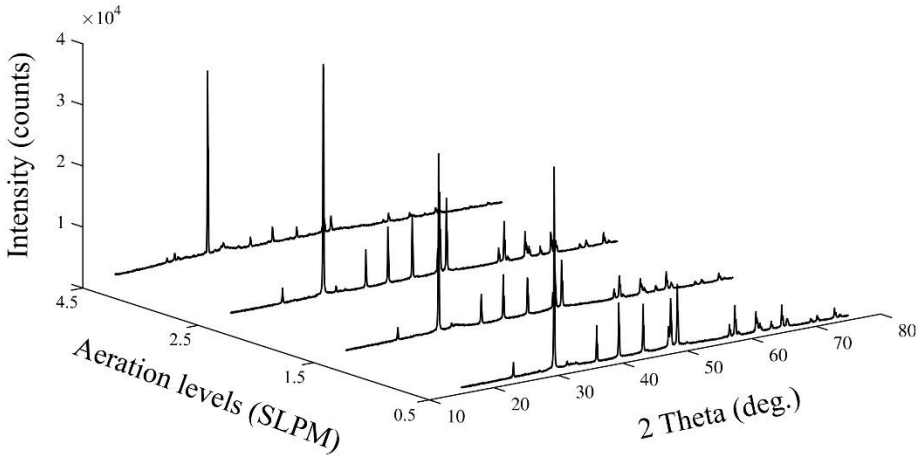

Figure 5-11 XRD spectra for the crystals precipitated over aeration controlled batch fermentations.

As shown in Figure 5-11, the most intensive peaks occurred at the angles of 27.1° and 29.3°, indicating the majority of crystals formed during aeration controlled batch fermentations were vaterite and calcite. As expected, no mineralogical changes were detected following the introduction of different aeration rates into the fermentor. However, pH was found to be a significant factor on changing the $CaCO_3$ morphology (Figure 5-12). The results indicate that the increase of pH to 10 led to precipitate a higher portion of vaterite, while the further increase of pH resulted in more calcite precipitation. Therefore it can be concluded that the most transformation of vaterite to calcite occurs at pH 10–11.

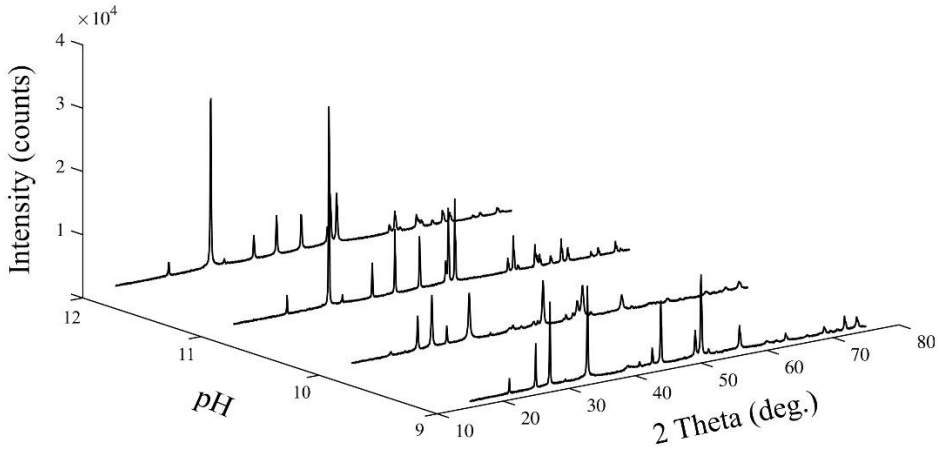

Figure 5-12 XRD spectra for the crystals precipitated over controlled pH batch fermentations.

5.3 Discussion

A diverse mineralization of crystals by bacteria have been comprehensively documented. The majority of investigations have been focused on the possibilities and mechanisms of producing minerals by bacteria in nature. However, the bacterial viability, metabolism and efficiency to induce biominerals are affected by medium composition, the availability of nucleation site, oxygen and pH [54]. In the previous chapter, the optimum concentration of nutritional compounds and inoculum as nucleation site were determined to maximize the production of $CaCO_3$. However, the effectiveness of bacterial compound (i.e., bacteria and nutrient) to induce $CaCO_3$ precipitation in the concrete matrix strictly relies on pH and availability of

oxygen [169]. Therefore this chapter investigates the effect of aeration and pH on the bacterial production of $CaCO_3$.

A real-time on-line monitoring of the effective factors on biomineralization of $CaCO_3$ in a bioreactor indeed helps to gain a comprehensive understanding of the biomineralization process. An uncontrolled-pH batch fermentation at the aeration rate of 0.5 SLPM was performed to observe the bacterial growth, $CaCO_3$ precipitation, and variation of pH and DO over the course of fermentation. During the first 18 h of fermentation no visible accumulations of inorganic material on the bacterial cell surfaces was observed. However, after 18 h, $CaCO_3$ crystals start to form and the turbidity increased. As depicted in Figure 5-1, the highest rate of $CaCO_3$ precipitation was obtained during the exponential bacterial growth phase. This might be due to the presence of abundant nucleation sites at exponential growth phase where the bacteria start to divide asexually by binary fission. Despite the precipitation of $CaCO_3$ during the prolonged stationary phase, its rate was considerably lower than the exponential phase. The decrease in $CaCO_3$ precipitation is attributed to the nutrient starvation and accumulation of toxic products of catabolism leading to a significant decline in the number of viable cells. These results confirm the significant contribution of viable bacterial cells as the nucleation site in the bioprecipitation of $CaCO_3$.

The consumption of oxygen by bacteria was evident during the fermentation, and this indicates that the bacteria require oxygen for the growth and, consequently, $CaCO_3$ production. As is shown in Figure 5-1, following inoculation, the concentration of DO in the bioreactor began to decrease until the end of exponential growth and then increased. This illustrates that the maximum oxygen uptake took place in the initial phase of the fermentation process.

5.3.1 Aeration controlled batch fermentations

Aeration and agitation are involved in different extent in overall mass and oxygen transfers in the fermentation process. Aeration provides oxygen to the bacteria and has a significant effect on the bulk mixing of the fermentation fluid, while agitation contributes to the distribution of nutrient and oxygen in the medium. DO has a low

solubility in the fermentation medium, while bacteria require it for growth, and enhancing the metabolic activity and yield. It is known that the metabolic pathway and the metabolic fluxes can be affected by oxygen transfer rate. Some bioprocesses demand a high oxygen transfer rate condition, while others require a controlled oxygen transfer rate in order to regulate oxygen uptake rate [172]. The effect of oxygen on the microbial growth and bioproduct has been previously documented. For instance, Zhang et al. [173] reported that the provision of oxygen supply can enhance the bacterial precipitation of $CaCO_3$. The same observation was noticed by Wang et al. [79] and Ramachandran et al. [174]. They examined the possibility of $CaCO_3$ precipitation in different parts of the concrete specimen. Their results demonstrate that the precipitates mostly concentrate in those areas where oxygen is sufficiently available.

For an efficient bacterial production of $CaCO_3$, it is important to keep the oxygen level at the optimum rate throughout the fermentation. The result obtained during fermentation show that the production of $CaCO_3$ can be enhanced if a sufficient amount of oxygen is available in the media. Overall, the *p*-value less than 0.05 indicates the significant effect of aeration on the bacterial growth, metabolic activity and $CaCO_3$ precipitation. Data demonstrate the higher aeration rate results in an increase in both $CaCO_3$ and cell concentration. High and low DO concentrations have a significant impact on the bacterial growth. Statistical analysis showed that there was no significant increase in the yield when the aeration rate increased from 0.5 SLPM to 1.5 SLPM. This might be attributed to the provision of an inadequate supply of oxygen into the fermentor to robust bacterial growth, increase the nucleation sites, and bacterial production of $CaCO_3$. Conversely, a significant increase in the bacterial yield was obtained when the airflow increased to 2.5 SLPM. In comparison to 0.5 SLPM airflow, higher growth was observed when a 2.5 SLPM aeration was used. Well-distribution and transportation of nutrients to the cells and adequate supply of oxygen for germination are the main reasons for increasing the yield.

Despite the increase of yield at 4.5 SLPM airflow, the statistical analysis displayed no significant improvement in the yield as compared to 2.5 SLPM. Although the concentration of $CaCO_3$ was increased when the aeration increased from 2.5 SLPM to 4.5 SLPM, the number of cells was not substantially enhanced.

This is attributed to maintaining DO concentration greater than its critical level. In this stage of the study, it was shown that the production of $CaCO_3$ is evidently correlated with the aeration rate. Since the provision of oxygen is required for bacterial germination, metabolism, and $CaCO_3$ precipitation, the utilization of oxygen releasing compounds is suggested to compensate for the lack of oxygen.

5.3.2 Controlled-pH batch fermentations

Another factor affecting the performance of bacteria to induce $CaCO_3$ precipitation is the medium pH. The preliminary study showed a pH variation during the fermentation of $CaCO_3$ which is due to factors including (i) NH_3(g) dissolution, (ii) CO_2(g) dissolution, and (iii) acid generation during the bacterial production of $CaCO_3$ [175, 176]. Based on the results, pH dropped from 7.6 to 7.2 at the beginning of fermentation due to the increased respiration, leading to enrichment in CO_2 and, consequently, acidifying the surrounding [177]. However, after 21 h of fermentation, bacteria maintained robust growth in exponential phase which resulted in releasing more NH_4^+ and, subsequently, pH was increased to 8.2 (Eqs. 5-1 to 5-3). According to Eq. 5-1 the hydrolysis of one mL of urea by bacteria generates one mole of NH_3 and NH_2COOH. As can be seen from Eq. 5-2, simultaneously one extra mole of NH_3 is produced from hydrolysis of NH_2COOH. The production of OH^- from the reaction between NH_3 and H_2O results in an increase in pH which favors $CaCO_3$ precipitation (Eq. 5-3) [67, 70].

$$CO(NH_2)_2 + H_2O \rightarrow NH_2COOH + NH_3 \quad (5\text{-}1)$$

$$NH_2COOH + H_2O \rightarrow NH_3 + H_2CO_3 \quad (5\text{-}2)$$

$$2NH_3 + 2H_2O \rightarrow 2NH_4^+ + 2OH^- \quad (5\text{-}3)$$

The results indicate that a greater rate of $CaCO_3$ precipitation was induced when the pH was increasing over the uncontrolled-pH fermentation process. Since the bacterial production of $CaCO_3$ is used in different environmental conditions, it is important to investigate the effect of pH on the efficiency of the biomineralization process. Controlled-pH batch fermentations were performed at different pH levels

to identify the effect of alkalinity on the viability and capability of producing $CaCO_3$ crystal. To simulate the concrete pH, the highest level of alkalinity was set to 12. To keep the pH constant over the course of fermentation, a proportional-integral-derivative (PID) controller was used.

The effect of pH on bacterial growth and mineral precipitation has been reported in the literature. Kaur et al. [178] isolated bacteria from calcareous soil (pH 11) and determined the ability of the isolates to induce $CaCO_3$ precipitation. It was found that some of the isolates, including *B. megaterium* and *B. cereus*, can grow in a pH range of 6.5 to 11.5, while the other isolates (*B. thuringiensis*, *B. subtilis* and *L. fusiformis*) were able to survive at a pH range of 6–10. In another investigation Kim et al. [170] tested different bacterial strains onto Difco nutrient broth with a pH of 11 to determine whether they were capable of growing in alkaline conditions. The colonies that were able to grow in these conditions were considered as possible $CaCO_3$-precipitating isolates. Among the isolates it was found that only *Sporosarcina sp* and *Bacillus sp* were capable of growing in such an alkaline environment. In general, bacterial cells are quickly adapting to environmental conditions at a lower pH by showing a shorter lag phase. However, their viabilities decrease with the increase of the alkalinity. This reduction is attributed to the inhibitory effect of alkalinity, which causes a prolonged lag in growth [179].The cells are highly sensitive to external pH; however, the selected bacteria are well adapted to grow in alkaline conditions, enabling them to induce precipitating $CaCO_3$ at high pH levels. The results disclose that the inoculation of bacteria in a higher pH medium has a negative effect on the cell viability. As the pH was increased, the number of cells decreased and reached its lowest value at a pH of 12, but still remained viable at concrete's pH. This proves the selected isolates are able to survive in more extreme pHs following a decrease in the number of the cells.

Although viability of bacteria in an alkaline environment is critical, the capability of producing $CaCO_3$ by bacteria in such a harsh condition is another important parameter to be considered. In contrast to viability, a higher pH was found to be significant in the production of $CaCO_3$. The higher precipitation of $CaCO_3$ at the higher level of pH might be due to the production of more enzyme which facilitates the generation of CO_3^{2-} and, consequently, more $CaCO_3$ crystals are induced. It has been stated that urease enzyme activities depend on pH value [68, 180]. More

urease released in the medium results in more production of CO_3^{2-}. Carbonate tends to dissolve in the medium at low pH levels rather than precipitate [181]. Therefore $CaCO_3$ precipitation is increased as the pH level in the medium is increased. In general, the soluble Ca^{2+} ion concentration shows a decreasing trend indicating the precipitation of $CaCO_3$ during time. The same trend was observed for the concentration of soluble Ca^{2+} ion when the pH increased. However, the rate of $CaCO_3$ precipitation was decreased with the increase in fermentation time. This might be due to the reduction in the number of viable cells in the medium.

Despite the decline in the cell viability, the ANOVA results indicate the increase of pH is effective to increase the yield. The same trend was also stated where the optimum medium showed the highest urease activity and $CaCO_3$ precipitation efficiency, but lower growth rate [180]. The comparison was made between each pair of batch results and it was concluded that pH 12 has the most significant influence on the yield. The controlled-pH fermentation experiments disclose that the selected isolates are alkali tolerant and their ability to induce $CaCO_3$ enhances with the increase of pH.

5.3.3 Morphological observation

Physical and chemical characteristics of $CaCO_3$ precipitates, such as crystal size, specific surface area, morphology, purity, and brightness, are the main criteria that are usually considered to be used in different industrial applications. Physical properties of $CaCO_3$, including density, solubility and hardness, largely depends on the percentage of each polymorph (i.e. calcite, vaterite and aragonite). Calcite and aragonite are the two most dominant $CaCO_3$ polymorphs precipitated in nature, while vaterite is the other anhydrous $CaCO_3$ polymorph that rarely occurs in nature. Morphological analysis using SEM is a common technique to evaluate the crystal properties and perform an elemental chemical analysis. Different saturation levels during mineralization leads to precipitate various $CaCO_3$ crystalline polymorphs. Furthermore, bacteria metabolic activities, cell surface characteristics, fermentation medium compositions, and the concentration of EPS are attributed to the production of different morphologies.

The fermentative $CaCO_3$ crystals induced in the aeration controlled batches displayed different morphologies from those formed in the controlled-pH batches. Most of the precipitated crystals in aeration controlled fermentation runs were a combination of egg-shaped or irregular shape, while the produced biominerals in controlled-pH runs were predominately regular spherical or egg-shaped at a lower alkalinity condition. It was also noticed that no aragonite crystals are precipitated over both fermentation stages. The formation of calcite attributed to the presence of EPS in the medium which inhibits vaterite precipitation and this can be used to biosynthesize the high-ordered $CaCO_3$ morphologies. The presence of rod-shape gaps (bacterial imprints) on the surface of bio-precipitates (Figure 5-5) implies the linkage between biomineralization and bacteria as nucleation sites allowing the Ca^{2+} ions to attach to a negatively charged cell wall.

$CaCO_3$ polymorphism and morphology can also be affected by abiotic factors. It has been reported that the pH not only facilitates the formation of $CaCO_3$ but it also has an influence on the morphology of $CaCO_3$ [182, 183]. Unlike the biominerals precipitated during aeration controlled batches, vaterite particles were found the predominant polymorphs at pH 9–10. This indicates that the pH has a regulatory effect on the morphology of the precipitated $CaCO_3$ crystals. The increase in pH from neutral to alkaline (up to pH 10) is assumed to inhibit the transformation of vaterite to calcite. However, the release of dissolved organic carbon (DOC) from the EPS at a high pH complexes Ca^{2+} ions in solution, leading to change the saturation level in the bulk solution and facilitating the transformation of vaterite to calcite [184]. Interestingly, a transition was found in the surface structure of precipitated crystals during controlled-pH fermentation runs. The smooth surface of $CaCO_3$ crystals was deposited when the pH was fixed to 9, while the porous and rough particles were formed at higher pH fermentation. The crystals formed at a higher alkaline condition appeared more poorly ordered with rougher crystal faces. The decrease of the bacterial cell and organic macromolecules somewhat contributes to changing the surface structure from smooth to rough. A distinct surface morphology was also observed during the course of fermentation at a pH of more than 10. The polycrystals' formation at high pH condition may arise from the quick adsorption of Ca^{2+} ions at different interfaces over biosynthesis of $CaCO_3$.

The same crystal structure for the spherical vaterite particles was previously observed during lysozyme mediated $CaCO_3$ mineralization [185].

5.3.4 Crystal characterization

The structural analysis provides a unique insight into the mechanism of $CaCO_3$ precipitations. Therefore the $CaCO_3$ crystals precipitated during biomineralization was examined by XRD. Figure 5-11 demonstrates XRD spectra for induced $CaCO_3$ particles during aeration controlled batch fermentations where the angles of 29.3° and 27.1° represent calcite and vaterite, respectively. The consistent XRD spectra during aeration controlled fermentations shows that the aeration has no effect on the $CaCO_3$ morphology transformation. In contrast to aeration controlled batches, calcite found the least polymorph precipitated at pH 9 and 10. This might be due to the inhibitory effect of pH on the conversion of vaterite to calcite. However, vaterite crystals transformed to calcite at extreme pH (11–12), and the concentration of vaterite reached its lowest level at pH 12. The crystal transformation possibly caused by changing the ionization degree. Moreover, the ionic strength in the aqueous medium affects the $CaCO_3$ solubility and therefore different morphologies are precipitated.

5.4 Chapter summary

In this chapter we have clearly shown the effect of aeration and pH on the bacterial growth and $CaCO_3$ precipitation. The data obtained in uncontrolled-pH fermentations disclose that the sudden changes in DO concentration and pH are indicative of metabolic shifts and formation of $CaCO_3$, respectively. Aeration controlled fermentation data show that the higher aeration rate increases both bacterial growth and $CaCO_3$ production and the *p*-value of less than 0.05 indicates that the aeration has a significant effect on the yield. On the other hand, the increase in aeration rate to 4.5 SLPM was not significant as compared to 2.5 SLPM. It was found that the utilization of 2.5 SLPM airflow is the optimum rate of aeration to obtain the highest level of yield. The result obtained by SEM and XRD point out that the aeration rate has no effect on the $CaCO_3$ morphology, and calcite and

vaterite were found the predominant polymorph precipitated at aeration controlled batches.

Since the bacteria and nutrients are incorporated into the concrete matrix, the effect of pH on the bacterial production of $CaCO_3$ was also investigated. The fermentations at different pH levels (9–12) were performed and the results indicate that the increase of pH leads to a decline in cell viability. However, the same condition results in an increase of $CaCO_3$ precipitation. According to statistical analysis, pH has the positive effect on yield, and the highest level of yield is obtained in more alkaline conditions. In contrast to aeration controlled batches, a morphological transition was observed when a different pH was used. The lower pH (9–10) found to be favorable of vaterite precipitation, while a higher pH (10–12) resulted in a transformation of vaterite to calcite. Notably, the increase of pH changed the surface structure of bio-precipitates from smooth to rough. Higher magnification images of induced crystals at high alkalinity fermentation displayed that $CaCO_3$ structures are composed of an oriented aggregate of crystal.

To be able to induce $CaCO_3$ precipitation in concrete matrix, the bacteria require oxygen to germinate and initiate the biomineralization process. Therefore the presence of oxygen releasing compounds that generate a steady amount of oxygen may address the oxygen shortcoming for bacterial growth and $CaCO_3$ biosynthesis in oxygen-limiting conditions.

Chapter 6

Enhanced bacterially induced $CaCO_3$ precipitation in oxygen-limiting conditions [4]

[4] This chapter forms the basis of a research paper published in the Journal of Biocatalysis and Agricultural Biotechnology, as referenced below.

[186] **Seifan, M.**, Samani, A.K., and Berenjian, A. *A novel approach to accelerate bacterially induced calcium carbonate precipitation using oxygen releasing compounds (ORCs).* Biocatalysis and Agricultural Biotechnology, 2017. 12: p. 299-307.

6.1 Introduction

The experiments in the previous chapter were performed to investigate the effect of aeration on biomineralization of $CaCO_3$. It was found that, in addition to the nutritional components, the performance of a bio self-healing concrete and capability of producing $CaCO_3$ relied on the presence of oxygen. The fermentation results indicate that the aeration has a positive effect on bacterial growth and $CaCO_3$ concentration.

Despite the recent progress in designing a biotechnological protocol for the crack treatment, $CaCO_3$ precipitation can only occur on the surface areas of the concrete. Achal et al. [187] performed an investigation to determine the possibility of $CaCO_3$ production by *Bacillus* sp. in mortar samples. Their results show that the production of $CaCO_3$ was only limited to the outer parts of the specimen and biomineralization occurred up to 27.2 mm from the surface. In another investigation Rodriguez-Navarroet et al. [188] demonstrated the effect of $CaCO_3$ biomineralization using *Myxococcus xanthus* on deteriorated ornamental stone. Although the authors noted that the newly formed $CaCO_3$ crystals were strongly attached to the substrate, the biomineralization was limited to a depth of one hundred micrometers. Over recent years, X-ray computed tomography (X-ray µCT) recognizes a non-destructive technique in material sciences, particularly for porosity analysis. Wang et al. [79] employed X-ray µCT to prove the feasibility of bacterial incorporation as a promising approach for self-healing concrete. It was found that the amount of $CaCO_3$ precipitation decreases with the increase of the crack's depth. Despite the filling of surface cracks by a layer of $CaCO_3$, the crust cannot guarantee the concrete to be watertight, as this loose layer may be subjected to peeling over the concrete lifespan.

Considering the positive effect of oxygen on bacterial growth and $CaCO_3$ production, the lack of oxygen might be the reason to limit mineral precipitation inside the cracks and pores. To be industrially applicable, a prompt action is in demand to address the current problem associated with the bio-self-healing approach.

The successful utilization of oxygen releasing compounds (ORCs) has been reported for bioremediation applications, such as removal of contaminants

biodegradation from ground water [189] and saturated soil [83]. It is therefore believed that the use of ORCs can be a solution to address the shortage of oxygen in deeper parts of the concrete. ORCs are mainly composed of chemicals which liberate oxygen in the presence of water or moisture, and provide the molecular oxygen needed for the aerobic microbial metabolic activity. Once a crack occurs in concrete, water or moisture penetrate into the deepest parts of cracks enabling the ORCs to generate oxygen for bacterial germination and possibly $CaCO_3$ biosynthesis. However, a higher concentration of oxygen (more than critical level) has an inhibitory effect on $CaCO_3$ precipitation.

To enhance the performance of bio self-healing concrete, the incorporated healing agent should be able to fill the entire cracks and pores. Therefore the experiments in this chapter were performed to: (i) screen the effect of different ORCs on bacterially induced $CaCO_3$ precipitation and (ii) determine the critical level of ORCs to maximize the biosynthesis of $CaCO_3$ in oxygen-limiting conditions.

6.2 Results

6.2.1 ORCs and $CaCO_3$ precipitation

The effect of ORCs on bacterially induced $CaCO_3$ precipitation was determined at the screening stage. Primarily, laboratory study was conducted to identify the appropriate compositions and the concentration of ORCs. In this case, four different types of peroxide, namely calcium peroxide (CP), urea-hydrogen peroxide (UP), zinc peroxide (ZP), and magnesium peroxide (MP) were evaluated for their oxygen releasing ability. Figure 6-1 shows the effect of different ORCs on the bacterial production of $CaCO_3$. The results indicate that the highest $CaCO_3$ precipitation took place in the fermentation media containing UP and MP, whereas the addition of CP and ZP showed an inhibitory effect on the bacterial precipitation of $CaCO_3$. The highest concentration of $CaCO_3$ (33.85 g/L) was achieved when 6.67 mg/L of MP was added to the fermentation medium. However, the increase in MP dosage from 6.67 to 33.33 mg/L resulted in a 19% decline in the biomineralization of $CaCO_3$. A significant decrease (10-fold) in $CaCO_3$ precipitation was observed when the concentration of MP further increased to 46.47 mg/L. Contrariwise, there was no

significant difference in the amount of $CaCO_3$ precipitation when the fermented medium was supplemented with different dosages of UP. Based on the results, a 10-times increase in UP concentration only resulted in 5% decline in the biomineralization of $CaCO_3$.

The increase of CP concentration from 1.67 to 6.67 mg/L resulted in 65% decrease in $CaCO_3$ precipitation. Although the increase of CP concentration to 6.67 mg/L significantly decreased $CaCO_3$ production, it led to precipitate 15 times higher $CaCO_3$ precipitation than the same dosage of ZP. The highest inhibitory effect ORCs occurred when ZP was supplemented in the fermentation ingredient. The lowest concentration of ZP resulted in 7.8 times lower $CaCO_3$ precipitation comparing the same concentration of CP, and surprisingly the further increase of ZP concentration to 33.33 mg/L completely inhibited the biosynthesis.

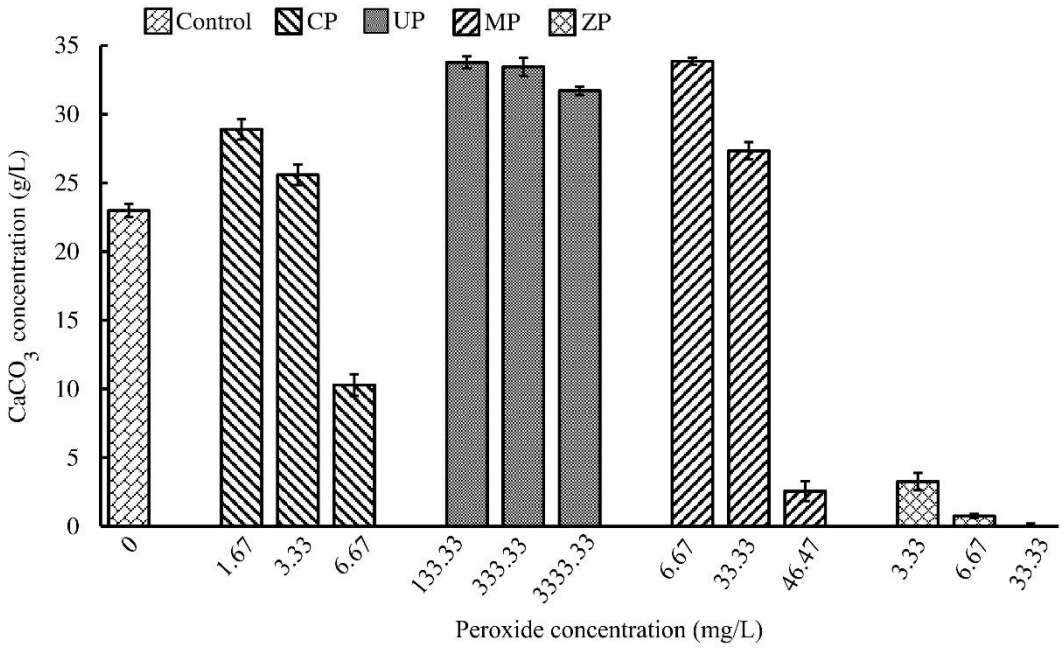

Figure 6-1 The effect of oxygen releasing compounds on bacterially induced $CaCO_3$ precipitation.

6.2.2 Optimization of significant ORCs using response surface methodology

It is particularly important to study the variables interaction at various concentrations, since toxicity is experienced by the cells, especially at a high concentration of peroxides. The screening study showed that CP and ZP significantly inhibited the bacterial precipitation of $CaCO_3$. Therefore UP and MP were selected for the optimization stage to further evaluate their effect on enhancing the bacterially induced $CaCO_3$ precipitation.

To enhance the $CaCO_3$ biosynthesis, the optimum concentrations of significant variables from the screening stage were determined using a RSM with a CCF design matrix. Table 6-1 presents the full experimental design with regard to their concentrations.

Table 6-1 Experimental conditions of the central composite face-centered (CCF) design and responses indicating both original and scaled factors.

Run	Factors [a]		Observed $CaCO_3$ (g/L)	Predicted $CaCO_3$ (g/L)
	X_1 (mg/L)	X_2 (mg/L)		
1	333.33 (-1)	6.67 (-1)	34.19	34.71
2	4333.33 (+1)	6.67 (-1)	34.39	33.32
3	333.33 (-1)	33.33 (+1)	4.08	5.92
4	4333.33 (+1)	33.33 (+1)	15.17	15.42
5	333.33 (-1)	20.00 (0)	33.49	31.12
6	4333.33 (+1)	20.00 (0)	34.26	35.18
7	2333.33 (0)	6.67 (-1)	34.36	34.91
8	2333.33 (0)	33.33 (+1)	13.66	11.57
9	2333.33 (0)	20.00 (0)	32.34	34.05
10	2333.33 (0)	20.00 (0)	34.19	34.05
11	2333.33 (0)	20.00 (0)	34.07	34.05

[a] Values are expressed as real and scaled levels, X_1 = Urea-hydrogen peroxide (UP) and X_2= Magnesium peroxide (MP)

The statistical analysis data containing the regression coefficients for the model are given in Table 6-2. The data obtained from RSM were then fitted via the response surface regression procedure using the second order polynomial equation. As shown in Eq. 6-1, the quadratic model for the bacterial precipitation of $CaCO_3$ was regressed for predicting the $CaCO_3$ precipitation as a function of significant peroxides (UP and MP).

$$Y = 34.05 + 2.03X_1 - 11.67X_2 - 0.89{X_1}^2 - 10.81{X_2}^2 + 2.72X_1X_2 \quad (6\text{-}1)$$

where Y, X_1 and X_2 are the predicted $CaCO_3$, UP and MP concentrations, respectively. The statistical analysis of the quadratic regression model shows that the model is highly significant (p-value < 0.000) with R^2 value of 0.985. The closer R^2 value to the unity results in a better empirical fit using the actual data. The R^2 value indicates that 98.5% of the sample variation for the response ($CaCO_3$) is explained by the independent variables, and this also implies that the model is not explained only 1.5% of sample variation. Based on the results, the linear interaction of variables is significant on the response, whereas the quadratic terms are found to be insignificant on $CaCO_3$ production.

Table 6-2 Statistical analysis from the central composite face-centered (CCF) design experiments.

Term	Coefficient	Standard error	*p-value*
Constant	34.05	0.99	3.95e-07
X_1	2.03	0.79	0.050
X_2	-11.67	0.79	2.56e-05
X_1^2	-0.89	1.22	0.494
X_2^2	-10.81	1.22	0.000
$X_1 X_2$	2.72	0.97	0.037

X_1: UP, X_2: MP, R^2=0.985, R^2(Adj.)=0.969 and Q^2=0.865

The statistical significance of the quadratic model was checked by *F*-test, and the results of ANOVA are listed in Table 6-3. The results indicate that the Fischer's *F*-test is highly significant (*p*-value < 0.000) for the regression. The model was further assessed for its suitability by examining the lack of fit, and the results show that the lack of fit is not significant for the model (*p*-value > 0.05). This indicates that there was only 16% chance that a lack of fit can occur due to the noise.

Table 6-3 Analysis of variance of the quadratic model for the central composite face-centered (CCF) design.

Source	DF	SS	MS	SD	*F*-value	*p*-value
Regression	5	1206.40	241.28	15.53	64.52	0.000
Residual	5	18.69	3.74	1.93	-	-
Lack of Fit	3	16.58	5.53	2.35	5.22	0.165
Pure error	2	2.12	1.06	1.03	-	-
Total corrected	10	1225.10	122.51	11.07	-	-

DF: degree of freedom, *SS*: sum of squares, *MS*: mean sum of squares, *SD*: standard deviation

6.2.3 Experimental verification

To determine the optimum level of ORCs, the regression equation was solved while remaining inside the experimental region. Figure 6-2 shows the contour curve plot indicating the experimental region to gain the highest concentration of $CaCO_3$.

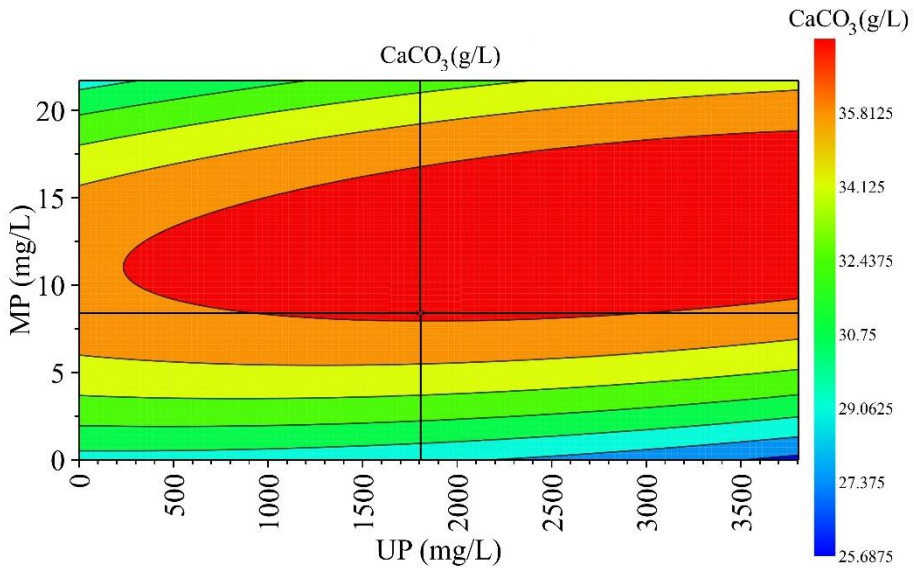

Figure 6-2 The review of the optimization; the contour curve plot of the optimum conditions to achieve the highest $CaCO_3$ precipitation.

Independent fermentation runs were carried out with the optimum levels of ORCs predicted by the model to verify the optimization results. The fermented medium was supplemented with the optimum concentrations of ORCs (1800 mg/L UP and 8.3 mg/L MP). The results indicate that the average value of $CaCO_3$ concentration obtained experimentally was only 4.5% lower than the predicted value of the model.

The variations of parametric factors on $CaCO_3$ biosynthesis in the optimum sample were checked and the results are shown in Figure 6-3 to Figure 6-4. The DO concentration was monitored during the fermentation to investigate the effect of ORCs on DO variation. The result in Figure 6-3 shows that the DO trend was consistent for the sample with ORCs and control experiments, while the DO level was significantly higher in the presence of ORCs than the control experiment. The concentration of DO started to decrease after 24 h of the fermentation period. After 48 h, the DO concentration rose and reached to a peak level. Overall, the addition of ORCs brought about 12.5% increase in DO concentration for the first 48 h of the fermentation, whereas the average level of DO was 3.3-times higher than the control run during the rest of the fermentation.

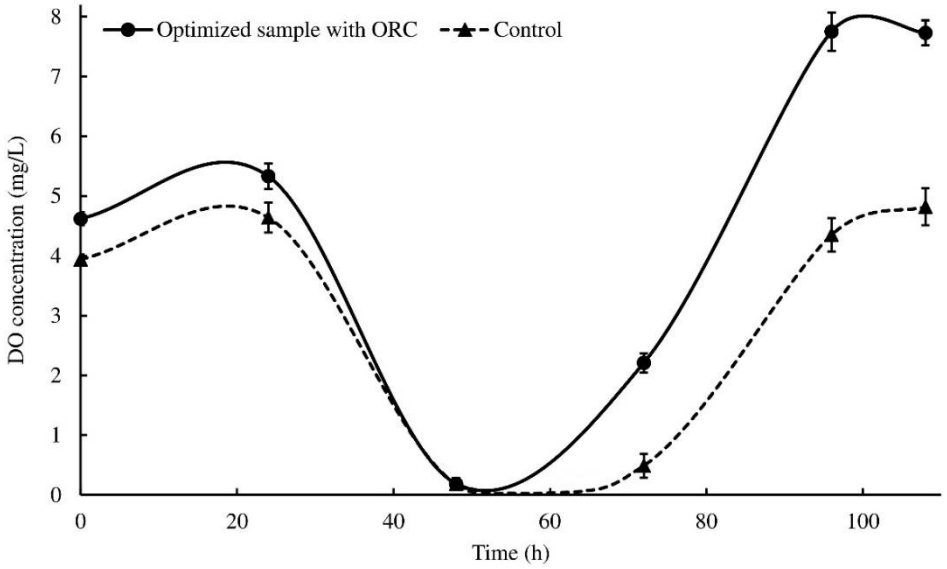

Figure 6-3 The variations of DO for the amended fermentation medium containing the optimum concentrations of selected ORCs.

The variation of pH was also monitored during the fermentation with ORCs, and the results are exhibited in Figure 6-4. The same strategy was noticed for the pH profiles in the presence of ORCs and control samples. However, the pH of control solution was higher than the medium supplemented with ORCs for the first 35 h of incubation. The pH profiles began to gradually decrease until 72 h, and followed an increase and reached the values of 8.51 and 8.10 for the sample containing ORCs and control, respectively. The results also disclose that the solution supplemented with ORCs had the higher pH after 35 h of fermentation as compared to the control sample. This might be attributed to the presence of ORCs which bring about a rise in pH by producing strong bases compounds, such as $Ca(OH)_2$ and $Mg(OH)_2$, which facilitates bacterial $CaCO_3$ precipitation.

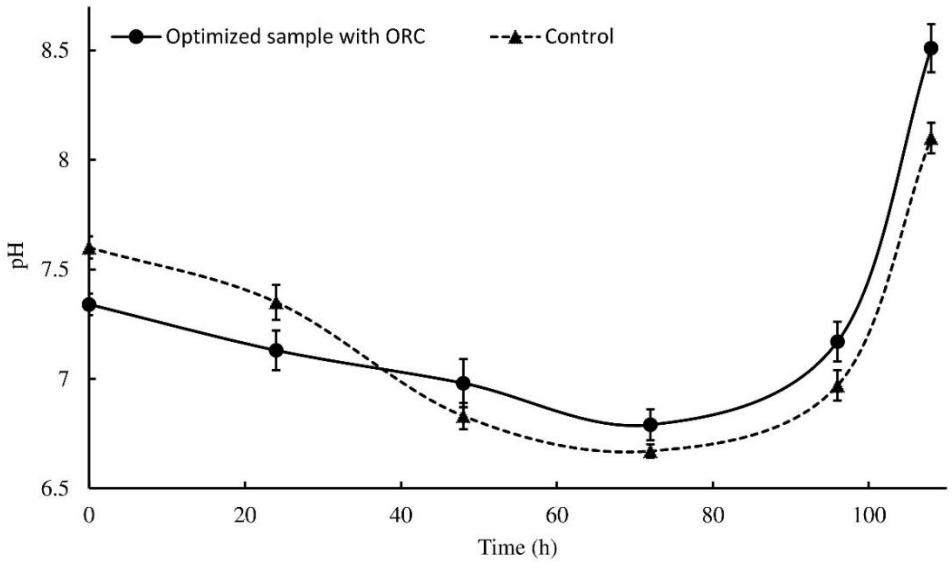

Figure 6-4 The variations of pH for the amended fermentation medium containing the optimum concentrations of selected ORCs.

6.2.4 Morphological observation

Crystal shapes of $CaCO_3$ particles are distinguishable by SEM. The morphology of $CaCO_3$ crystals is more complex in the enzymatic systems, and it can be affected by the presence of the enzyme. Sondi and Matijević [190] reported the regulatory effect of the enzyme on the morphology of the $CaCO_3$ crystals. Morphologies of the $CaCO_3$ crystals precipitated in the presence of various ORCs during the screening are presented in Figure 6-5 to Figure 6-8.

Based on the results obtained at screening study, it is visually confirmed that different shapes of crystals, including small rounded body and rhombohedral, were precipitated. As depicted in Figure 6-5 to Figure 6-7, the mixture of $CaCO_3$ particles consisting of vaterite and calcite was induced in the media containing MP, UP, and CP. However, as can be seen from Figure 6-8, the majority of crystals precipitated in the presence of ZP were rhombohedral (calcite). It is worth noting that the average size of induced vaterite particles was ~10–30 µm, while different sizes of calcite crystals were observed at the screening stage. It was found that the size of calcite particles was mainly 20–40 µm in the presence of MP and UP, and 5–15 µm when CP and ZP were added to the fermentation media.

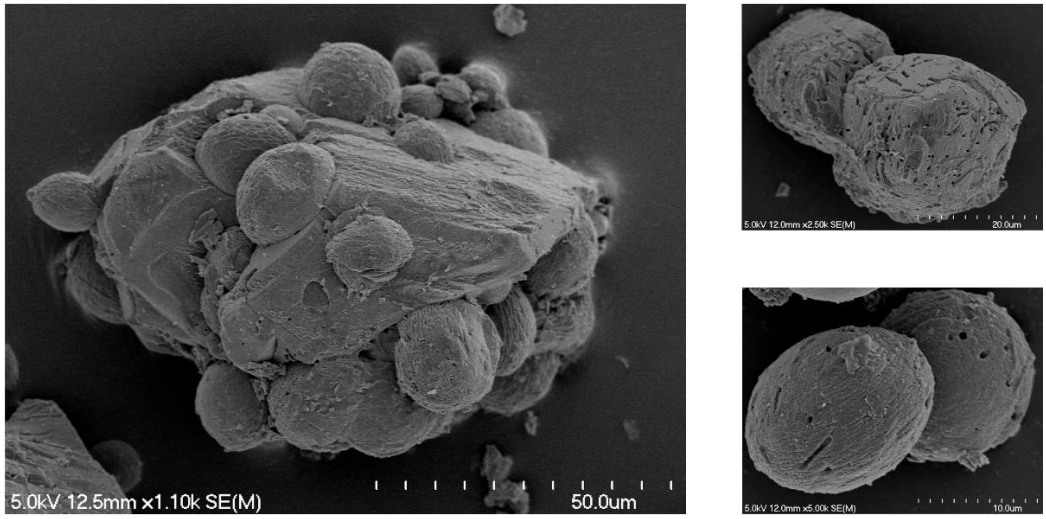

Figure 6-5 SEM micrograph of $CaCO_3$ crystals at the screening stage for the medium supplemented with MP.

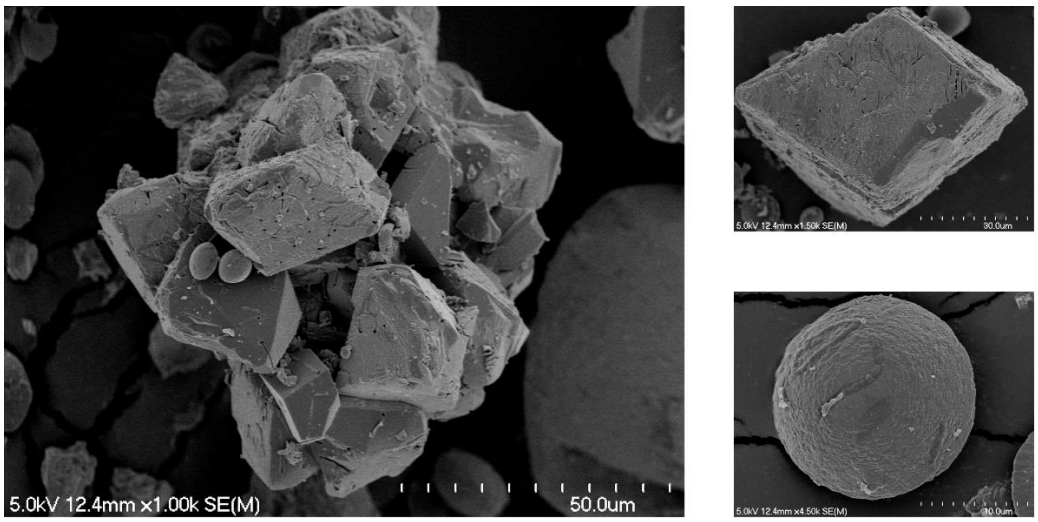

Figure 6-6 SEM micrograph of $CaCO_3$ crystals at the screening stage for the medium supplemented with UP.

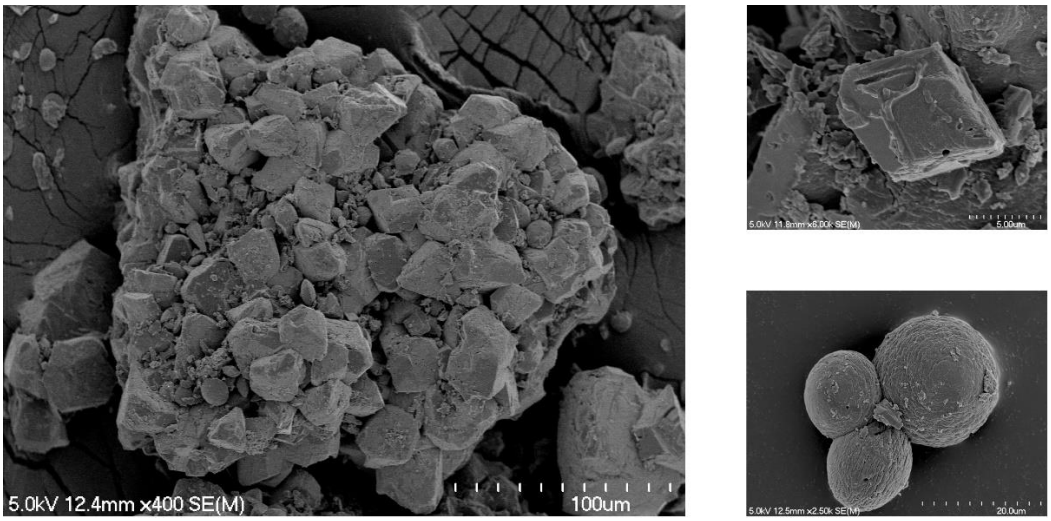

Figure 6-7 SEM micrograph of $CaCO_3$ crystals at the screening stage for the medium supplemented with CP.

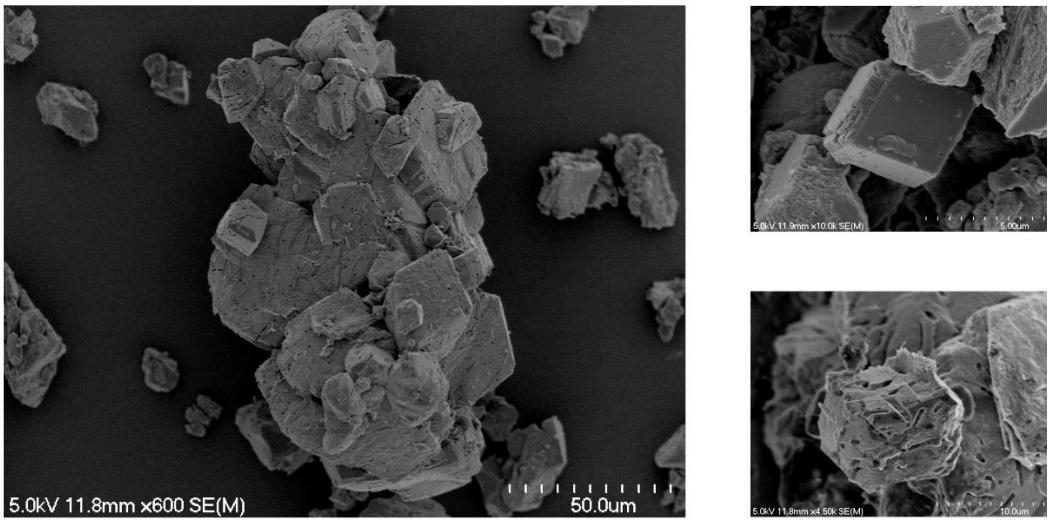

Figure 6-8 SEM micrograph of $CaCO_3$ crystals at the screening stage for the medium supplemented with ZP.

The morphologies of induced $CaCO_3$ precipitation in the presence ORCs during the optimization study were also investigated. As expected, a combination of vaterite and calcite was induced by the addition of the optimum concentrations of selected ORCs, and the SEM micrographs for the optimum sample are displayed in Figure 6-9.

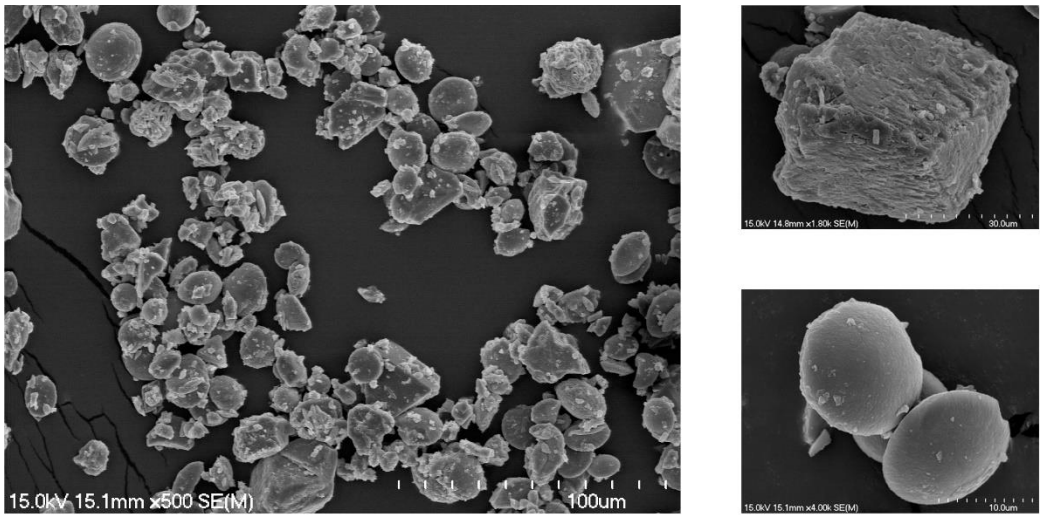

Figure 6-9 SEM micrograph of $CaCO_3$ precipitation when the media was supplemented with the optimum concentrations of ORCs.

The collected dry biosynthesis products were also examined using EDS analysis to observe the elemental compositions. As shown in Figure 6-10, the EDS spectra for the optimum sample (containing ORCs) closely resembled the pure $CaCO_3$, indicating the formed crystals were either calcite, vaterite and/or aragonite. Since aragonite particles were not detected by SEM and XRD, it can be concluded that the precipitated crystals are calcite and vaterite.

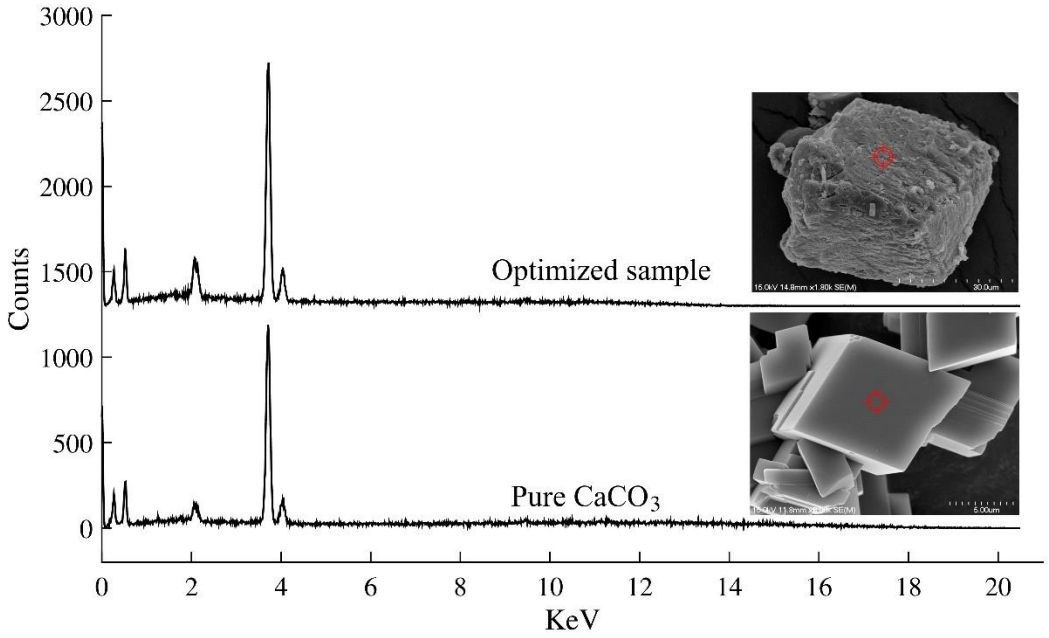

Figure 6-10 EDS spectra for the pure $CaCO_3$ crystal and the particle precipitated in the media supplemented with optimum concentrations of ORCs.

6.2.5 Characterization of crystals

The XRD peaks are appropriate indicators for qualitative and quantitative determination of bacterially induced $CaCO_3$ precipitation. Therefore the precipitated $CaCO_3$ powders at screening study were subjected to XRD measurement and the patterns are shown in Figure 6-11. Interestingly, the presence of different ORCs at the screening stage resulted in a different portion of $CaCO_3$ polymorphs. The highest portion of calcite was precipitated in the solution containing ZP, while the lowest concentration of calcite induced in the medium supplemented with MP. The comparison between UP and CP revealed that the solution containing CP induced a higher portion of calcite than UP. It was also found that no aragonite was induced during the fermentation process. On the other hand, the addition of MP to the fermentation medium led to induce the highest portion of vaterite precipitation. The investigation also indicates that a higher portion of vaterite was induced in the solution with UP as compared to CP. However, no vaterite particles were detected when ZP was added to the fermentation medium.

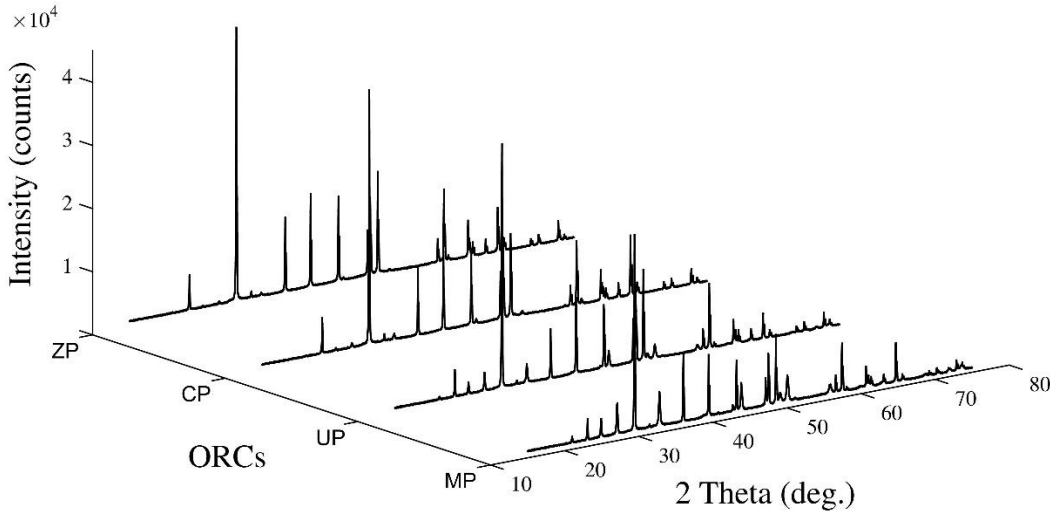

Figure 6-11 XRD spectra of bacterially induced $CaCO_3$ precipitation in the screening study.

XRD analysis was also performed for the optimization media and the spectra are given in Figure 6-12. As expected, a combination of vaterite and calcite was induced when the optimum concentrations of ORCs were added to the fermentation solution (Figure 6-13).

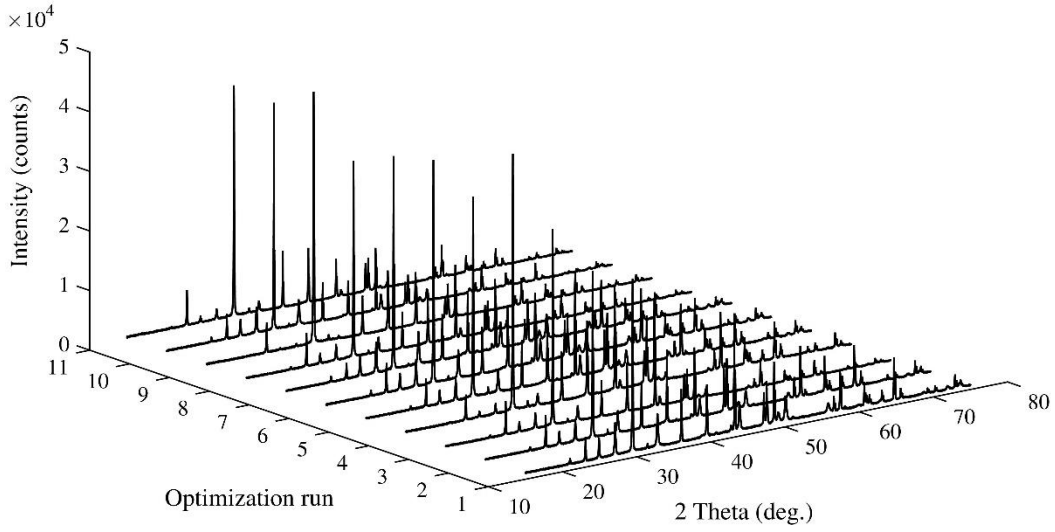

Figure 6-12 XRD spectra of bacterially induced $CaCO_3$ precipitation in the optimization study.

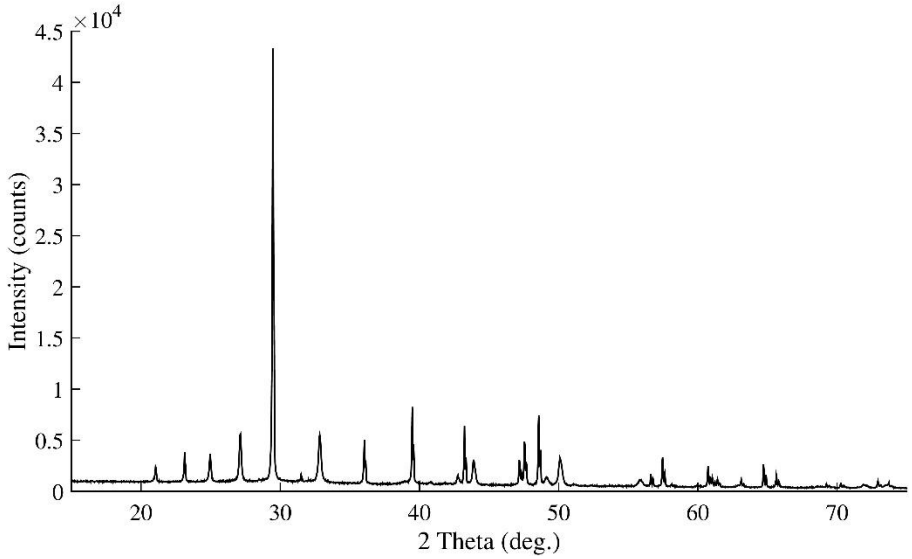

Figure 6-13 XRD spectra of bacterially induced $CaCO_3$ precipitation in the media supplemented with optimum concentrations of ORCs.

6.3 Discussion

6.3.1 ORCs and $CaCO_3$ precipitation

The applications of oxygen releasing materials, including sodium percarbonate or metal peroxides, have been reported to support in situ aerobic biosynthesis [83, 191]. In this sense, the aerobic biodegradation of contaminants by the addition of ORCs has been proposed under oxygen-limiting conditions [80, 82]. However, the aerobic fermentation can be affected by many physical, chemical and biological conditions that influence the overall $CaCO_3$ biosynthesis efficiency. Our previous study demonstrated that aeration has a positive effect on the bacterial production of $CaCO_3$ by providing a higher level of DO [169]. In general, the ORCs significantly affect the quantity of released oxygen and the pH [81]. The introduction of pure oxygen rather than air in the fermentation media can significantly increase the DO concentration [192], and, consequently, this contributes to enhancing the biomineralization efficiency. However, maintaining DO concentration greater than its critical level would be toxic for microorganisms [193], and bacterially induced $CaCO_3$ precipitation is affected accordingly.

The ORC materials tend to release oxygen at a controlled rate to enhance the aerobic biomineralization processes by providing more oxygen. Eqs. 6-2 and 6-3 show the chemical reactions of peroxides towards the production of hydrogen peroxide and subsequently oxygen liberation, where M represents the divalent metal [83, 194]. As shown in the Eq. 6-2, hydrogen peroxide is produced by the reaction between peroxide (ORC) and water. This process is subsequently followed by decomposition of hydrogen peroxide into oxygen (Eq. 6-3).

$$MO_2 + 2H_2O \rightarrow M(OH)_2 + H_2O_2 \quad (6\text{-}2)$$

$$2H_2O_2 \rightarrow O_2 + 2H_2O \quad (6\text{-}3)$$

It has been reported that oxygen is required to initiate and maintain the bacterial activity for the biomineralization of $CaCO_3$ which is induced through urea hydrolysis or oxidation of organic carbon pathways [195]. Considering the poor solubility of oxygen in the water, the bio self-healing approach for concrete crack

treatment is only limited to the surface areas where a sufficient amount of oxygen is available. To address this issue, we proposed the addition of ORCs. However, the addition of various ORCs results in the production of different $CaCO_3$ concentrations. It was found that UP and MP are significant ORCs on enhancing $CaCO_3$ precipitation, while CP and ZP have a negative effect on $CaCO_3$ biomineralization. Zhang et al. [173] reported that CP can increase the bacterially induced $CaCO_3$ precipitation in the presence of *Bacillus* species. However, our data show that UP and MP have more significant influence on producing $CaCO_3$. This might be due to the rapid oxygen-releasing rate of CP at the early stage of the fermentation [196], which leads to exceeding its critical level and, consequently, $CaCO_3$ precipitation is inhibited.

Based on screening results, among the investigated ORCs, the presence of ZP in fermentation media results in the drastic decline in bacterial $CaCO_3$ precipitation. As compared to the control experiment, a considerable reduction in $CaCO_3$ precipitation was observed due to the presence of the lowest concentration of ZP (3.33 g/L). This shows that the availability of ZP has the most detrimental effect on the biomineralization process. Previously, Rothenstein et al. [197] reported that the presence of zinc in culture media can affect the growth rate of *Halomonas halophila.* It is hypothesized that the zinc is extracellularly bound to the cells and consequently affects the $CaCO_3$ precipitation. On the other hand, a low concentration of UP and MP resulted in a slight increase in $CaCO_3$ precipitation. Due to a low solubility and slow reaction rate of MP with water, it has the slowest oxygen-releasing capability [198] which provides a sustained release of oxygen during the fermentation. Dissolution of UP in water not only releases oxygen but also provides a higher supply of urea which is essential to inducing carbonate during biosynthesis. However, a greater amount of urea than it can be consumed by bacteria to initiate the biomineralization process remains unused. Overall, the screening results suggest that UP and MP are the most promising sources for the support of bacterial production of $CaCO_3$, and therefore an optimization study was performed for further enhancement of $CaCO_3$ biosynthesis.

6.3.2 Optimization of significant ORCs for $CaCO_3$ precipitation

Adequate oxygen supply to the cells is often critical in aerobic fermentation; however, the excessive release of oxygen by ORCs might adversely affect the bioprocesses [199]. Furthermore, it has been noted that the irreversible cell damage can occur as a result of temporary oxygen depletion [200]. Therefore the optimization was carried out to propose the optimum concentrations for the selected ORCs which can provide a continuous supply of oxygen, and facilitates the bacteria to induce $CaCO_3$ under oxygen-limiting conditions. The CCF design matrix used in the present investigation enabled us to study and explore the effect of various concentrations of potent ORCs on $CaCO_3$ precipitation. The regression analysis of the experimental design listed in Table 6-2 reflects that all single factor and quadratic model terms, excluding X_1^2, are significant (p-value<0.05) on bacterial precipitation of $CaCO_3$. A p-value of less than 0.05 also shows that the interactive term of X_1X_2 significantly affects the biosynthesis of $CaCO_3$. The error associated with repetitions was determined based on the replicates of the central points. The analysis of variance results indicates an R^2 value of 0.985 which ensures a satisfactory adjustment of the model to the experimental data. As given in Table 6-3, the significant regression and the non-significant lack of fit also suggest that the model has been well fitted to the experimental data.

Figure 6-14 and Figure 6-15 depict the single and synergic effects of significant ORCs (UP and MP) on predicted $CaCO_3$ precipitation, respectively. As shown in Figure 6-15, a 3D response surface plot was constructed to illustrate the interactive effects of the influential ORCs and to provide a visual interpretation for the location of the optimal concentrations. The shape of the corresponding plot shows the mutual interaction between variables is significant, and $CaCO_3$ precipitation is considerably affected by the concentration of UP and MP. The data indicate that the low and high concentrations of both UP and MP adversely affect the biomineralization of $CaCO_3$. The oxygen released by the low concentrations of ORCs could not meet the cell requirement, and the high levels of ORCs showed toxicity by releasing an excessive amount of oxygen than required by bacteria. The precipitation of $CaCO_3$ was enhanced with increases in the concentrations of UP and MP to approximately 3300 and 12 mg/L, respectively. However, further increases in the concentration of UP and MP led to a decrease in $CaCO_3$

concentration. The high concentrations of UP and MP cause the oxygen releasing process to take place too quickly, and the resulted supersaturation state inhibits the bacterial activity. Another possible explanation for the inhibitory effect of high concentrations of UP and MP is due to oxygen toxicity which causes inhibition of metabolism and respiration in microorganisms [201].

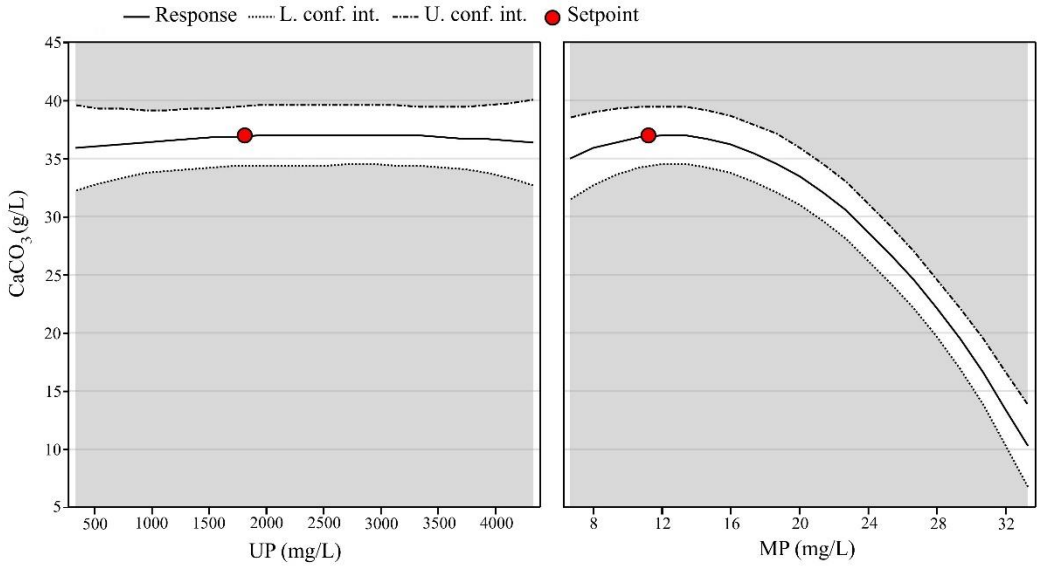

Figure 6-14 Single effect of influential ORCs (UP and MP) on bacterial induced $CaCO_3$ precipitation.

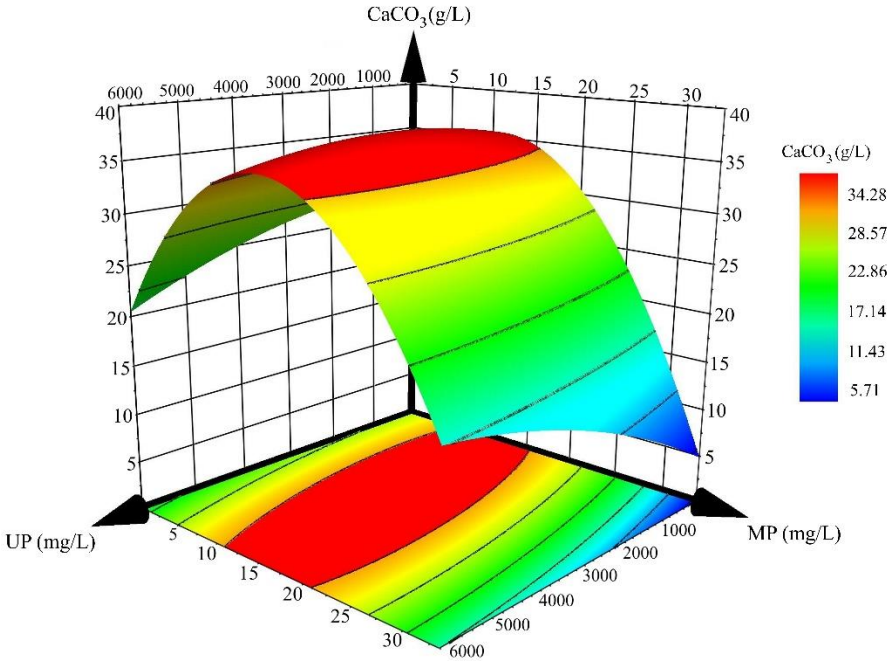

Figure 6-15 Response surface plot shows the synergistic effects of influential ORCs (UP and MP) on bacterial induced $CaCO_3$ precipitation.

6.3.3 Experimental verification

In order to validate the optimization results, verification experiments were performed at the predicted values derived from the model. The review of the optimization as a contour curve plot given in Figure 6-15 shows the relative effects of UP and MP on $CaCO_3$ precipitation. To evaluate the performance of optimized ORCs on the biomineralization process, the critical parameters such as DO and pH were monitored. The validation experiments showed that there is an increase in bacterial precipitation of $CaCO_3$ as compared to the control run, and it has only a negligible difference with the value predicted by the model. More importantly, the optimized sample could accelerate the biomineralization of $CaCO_3$. The presence of ORCs resulted in a 22.5% increase in $CaCO_3$ precipitation at 72 h of fermentation. Taking into account that the majority of the concrete cracks are generated at the early age, an ideal bio self-healing compound requires to activate immediately upon the crack formation and fill the entire crack in a short period of time. Moreover, it has been noted that the ORCs are able to last from four months to over a year [82]. Therefore the addition of proposed optimum ORCs as a supplementary bio self-

healing agent can enhance the concrete performance by efficiently filling the concrete cracks upon their formation.

The bacterial metabolic activity has an important role in the biomineralization process, and it can be affected by the level of DO. As shown in Figure 6-3, the samples containing the optimum concentrations of UP and MP have a higher level of DO throughout the fermentation as compared to the control samples. The higher DO level during fermentation not only boosts the cell populations but also contributes to bacterial growth in oxygen-limiting conditions. The bacterial cell has an important role in the biosynthesis of $CaCO_3$ precipitation. Stocks-Fischer et al. [68] reported that the bacterial cells serve as nucleation sites in the biomineralization process. These higher nucleation sites provide a favorable condition to further increase $CaCO_3$ precipitation due to the controlled and continuous supply of oxygen which meets the requirement for bacteria to initiate the biomineralization process. Eqs. 6-4 to 6-9 represent the bacterially induced $CaCO_3$ precipitation process through urea hydrolysis pathway [1, 70].

$$CO(NH_2)_2 + H_2O \xrightarrow{Microorganism} NH_2COOH + NH_3 \quad (6\text{-}4)$$

$$NH_2COOH + H_2O \rightarrow NH_3 + H_2CO_3 \quad (6\text{-}5)$$

$$2NH_3 + 2H_2O \rightarrow 2NH_4^+ + 2OH^- \quad (6\text{-}6)$$

$$2OH^- + H_2CO_3 \rightarrow CO_3^{2-} + 2H_2O \quad (6\text{-}7)$$

$$Ca^{2+} + Cell \rightarrow Cell - Ca^{2+} \quad (6\text{-}8)$$

$$Cell - Ca^{2+} + CO_3^{2-} \rightarrow Cell - CaCO_3 \quad (6\text{-}9)$$

In general, a higher concentration of bacterial cells increases the urease concentration which catalyzes the hydrolysis of urea into carbonate [159]. Therefore urea hydrolysis has a direct relationship with bacterial cell concentration, and this has a direct effect on $CaCO_3$ precipitation. On the other hand, one of the most common issues associated with the presence of ORCs is the sudden release of oxygen, which may affect the bacterial metabolism and $CaCO_3$ precipitation capacity. Since MP content in the optimized sample has a low solubility in water, it guarantees a gradual and continuous release of oxygen [81].

pH is another significant parameter on biomineralization of $CaCO_3$ by affecting the bacterial urease activity [161]. Our results also confirm the effect of pH on biomineralization of $CaCO_3$. It was noticed that the control experiment had a higher pH, and more $CaCO_3$ was precipitated over the first 35 h of fermentation. However, the optimized sample had higher pH and more $CaCO_3$ precipitation as compared to the control for the rest of fermentation period. This is due to the fact that carbonate tends to dissolve rather than precipitate at a low pH level [181]. The increase of H^+ in solution caused a decline in pH for both optimized and control experiments due to CO_2 dissolution. On the other hand, after 72 h of fermentation, the produced OH^- neutralized H^+ in fermentation medium through the dissolution of $NH_3(g)$ and, consequently, pH increased [202, 203]. Overall, a greater pH fluctuation was observed in the control solution during the dropping of pH, while in both fermentation runs, the pH increased more steadily. Over the oxygen liberating period, the reaction between ORCs and water results in an increase in pH, and this leads to stabilizing the pH variation.

6.3.4 Morphological observation and crystal characterization

The EDS spectrum taken for the bio-precipitates clearly showed that the main compositions are Ca, O, and C. A high degree of similarity between the pure $CaCO_3$ and precipitated crystals is another indication that the presence of ORCs can successfully facilitate the $CaCO_3$ biosynthesis process. Bioprecipitation of $CaCO_3$ may result in the production of different polymorphs, including calcite, vaterite, aragonite, and two hydrated crystalline phases, monohydro calcite and ikaite [178]. It has been noted that the production of the polymorphs depends on bacterial strains, growing environments, and their chemical nature [204, 205]. Taking into account that $CaCO_3$ polymorphs have different mechanical and physical properties (i.e., density, hardness and solubility), and they may be used in various applications, it requires determining whether the presence of ORCs will change the $CaCO_3$ polymorphs. Bacterial cell wall characteristics and growth medium composition are the main factors influencing the bacterially induced $CaCO_3$ morphology. Furthermore, a number of previous studies have demonstrated the role of EPS in the bacterial production of $CaCO_3$ polymorphs [167, 206]. Specifically, Bosak and

Newman [207] noted that the presence of EPS encourages the precipitation of vaterite particles rather than calcite. In our investigation the results obtained by XRD and SEM disclose that the presence of ZP has an effect on the $CaCO_3$ morphology and vaterite formation is suppressed. This might be due to the changes in nucleation energy caused by extracellular attachment of zinc onto the bacterial cell wall. This result corresponds with the finding of Rothenstein et al. [197] who observed that the availability of zinc in a fermentation solution had an effect on the morphology of induced $CaCO_3$ precipitation.

6.4 Chapter summary

The objective of the present chapter was to investigate the influence of ORCs addition on the bacterial $CaCO_3$ precipitation. The significance of bacterial activity by introducing more supply of oxygen in the biomineralization processes was successfully demonstrated. In this study we proposed a simple, active and long-term protocol to enhance and accelerate the bacterial production of $CaCO_3$. Accordingly, the results showed the availability of a higher oxygen supply by addition of CP and ZP can inhibit the precipitation of $CaCO_3$. Nevertheless, the presence of the optimum concentration of UP and MP can successfully enhance both oxygen level and $CaCO_3$ precipitation. The experimental results clearly show that the $CaCO_3$ precipitation and DO are enhanced by the addition of optimum concentrations of UP and MP. It is believed that the optimum concentrations of ORCs are promising to enhance the bio self-healing concrete performance. The addition of proposed compounds can terminate further crack development in the concrete structures by activation and supporting the biomineralization process in oxygen-limiting areas such as deep cracks and interior parts of the concrete matrix.

Chapter 7

Magnetic immobilization of bacterial cells with iron oxide nanoparticles (IONs) to improve the bio-concrete properties [5]

[5] This chapter forms the basis of two research papers published in the Journal of Applied Microbiology and Biotechnology, as referenced below.

[208] **Seifan, M.**, Ebrahiminezhad, A., Ghasemi, Y., Samani,A.K., and Berenjian, A. *Amine-modified magnetic iron oxide nanoparticle as a promising carrier for application in bio self-healing concrete.* Applied Microbiology and Biotechnology, 2018. 102: p. 175-184.

[209] **Seifan, M.**, Ebrahiminezhad, A., Ghasemi, Y., Samani,A.K., and Berenjian, A. *The role of magnetic iron oxide nanoparticles on bacterially induced calcium carbonate precipitation.* Applied Microbiology and Biotechnology. 2018. doi: 10.1007/s00253-018-8860-5

7.1 Introduction

Apart from the concrete mixture proportioning, a bio-concrete performance relies on many factors, such as appropriate bacterial species and nutrient ingredients, availability of oxygen to initiate $CaCO_3$ biomineralization, the viability of bacteria to withstand in a concrete environment, and capability of cells to induce $CaCO_3$ precipitation upon crack formation for a long period of time. In the previous chapters, the MICP process was successfully optimized by selecting the most $CaCO_3$-inducing bacteria and nutrients at their optimum concentrations. It was also found that the availability of oxygen is critical on MICP. To address the oxygen-limitation, a novel approach was proposed using ORCs, and the results indicate that the presence of the optimum concentration of ORCs can maintain the DO level higher than the control experiment and, consequently, biosynthesis of $CaCO_3$ is enhanced. However, the bacterial cell protection in a concrete environment is a matter of challenge.

The durability of the concrete is mainly related to the characteristics of its pore structure, and the concrete degradation often relies on the way potentially aggressive chemicals seep into the matrix. Porosity and the pores' connectivity are the main factors affecting the concrete permeability [210]. Clearly, the more porous concrete structure has a lower durability performance when exposed to water, moisture or aggressive substances, and it makes the concrete susceptible to degradation. The addition of the proposed bio self-healing agent can decrease the concrete porosity and voids by inducing $CaCO_3$ crystals. The bio self-healing mechanism can increase the durability of the concrete through decreasing fluid absorption. Although the presence of bio self-healing compounds is effective for durability of the concrete, it cannot guarantee the integrity of the structure. The addition of nutrients, specifically nitrogen sources, has a negative impact on cement binding efficiency, and it may affect the mechanical properties of concrete.

On the other hand, the survivability of bacteria is the main challenge in designing the bio-concrete. Over recent years, several studies have been devoted to immobilization of bacteria in/on protective carrier as a promising approach to not only adapt the microorganism to the new surroundings but also protect them from harsh environmental conditions. Unlike the application of bio self-healing agent on

the concrete surface, more challenges emerge when the bio-agent is embedded in concrete. Considering the pore size of the concrete and bacterial cell, there is a high risk for the cells to squeeze upon cement hydration. On the other hand, the shear force on bacterial cells during the concrete mixing and casting as well as gradual shrinkage of the concrete may influence the bacterial cell activity and the bio self-healing concrete performance.

Different bacterial carriers, such as lightweight aggregate, hydrogel, polyurethane, silica gel, and diatomaceous earth, have been reported as the cell protective vehicles to enhance the bacterial survival and concrete characteristics. Polyurethane foam was first reported by Bang et al. [156] for bacterial immobilization to enhance the concrete crack filling efficiency. A few years later, Wang et al. [139] used polyurethane and silica gel as the carrier for the bacteria protection. Despite the fact that a higher $CaCO_3$ precipitation was induced by immobilized bacteria in silica gel than polyurethane, a lower strength regain was observed in those samples containing silica gel immobilized bacteria. In another investigation diatomaceous earth was proposed as a promising protective carrier and the results indicate that the immobilized cells had much higher ureolytic activity (~ 15 times) than that of un-immobilized cells [10].

To date, different types of chemical admixtures, such as superplasticizers, retarders, accelerators, and air-entraining additives, have been introduced to the market to control or modify the concrete properties. Traditionally, different mineral additives, including silica fume and fly ash, have been used in cement composites due to their ability to fill in micro and macro voids as well as showing a partial binding effect [89]. Over recent years, nanotechnology has attracted considerable attention as an alternative to conventional technologies. Nanotechnology refers to a field of technology dealing with materials with dimensions of the order of 100 nm or smaller. The advances in nanotechnology can be seen in many technologies and industry sectors, such as electronics, energy, medicines, chemical sensors, cosmetics, food, and fabrics, due to their specific physicochemical characteristics. Nanotechnology has also become a strategically important research in construction materials, such as concrete. For instance, the effects of nano Fe_2O_3 [211], nano montmorillonite clay [212], nano silica [91, 95], nano $CaCO_3$ [213], nano TiO_2 [214], and carbon nanotubes (CNTs) [215] on improving the mechanical properties

of concrete and enhancing the kinetics and hydration of cement have been well demonstrated [92, 93]. The nano scale-size of particles are able to enhance the concrete properties from conventional grain-size materials of the same chemical composition. The unique characteristics of nano-sized particles, including a larger surface area and greater electrostatic force, result in a higher capability to fill in voids as compared to the conventional mineral additives. On the other hand, the addition of proper nano scale-size particles can influence the mechanical performance of the concrete. Li et al. [93] reported a higher compressive and flexural strength when nano-Fe_2O_3 and nano-SiO_2 were added to the mortar as compared to the plain cement mortar. Likewise, Oltulu et al. [89] investigated the effects of nano-sized particles on the compressive strength of cement mortars. It was found that the presence of nano-SiO_2, nano-Al_2O_3 and nano-Fe_2O_3 at a ratio of 1.25 wt% of the binder can enhance the compressive strength of the mortar specimens. Moreover, the addition of selected nano powders reported to decreasing in capillary absorption (14%) as compared to the control specimen.

Apart from the different applications of nanoparticles, the unique biological and chemical properties of nanoparticles make them potential for biotechnological processes. Among all nanoparticles, the application of nanostructures of magnetic iron oxide materials is increasing due to their unique physical and chemical properties caused by their high intrinsic anisotropy and surface activity [216]. It has been noted that the IONs not only influence the biosynthesis of products and metabolites but also reduce the downstream processes [217]. Due to efficient cell capture, IONs have the potential to be used as a carrier for immobilization of bacterial cells.

Considering the positive effect of nano-scaled sized particles on concrete properties, the possibility of bacterial immobilization onto these carriers, and more importantly, addressing the shortcomings associated with the direct incorporation of bacterial cells into the concrete, the experiments in this chapter were performed to investigate the feasibility of MICP using different magnetically immobilized IONs and their effects on bacterial growth.

7.2 Results

7.2.1 Synthesis and characterization of iron oxide nanoparticles

7.2.1.1 IONs synthesis

Co-precipitation is one of the most conventional techniques to synthesize Fe_3O_4 or ɣ-Fe_2O_3 [134]. In this approach the nanoparticles are formed upon the addition of a highly basic solution to the mixture of ferric and ferrous ions. Further continuing the reaction with vigorous mixing leads to growing the larger magnetic nanoparticles. In this study magnetite nanoparticles with uniform morphology and narrow size distribution were synthesized via the co-precipitation technique using the solution of $FeSO_4$ and $FeCl_3$. Over synthesis, to prevent the oxidation of γ-Fe_2O_3 and also enable the maghemite formation, inert gas atmosphere (N_2) was continuously introduced into the reaction chamber. The black precipitates were formed upon the addition of a basic solution (ammonium hydroxide) and the larger nanoparticles were obtained by continuing the reaction for 60 min. As it can be seen from Figure 7-1, the magnetic response of fabricated nanoparticles was tested by placing a permanent magnet close to the vials containing a well-dispersed solution of IONs in water. The right vial (Figure 7-1b) illustrates the prepared particles were successfully attracted to the magnet.

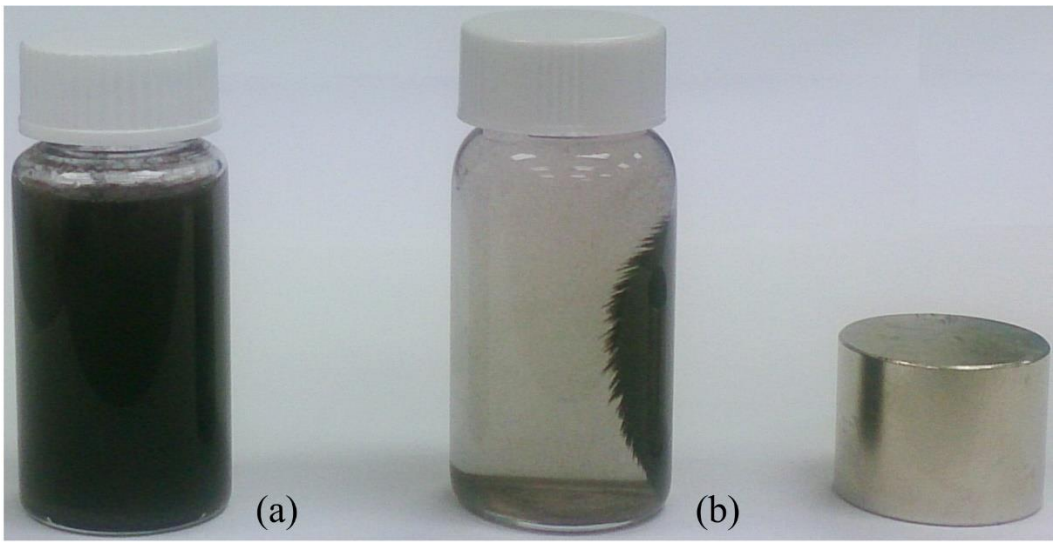

Figure 7-1 Photograph of magnetite IONs; (a) left vial contains suspended IONs and b) right vial contains IONs subjected to a permanent magnet.

7.2.1.2 Transmission electron microscopy (TEM)

Different techniques have been utilized to characterize the fabricated magnetic IONs. The morphology of nanoparticles was analyzed by using a transmission electron microscope (TEM). Figure 7-2 and Figure 7-3 show the morphology of the fabricated naked and APTS-coated IONs, respectively. Both TEM micrographs confirmed the fabrication of monodisperse spherical particles. Image analysis package (ImageJ software) was used to determine the particle size. Image analysis showed a fairly uniform particle size; however, the size of APTES-coated IONs was slightly bigger than naked IONs. The results for naked IONs show a fairly uniform particle size ranging 8–15 nm, while the particles size distribution ranging from 10 to 18 nm were noticed for APTES-coated IONs.

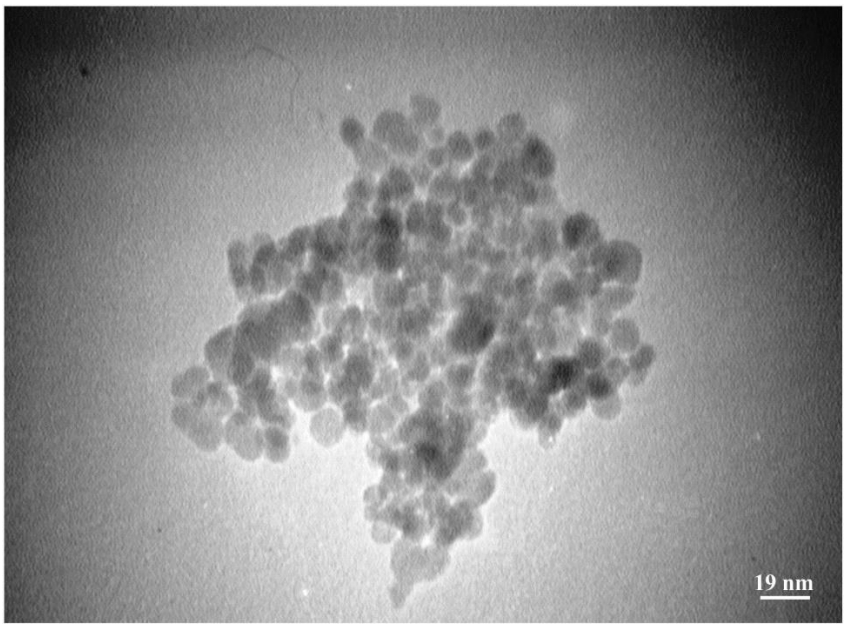

Figure 7-2 Transmission electron microscopy (TEM) images of prepared naked magnetic IONs.

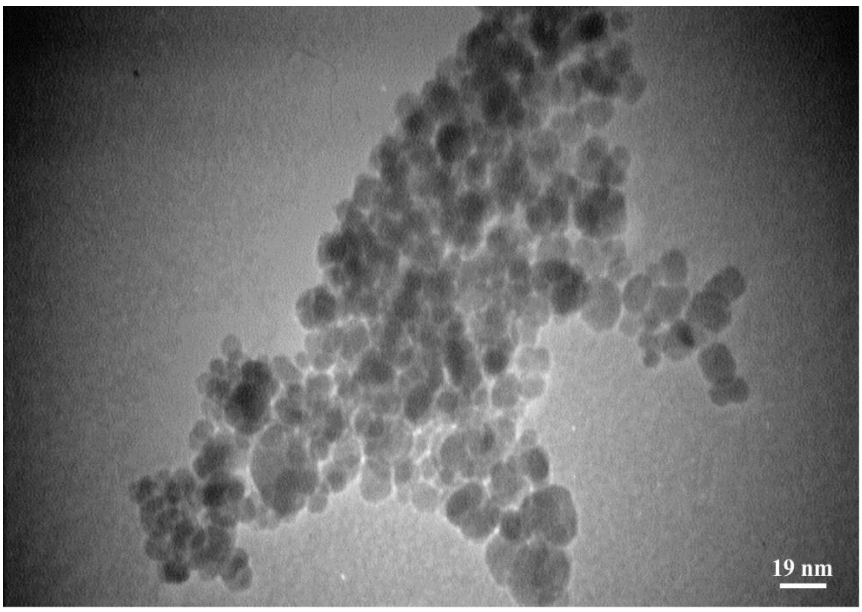

Figure 7-3 Transmission electron microscopy (TEM) images of prepared APTES-coated magnetic IONs.

7.2.1.3 Fourier-transform infrared spectroscopy (FTIR)

Fourier transform infrared spectroscopy (FTIR) is one of most important and emerging tools used for identification and characterization of nanoparticles by providing information about the vibrational and rotational modes of motion of the particles. Figure 7-4 illustrates the FTIR spectra of the fabricated naked IONs. The formation of IONs was characterized by the characteristics peaks of Fe–O bond at 644.53 cm^{-1} and 450.46 cm^{-1}. During co-precipitation synthesis, the surface of the magnetite nanoparticles was modified by OH groups from the aqueous medium. The stretching vibrations of the O–H groups appeared as a wide peak (stretching point) at 3433.92 cm^{-1} and a sharp peak (deforming point) at 1629.48 cm^{-1}.

The success of nanoparticle saline coating functionalization was also confirmed by FTIR analysis and the result is shown in Figure 7-5. The strong absorption at 637.20 cm^{-1} and 457.28 cm^{-1} arise from the Fe–O characteristic of APTES-coated Fe_3O_4 nanoparticles. The characteristics peaks due to surface OH groups of IONs were observed at 1636.80 cm^{-1} and 3441.24 cm^{-1}. The stretching vibration bond at 1032.65 cm^{-1} corresponds the Si–O bond in APTES-coated IONs. The peak at about 2900 cm^{-1} is attributed to the asymmetric and symmetric C–H stretching vibrations. The obtained FTIR spectra demonstrates the successful amino acid coating of IONs.

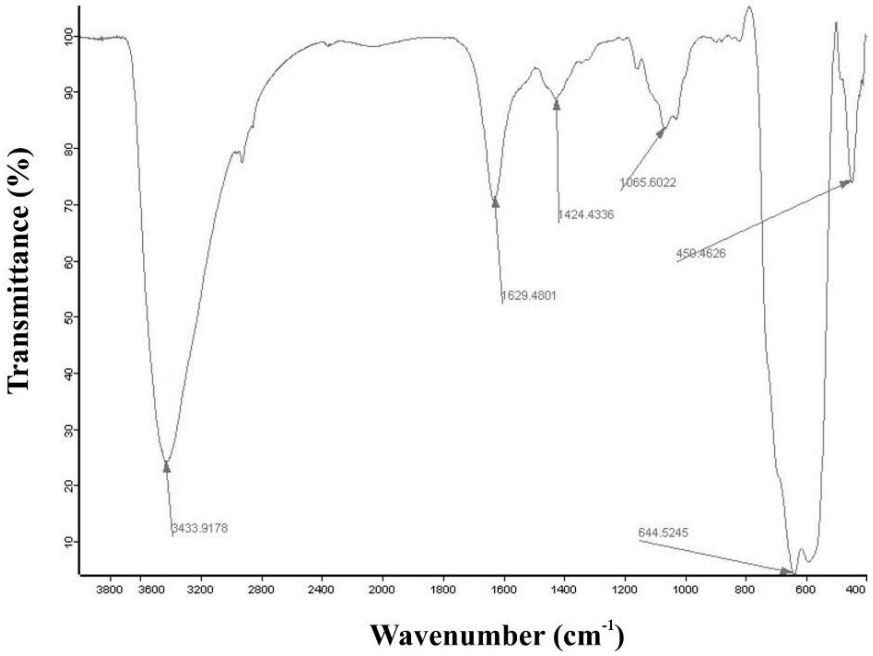

Figure 7-4 Fourier-transform infrared spectroscopy (FTIR) spectra of naked magnetic IONs.

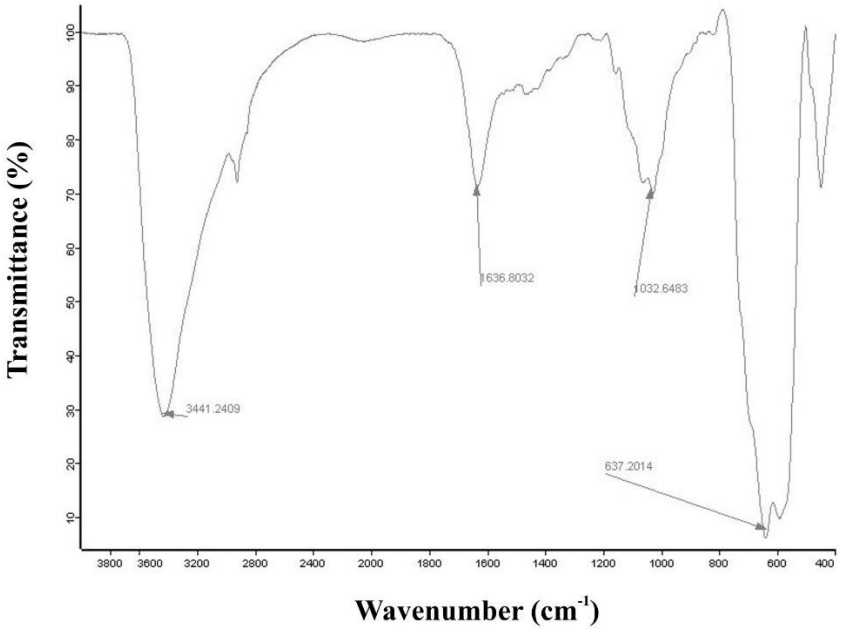

Figure 7-5 Fourier-transform infrared spectroscopy (FTIR) spectra of APTES-coated magnetic IONs.

7.2.1.4 X-ray diffraction (XRD)

X-ray diffraction (XRD) analysis was also performed to characterize the fabricated IONs. As depicted in Figure 7-6, XRD spectra of the prepared IONs were validated by characteristic features of magnetite nanoparticles at 2θ of 30.2°, 35.5°, 43.1°, 53.5°, 57.1°, 62.6° and 74.4°, corresponding to the diffractions of 220, 311, 400, 422, 511, 440 and 533 crystal faces of iron oxide (III) spinel structure. The XRD characteristics of the prepared IONs (positions and relative intensities) correspond with the XRD diffraction peaks of standard IONs, and show that the fabricated precipitates are magnetite nanoparticles. The crystallite size of synthesized nanoparticles was calculated based on the Scherrer's equation (Eq. 7-1):

$$D = \frac{K.\lambda}{\beta.\cos(\theta)} \qquad (7\text{-}1)$$

where D is the average crystallite diameter. K, λ, β and θ are the shape factor (0.94), the X-ray wavelength, the line broadening at half the maximum intensity (FWHM), and the Bragg's angle in degree, respectively. The average crystallite size of APTES-coated IONs for the plane refraction peak of 311 was estimated to be 17 nm.

XRD analysis was also performed for the amine-modified nanoparticles. As shown in Figure 7-7, a series of characteristic peaks of 30.2°, 35.5°, 43.1°, 53.6°, 57.2°, 62.7° and 74.2° marked by their indices 220, 311, 400, 422, 511, 440, and 533 were identified in the XRD spectra of APTES-coated IONs. The XRD pattern also showed sharp peaks indicating that the fabricated particles had good crystalline structure.

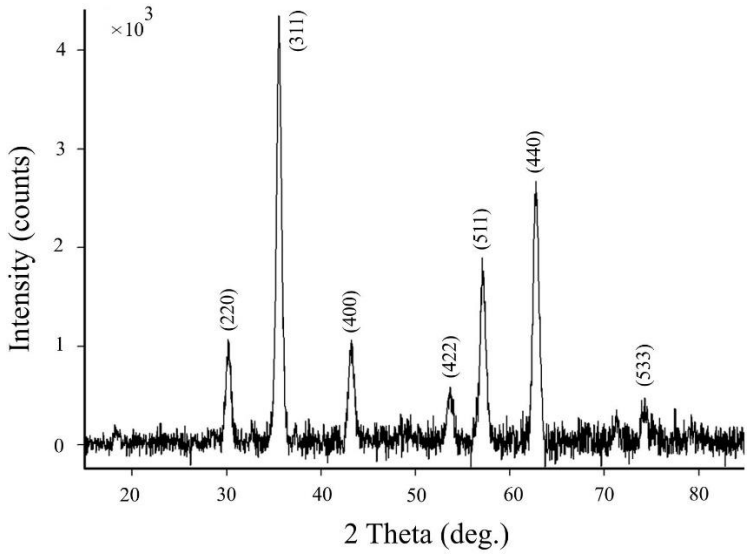

Figure 7-6 X-ray diffraction (XRD) spectra of the prepared naked magnetic IONs.

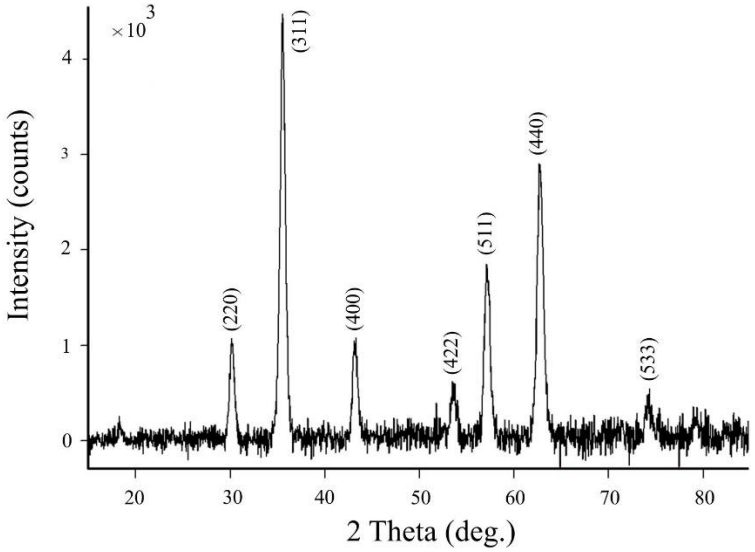

Figure 7-7 X-ray diffraction (XRD) spectra of the prepared APTES-coated magnetic IONs.

7.2.2 Visualization and interaction of IONs with bacterial cell surface

Visualization using SEM was performed to gain insight into the interaction of nanoparticles and bacterial cells upon the exposure to different types of IONs (Naked and APTES-coated). The adsorption of nanoparticles onto the bacterial cell walls is accomplished by the interaction of magnetic IONs and bacterial cell walls due to electrostatic attraction or repulsion. Furthermore, the presence of functional groups, such as carboxyl, hydroxyl and phosphate in EPS can also facilitate the

robust attachment between IONs and cell walls [217]. In this case, the IONs can be adsorbed on the bacterial cell walls using hydrogen bonds [218, 219]. Figure 7-8a and Figure 7-9a present the SEM micrograph of free floating bacterial cells. The decoration and immobilization of bacterial cells with naked and APTES-coated IONs are shown in Figure 7-8b and Figure 7-9b, respectively. The SEM micrographs of decorated cells with both naked and APTES magnetic IONs confirmed that the dispersed Fe_3O_4 nanoparticles were self-assembled on the bacterial surface. It was also observed that a larger amount of APTES-coated IONs were adsorbed on the bacterial cell walls as compared to the uncoated IONs. Since both fabricated IONs had the same magnitude of magnetizing force, this might be attributed to the more biocompatible behavior of amino acid coated nanoparticles.

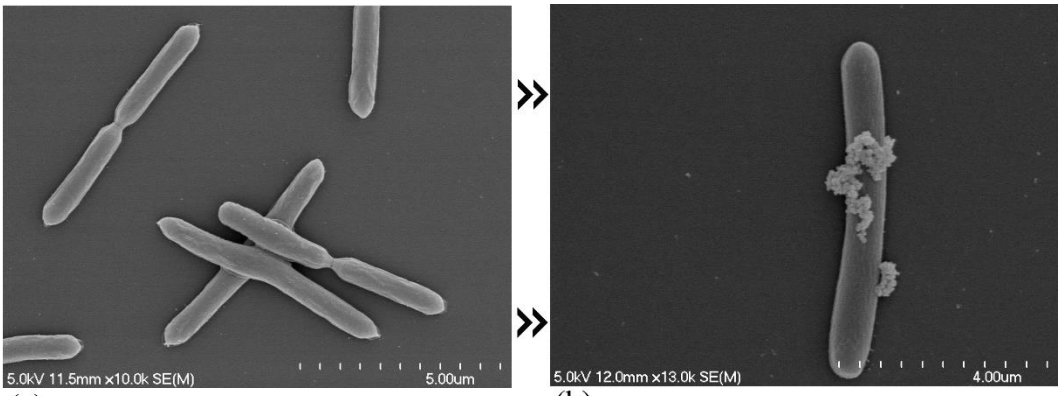

Figure 7-8 SEM micrographs of: a) bacterial cells and b) decorated cell with naked IONs indicating the successful attachment of nanoparticles to the cell surface.

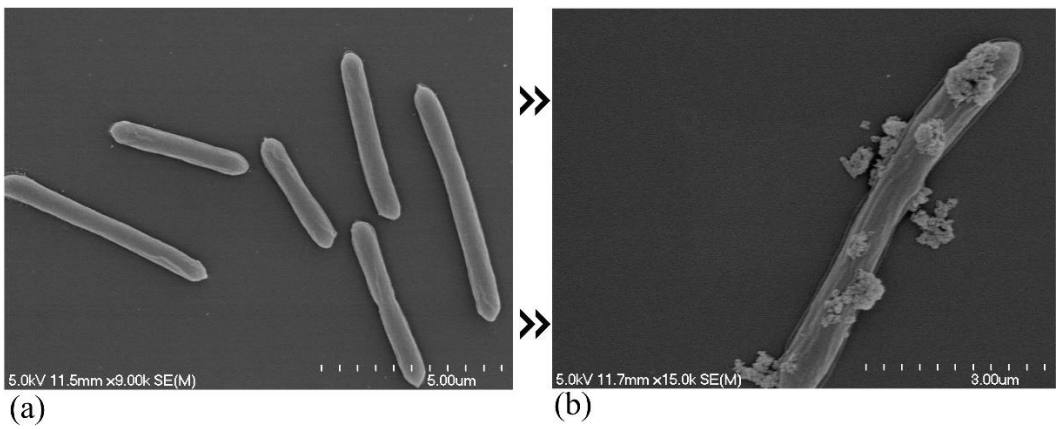

Figure 7-9 SEM micrographs of a) bacterial cells and b) decorated cell with APTES-coated IONs indicating the successful attachment of nanoparticles to the cell surface.

7.2.3 Effect of IONs on bacterial growth

To analyze the activities and growth of immobilized bacterial cells, a comparative study was conducted by performing fermentation experiments in the presence of varying concentrations of IONs. Owing to experimental limitation (further increase in IONs concentration more than 300 μg/mL leads to sudden agglomeration and sedimentation IONs and bacterial cells), a lower concentration of IONs than 300 μg/mL were used for the screening study. As shown in Figure 7-10, the bacterial growth was affected when the cells were immobilized with nanoparticles.

As given in Table 7-1, the statistical analysis shows that the increase in the concentration of naked IONs resulted in significant difference in the bacterial cell growth (p-value<0.05). Immobilization of bacteria using 50 μg/mL of naked IONs did not promote the growth as compared to the free-floating cell. Likewise, further increase in naked ION concentration to 100 μg/mL had no significant effect on bacterial growth. At the end of the fermentation process, the highest cell concentration was achieved when the bacteria were immobilized on 150 μg/mL of naked IONs (p-value<0.05). On the other hand, further increase in naked ION concentration (up to 250 μg/mL) had an inhibitory effect on bacterial growth as compared to the addition of 150 μg/mL nanoparticles, but still higher than free cell. However, the growth promotion caused by the addition of these concentrations of IONs (200–250 μg/mL) was not significant as compared to the media containing free floating cells. The results show that the highest inhibition occurred when the fermentation media were inoculated with immobilized bacterial cells on 300 μg/mL of naked IONs.

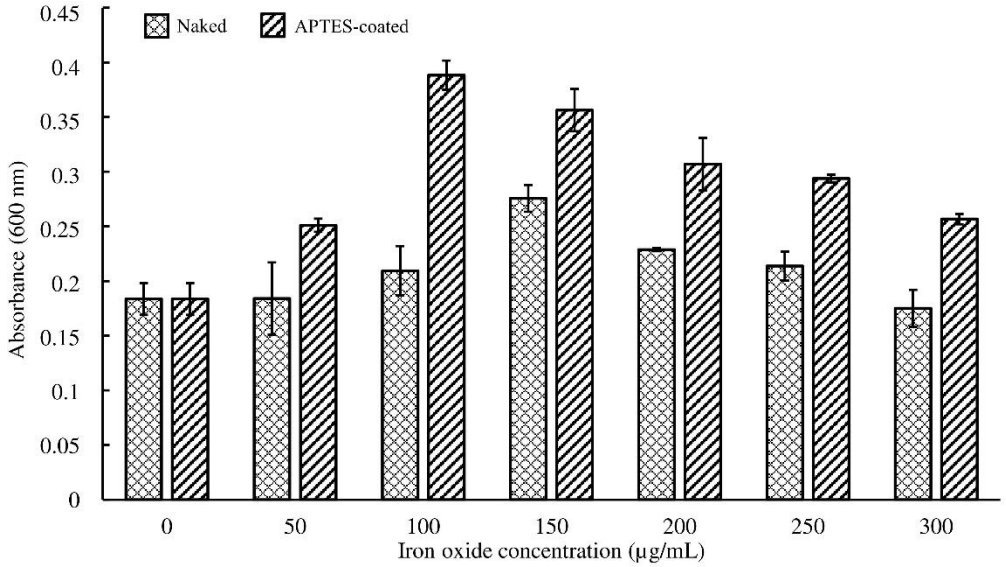

Figure 7-10 Bacterial growth at various concentrations of naked and APTES-coated magnetic IONs ranging from 0 to 300 µg/mL.

Table 7-1 Analysis of variance showing the significance of magnetic immobilized cells with naked nanoparticles on the bacterial growth.

Source of variation	SS	DF	MS	*F*-value	*p*-value
Between Groups	0.022	6	0.004	3.478	0.026
Within Groups	0.015	14	0.001	-	-
Total	0.036	20	-	-	-

DF: degree of freedom, *SS*: sum of squares, *MS*: mean sum of squares

The bacterial growth was also monitored when the fermentation media were inoculated with immobilized cells on APTES-coated IONs. The ANOVA results on Table 7-2 indicate that the immobilization of bacterial cells on APTES-coated IONs has a significant effect on bacterial growth (p-value<0.05). In comparison to the free-floating cell, the presence of APTES-coated IONs resulted in the higher cell density and the maximum bacterial growth was obtained in the presence of 100 µg/mL of APTES-coated nanoparticles. Despite the significant increase in cell concertation as compared to control, the further increase in nanoparticle concentration (more than 100 µg/mL) resulted in a decline in cell density. As can be seen in Figure 7-10, the magnetic immobilization on different concentrations of

APTES-coated ION contributed to the higher cell growth as compared to the counterparts with uncoated IONs.

Table 7-2 Analysis of variance showing the significance of magnetic immobilized cells with APTES-coated nanoparticles on the bacterial growth.

Source of variation	SS	DF	MS	*F*-value	*p*-value
Between Groups	0.085	6	0.014	23.355	0.000
Within Groups	0.008	14	0.001	-	-
Total	0.093	20	-	-	-

DF: degree of freedom, *SS*: sum of squares, *MS*: mean sum of squares

7.2.4 Effect of IONs on biosynthesis of $CaCO_3$

The capability of inducing $CaCO_3$ precipitation in the presence of magnetically immobilized cells was investigated and the results are presented in Figure 7-11. As shown in Table 7-3, the increase in IONs concentration from 50 μg/mL to its highest level (300 μg/mL) resulted in a significant difference in $CaCO_3$ concentration (*p*-value<0.05). Statistically, the addition of 50 μg/mL IONs significantly decreased the $CaCO_3$ precipitation. Similarly, increasing the IONs concentration to 150 μg/mL had an inhibitory effect on $CaCO_3$ biosynthesis; however, this reduction was not significant. In contrast to the lower concentrations of IONs, the statistical analysis showed that further increase in ION concentrations was in favor of $CaCO_3$ production. The results show that the highest concentration of $CaCO_3$ was obtained when the bacteria were immobilized on 300 μg/mL of IONs. However, an independent t-test showed no significant improvement in $CaCO_3$ biosynthesis when the concentration of IONs increased from 250 μg/mL to 300 μg/mL.

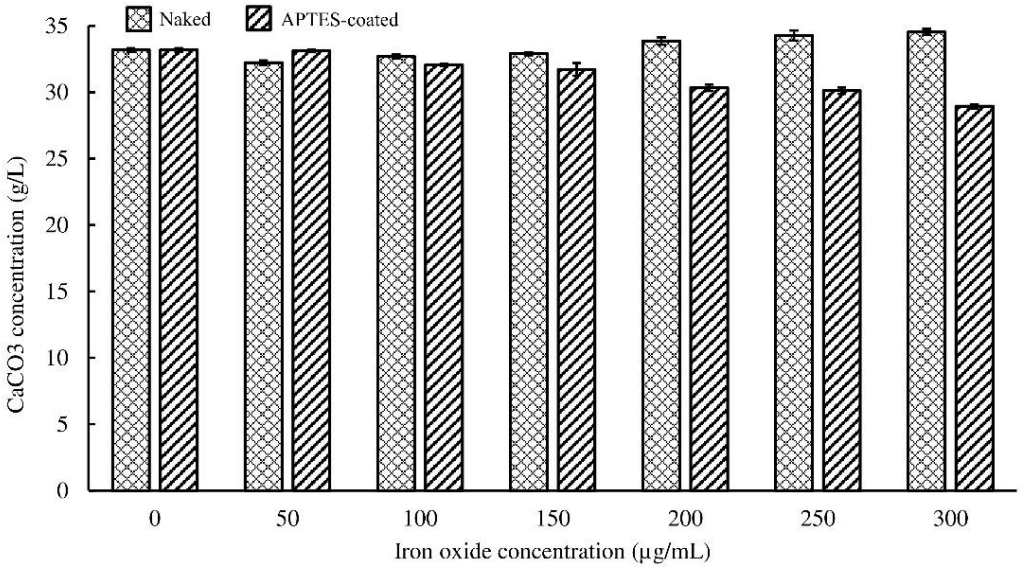

Figure 7-11 Bacterially induced $CaCO_3$ precipitation at various concentrations of naked and APTES-coated magnetic IONs ranging from 0 to 300 µg/mL.

Table 7-3 Analysis of variance showing the significant effect of naked IONs on the bacterial production of $CaCO_3$.

Source of variation	SS	DF	MS	*F*-value	*p*-value
Between Groups	13.327	6	2.221	14.791	0.000
Within Groups	2.102	14	0.150	-	-
Total	15.429	20	-	-	-

DF: degree of freedom, *SS*: sum of squares, *MS*: mean sum of squares

As given in Table 7-4, ANOVA results indicate that the presence of APTES-coated IONs had a significant effect on biosynthesis of $CaCO_3$. As compared to the control experiment, the magnetic immobilization of cells with different concentrations of APTES-coated ION inhibited the $CaCO_3$ production. Although the presence of 50 µg/mL of APTES-coated IONs did not significantly affect the biosynthesis of $CaCO_3$ (p-value>0.05), a further increase in APTES-coated ION concentration resulted in a significant decrease in biomineralization of $CaCO_3$ (p-value<0.05). The highest inhibition in $CaCO_3$ precipitation was observed when the fermentation media were inoculated with immobilized bacterial cells with 300 µg/mL of APTES-coated nanoparticles.

Table 7-4 Analysis of variance showing the significant effect of APTES-coated IONs on the bacterial production of $CaCO_3$.

Source of variation	SS	DF	MS	*F*-value	*p*-value
Between Groups	46.456	6	7.743	45.277	0.000
Within Groups	2.394	14	0.171	-	-
Total	48.851	20	-	-	-

DF: degree of freedom, *SS*: sum of squares, *MS*: mean sum of squares

7.2.5 Validation runs

The initial screening disclosed that the magnetic immobilization of cells with naked IONs contributes to an increase in $CaCO_3$ precipitation, whereas the presence of APTES-coated IONs as a carrier for bacterial cells leads to inhibiting the biosynthesis of $CaCO_3$. Statistical analysis showed that the presence of 250 μg/mL naked IONs contributes to an increase in $CaCO_3$ precipitation. Therefore, to maximize $CaCO_3$ precipitation, the fermentation media were inoculated with immobilized bacterial cells with 250 μg/mL naked IONs and the pH variations were monitored over the course of fermentation.

Figure 7-12 exhibits the variation of pH over fermentation in the presence or absence of IONs. It was observed that the media inoculated with immobilized bacteria resulted in a slight reduction in pH for the first ~80 h of biomineralization. During this period, pH began to decline gradually and reached its lowest level at 6.88 and 6.82 for free-floating bacteria and immobilized cells, respectively. However, after 72 h the pH started to rise for both fermentation conditions. In this stage, the pH of the samples containing immobilized cells increased faster than the control solution. This might be due to more ammonia production during decomposition of urea by immobilized bacteria than free cells.

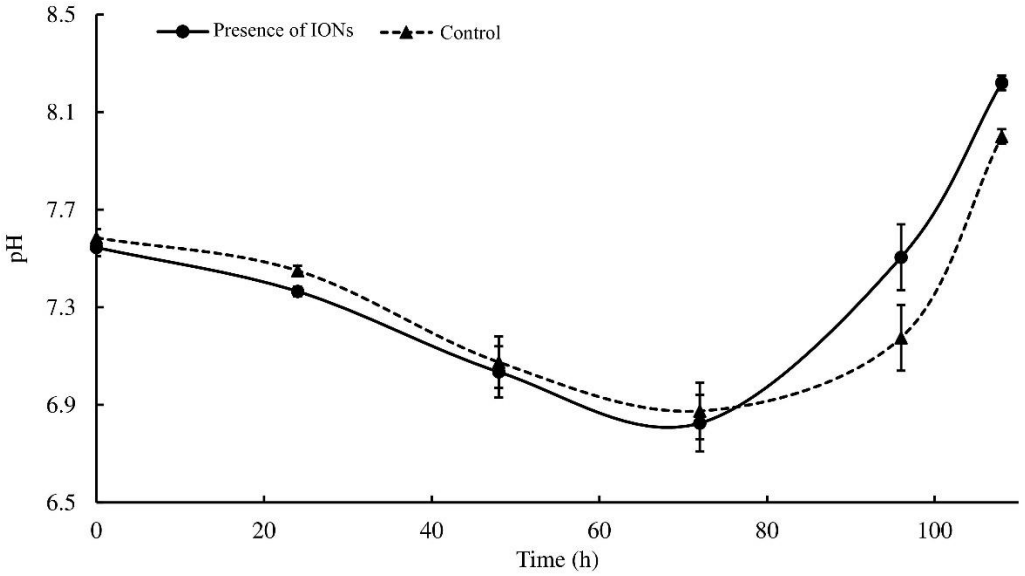

Figure 7-12 pH profiles when the fermentation solutions were inoculated with free floating cells and immobilized cells with 250 μg/mL IONs.

7.2.6 SEM observation and mineralogical study

SEM was used to observe the fabricated nanoparticles and the morphology of precipitated $CaCO_3$ crystals during the biomineralization process. SEM micrographs could evidently display the morphology of the prepared nanoparticles (Figure 7-13). Since no dispersion was performed prior to SEM imaging, the nanoparticles were assembled and stuck together. It was observed that the naked IONs had a bigger cluster than APTES-coated particles. It has been reported that naked IONs tend to aggregate to minimize the high surface energies [134]. The fabricated IONs were mostly spherical and had a uniform particle size distribution. This is in agreement with the results obtained by TEM.

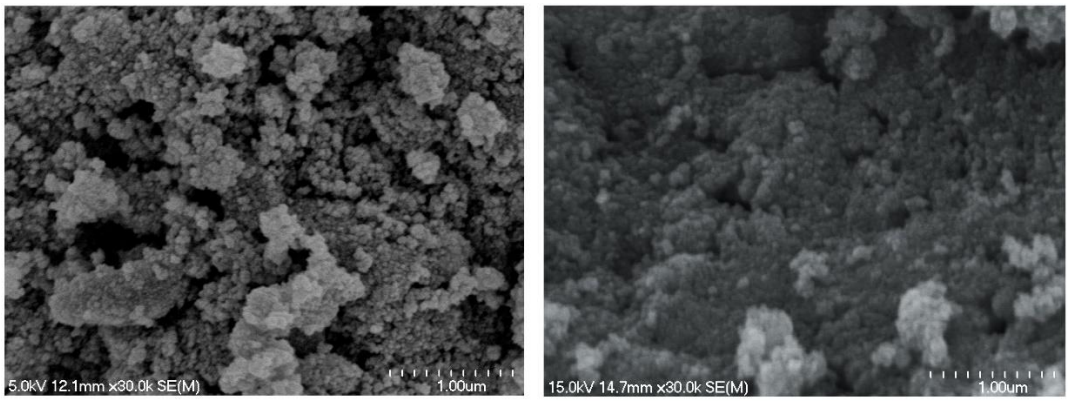

(a) (b)

Figure 7-13 SEM micrographs indicating the morphology of fabricated nanoparticles: a) naked magnetic IONs and b) APTES-coated magnetic IONs.

The morphology of induced $CaCO_3$ crystals in the presence of nanoparticles was also analyzed by using SEM and the micrographs are displayed in Figure 7-14. The assemblages of induced $CaCO_3$ crystals in the presence of naked and APTES-coated IONs, which were mainly spherical particles, are shown in Figure 7-14a and Figure 7-14b, respectively. Biosynthesis of $CaCO_3$ via immobilized bacterial cells with both nanoparticles did not change the morphology of precipitated crystals as compared to the particles induced by free-floating cells. Interestingly, the enlarged photo of precipitated $CaCO_3$ (Figure 7-14c) shows the presence of nanoparticles on the surface of the $CaCO_3$ crystals. Figure 7-14d represents the enlarged area of the precipitated $CaCO_3$ crystal. It is evident that a thin layer of IONs was adsorbed on the surface of $CaCO_3$ particles. Moreover, no morphological changes were observed for the synthesized IONs after the fermentation process.

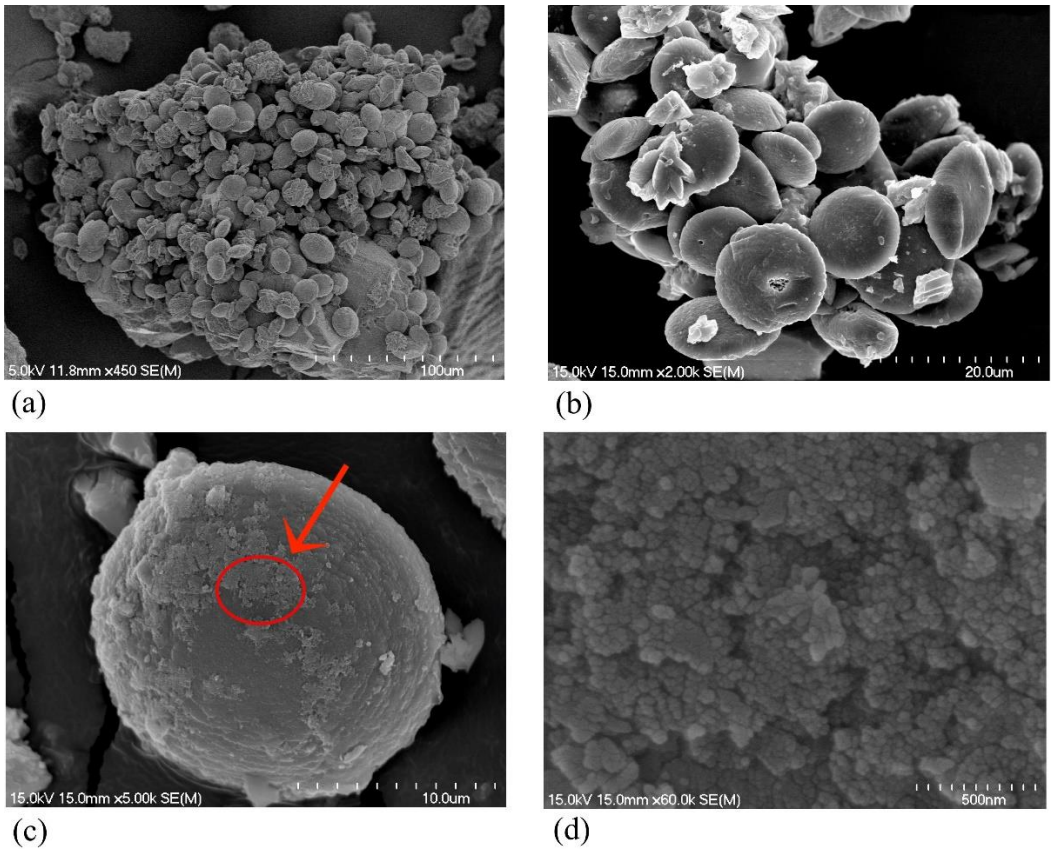

Figure 7-14 SEM images representing: a) an assemblage of bacterially induced $CaCO_3$ precipitation in the presence of naked IONs, b) an assemblage of bacterially induced $CaCO_3$ precipitation in the presence of APTES-coated IONs, c) enlarged $CaCO_3$ crystal surrounded by IONs and d) the morphology of IONs attached to the precipitated $CaCO_3$ crystal.

In addition to SEM imaging, EDS analysis was performed to identify the elemental compositions of the bacterially induced $CaCO_3$ precipitates. EDS spectra for two spots on the precipitated $CaCO_3$ are presented in Figure 7-14. The elemental compositions of the mineralization product at spot one showed a large amount of Ca along with small amounts of C and O. On the other hand, Fe was also detected in addition to Ca, C and O in the spectra for the second spot. As expected for the second spot, EDS analysis confirmed that the attached nanoparticles on the surface of $CaCO_3$ crystal are IONs.

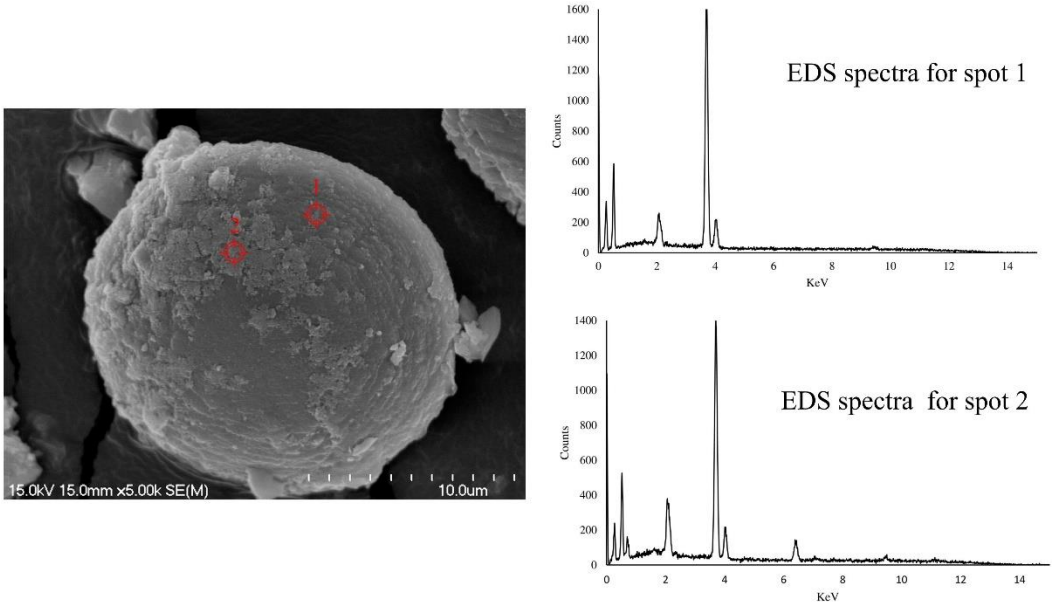

Figure 7-15 EDS spectra for $CaCO_3$ crystals precipitated in the presence of IONs.

7.2.7 Structural characterization of precipitated $CaCO_3$ crystals

In order to deepen the understanding of the presence of decorated cells with IONs in the fermentation media and its effect on $CaCO_3$ morphology, the precipitated crystals were examined by XRD. The XRD patterns for precipitated $CaCO_3$ in the presence of naked and APTES-coated IONs are presented in Figure 7-16 and Figure 7-17, respectively. The data show that the presence of immobilized bacteria with both types of nanoparticles had no effect on the morphology of $CaCO_3$ crystals as compared to free-floating cells. Calcite and vaterite were found to be the most predominant polymorphs precipitated in the media, while no aragonite was detected in the presence of immobilized bacterial cells.

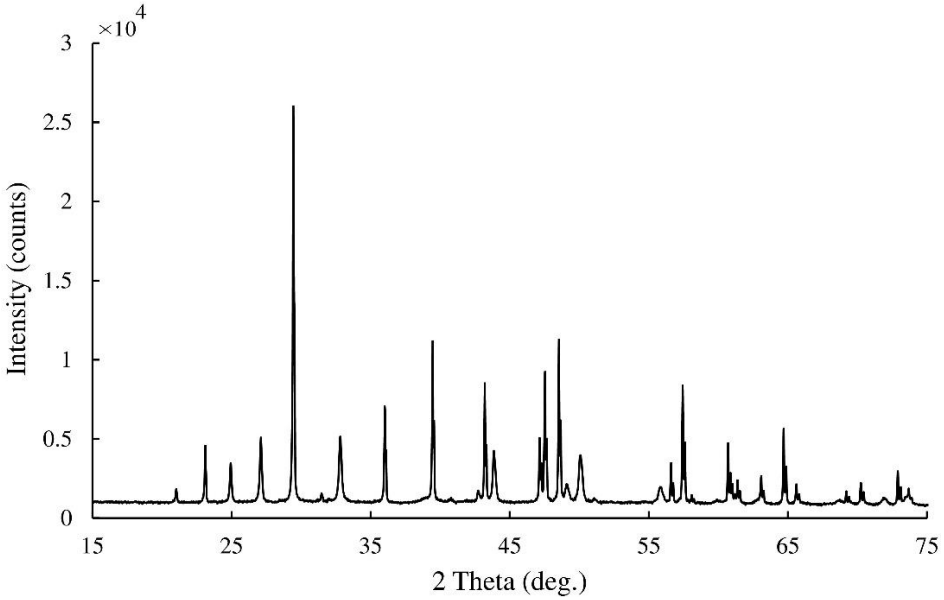

Figure 7-16 XRD spectra for precipitated $CaCO_3$ crystals in the presence of naked IONs.

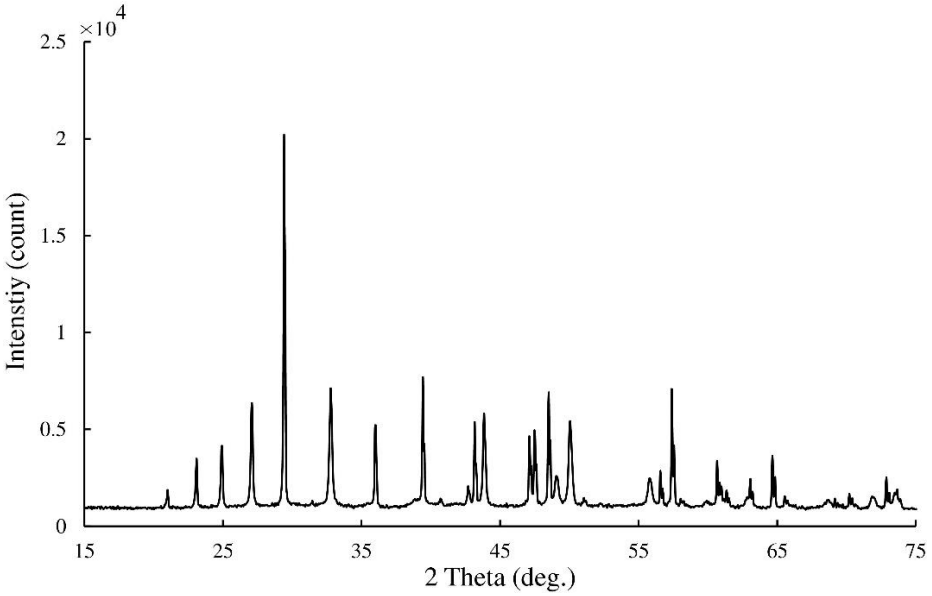

Figure 7-17 XRD spectra for precipitated $CaCO_3$ crystals in the presence of APTES-coated IONs.

7.3 Discussion

7.3.1 Synthesis and surface modification of IONs

In general, there are two critical steps towards crystals formation from a solution, namely nucleation and crystal growth. Monodispersed nanoparticles are generated when the solution reaches its critical supersaturation level and, consequently, the crystals began to grow due to diffusion of solute particles until a desired size is achieved [220, 221]. Different procedures have been described to synthesize the magnetic IONs. Among the various protocols that have been described for the synthesis of magnetic IONs, the aqueous co-precipitation method is the most efficient technique. In this approach, magnetic IONs are synthesized by adding a strong alkaline solution to the aqueous iron salt solutions (ferric and ferrous). In the 1980s, Massart [222] could successfully synthesize magnetite by adding ferric and ferrous chloride solutions to an ammonia solution. However, the yield, particle size, distribution and morphology of these particles depend on different factors, such as the type of solution salts (chlorides, sulfates, nitrates and perchlorates), the ferric and ferrous ratio, ionic strength of the solution, the pH and temperature of the mixture, the speed of basic solution addition, mixing speed and reaction time [134, 223].

IONs show the great promises in different biomedical and biotechnological applications, such as magnetic resonance imaging [224], hyperthermia [225], drug delivery [226], and magnetic separation of bacterial cells, due to their unique characteristics including biocompatibility, the large surface area to volume, and potential of magnetically recovering. However, particle agglomeration, rapid biodegradation, low stability, and alteration of magnetic properties are the main shortcomings associated with the direct addition of uncoated IONs to the biological systems [96, 227]. Surface functionalization can be a promising approach to address the issues associated with uncoated IONs. Different types of surface coating techniques, including encapsulation in polymeric coatings materials and silane coupling agents, have been introduced. Recently silane-treated Fe_2O_3 nanoparticles were proposed as one of the most biocompatible approaches to modify the naked ION characteristics. The amine-modified magnetic surface coating can be achieved through the nanoparticle coating process using APTES, APTS, APDES, and ADES.

It has been reported that various factors, such as pH, reaction temperature and time, can affect the morphology, structure and magnetic properties of these nanoparticles [228, 229].

7.3.2 Characterization of IONs and interaction with bacterial cells

In this chapter, different characterization techniques were employed to analyze the fabricated IONs. The particle size is one of the most critical features affecting the electrical, optical, and magnetic behavior of these nanoparticles [230]. The TEM images confirm that the fabricated nanoparticles are uniform, spherical and monodisperse. Although the IONs' surface coating prevents the core oxidation, it may affect the nanoparticle structures. The results show that the nanoparticle functionalization using APTES had no negative effect on the structure of IONs.

Nanobiotechnology can substantially facilitate the selective separation and reduces the downstream processing and cost by providing a new horizon for the immobilization of bacteria, enzymes, peptides and proteins on magnetic nanoparticles. The cell surface charge is one of the key features of bacterial strains, making them attractive candidates for magnetic immobilization in biotechnological applications. It is known that the bacterial cell walls have a strain dependent net negative charge. The presence of carboxyl or phosphate groups in teichoic acids linked to either the peptidoglycan or the underlying plasma membrane in Gram positive strain results in the cell walls possessing the negative charge [103], while the availability of phospholipids and lipopolysaccharides in Gram negative bacteria is the main reason to impart a negative charge. Apart from the cell wall characteristics, the high surface area to volume ratio of nanoparticles provides a promising site for bacterial capture. However, the successful attachment of bacterial cells with nanoparticles have a significant effect on the cell activity and the efficiency of the bioprocess. As shown in Figure 7-8 and Figure 7-9, the interaction between IONs and bacterial cell walls due to electrostatic attraction or repulsion contributes to adsorption of nanoparticles onto the bacterial cells.

7.3.3 The effect of IONs on the bacterial growth

Over recent years, ION immobilization has been widely reported as a promising technique for biotechnological purposes due to their unique physicochemical properties. Despite the potential applications, immobilization of bacterial cells on IONs is associated with considerations. By reviewing the literature, it can be concluded that IONs have contradictory effects on bacterial cells. Some investigations show that the IONs have a negative effect on normal cell functionalities and contribute to inhibiting the bacterial growth [106]. On the other hand, other studies show that the presence of IONs not only has no negative toxicity or inhibitory influence on the bacterial cells but also contributes to stimulate the bacterial growth [108, 109]. The cells' physiology and ION concentration are the main influential factors which can stimulate or inhibit the bacterial growth [110]. Our results demonstrate that the naked IONs can affect the growth of *Bacillus* species in a dosage-dependent manner. Although the addition of 50 µg/ml of IONs resulted in a decrease in cell growth, further increase in naked IONs concentration led to promote the bacterial growth and the maximum growth was observed in the presence of 150 µg/ml naked IONs.

In order to stabilize the naked IONs, prevent undesired particle agglomeration and provide monodispersibility and biocompatibility, the nanoparticles were surface coated with APTES. ION surface modification offers a promising approach to enhance the bacterial growth. Another advantage of nanoparticle coating is the protection of the magnetic core against oxidation which preserves the magnetic characteristics for a long period of time. However, a lower saturation magnetization capacity caused by surface coating might be the main disadvantage of functionalized nanoparticles. The comparative study on the growth of bacteria in the presence of APTES-coated IONs revealed the important role of Fe nanoparticles on bacterial growth. As expected, surface modification of naked IONs resulted in a higher bacterial growth due to its biocompatibility as compared to uncoated IONs.

In general, nanotoxicity can occur due to: (i) a chemical toxicity based on the chemical composition, and (ii) a stress or stimuli caused by the surface, size and/or shape of the particles [231]. Moreover, the cell viability reduction might be due to the reactive oxygen species (ROS) along with superoxide radicals (O^{2-}), hydroxide

radical (OH^-), and singlet oxygen ($^1O_2$) generated by the IONs [106, 232]. ROS production is one of the most accepted mechanisms causing cell toxicity. ROS are natural byproducts of cellular oxidative metabolism and it is known that many metal oxide nanoparticles have the potential of producing ROS. ROS can affect the modulation of cell survival, death and signaling, as well as differentiation and inflammation-related factor production [233]. Different factors, including particle size, shape, surface area, and chemical composition of nanoparticles, have a direct influence on ROS generation. Oxidative stress, inflammation and consequent damage to the bacterial cell membranes, proteins oxidation and DNA breakage are among the main nanotoxicity mechanisms caused by ROS generation [106]. As shown in Eqs. 7-2 to 7-4, the reduction in molecular dissolved oxygen by nanoparticles containing Fe^0 and Fe(II) in the aqueous solution can contribute to the production of ROS or ferryl-oxo complexes [234].

$$Fe(II) + O_2 \rightarrow Fe(IV)O^{2+} \quad (7\text{-}2)$$

$$Fe(II) + O_2 \rightarrow Fe(III) + HO_2^0/O_2^{-0} \quad (7\text{-}3)$$

$$\equiv Fe(II) + O_2(aq) \rightarrow \equiv Fe(III) + HO_2^0/O_2^{-0} \quad (7\text{-}4)$$

The efficiency of bacterial attachment to the fabricated IONs has also a significant influence on the growth and metabolic activity of bacterial cells. The entrapment of bacterial cells with the high concentration of nanoparticles decreases the cell permeation, while the bacterial cell protection may not be achieved when the low concentration of IONs present around the cells. Therefore the identification of the optimum concentration of nanoparticles is of critical importance.

7.3.4 The effect of IONs on the biosynthesis of $CaCO_3$

The effectiveness of magnetically immobilized cells on nanobiotechnological applications is another significant factor that needs to be investigated. Numerous reports in the literature have demonstrated the potential applications of nanoparticles in the concrete matrix to enhance the mechanical properties. It is believed that Fe_2O_3 nanoparticles are able to act as nano-fillers and to recover the

pore structure of the specimens. This behavior results in improving the concrete water permeability and consequently the performance of the concrete. On the other hand, the direct incorporation of bacterial cells into the concrete mixture during casting leads to decreasing the viability of bacterial cells and the efficiency of the bio-concrete [1, 10]. In this investigation a comparative study on the possibility of inducing $CaCO_3$ precipitation by magnetically immobilized cells was performed. The presence of naked and APTES-coated IONs have a significant effect on biomineralization of $CaCO_3$, however, in a different manner. The experimental results show that the immobilized bacterial cell onto IONs can enhance the mineralization of $CaCO_3$ at higher concentrations of naked IONs, and the highest $CaCO_3$ precipitation is achieved in the presence of 300 μg/mL IONs. However, the results indicate that there was no significant increase in $CaCO_3$ precipitation when the concentration of IONs increased from 250 μg/mL to 300 μg/mL. Therefore 250 μg/mL was selected as the final concentration for application in bio self-healing concrete. On the other hand, the addition of APTES-coated IONs showed a significant negative effect on $CaCO_3$ precipitation as compared to the free-floating bacterial cells. Reduction in the formation of primary and secondary metabolites may be due to stress or stimuli caused by the surface, size and shape of the nanoparticles [217].

7.4 Chapter summary

It has been widely reported that the presence of IONs in the concrete matrix lead to enhance the concrete performance by filling the pores and increasing the cement hydration. The attachment of bacterial cells in/on protective carriers offer a promising approach to protect the bacteria from the resulted shear forces caused by mixing and drying shrinkage of concrete. In this chapter, naked and APTES-coated IONs were successfully synthesized by co-precipitation technique and the fabricated nanoparticles were characterized using TEM, FTIR, SEM and XRD. It was confirmed that the nanoparticles were uniform and monodisperse and the amino acid coating had no significant impact on the size. The fermentation process was performed to investigate the effect of magnetically immobilized cells on bacterial growth and $CaCO_3$ precipitation. It was clearly shown that although

APTES-coated IONs have a significant effect of bacterial growth due to their biocompatible nature, the biomineralization of $CaCO_3$ is adversely affected by an increase in APTES-coated ION concentration. On the other hand, the results indicate the presence of naked IONs is in favor of $CaCO_3$ biosynthesis. Considering the significant effect of nanoparticles on cement hydration and efficient bonding with the concrete matrix, the magnetic immobilization of $CaCO_3$-inducing cells would be a cutting-edge solution to address the shortcomings associated with the direct incorporation of cells into the concrete matrix.

Chapter 8

Evaluating the durability and mechanical properties of the designed bio self-healing concrete [6]

[6] This chapter forms the basis of two research papers published in the Journal of Applied Microbiology and Biotechnology, as referenced below.

[235] **Seifan, M.**, Saramah, K.A., Ebrahiminezhad, A., Ghasemi, Y., Samani, A.K., and Berenjian, A. *Bio-reinforced self-healing concrete using magnetic iron oxide nanoparticles.* Applied Microbiology and Biotechnology, 2018. 102: p. 2167-2178.

[236] **Seifan, M.**, Saramah, K.A., Samani, A.K., Ebrahiminezhad, A., Ghasemi, Y., and Berenjian, A. *Mechanical properties of bio self-healing concrete containing immobilized bacteria with iron oxide nanoparticles.* Applied Microbiology and Biotechnology, 2018.

8.1 Introduction

Concrete is one of the world's most versatile and widely used construction materials. High compressive strength, versatility, availability, affordability, simple preparation, fire resistance, excellent thermal mass, compatibility with steel reinforcement bar and the possibility of casting in desired shapes are the most important features of concrete. Despite the advantages of concrete, it has a low tensile strength and is susceptible to cracking under internal and external stresses. To address the low tensile strength and ductility, concrete is mostly reinforced with embedded bars. In this case, the reinforced concrete (with reinforcement bars) resists not only compression but also bending and other exerted tensile stresses. Therefore an intelligent design will result in concrete resists in both compression and tensile stresses. Reinforcement bars have a positive effect on crack width restriction by controlling plastic shrinkage. However, they cannot prevent crack formation.

Once a crack occurs in concrete, the aggressive chemicals penetrate into the matrix. This results in the reinforcement bars' corrosion and decreasing the concrete integrity and service life. As a result of this phenomenon, more cement is needed to replace the degraded concrete. The massive production of concrete has an adverse impact on the environment through the production of cement as the main constituent of the concrete. Cement is produced by heating the raw materials including $CaCO_3$, silica, alumina and iron ore. Therefore an urgent action is in high demand due to the limitation of natural resources to produce cement, and also considerable maintenance costs of degraded concrete structures.

Currently, there are different types of passive crack treatments which are applicable for the detected cracks. The application of chemical and polymer sealers as the external coating agent is a common approach to seal the visible cracks. However, these techniques are associated with considerable shortcomings, such as poor weathering and low heat resistance, sensitivity to moisture and temperature, poor bonding with concrete, susceptibility to degradation, and delamination with age and short lifespan. An ideal healing approach should have quality, long shelf life, pervasiveness, and the ability to heal cracks repeatedly an unlimited number of times. One promising solution to address the cracking issue would be the

incorporation of self-healing mechanisms into the concrete matrix. Dry [237] reported that the encapsulation of adhesives or sealants into the concrete matrix can contribute to fabricate a self-healing concrete. It was found that the release of the healing agent from the porous-walled fibers incorporated into the matrix results in filling the crack. The healing agent can be incorporated in short fiber or long tubes. The incorporation of expansive materials is another approach for designing self-healing concrete. Upon crack formation, the expansive materials are activated and started to expand when triggered by water, moisture or carbonation penetration [238]. In spite of the positive effect of encapsulation methods on crack sealing properties, these approaches are not repetitive and cannot guarantee the concrete integrity.

Over recent years, a sustainable biotechnological approach has emerged as an alternative approach to conventional techniques to heal the concrete cracks. Incorporation of bio healing agent (bacteria and nutrients) offers a promising approach to design an efficient self-healing concrete. Despite the recent progress in improving concrete properties by incorporation of the microbial agent, there are still some shortcomings needed to be addressed. In previous chapters we could address the limitations associated with the bio self-healing concrete.

In this chapter the designed bio-agent compound is incorporated into the concrete matrix to evaluate the performance of the bio self-healing mechanism. The characteristics of bio-concrete in terms of crack filling capacity, compressive strength, drying shrinkage, sorptivity, and water absorption are determined. Moreover, a characterization study is performed to analyze the precipitated $CaCO_3$ crystals.

8.2 Results

The concrete samples were mixed and casted according to ASTM standard specifications noted in Chapter 3. To cast the bio-concrete specimens, bio-agent compounds, including the nutrients and immobilized bacterial cells, were dissolved in tap water and the mass adjusted to the same levels as the control specimens

required. All the samples were cured in the moist condition and the following results were obtained.

8.2.1 Water absorption

The influence of bio-agent on water absorption of concrete specimens was investigated. Figure 8-1 shows the samples used to determine water absorption of specimens in accordance with ASTM C642-97. The results obtained for water absorption is shown in Figure 8-2. The results indicate that the inclusion of proposed bio-agent decreased the water absorption capacity after immersion and boiling of the concrete specimens due to $CaCO_3$ precipitation as a result of the bacterial metabolic activity. The reduction in volume permeable pore space in bio-concrete samples implies the precipitation of $CaCO_3$ could fill the pores and cavities.

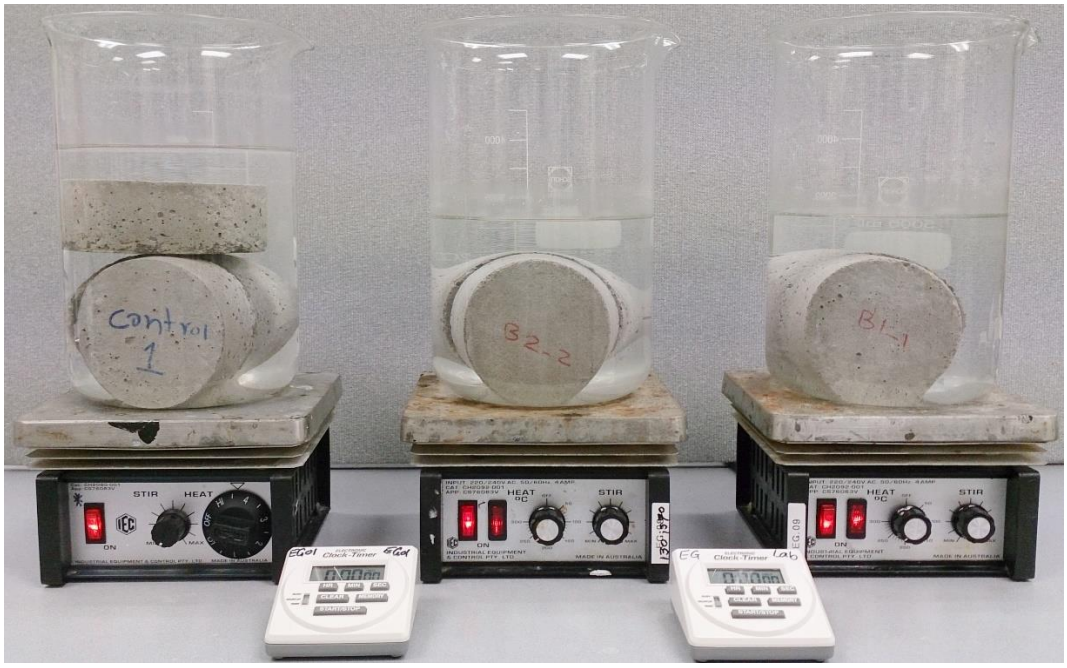

Figure 8-1 Experimental setup of the water absorption test (according to ASTM C642-97).

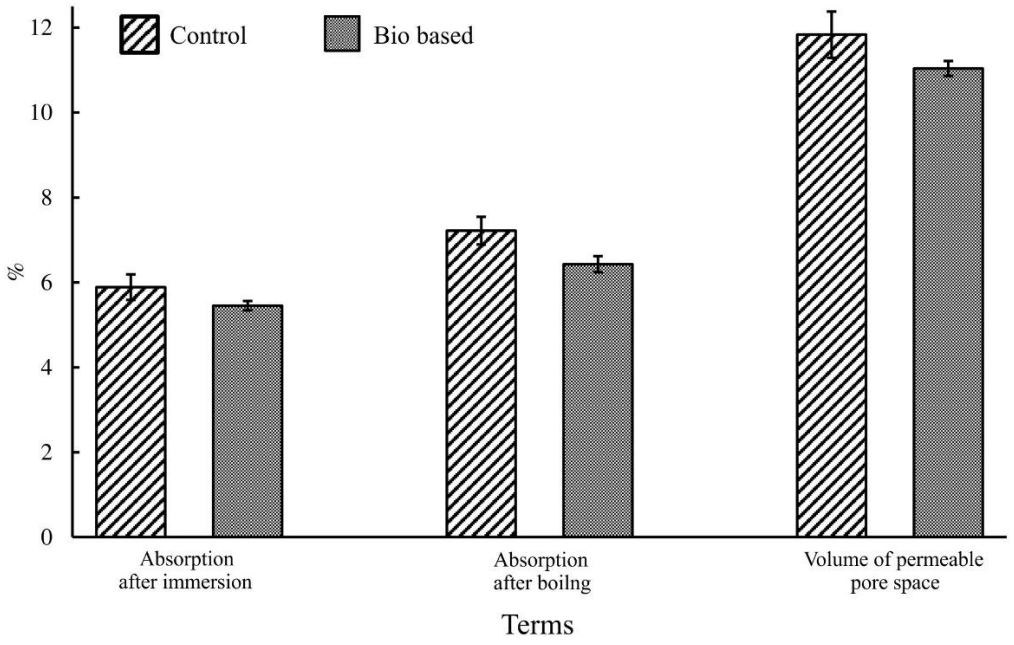

Figure 8-2 Effect of bio-agent addition on water absorption, after immersion and boiling, and volume of permeable pore space of concrete specimens.

8.2.2 Water sorptivity

Concrete sorptivity over time is another characteristic that can affect the concrete properties. To investigate the effect of proposed bio-agent on concrete water absorption rate, the experiments were performed according to ASTM C1585-04. Figure 8-3 shows the samples were used to determine water absorption rate.

Figure 8-3 Experimental setup of water absorption rate (according to ASTM C1585-04).

The results for the water absorption rate over a period of 9 days is presented in Figure 8-4. It was noticed that the presence of bio-agent in concrete resulted in a significant decrease of the water uptake as compared to control specimens.

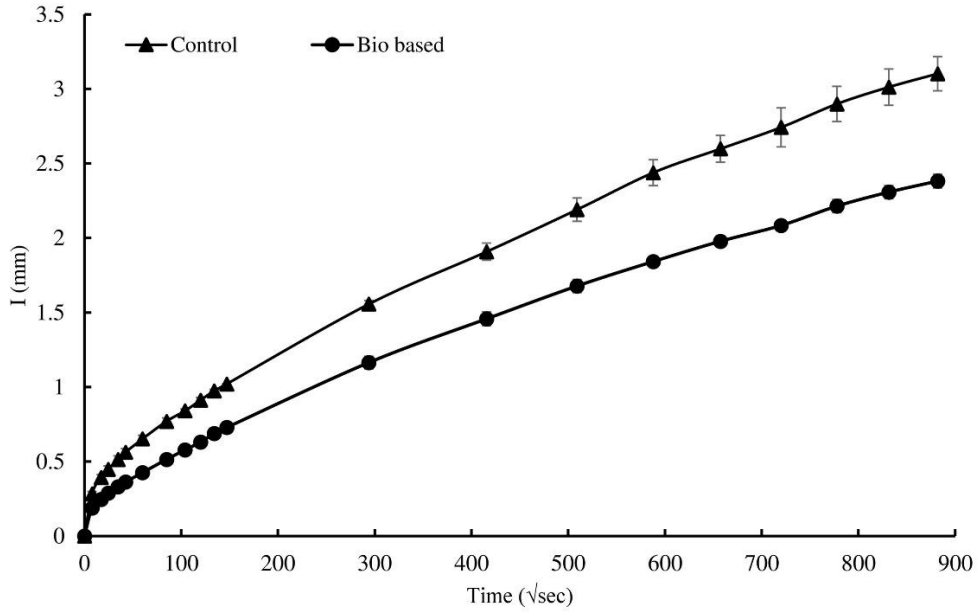

Figure 8-4 Capillary water absorption of the specimens as a function of time.

Water uptake takes place in two stages namely initial and secondary absorption. The initial rate of water absorption is defined as the slope of the line, which is constructed using least squares, linear regression analysis, to fit the curve of absorption (I) versus the square root of time (√sec) for the first 6 h of the testing. The secondary rate of water absorption is defined as the slope of the line that is drawn using least squares, to fit the curve of absorption (I) against the square root of time (√sec) from 1 d to 9 d. The initial and secondary absorption rate of control and bio-based specimens is presented in Table 8-1. The presence of bio-agent in concrete had positive effects on both initial and secondary water absorption stages. The results indicate that the control specimens absorbed 35% higher water than bio-based samples during initial absorption stage. A similar trend was observed over the secondary absorption stage where water uptake in control samples was 28% higher than bio-based samples.

Table 8-1 Initial and secondary absorption rate of the bio-based and the control concrete specimens.

	Initial absorption		Secondary absorption	
	S_i (mm/√sec)	R^2	S_s (mm/√sec)	R^2
Control specimen	5×10^{-3}	0.984	2.7×10^{-3}	0.995
Bio-based specimen	3.7×10^{-3}	0.995	2.1×10^{-3}	0.996

8.2.3 Compressive strength

Figure 8-5 presents the average compressive strength of the control and bio-based concrete specimens at 3, 7 and 28 days. As compared to the control specimens, the concrete samples containing bio-agent had the higher compressive strength at all ages. The incorporation of designed bio-agent into concrete resulted in 74% higher compressive strength after 3 days. Likewise, the compressive strengths of bio-concrete samples were increased by 43% and 15% after 7 and 28 days, respectively. Despite the positive effect of bio-agent on compressive strength, the aging caused higher compressive strength recovery for the control samples than bio-concrete specimens.

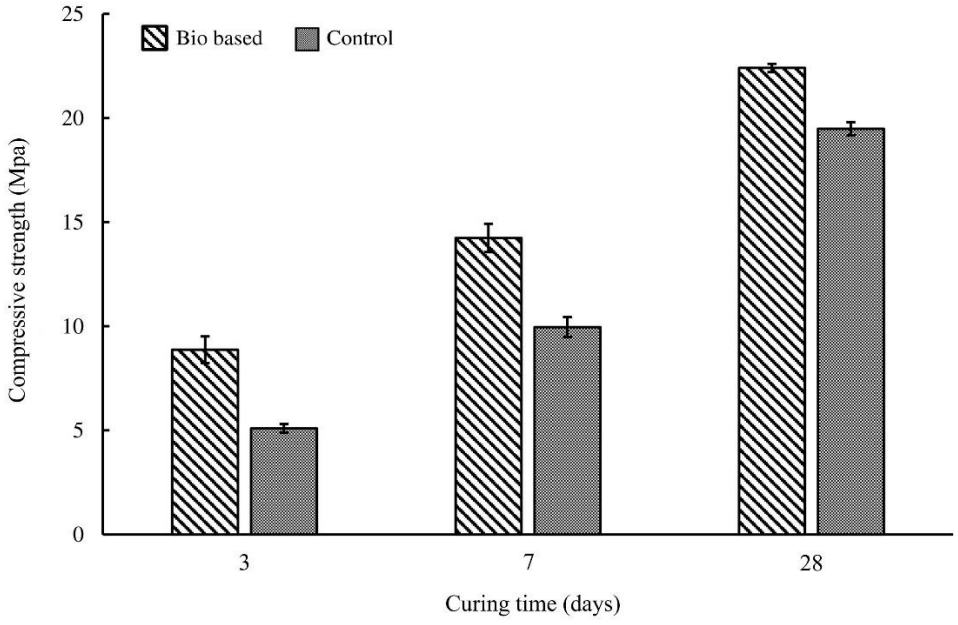

Figure 8-5 Comparison of compressive strength of the control and the bio-based concrete samples for 3, 7 and 28 days.

8.2.4 Drying shrinkage

Drying shrinkage samples and the apparatus to measure the length is shown in Figure 8-6. The drying shrinkage measurements for all concrete specimens up to 60 days are presented in Figure 8-7. The values in this figure shows the average of three measurements. The experimental results disclose that the inclusion of bio-agent into the concrete mixture resulted in a higher free shrinkage than control samples. The drying shrinkage of all concrete samples increased very quickly during the first 14 days of drying storage; however, the strain values slightly changed after that time.

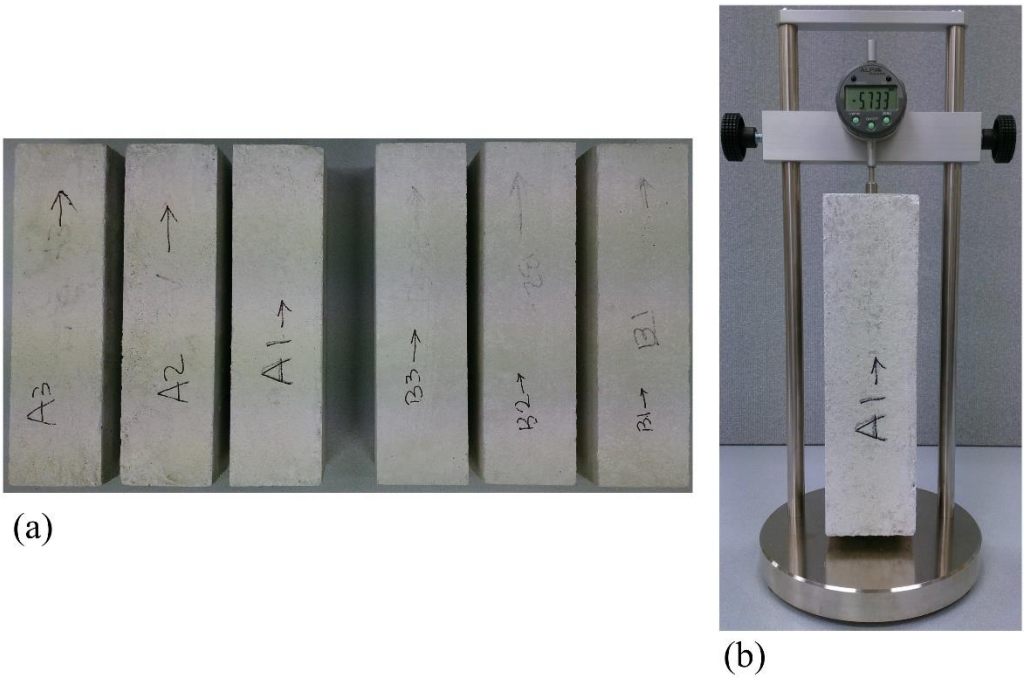

Figure 8-6 Experimental set up for drying shrinkage measurement a) prismatic concrete specimens and b) length comparator.

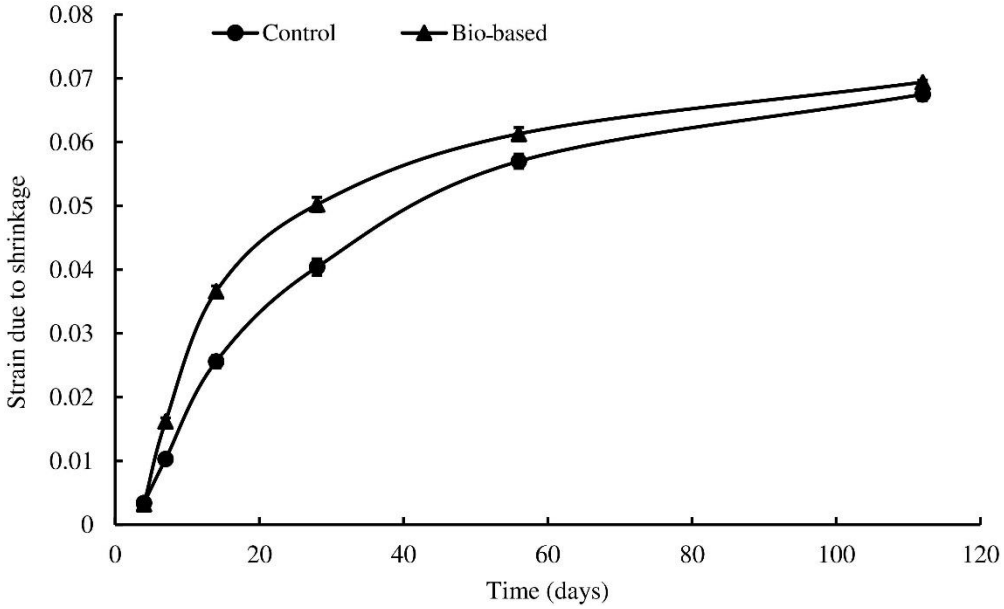

Figure 8-7 Comparison of drying shrinkage of the control and the bio-based concrete samples.

8.2.5 Crack closure observation

After evaluating the mechanical characteristics of concrete specimens, an experiment was performed to visualize the crack closure by $CaCO_3$ deposition. The surface of the concrete samples was observed and photographed with a light microscope equipped with a camera. The crack healing ratio varied depending on the initial crack width and the availability of bio-agent. Figure 8-8 to Figure 8-11 display the direct stereomicroscopic observation of cracks closure in bio-based and control concrete specimens before and after exposure to water. As shown in Figure 8-8, the bio-concrete specimen possessed a high crack sealing capacity after the healing process. Figure 8-9a–b present the enlarged photos of the cracks filled by $CaCO_3$. In general, the smaller crack width showed the higher sealing capacity. Apart from crack sealing, the results indicate that the bio-concrete is also able to seal the pores created during casting. Similar sealing behavior was also observed for the pores and the results are demonstrated in Figure 8-9c–d. However, it was noticed that the efficiency of the bio-concrete to recover the cracks is slightly higher than pores and cavities. This might be due to the higher surface area and the ease of nutrient transportation in cracks which increases the availability of bio-agent and

consequently more $CaCO_3$ is induced. It is worth noting that the crack sealing efficiency was enhanced with an increase in the incubation period.

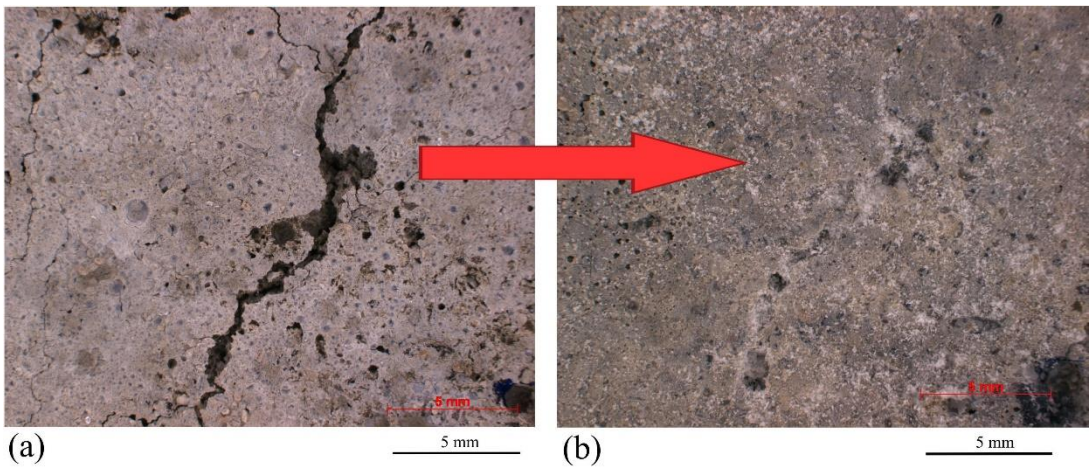

Figure 8-8 Stereomicroscopic images of the crack healing process in bio-concrete specimen (a) before and (b) 28 days after water exposure.

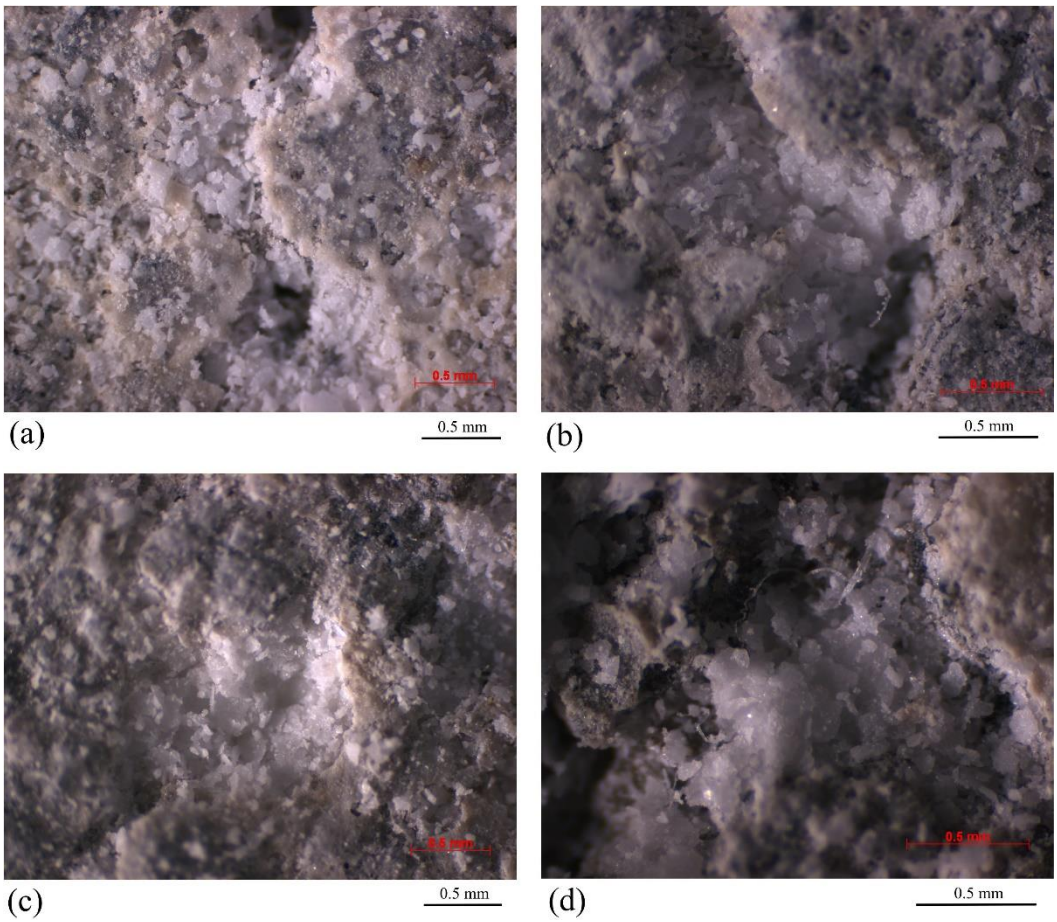

Figure 8-9 Stereomicroscopic images of induced $CaCO_3$ precipitation after 28 days water exposure in (a–b) cracks and (c–d) pores.

On the other hand, no significant crack healing occurred in the control specimens and the majority of the final crack widths remained the same as the initial ones (Figure 8-10). The control samples showed a limited crack sealing capacity, possibly due to autogenous healing after submersion in water. Young concrete has the ability to heal the surface microcracks upon hydration of unhydrated cement particles; however, this highly depends on the presence of unreacted cement around cracks and pores. The stereomicroscopic images in Figure 8-11 illustrate a thin layer of crystal on crack walls. Although this confirms the autogenous healing capacity of the concrete, it was not significant as compared to bio-based agent healing efficiency and could not seal the cracks.

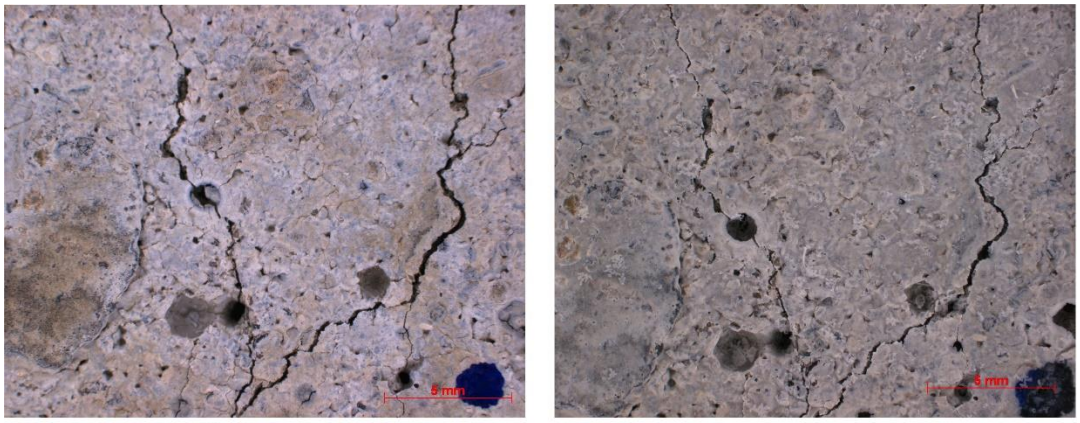

Figure 8-10 Stereomicroscopic images of the crack in control specimen (a) before and (b) 28 days after water exposure.

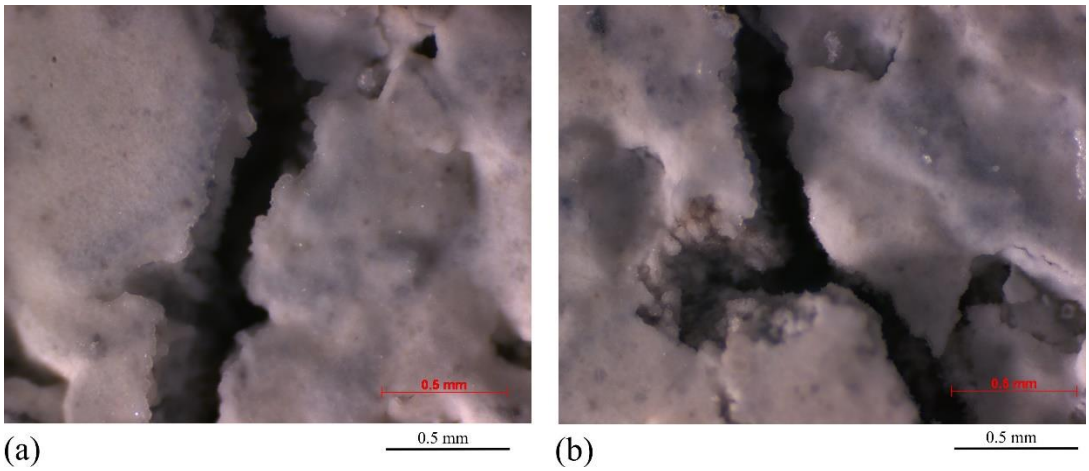

Figure 8-11 Stereomicroscopic images of crack in control specimen after 28 days water exposure.

8.2.6 Visualization and analysis of deposited $CaCO_3$

SEM analysis was performed to characterize the precipitated crystals in bio-concrete specimens. Figure 8-12a and b, shows a massive columnar precipitate induced in bio-concrete samples after 28 days healing process. The deformed lamellar rhombohedra was observed as the main morphology for the precipitated crystals. Since this crystal morphology was observed in cracks, pores and those areas contacted with water, it can be concluded that its formation was related to activation of the incorporated bio-based agent. Once a cracking occurs, the designed bio-based agent is activated and the sealing process starts. This mechanism can clearly be seen from Figure 8-13. In case of cracking (Figure 8-13a), $CaCO_3$ is induced on both surfaces of the crack as a result of bacterial activity. The healing process continues until the crack is entirely sealed. The same scenario happens for the voids and pores; however, as shown in Figure 8-13b, the $CaCO_3$ is induced from the bottom of the cavity as well.

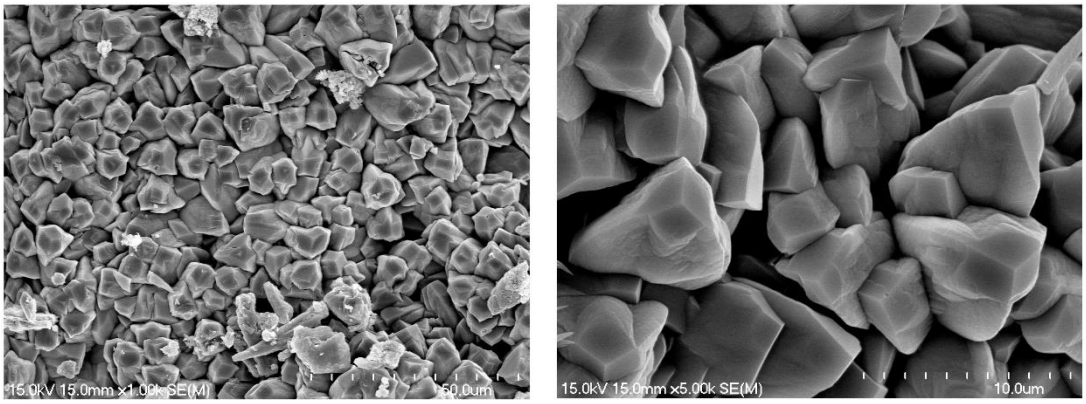

(a) (b)

Figure 8-12 SEM micrographs of the precipitated crystals in the concrete specimens containing the bio-based agent.

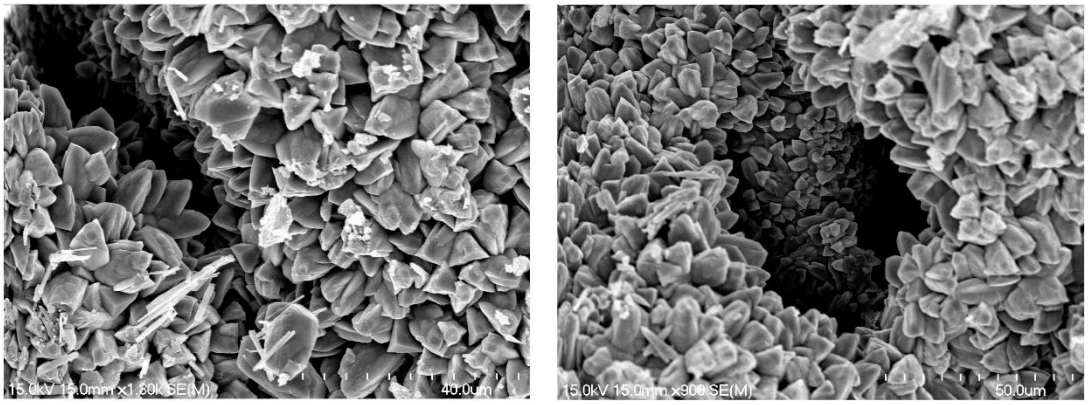

(a) (b)

Figure 8-13 SEM micrographs indicating the deposition of bacterially induced $CaCO_3$ in micro a) crack and b) pore.

During SEM imaging, EDS was performed to analyze the elemental composition of minerals precipitated during healing (Figure 8-14). The EDS results show that Ca, C and O were the main compositions of the precipitated crystals in bio-concrete specimens. Considering the ratio of the elements, it suggests that the precipitates were $CaCO_3$. To gain an insight into the distribution and the composition of chemicals present at the inner crack surface, the elemental composition mapping was performed and the results are presented in Figure 8-15. The EDS maps of the broken cracked specimen show a high concentration of Si and a low distribution of Ca in the crack surface wall. In contrast to the crack surface, a higher concentration of Ca was detected over the precipitated crystals. Based on the distributions of elements in the crack area, it can be concluded that the crack sealing due to bacterial activity was successfully achieved.

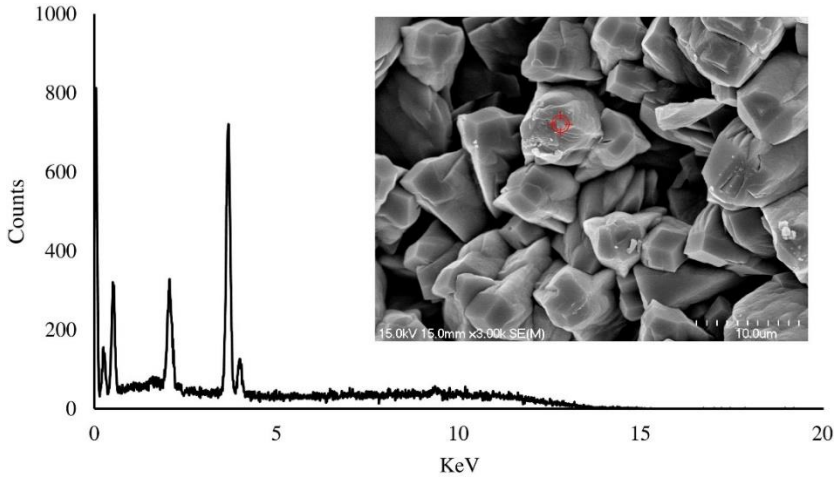

Figure 8-14 EDS spectra of the precipitated crystals in bio-concrete.

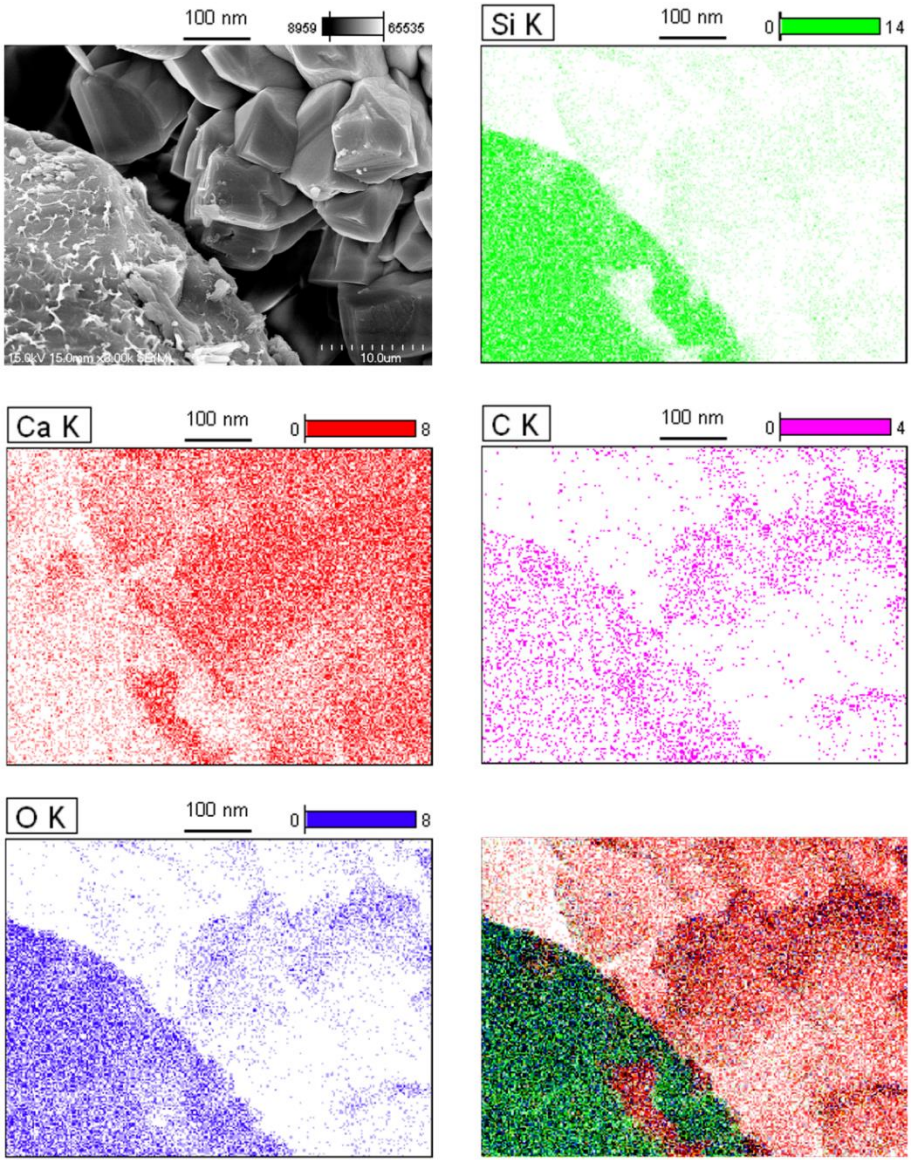

Figure 8-15 EDS chemical composition mapping of deposited bacterially induced $CaCO_3$ in a broken cracked specimen.

8.3 Discussion

8.3.1 Water absorption and sorptivity

Fluid transport in porous structures, such as concrete and mortar, plays an important role in determining the durability of these materials. The pores and voids left inside the concrete matrix create capillaries upon the evaporation of excess water from the concrete paste. The permeability is related to the pore structure of the concrete matrix. It has been reported that the presence of supplementary materials, which serve to occupy the pores and microcracks as well as the degree of cement hydration, can affect the permeability [140]. As presented in water absorption results, the specimens containing bio-agent showed a higher water penetration resistance as compared to the control samples. The reduction in water penetration is attributed to the bacterially induced $CaCO_3$ crystals and the presence of IONs which fill the concrete pores and void. Moreover, the lower volume of permeable pore space in the bio-agent samples confirms the filling of the concrete pores by precipitated $CaCO_3$. This demonstrates the successful implementation of bio self-healing agent into the concrete matrix to minimize the water absorption of the structure.

Apart from water absorption, the sorptivity of concrete over time significantly affects its properties. There are different factors influencing the water sorptivity of a concrete as follows [152]:

- Concrete mixture proportions
- The presence of chemical admixtures and supplementary cementitious materials
- The composition and physical characteristics of the cementitious component and aggregates
- The entrained air content
- The type and duration of curing
- The degree of hydration or age
- The presence of microcracks
- The presence of surface treatments such as sealers
- Placement method including consolidation and finishing
- The moisture condition of the concrete at the time of testing

The results show that the bio-concrete had a lower water uptake rate over 9 days of exposure. As can be seen from Figure 8-4, the water absorption curves have three main regions namely the (i) short-term water absorption, (ii) transition, and (iii) long-term water absorption. The initial and secondary sorptivity refer to the short-term and long-term absorption rates which can be obtained from the equations of the curve in each region. The initial absorption is an indication of how quickly the water penetrates and fills the large pores and cracks. Whereas, the secondary absorption implies how quickly and easily the water fills the small pores and air voids. The bio-concrete specimens possessed lower short-term and long-term values of water absorption. It was also noticed that the secondary absorption was considerably lower than initial absorption since the higher percentage of water was already absorbed during the first hours of the test. The experimental results show that the deposition of bacterially induced $CaCO_3$ crystals in the concrete cracks and pores resulted in a decrease in permeation capacity. This indicates that the inclusion of designed bio-agent in concrete limits the ingress of harmful chemicals, and as a result the structure life span will be increased.

8.3.2 Compressive strength

Compressive strength is another important property of concrete. The results indicate that the incorporation of bio-agent into the concrete matrix had a significant effect on compressive strength. $CaCO_3$ deposition in porous matrix is the main reason to enhance the compressive strength in bio-concrete specimens. Moreover, the addition of IONs has a significant effect on mechanical properties of concrete. The embedment of bacterial cells in/on milli/macro-scale particles minimizes the cell interaction with surrounding and nutrients. However, the immobilization of bacterial cells with nanoscale sized particles such as IONs can protect the cells from the concrete harsh environment without compromising on the interaction of bacterial cells with surrounding. Furthermore, the addition of IONs can contribute to enhancing the concrete mechanical properties in two ways [94]: (i) acts as a nucleus to tightly bond with cement hydrate, and (ii) promote the cement hydration as a result of their high activity. Although the presence of bio-agent resulted in a higher compressive strength than control samples, the higher improvement was

observed in early ages. Since the concrete matrix is still porous during the initial curing period, there is a high chance of reaching nutrients to the bacteria. Deposition of $CaCO_3$ in early ages contributes partial filling of pores and voids. This phenomenon may result in the blockage of nutrients and oxygen flow to the bacterial cells, and consequently the bacterial cells turn into endospores and $CaCO_3$ precipitation is decreased. Another explanation for this phenomenon is a fast rate of hydration during the early ages of concrete curing in the samples containing decorated bacterial cells with IONs [104].

8.3.3 Drying shrinkage

Water is one of the main constituents of the concrete and its excess loss from the matrix as it hardens results in a volume reduction. Drying shrinkage is the volume reduction as a result of moisture loss during the concrete hardened state. The internal parameters, such as concrete mix design, water-cement ratio, admixtures, and the type of cement and aggregates, can affect the moisture loss from the concrete. Whereas the ambient conditions (i.e., temperature, pressure, and relative humidity), size and shape of the concrete are recognized as the external factors influencing the drying shrinkage. Although the drying shrinkage alone cannot provide necessary information on the behavior of the structures (due to the fact that the majority of the concretes are restrained by reinforcement or the structure), it can offer valuable information on shrinkage stress development [239].

The free drying shrinkage data show a higher strain in bio-based specimens than control samples. Compared to the control samples, the bio-concrete specimens contained additional chemicals such as IONs and nutrients. Therefore the reason for the higher shrinkage in bio samples might be due to autogenous shrinkage which occurs as a result of these chemical reactions during cement hydration. The test results obtained herein agree with the findings of the study conducted by Sierra-Beltran et al. [142] which reported a higher shrinkage strain in the samples containing bio-based agent (*B. cohnii* and calcium lactate). To address this issue, the concrete reinforcement is a promising solution to control and restrain the concrete shrinkage strain.

8.3.4 Visualization of crack sealing and precipitate

As evidenced in the stereomicroscopic image (Figure 8-8), the incorporation of designed bio-based agent could successfully seal the concrete cracks as compared to the reference samples (Figure 8-10). To gain a deeper understanding of the precipitate morphology and the mechanism of the healing process, SEM analysis was performed. The SEM micrographs provided a unique overview of the mechanism of healing defects in concrete. The SEM micrographs show that the deposition of $CaCO_3$ starts from the crack surface and continues until the crack is filled. Moreover, the morphology of the induced crystals had rhombohedral structure. This morphology is similar to the morphology of $CaCO_3$ reported by Wiktor et al. [66] and Wang et al. [87]. EDS analysis was conducted to analyze the elemental composition of the deposited crystals in the crack. The EDS pattern confirms the precipitation of $CaCO_3$ crystals in the crack. Moreover, elemental mapping was performed to visualize the concrete response to crack initiation. As displayed in Figure 8-14 and Figure 8-15, the elemental composition of precipitated crystals in the crack suggested $CaCO_3$ was induced inside the concrete crack due to the presence of immobilized bacterial cells.

8.4 Chapter summary

The main objective of this chapter was to investigate the effect of the designed bio-agent on the concrete properties. To achieve this, the efficiency of bio-concrete to seal the crack was studied by using microscopic observation. The stereomicroscopic images illustrate that the designed bio-concrete can successfully sense the damages and heal the defects. Indeed, the bio self-healing possess a superior crack-sealing capacity as compared to untreated concrete. The effects of bio-agent on the concrete mechanical properties were also investigated. The results indicate that the inclusion of immobilized bacterial cells with IONs in concrete increases the compressive strength. Bio-deposition of $CaCO_3$ in cracks and voids brought about a lower water absorption and sorptivity as compared to the control specimens. However, a higher strain due to drying shrinkage was observed in those samples containing bio-agent.

Chapter 9

Conclusions and recommendations

It is evident that the cracking phenomenon in concrete is a complex issue since it can occur under different conditions. Designing a concrete with self-healing characteristics has drawn much attention to prevent the structure deterioration. Self-healing mechanism in concrete can be achieved through physical, chemical and mechanical approaches. Concrete itself has the ability to partially heal microcrack via autogenous healing. However, the efficiency of autogenous healing is not enough to heal all generated cracks, and, more importantly, its success relies on many factors. Therefore a novel bio self-healing mechanism has been proposed to address the concrete issue by producing the most compatible material with concrete. This chapter remarks on the investigation performed in the previous chapters by summarizing the conclusions and prospectives.

9.1 Fundamental approach

One promising approach for designing the new generation of more durable concrete structures is the incorporation of self-healing agents into the concrete matrix. Among the potential self-healing agent, a bio-based healing agent distinguishes itself by inducing a highly compatible compound with concrete matrix ($CaCO_3$). This novel idea has attracted much attention; however, prior to practical implementation in a real situation, a laboratory proof of concept is required. The laboratory experimental investigation allows the exploration of different concepts and possibilities of this innovative technology. The process development strategies for bio self-healing concrete are as follow:

9.2 Design of a potent bio-agent to induce $CaCO_3$

The effectiveness of a bio self-healing concrete highly relies on the capability of inducing $CaCO_3$. The utilization of suitable microbial compounds at their optimum levels can significantly enhance the efficiency of bio self-healing concrete by filling the entire cracks and pores. In Chapter 4, different genera of bacteria, nutrients, Ca sources and operating conditions were screened to identify the potent variables on the MICP process. For this purpose, a simple and cost efficient screening in shake flask scale was conducted. It has been demonstrated that *B. sphaericus*, *B.*

licheniformis, yeast extract, urea, calcium chloride, and agitation speed have a significant effect on the biosynthesis of $CaCO_3$. Thereafter an optimization study was performed to determine the optimum concentrations of potent variables on the biomineralization of $CaCO_3$. However, the capability of isolates to induce $CaCO_3$ precipitation in the concrete environment needs to be investigated.

9.3 Capability of inducing $CaCO_3$ in high pH and investigation into the role of oxygen in $CaCO_3$ precipitation efficiency

The applicability of the optimized bio-agent to induced $CaCO_3$ in the concrete environment was tested using a fermentor in Chapter 5. A real-time on-line monitoring of the effective factors on biomineralization of $CaCO_3$ in a bioreactor indeed helps to gain a comprehensive understanding of the basis of the biomineralization process. To achieve this the fermentations were performed at different pH levels ranging from 9 to 12. The results indicate that the pH has a significant effect on $CaCO_3$ precipitation; however, the increase of pH leads to a decline in cell viability. It was also found that the selected isolates are capable of withstanding in concrete pH. Morphological observation and the crystal characterization studies demonstrated that the pH is a potential factor on $CaCO_3$ morphology. The lower pH (9–10) found to be favorable of vaterite precipitation, while a higher pH (10–12) resulted in a transformation of vaterite to calcite. Notably, the increase of pH changed the surface structure of bio-precipitates from smooth to rough. Higher magnification images of induced crystals at high alkalinity fermentation display that $CaCO_3$ structures are composed of an oriented aggregate of crystal.

By reviewing the literature, it can be concluded that the bio self-healing mechanism is limited to the specific depth of the crack. The reduction in bio self-healing efficiency is attributed to the oxygen limitation inside the cracks. To investigate the effect of oxygen level on biomineralization of $CaCO_3$, the aeration controlled fermentation at different levels of airflow (0.5–4.5 SLPM) were performed. The results indicate that aeration has a significant effect on both bacterial growth and $CaCO_3$ precipitation. In contrast to aeration controlled batches,

the result obtained by SEM and XRD point out that aeration rate has no effect on the $CaCO_3$ morphology, and calcite and vaterite were found the predominant polymorph precipitated at aeration controlled batches.

9.4 Promising approach to increase the oxygen level inside the concrete crack

Since the bio self-healing efficiency depends on the availability of oxygen in the concrete crack, Chapter 6 focuses on designing a new approach to introduce oxygen inside the concrete matrix. A simple, active and long-term protocol was proposed to not only enhance but also accelerate the bacterial $CaCO_3$ precipitation. In the first stage, the effect of various ORCs on $CaCO_3$ biosynthesis was investigated. The results show that the addition of CP and ZP inhibits the precipitation of $CaCO_3$, while UP and MP contribute to enhancing $CaCO_3$. Therefore an optimization study was performed to maximize the production of $CaCO_3$. It was demonstrated that the $CaCO_3$ precipitation and cell growth are enhanced by the addition of optimum concentrations of UP and MP. It is hypothesized that the addition of the designed ORCs can terminate further crack development in the concrete structures by activation and support the biomineralization process in oxygen-limiting areas.

9.5 Nanotechnological approach for the bacterial cell protection

The direct incorporation of bacterial cells into the concrete matrix is associated with several drawbacks. These shortcomings are (i) decreasing in the cell viability at high pH, (ii) high risk of cells squeezing upon the cement hydration, and (iii) excreting the shear force on bacterial cells during concrete preparation. To address these limitations a novel nanotechnological approach was proposed in Chapter 7. Nanotechnology has emerged as a promising way in many industrial sectors such as construction. Moreover, the unique biological and chemical properties of nanoparticles, such as IONs, make them potential for biotechnological processes. Considering the positive effect of nano-scaled sized particles on concrete properties, possibility of bacterial immobilization with these carriers was investigated. Chapter 7 was performed to study the feasibility of MICP using different magnetically

immobilized IONs. In this chapter, naked and APTED-coated IONs were successfully synthesized and the prepared particles were characterized using different techniques including TEM, FTIR, SEM and XRD. The characterization studies confirm the formation of uniform and monodisperse IONs. To evaluate the effects of magnetically immobilized bacterial cells on the biomineralization of $CaCO_3$ and bacterial growth, the fermentation study using different concentrations of naked and APTES-coated IONs was performed. As expected, the amino acid coating of IONs resulted in a higher bacterial growth due to the biocompatible nature of APTES-coated IONs. However, the presence of APTES-coated IONs contributed to a significant decrease in $CaCO_3$ biosynthesis. On the other hand, the results show that the presence of naked IONs is in favor of $CaCO_3$ biosynthesis. Considering the significant effect of nanoparticles on cement hydration and efficient bonding with the concrete matrix, the immobilization of bacterial cells with naked IONs is proposed as a promising approach in the application of bio self-healing concrete.

9.6 Performance of the designed bio self-healing concrete

In Chapter 8 the performance of the designed nanobiotechnological self-healing concrete was investigated. The efficiency of the proposed bio self-healing concrete was determined using various laboratory tests such as compressive strength, water absorption, drying shrinkage, and crack healing observation. The results indicate that the inclusion of immobilized bacterial cells with IONs in concrete increases the compressive strength. Bio-deposition of $CaCO_3$ in cracks and voids brought about a lower water absorption and sorptivity as compared to the control specimens. However, a higher strain due to drying shrinkage was observed in those samples containing bio-agent. The microscopic images illustrate that the proposed bio-concrete can successfully sense the cracks and heal them accordingly. The overall results indicate that the novel development of bio self-healing mechanism, indeed improve the concrete mechanical properties and show a high crack sealing efficiency.

9.7 Outlook

The new generation of bio self-healing concrete has been developed and tested in the laboratory scale. The experimental results proved that the incorporation of the designed bio-agent in concrete can substantially enhance the concrete properties such as crack sealing capacity, compressive strength and water absorption.

To be industrially applicable, an up-scale investigation needs to be performed. The bio self-healing cost is another subject that needs to be considered. The main sources of costs are for the nutrients, bacterial preparation and immobilization. Since the concrete is relatively cheap, the price of bio self-healing concrete must be competitive enough to attract contractors. To achieve this, the application of alternative nutrients compound from waste is suggested. In this case, a screening study is required to investigate the effect of different nutrients on MICP process.

Water plays a key role in the MICP process. Since water is required to initiate $CaCO_3$ precipitation, the addition of water based polymers can significantly accelerate the concrete crack healing process.

It is believed that the numerical modeling of the proposed bio self-healing concrete contributes to gain a better understanding about the system behavior, specifically with reinforcement bars.

References

1. Seifan, M., A.K. Samani, and A. Berenjian, *Bioconcrete: next generation of self-healing concrete*. Applied Microbiology and Biotechnology 2016. **100**(6): p. 2591-2602.

2. Seifan, M., et al., *The effectiveness of microbial crack treatment in self healing concrete* in *High Value Processing Technologies*, A. Berenjian, H. Jafarizadeh-Malmiri, and Y. Song, Editors. 2016, Nova Science Publishers, Inc.: New York, USA. p. 97-124.

3. Neville, A.M. and J.J. Brooks, *Concrete technology*. Second ed. 2010, Harlow, UK: Longman Scientific & Technical.

4. Khan, M.A., *Bridge and highway structure rehabilitation and repair*. 2010, New York, USA: McGraw-Hill Companies, Inc.

5. Bang, S.S., et al., *Microbial calcite, a bio-based smart nanomaterial in concrete remediation.* International Journal of Smart and Nano Materials, 2010. **1**(1): p. 28-39.

6. Federal Highway Administration (FHWA) and Office of Infrastructure Research and Development, *Corrosion cost and preventive strategies in the United States*. 2001: USA.

7. Cailleux, E. and V. Pollet. *Investigations on the development of self-healing properties in protective coatings for concrete and repair mortars*. in *2nd International Conference on Self-Healing Materials*. 2009. Chicago, IL, USA.

8. Silva, F.B., et al., *Industrial application of biological self-healing concrete: Challenges and economical feasibility.* Journal of Commercial Biotechnology, 2015. **21**(1): p. 31-38.

9. Worrell, E., et al., *Carbon dioxide emissions from the global cement industry.* Annual Review of Environment and Resources, 2001. **26**: p. 303-329.

10. Wang, J.Y., N. De Belie, and W. Verstraete, *Diatomaceous earth as a protective vehicle for bacteria applied for self-healing concrete.* Journal of Industrial Microbiology and Biotechnology, 2012. **39**(4): p. 567-577.

11. Pacheco-Torgal, F. and J.A. Labrincha, *Biotech cementitious materials: Some aspects of an innovative approach for concrete with enhanced durability.* Construction and Building Materials, 2013. **40**: p. 1136-1141.

12. De Muynck, W., et al., *Bacterial carbonate precipitation as an alternative surface treatment for concrete.* Construction and Building Materials, 2008. **22**(5): p. 875-885.

13. De Muynck, W., et al., *Bacterial carbonate precipitation improves the durability of cementitious materials.* Cement and Concrete Research, 2008. **38**(7): p. 1005-1014.

14. Dhami, N., A. Mukherjee, and M.S. Reddy, *Biofilm and microbial applications in biomineralized concrete*, in *Advanced Topics in Biomineralization*, J. Seto, Editor. 2012, InTech.

15. Van Tittelboom, K., et al., *Use of bacteria to repair cracks in concrete.* Cement and Concrete Research, 2010. **40**(1): p. 157-166.

16. De Rooij, M., et al., *Self-healing phenomena in cement-based materials: state-of-the-art report of RILEM technical committee 221-SHC: self-Healing phenomena in cement-Based materials*. Vol. 11. 2013: Springer.

17. Edvardsen, C., *Water permeability and autogenous healing of cracks in concrete.* Materials Journal, 1999. **96**(4): p. 448-454.

18. Hearn, N., *Self-sealing, autogenous healing and continued hydration: What is the difference?* Materials and Structures/Materiaux et Constructions, 1998. **31**(212): p. 563-567.

19. Savija, B. and E. Schlangen, *Autogeneous healing and chloride ingress in cracked concrete.* Heron, 2016. **61**(1): p. 15-32.

20. Schlangen, H., et al. *Recent advances on self healing of concrete*. in *FraMCos-7: Proceedings of the 7th International Conference on Fracture Mechanics of Concrete and Concrete Structures, Jeju Island, Korea, 23-28 May 2010*.

21. Blaiszik, B.J., et al., *Self-healing polymers and composites.* Annual Review of Materials Research, 2010. **40**: p. 179-211.

22. Ramm, W. and M. Biscoping, *Autogenous healing and reinforcement corrosion of water-penetrated separation cracks in reinforced concrete.* Nuclear Engineering and Design, 1998. **179**(2): p. 191-200.

23. Edvardsen, C., *Water permeability and autogenous healing of cracks in concrete.* ACI Materials Journal, 1999. **96**(4): p. 448-454.

24. Van Tittelboom, K. and N. De Belie, *Self-healing in cementitious materials-a review.* Materials, 2013. **6**(6): p. 2182-2217.

25. Wang, X., et al., *Experimental study on cementitious composites embedded with organic microcapsules.* Materials, 2013. **6**(9): p. 4064-4081.

26. Wang, J.Y., et al., *Self-healing concrete by use of microencapsulated bacterial spores.* Cement and Concrete Research, 2014. **56**: p. 139-152.

27. Şahmaran, M., et al., *Self-healing of mechanically-loaded self consolidating concretes with high volumes of fly ash.* Cement and Concrete Composites, 2008. **30**(10): p. 872-879.

28. Reinhardt, H.W. and M. Jooss, *Permeability and self-healing of cracked concrete as a function of temperature and crack width.* Cement and Concrete Research, 2003. **33**(7): p. 981-985.

29. Clear, C.A., *The effects of autogenous healing upon the leakage of water through cracks in concrete*. 1985, Cement and Concrete Association: England.

30. Van der Zwaag, S., *Self healing materials: An alternative approach to 20 centuries of materials science*. 2007, Netherland: Springer Series in Materials Science.

31. Li, V.C. and E. Herbert, *Robust self-healing concrete for sustainable infrastructure.* Journal of Advanced Concrete Technology, 2012. **10**(6): p. 207-218.

32. Stabnikov, V., V. Ivanov, and J. Chu, *Construction Biotechnology: a new area of biotechnological research and applications.* World Journal of Microbiology and Biotechnology, 2015. **31**(9): p. 1303.

33. Plank, J., *Applications of biopolymers and other biotechnological products in building materials.* Applied microbiology and biotechnology, 2004. **66**(1): p. 1-9.

34. Rivadeneyra, M.A., et al., *Precipatation of calcium carbonate by Vibrio spp. from an inland saltern.* FEMS Microbiology Ecology, 1994. **13**(3): p. 197-204.

35. Ronholm, J., et al., *A mineralogical characterization of biogenic calcium carbonates precipitated by heterotrophic bacteria isolated from cryophilic polar regions.* Geobiology, 2014. **12**(6): p. 542-556.

36. Banks, E.D., et al., *Bacterial calcium carbonate precipitation in cave environments: A function of calcium homeostasis.* Geomicrobiology Journal, 2010. **27**(5): p. 444-454.

37. Rusznyák, A., et al., *Calcite biomineralization by bacterial isolates from the recently discovered pristine karstic herrenberg cave.* Applied and Environmental Microbiology, 2012. **78**(4): p. 1157-1167.

38. Folk, R.L., *Interaction between bacteria, nannobacteria, and mineral precipitation in hot springs of central Italy.* Géographie physique et Quaternaire, 1994. **48**(3): p. 233-246.

39. Tiano, P., L. Biagiotti, and G. Mastromei, *Bacterial bio-mediated calcite precipitation for monumental stones conservation: Methods of evaluation.* Journal of Microbiological Methods, 1999. **36**(1-2): p. 139-145.

40. Fujita, Y., et al., *Calcium carbonate precipitation by ureolytic subsurface bacteria.* Geomicrobiology Journal, 2000. **17**(4): p. 305-318.

41. Dhami, N.K., M.S. Reddy, and A. Mukherjee, *Bacillus megaterium mediated mineralization of calcium carbonate as biogenic surface treatment of green building materials.* World Journal of Microbiology and Biotechnology, 2013. **29**(12): p. 2397-2406.

42. Sarda, D., et al., *Biocalcification by Bacillus pasteurii urease: A novel application.* Journal of Industrial Microbiology and Biotechnology, 2009. **36**(8): p. 1111-1115.

43. Dhami, N.K., M.S. Reddy, and A. Mukherjee, *Improvement in strength properties of ash bricks by bacterial calcite.* Ecological Engineering, 2012. **39**: p. 31-35.

44. Warren, L.A., et al., *Microbially mediated calcium carbonate precipitation: Implications for Interpreting calcite precipitation and for solid-phase capture of inorganic contaminants.* Geomicrobiology Journal, 2001. **18**(1): p. 93-115.

45. Van Hamme, J.D., A. Singh, and O.P. Ward, *Recent advances in petroleum microbiology.* Microbiology and Molecular Biology Reviews, 2003. **67**(4): p. 503-549.

46. DeJong, J.T., M.B. Fritzges, and K. Nüsslein, *Microbially induced cementation to control sand response to undrained shear.* Journal of Geotechnical and Geoenvironmental Engineering, 2006. **132**(11): p. 1381-1392.

47. van Paassen, L.A., et al., *Potential soil reinforcement by biological denitrification.* Ecological Engineering, 2010. **36**(2): p. 168-175.

48. Burbank, M.B., et al., *Precipitation of calcite by indigenous microorganisms to strengthen liquefiable soils.* Geomicrobiology Journal, 2011. **28**(4): p. 301-312.

49. Mitchell, A.C., et al., *Microbially enhanced carbon capture and storage by mineral-trapping and solubility-trapping.* Environmental Science and Technology, 2010. **44**(13): p. 5270-5276.

50. Tebo, B.M., et al., *Geomicrobiology of manganese(II) oxidation.* Trends in Microbiology, 2005. **13**(9): p. 421-428.

51. Bazylinski, D.A. and B.M. Moskowitz, *Microbial biomineralization of magnetic iron minerals: microbiology, magnetism and environmental significance.* Reviews in Mineralogy, 1997. **35**: p. 217-223.

52. Mann, S., *Biomineralization: Principles and concepts in bioinorganic materials chemistry*. 6th ed. 2001: Oxford University Press.

53. Barton, L.L. and D.E. Northup, *Microbes at work in nature: Biomineralization and microbial weathering*, in *Microbial Ecology*. 2011, John Wiley & Sons, Inc.: Hoboken, NJ, USA. p. 299-326.

54. Hammes, F. and W. Verstraete, *Key roles of pH and calcium metabolism in microbial carbonate precipitation.* Reviews in Environmental Science and Biotechnology, 2002. **1**(1): p. 3-7.

55. Castanier, S., G. Le Métayer-Levrel, and J.P. Perthuisot, *Ca-carbonates precipitation and limestone genesis - the microbiogeologist point of view*. Sedimentary Geology, 1999. **126**(1-4): p. 9-23.

56. Castainer, S., M. Le, and J. Perthuisot, *Bacterial roles in the precipitation of carbonate minerals*, in *Microbial Sediments*, R.E. Riding and S.M. Awramik, Editors. 2000. p. 32-39.

57. Okafor, N., *Environmental microbiology of aquatic and waste systems*. 2011, USA: Springer Science & Business Media.

58. Munn, C.B., *Marine microbiology: Ecology and applications*. 2004, London: Bios Scientific Publisher.

59. Knorre, H. and K.E. Krumbein, *Bacterial calcification*, in *Microbial Sediments*, R.E. Riding and S.M. Awramik, Editors. 2000, Springer: Berlin. p. 25-31.

60. Groth, I., et al., *Geomicrobiological study of the Grotta dei Cervi, Porto Badisco, Italy.* Geomicrobiology Journal, 2001. **18**(3): p. 241-258.

61. Cacchio, P., et al., *Calcium carbonate precipitation by bacterial strains isolated from a limestone cave and from a loamy soil.* Geomicrobiology Journal, 2003. **20**(2): p. 85-98.

62. Ehrlich, H.L., *Geomicrobiology*. 1995, New York: Marcel Dekker Inc.

63. Perito, B. and G. Mastromei, *Molecular basis of bacterial calcium carbonate precipitation*, in *Molecular Biomineralization*, W.E.G. Müller, Editor. 2011, Springer Berlin Heidelberg. p. 113-139.

64. Belie, N.D. and W. Muynck, *Crack repair in concrete using biodeposition*, in *Concrete Repair, Rehabilitation and Retrofitting II*. 2008: Cape Town, South Africa.

65. Jonkers, H.M., et al., *Application of bacteria as self-healing agent for the development of sustainable concrete.* Ecological Engineering, 2010. **36**(2): p. 230-235.

66. Wiktor, V. and H.M. Jonkers, *Quantification of crack-healing in novel bacteria-based self-healing concrete.* Cement and Concrete Composites, 2011. **33**(7): p. 763-770.

67. Dick, J., et al., *Bio-deposition of a calcium carbonate layer on degraded limestone by Bacillus species.* Biodegradation, 2006. **17**(4): p. 357-367.

68. Stocks-Fischer, S., J.K. Galinat, and S.S. Bang, *Microbiological precipitation of $CaCO_3$.* Soil Biology and Biochemistry, 1999. **31**(11): p. 1563-1571.

69. Muynck, W., N. Belie, and W. Verstraete, *Improvement of concrete durability with the aid of bacteria*, in *In Proceedings of the first international conference on self healing materials*. 2007, Springer.

70. Burne, R.A. and Y.Y.M. Chen, *Bacterial ureases in infectious diseases.* Microbes and Infection, 2000. **2**(5): p. 533-542.

71. Karatas, I., *Microbiological improvement of the physical properties of soils*. 2008: Arizona State University.

72. Erşan, Y.Ç., N.d. Belie, and N. Boon, *Microbially induced $CaCO_3$ precipitation through denitrification: An optimization study in minimal nutrient environment.* Biochemical Engineering Journal, 2015. **101**: p. 108-118.

73. Kar, S.Z. and A. Berenjian, *Soil formation by ecological factors: Critical review.* American Journal of Agricultural and Biological Science, 2013. **8**(2): p. 114-116.

74. De Muynck, W., N. De Belie, and W. Verstraete, *Microbial carbonate precipitation in construction materials: A review.* Ecological Engineering, 2010. **36**(2): p. 118-136.

75. Hammes, F., et al., *Strain-specific ureolytic microbial calcium carbonate precipitation.* Applied and environmental microbiology, 2003. **69**(8): p. 4901-4909.

76. Wang, Y.H. and X. Zhang, *Influence of agitation and aeration on growth and antibiotic production by Xenorhabdus nematophila.* World Journal of Microbiology and Biotechnology, 2007. **23**(2): p. 221-227.

77. Gollapudi, U.K., et al., *A new method for controlling leaching through permeable channels.* Chemosphere, 1995. **30**(4): p. 695-705.

78. Qian, C., et al., *Microbial self-healing effects of concrete cracks.* Dongnan Daxue Xuebao (Ziran Kexue Ban)/Journal of Southeast University (Natural Science Edition), 2013. **43**(2): p. 360-364.

79. Wang, J., et al., *X-ray computed tomography proof of bacterial-based self-healing in concrete.* Cement and Concrete Composites, 2014. **53**: p. 289-304.

80. Heitkamp, M.A., *Effects of oxygen-releasing materials on aerobic bacterial degradation processes.* Bioremediation Journal, 1997. **1**(2): p. 105-114.

81. Walawska, B., et al., *Solid inorganic peroxy compounds in environmental protection.* Polish Journal of Chemical Technology, 2007. **9**(3): p. 68–72.

82. Koenigsberg, S.S. and C.A. Sandefur, *The use of oxygen release compound for the accelerated bioremediation of aerobically degradable contaminants: The advent of time-release electron acceptors.* Remediation Journal, 1999. **10**(1): p. 3-29.

83. Cassidy, D.P. and R.L. Irvine, *Use of calcium peroxide to provide oxygen for contaminant biodegradation in a saturated soil.* Journal of Hazardous Materials, 1999. **69**(1): p. 25-39.

84. Zappi, M., et al., *The fate of hydrogen peroxide as an oxygen source for bioremediation activities within saturated aquifer systems.* Journal of the Air & Waste Management Association, 2000. **50**(10): p. 1818-1830.

85. Schlegel, H.G. and C. Zaborosch, *General microbiology*. 7th ed. 1993: Cambridge: University Press.

86. Jonkers, H.M., *Bacteria-based self-healing concrete.* Heron, 2011. **56**(1-2): p. 5-16.

87. Wang, J.Y., et al., *Application of hydrogel encapsulated carbonate precipitating bacteria for approaching a realistic self-healing in concrete.* Construction and Building Materials, 2014. **68**(0): p. 110-119.

88. De Belie, N., *Application of bacteria in concrete: a critical evaluation of the current status.* RILEM Technical Letters, 2016. **1**: p. 56-61.

89. Oltulu, M. and R. Şahin, *Effect of nano-SiO_2, nano-Al_2O_3 and nano-Fe_2O_3 powders on compressive strengths and capillary water absorption of cement mortar containing fly ash: A comparative study.* Energy and Buildings, 2013. **58**: p. 292-301.

90. Sanchez, F. and K. Sobolev, *Nanotechnology in concrete - A review.* Construction and Building Materials, 2010. **24**(11): p. 2060-2071.

91. Qing, Y., et al., *Influence of nano-SiO_2 addition on properties of hardened cement paste as compared with silica fume.* Construction and Building Materials, 2007. **21**(3): p. 539-545.

92. Oltulu, M. and R. Şahin, *Single and combined effects of nano-SiO_2, nano-Al_2O_3 and nano-Fe_2O_3 powders on compressive strength and capillary permeability of cement mortar containing silica fume.* Materials Science and Engineering A, 2011. **528**(22-23): p. 7012-7019.

93. Li, H., et al., *Microstructure of cement mortar with nano-particles.* Composites Part B: Engineering, 2004. **35**(2): p. 185-189.

94. Li, H., H.G. Xiao, and J.P. Ou, *A study on mechanical and pressure-sensitive properties of cement mortar with nanophase materials.* Cement and Concrete Research, 2004. **34**(3): p. 435-438.

95. Jo, B.W., et al., *Characteristics of cement mortar with nano-SiO_2 particles.* Construction and Building Materials, 2007. **21**(6): p. 1351-1355.

96. Dias, A., et al., *A biotechnological perspective on the application of iron oxide magnetic colloids modified with polysaccharides.* Biotechnology Advances, 2011. **29**(1): p. 142-155.

97. Corchero, J.L. and A. Villaverde, *Biomedical applications of distally controlled magnetic nanoparticles.* Trends in Biotechnology, 2009. **27**(8): p. 468-476.

98. Xu, Z.P., et al., *Subcellular compartment targeting of layered double hydroxide nanoparticles.* Journal of Controlled Release, 2008. **130**(1): p. 86-94.

99. Liu, J.F., Z.S. Zhao, and G.B. Jiang, *Coating Fe_3O_4 magnetic nanoparticles with humic acid for high efficient removal of heavy metals in water.* Environmental science & technology, 2008. **42**(18): p. 6949-6954.

100. Fornara, A., et al., *Tailored magnetic nanoparticles for direct and sensitive detection of biomolecules in biological samples.* Nano letters, 2008. **8**(10): p. 3423-3428.

101. Jing, Y., et al., *Blood progenitor cell separation from clinical leukapheresis product by magnetic nanoparticle binding and magnetophoresis.* Biotechnology and Bioengineering, 2007. **96**(6): p. 1139-1154.

102. Okoli, C., et al., *Application of magnetic iron oxide nanoparticles prepared from microemulsions for protein purification.* Journal of Chemical Technology and Biotechnology, 2011. **86**(11): p. 1386-1393.

103. Scott, J.R. and T.C. Barnett, *Surface proteins of gram-positive bacteria and how they get there.* Annual Review of Microbiology, 2006. **60**: p. 397-423.

104. Rashad, A.M., *A synopsis about the effect of nano-Al_2O_3, nano-Fe_2O_3, nano-Fe_3O_4 and nano-clay on some properties of cementitious materials - A short guide for Civil Engineer.* Materials and Design, 2013. **52**: p. 143-157.

105. Dhawan, A., V. Sharma, and D. Parmar, *Nanomaterials: A challenge for toxicologists.* Nanotoxicology, 2009. **3**(1): p. 1-9.

106. Chatterjee, S., A. Bandyopadhyay, and K. Sarkar, *Effect of iron oxide and gold nanoparticles on bacterial growth leading towards biological application.* Journal of Nanobiotechnology, 2011. **9**(1): p. 34-41.

107. Berry, C.C., et al., *Cell response to dextran-derivatised iron oxide nanoparticles post internalisation.* Biomaterials, 2004. **25**(23): p. 5405-5413.

108. Borcherding, J., et al., *Iron oxide nanoparticles induce Pseudomonas aeruginosa growth, induce biofilm formation, and inhibit antimicrobial peptide function.* Environmental Science: Nano, 2014. **1**(2): p. 123-132.

109. Grumezescu, A.M., et al., *In vitro assay of the antimicrobial activity of Fe_3O_4 and $CoFe_2O_4$/oleic acid - core/shell on clinical isolates of bacterial and fungal strains.* Optoelectronics and Advanced Materials, Rapid Communications, 2010. **4**(11): p. 1798-1801.

110. Dinali, R., et al., *Iron oxide nanoparticles in modern microbiology and biotechnology.* Critical Reviews in Microbiology, 2017. **43**(4): p. 493-507.

111. Vatta, L.L., R.D. Sanderson, and K.R. Koch, *Magnetic nanoparticles: properties and potential applications.* Pure and applied chemistry, 2006. **78**(9): p. 1793-1801.

112. Demirer, G.S., A.C. Okur, and S. Kizilel, *Synthesis and design of biologically inspired biocompatible iron oxide nanoparticles for biomedical applications.* Journal of Materials Chemistry B, 2015. **3**(40): p. 7831-7849.

113. Berry, C.C., et al., *Cell response to dextran-derivatised iron oxide nanoparticles post internalisation.* Biomaterials, 2004. **25**(23): p. 5405-5413.

114. Zhang, Y., N. Kohler, and M. Zhang, *Surface modification of superparamagnetic magnetite nanoparticles and their intracellular uptake.* Biomaterials, 2002. **23**(7): p. 1553-1561.

115. Ebrahiminezhad, A., et al., *Preparation of novel magnetic fluorescent nanoparticles using amino acids.* Colloids and Surfaces B: Biointerfaces, 2013. **102**: p. 534-539.

116. Shen, M., et al., *Facile one-pot preparation, surface functionalization, and toxicity assay of APTS-coated iron oxide nanoparticles.* Nanotechnology, 2012. **23**(10): p. 105601.

117. Ebrahiminezhad, A., et al., *Synthesis and application of amine functionalized iron oxide nanoparticles on Menaquinone-7 fermentation: A step towards process intensification.* Nanomaterials, 2015. **6**(1): p. 1-9.

118. Kwon, S.G., et al., *Kinetics of monodisperse iron oxide nanocrystal formation by "heating-up" process.* Journal of the American Chemical Society, 2007. **129**(41): p. 12571-12584.

119. Roca, A., et al., *Structural and magnetic properties of uniform magnetite nanoparticles prepared by high temperature decomposition of organic precursors.* Nanotechnology, 2006. **17**(11): p. 2783.

120. Bronstein, L.M., et al., *Influence of iron oleate complex structure on iron oxide nanoparticle formation.* Chemistry of Materials, 2007. **19**(15): p. 3624-3632.

121. Kim, E.H., et al., *Synthesis of ferrofluid with magnetic nanoparticles by sonochemical method for MRI contrast agent.* Journal of Magnetism and Magnetic Materials, 2005. **289**: p. 328-330.

122. Bang, J.H. and K.S. Suslick, *Sonochemical synthesis of nanosized hollow hematite.* Journal of the American Chemical Society, 2007. **129**(8): p. 2242-2243.

123. Pinkas, J., et al., *Sonochemical synthesis of amorphous nanoscopic iron(III) oxide from $Fe(acac)_3$.* Ultrasonics Sonochemistry, 2008. **15**(3): p. 257-264.

124. Vijayakumar, R., et al., *Sonochemical synthesis and characterization of pure nanometer-sized Fe_3O_4 particles.* Materials Science and Engineering: A, 2000. **286**(1): p. 101-105.

125. Giri, S., et al., *Magnetic properties of α-Fe_2O_3 nanoparticle synthesized by a new hydrothermal method.* Journal of Magnetism and Magnetic Materials, 2005. **285**(1): p. 296-302.

126. Jing, Z. and S. Wu, *Synthesis and characterization of monodisperse hematite nanoparticles modified by surfactants via hydrothermal approach.* Materials Letters, 2004. **58**(27): p. 3637-3640.

127. Hu, X., J.C. Yu, and J. Gong, *Fast production of self-assembled hierarchical α-Fe_2O_3 nanoarchitectures.* The Journal of Physical Chemistry C, 2007. **111**(30): p. 11180-11185.

128. Chin, A.B. and I.I. Yaacob, *Synthesis and characterization of magnetic iron oxide nanoparticles via w/o microemulsion and Massart's procedure.* Journal of materials processing technology, 2007. **191**(1): p. 235-237.

129. Vidal-Vidal, J., J. Rivas, and M.A. López-Quintela, *Synthesis of monodisperse maghemite nanoparticles by the microemulsion method.* Colloids and Surfaces A: Physicochemical and Engineering Aspects, 2006. **288**(1): p. 44-51.

130. Mehta, R., et al., *Direct binding of protein to magnetic particles.* Biotechnology Techniques, 1997. **11**(7): p. 493-496.

131. Bomatí-Miguel, O., et al., *Calorimetric study of maghemite nanoparticles synthesized by laser-induced pyrolysis.* Chemistry of Materials, 2008. **20**(2): p. 591-598.

132. Pascal, C., et al., *Electrochemical synthesis for the control of γ-Fe_2O_3 nanoparticle size. Morphology, microstructure, and magnetic behavior.* Chemistry of materials, 1999. **11**(1): p. 141-147.

133. Bharde, A.A., et al., *Bacteria-mediated precursor-dependent biosynthesis of superparamagnetic iron oxide and iron sulfide nanoparticles.* Langmuir, 2008. **24**(11): p. 5787-5794.

134. Wu, W., Q. He, and C. Jiang, *Magnetic iron oxide nanoparticles: Synthesis and surface functionalization strategies.* Nanoscale Research Letters, 2008. **3**(11): p. 397-415.

135. Roh, Y., et al., *Extracellular synthesis of magnetite and metal-substituted magnetite nanoparticles.* Journal of nanoscience and nanotechnology, 2006. **6**(11): p. 3517-3520.

136. Liu, Z.L., et al., *Synthesis and characterization of ultrafine well-dispersed magnetic nanoparticles.* Journal of Magnetism and Magnetic Materials, 2004. **283**(2): p. 258-262.

137. Kim, D., et al., *Synthesis and characterization of surfactant-coated superparamagnetic monodispersed iron oxide nanoparticles.* Journal of Magnetism and Magnetic Materials, 2001. **225**(1): p. 30-36.

138. Mahdavi, M., et al., *Synthesis, surface modification and characterisation of biocompatible magnetic iron oxide nanoparticles for biomedical applications.* Molecules, 2013. **18**(7): p. 7533-7548.

139. Wang, J., et al., *Use of silica gel or polyurethane immobilized bacteria for self-healing concrete.* Construction and Building Materials, 2012. **26**(1): p. 532-540.

140. Chahal, N., R. Siddique, and A. Rajor, *Influence of bacteria on the compressive strength, water absorption and rapid chloride permeability of fly ash concrete.* Construction and Building Materials, 2012. **28**(1): p. 351-356.

141. Erşan, Y.Ç., et al., *Screening of bacteria and concrete compatible protection materials.* Construction and Building Materials, 2015. **88**: p. 196-203.

142. Sierra-Beltran, M.G., H.M. Jonkers, and E. Schlangen, *Characterization of sustainable bio-based mortar for concrete repair.* Construction and Building Materials, 2014. **67**(PART C): p. 344-352.

143. Turnbull, P.C.B., *Medical Microbiology*. Vol. 4th. 1996: University of Texas Medical Branch at Galveston.

144. E. Boquet, A. Boronate, and A. Boronate, *Production of calcite (calcium carbonate) crystals by soil bacteria is a general phenomenon.* Nature, 1973. **246**: p. 527-529.

145. Seifan, M., et al., *The screening and morphological quantification of bacterial production of calcium carbonate*, in *Chemeca 2016: Chemical Engineering, Regeneration, Recovery and Reinvention*. 2016: Adelaide, Australia.

146. Zhou, G.T., et al., *Sonochemical synthesis of aragonite-type calcium carbonate with different morphologies.* New Journal of Chemistry, 2004. **28**(8): p. 1027-1031.

147. Mori, Y., T. Enomae, and A. Isogai, *Preparation of pure vaterite by simple mechanical mixing of two aqueous salt solutions.* Materials Science and Engineering C, 2009. **29**(4): p. 1409-1414.

148. *ASTM C39 / C39M-99, Standard test method for compressive strength of cylindrical concrete specimens, ASTM International, West Conshohocken, PA*. 1999.

149. *ASTM C157 / C157M-99, Standard test method for length change of hardened hydraulic-cement mortar and concrete, ASTM International, West Conshohocken, PA*. 1999.

150. *ASTM C511-98, Standard specification for mixing rooms, moist cabinets, moist rooms, and water storage tanks used in the testing of hydraulic cements and concretes, ASTM International, West Conshohocken, PA*. 1998.

151. *ASTM C617-98, Standard practice for capping cylindrical concrete specimens, ASTM International, West Conshohocken, PA*. 1998.

152. *ASTM C1585-04, Standard test method for measurement of rate of absorption of water by hydraulic-cement concretes, ASTM International, West Conshohocken, PA*. 2004.

153. *ASTM C490-00, Standard practice for use of apparatus for the determination of length change of hardened cement paste, mortar, and concrete, ASTM International, West Conshohocken, PA*. 2000.

154. Seifan, M., A.K. Samani, and A. Berenjian, *Induced calcium carbonate precipitation using Bacillus species.* Applied Microbiology and Biotechnology, 2016. **100**(23): p. 9895-9906.

155. Vučak, M., et al., *Effect of precipitation conditions on the morphology of calcium carbonate: Quantification of crystal shapes using image analysis.* Powder Technology, 1998. **97**(1): p. 1-5.

156. Bang, S.S., J.K. Galinat, and V. Ramakrishnan, *Calcite precipitation induced by polyurethane-immobilized Bacillus pasteurii.* Enzyme and Microbial Technology, 2001. **28**(4-5): p. 404-409.

157. Yoshida, N. and E. Higashimura, *Catalytic biomineralization of fluorescent calcite by the thermophilic bacterium geobacillus thermoglucosidasius.* Applied and Environmental Microbiology, 2010. **76**(21): p. 7322-7327.

158. Nemati, M., E.A. Greene, and G. Voordouw, *Permeability profile modification using bacterially formed calcium carbonate: Comparison with enzymic option.* Process Biochemistry, 2005. **40**(2): p. 925-933.

159. Okwadha, G.D.O. and J. Li, *Optimum conditions for microbial carbonate precipitation.* Chemosphere, 2010. **81**(9): p. 1143-1148.

160. Kistiakowsky, G.B., et al., *The effects of electrolytes on urease activity.* Journal of the American Chemical Society, 1952. **74**(20): p. 5015-5020.

161. Gorospe, C.M., et al., *Effects of different calcium salts on calcium carbonate crystal formation by Sporosarcina pasteurii KCTC 3558.* Biotechnology and Bioprocess Engineering, 2013. **18**(5): p. 903-908.

162. Xu, J., et al., *Effects of calcium source on biochemical properties of microbial $CaCO_3$ precipitation.* Frontiers in Microbiology, 2015. **6**(DEC).

163. Prasad, R., T.K. Abraham, and A.J. Nair, *Scale up of production in a bioreactor of a halotolerant protease from moderately halophilic Bacillus sp. isolated from soil.* Brazilian Archives of Biology and Technology, 2014. **57**(3): p. 448-455.

164. Laxman, R.S., et al., *Optimization and scale up of production of alkaline protease from Conidiobolus coronatus.* Process Biochemistry, 2005. **40**(9): p. 3152-3158.

165. Sooch, B.S. and B.S. Kauldhar, *Influence of multiple bioprocess parameters on production of lipase from Pseudomonas sp. BWS-5.* Brazilian Archives of Biology and Technology, 2013. **56**(5): p. 711-721.

166. Bendinger, B., et al., *Physicochemical cell surface and adhesive properties of coryneform bacteria related to the presence and chain length of mycolic acids.* Applied and Environmental Microbiology, 1993. **59**(11): p. 3973-3977.

167. Braissant, O., et al., *Bacterially induced mineralization of calcium carbonate in terrestrial environments: The role of exopolysaccharides and amino acids.* Journal of Sedimentary Research, 2003. **73**(3): p. 485-490.

168. Sanchez-Moral, S., et al., *Biomediated precipitation of calcium carbonate metastable phases in hypogean environments: A short review.* Geomicrobiology Journal, 2003. **20**(5): p. 491-500.

169. Seifan, M., A.K. Samani, and A. Berenjian, *New insights into the role of pH and aeration in the bacterial production of calcium carbonate ($CaCO_3$).* Applied Microbiology and Biotechnology, 2017. **101**: p. 3131–3142.

170. Kim, H.J., et al., *Calcium carbonate precipitation by Bacillus and sporosarcina strains isolated from concrete and analysis of the bacterial community of concrete.* Journal of Microbiology and Biotechnology, 2016. **26**(3): p. 540-548.

171. Li, W., et al., *Influence of initial pH on the precipitation and crystal morphology of calcium carbonate induced by microbial carbonic anhydrase.* Colloids and Surfaces B: Biointerfaces, 2013. **102**: p. 281-287.

172. Çalík, P., G. Çalík, and T.H. Özdamar, *Oxygen transfer effects in serine alkaline protease fermentation by Bacillus licheniformis: Use of citric acid as the carbon source.* Enzyme and Microbial Technology, 1998. **23**(7-8): p. 451-461.

173. Zhang, J.L., et al., *A binary concrete crack self-healing system containing oxygen-releasing tablet and bacteria and its Ca^{2+}-precipitation performance.* Applied Microbiology and Biotechnology, 2016: p. 1-12.

174. Ramachandran, S.K., V. Ramakrishnan, and S.S. Bang, *Remediation of concrete using micro-organisms.* ACI Materials Journal, 2001. **98**(1): p. 3-9.

175. Jiménez-López, C., et al., *Chemical, mineralogical and isotope behavior, and phase transformation during the precipitation of calcium carbonate minerals from intermediate ionic solution at 25°C.* Geochimica et Cosmochimica Acta, 2001. **65**(19): p. 3219-3231.

176. Jimenez-Lopez, C., et al., *Influence of lysozyme on the precipitation of calcium carbonate: a kinetic and morphologic study.* Geochimica et Cosmochimica Acta, 2003. **67**(9): p. 1667-1676.

177. Gat, D., et al., *Accelerated microbial-induced $CaCO_3$ precipitation in a defined coculture of ureolytic and non-ureolytic bacteria.* Biogeosciences, 2014. **11**(10): p. 2561-2569.

178. Kaur, N., M.S. Reddy, and A. Mukherjee, *Biomineralization of calcium carbonate polymorphs by the bacterial strains isolated from calcareous sites.* Journal of Microbiology and Biotechnology, 2013. **23**(5): p. 707-714.

179. Wilks, J.C., et al., *Acid and base stress and transcriptomic responses in Bacillus subtilis.* Applied and Environmental Microbiology, 2009. **75**(4): p. 981-990.

180. Onal Okyay, T. and D. Frigi Rodrigues, *Optimized carbonate micro-particle production by Sporosarcina pasteurii using response surface methodology.* Ecological Engineering, 2014. **62**: p. 168-174.

181. Loewenthal. R.E and G. van Rooyen Marais, *Carbonate chemistry of aquatic systems: theory and application*. 1976, Michigan, USA: Ann Arbor Science.

182. Ma, Y.F., Y.H. Gao, and Q.L. Feng, *Effects of pH and temperature on $CaCO_3$ crystallization in aqueous solution with water soluble matrix of pearls.* Journal of Crystal Growth, 2010. **312**(21): p. 3165-3170.

183. Hu, Y.B., et al., *Effect of pH and phosphate on calcium carbonate polymorphs precipitated at near-freezing temperature.* Crystal Growth and Design, 2015. **15**(4): p. 1596-1601.

184. Tourney, J. and B.T. Ngwenya, *Bacterial extracellular polymeric substances (EPS) mediate $CaCO_3$ morphology and polymorphism.* Chemical Geology, 2009. **262**(3-4): p. 138-146.

185. Wang, X., et al., *Lysozyme mediated calcium carbonate mineralization.* Journal of Colloid and Interface Science, 2009. **332**(1): p. 96-103.

186. Seifan, M., A.K. Samani, and A. Berenjian, *A novel approach to accelerate bacterially induced calcium carbonate precipitation using oxygen releasing compounds (ORCs).* Biocatalysis and Agricultural Biotechnology, 2017. **12**: p. 299-307.

187. Achal, V., A. Mukerjee, and M. Sudhakara Reddy, *Biogenic treatment improves the durability and remediates the cracks of concrete structures.* Construction and Building Materials, 2013. **48**: p. 1-5.

188. Rodriguez-Navarro, C., et al., *Conservation of ornamental stone by Myxococcus xanthus-induced carbonate biomineralization.* Applied and Environmental Microbiology, 2003. **69**(4): p. 2182-2193.

189. Vogt, C., et al., *Bioremediation of chlorobenzene-contaminated ground water in an in situ reactor mediated by hydrogen peroxide.* Journal of Contaminant Hydrology, 2004. **68**(1-2): p. 121-141.

190. Sondi, I. and E. Matijević, *Homogeneous precipitation of calcium carbonates by enzyme catalyzed reaction.* Journal of Colloid and Interface Science, 2001. **238**(1): p. 208-214.

191. Narendranath, N.V., K.C. Thomas, and W.M. Ingledew, *Urea hydrogen peroxide reduces the numbers of Lactobacilli, nourishes yeast, and leaves no residues in the ethanol fermentation.* Applied and Environmental Microbiology, 2000. **66**(10): p. 4187-4192.

192. Tsai, T.T., et al., *Enhanced bioremediation of fuel-oil contaminated soils: Laboratory feasibility study.* Journal of Environmental Engineering, 2009. **135**(9): p. 845-853.

193. Kazzaz, J.A., et al., *Cellular oxygen toxicity: Oxidant injury without apoptosis.* Journal of Biological Chemistry, 1996. **271**(25): p. 15182-15186.

194. Kao, C.M., et al., *Remediation of PCE-contaminated aquifer by an in situ two-layer biobarrier: Laboratory batch and column studies.* Water Research, 2003. **37**(1): p. 27-38.

195. Tziviloglou, E., et al., *Bio-based self-healing concrete: From research to field application,* in *Advances in Polymer Science*. 2016. p. 345-386.

196. Lee, C.-S., et al., *Fabrication of novel oxygen-releasing alginate beads as an efficient oxygen carrier for the enhancement of aerobic bioremediation of 1,4-dioxane contaminated groundwater.* Bioresource Technology, 2014. **171**: p. 59-65.

197. Rothenstein, D., et al., *Influence of zinc on the calcium carbonate biomineralization of Halomonas halophila.* Aquatic Biosystems, 2012. **1**: p. 8-31.

198. Camci-Unal, G., et al., *Oxygen-releasing biomaterials for tissue engineering.* Polymer International, 2013. **62**(6): p. 843-848.

199. Spain, J.C., et al., *Excessive bacterial decomposition of H_2O_2 during enhanced biodegradation.* Groundwater, 1989. **27**(2): p. 163-167.

200. Lee, J.M., *Biochemical engineering*. 1992, Englewood Cliffs, NJ, USA: Prentice Hall.

201. Haugaard, N., *Cellular mechanisms of oxygen toxicity.* Physiological Reviews, 1968. **48**(2): p. 311-373.

202. Becker, A., et al., *In-vitro crystallization of calcium carbonate in the presence of biological additives- comparison of the ammonium carbonate method with double-diffusion techniques.* Zeitschrift fur Anorganische und Allgemeine Chemie, 2003. **629**(12-13): p. 2305-2311.

203. Li, W., et al., *Influence of initial calcium ion concentration on the precipitation and crystal morphology of calcium carbonate induced by bacterial carbonic anhydrase.* Chemical Engineering Journal, 2013. **218**: p. 65-72.

204. Wei, S., et al., *Biomineralization processes of calcite induced by bacteria isolated from marine sediments.* Brazilian Journal of Microbiology, 2015. **46**(2): p. 455-464.

205. González-Muñoz, M.T., et al., *Bacterial biomineralization: New insights from Myxococcus-induced mineral precipitation*, in *Geological Society Special Publication*. 2010. p. 31-50.

206. Kawaguchi, T. and A.W. Decho, *A laboratory investigation of cyanobacterial extracellular polymeric secretions (EPS) in influencing CaCO3 polymorphism.* Journal of Crystal Growth, 2002. **240**(1–2): p. 230-235.

207. Bosak, T. and D.K. Newman, *Microbial kinetic controls on calcite morphology in supersaturated solutions.* Journal of Sedimentary Research, 2005. **75**(2): p. 190-199.

208. Seifan, M., et al., *Amine-modified magnetic iron oxide nanoparticle as a promising carrier for application in bio self-healing concrete.* Applied Microbiology and Biotechnology, 2018. **102**(1): p. 175-184.

209. Seifan, M., et al., *The role of magnetic iron oxide nanoparticles in the bacterially induced calcium carbonate precipitation.* Applied microbiology and biotechnology, 2018: p. 1-12.

210. Achal, V., A. Mukherjee, and M.S. Reddy, *Microbial concrete: Way to enhance the durability of building structures.* Journal of Materials in Civil Engineering, 2011. **23**(6): p. 730-734.

211. Sikora, P., et al., *The Influence of nano-Fe_3O_4 on the microstructure and mechanical properties of cementitious composites.* Nanoscale Research Letters 2016. **11**(1): p. 182.

212. Chang, T.-P., et al., *Material properties of Portland cement paste with nano-montmorillonite.* Journal of Materials Science, 2007. **42**(17): p. 7478-7487.

213. Sato, T. and F. Diallo, *Seeding effect of nano-$CaCO_3$ on the hydration of tricalcium silicate.* Transportation Research Record: Journal of the Transportation Research Board, 2010. (2141): p. 61-67.

214. Jayapalan, A., et al., *Influence of additions of anatase TiO_2 nanoparticles on early-age properties of cement-based materials.* Transportation research record: journal of the transportation research board, 2010. (2141): p. 41-46.

215. Konsta-Gdoutos, M.S., Z.S. Metaxa, and S.P. Shah, *Highly dispersed carbon nanotube reinforced cement based materials.* Cement and Concrete Research, 2010. **40**(7): p. 1052-1059.

216. Wu, W., et al., *Synthesis and magnetic properties of maghemite (γ-Fe_2O_3) short-nanotubes.* Nanoscale Research Letters, 2010. **5**(9): p. 1474.

217. Ebrahiminezhad, A., et al., *Magnetic immobilization of Bacillus subtilis natto cells for menaquinone-7 fermentation.* Applied Microbiology and Biotechnology, 2016. **100**(1): p. 173-180.

218. Larsen, M.U., et al., *Biocompatible nanoparticles trigger rapid bacteria clustering.* Biotechnology Progress, 2009. **25**(4): p. 1094-1102.

219. Bromberg, L., et al., *Bactericidal core-shell paramagnetic nanoparticles functionalized with poly (hexamethylene biguanide).* Langmuir, 2010. **27**(1): p. 420-429.

220. Lamer, V.K. and R.H. Dinegar, *Theory, production and mechanism of formation of monodispersed hydrosols.* Journal of the American Chemical Society, 1950. **72**(11): p. 4847-4854.

221. Wahajuddin and S. Arora, *Superparamagnetic iron oxide nanoparticles: Magnetic nanoplatforms as drug carriers.* International Journal of Nanomedicine, 2012. **7**: p. 3445-3471.

222. Massart, R., *Preparation of aqueous magnetic liquids in alkaline and acidic media.* IEEE Transactions on Magnetics, 1981. **17**(2): p. 1247-1248.

223. Melnyczuk, J.M. and P. Soubantika, *Synthesis and characterization of Iron oxide nanoparticles,* in *Handbook of Research on Nanoscience, Nanotechnology, and Advanced Materials*. 2014. p. 89-107.

224. Lee, N. and T. Hyeon, *Designed synthesis of uniformly sized iron oxide nanoparticles for efficient magnetic resonance imaging contrast agents.* Chemical Society Reviews, 2012. **41**(7): p. 2575-2589.

225. Laurent, S., et al., *Magnetic fluid hyperthermia: Focus on superparamagnetic iron oxide nanoparticles.* Advances in Colloid and Interface Science, 2011. **166**(1): p. 8-23.

226. Gupta, A.K. and M. Gupta, *Synthesis and surface engineering of iron oxide nanoparticles for biomedical applications.* Biomaterials, 2005. **26**(18): p. 3995-4021.

227. Santra, S., et al., *Synthesis and characterization of silica-coated iron oxide nanoparticles in microemulsion: the effect of nonionic surfactants.* Langmuir, 2001. **17**(10): p. 2900-2906.

228. Martin, S.T., C.L. Morrison, and M.R. Hoffmann, *Photochemical mechanism of size-quantized vanadium-doped TiO_2 particles.* The Journal of Physical Chemistry, 1994. **98**(51): p. 13695-13704.

229. Sundaram, P.A., R. Augustine, and M. Kannan, *Extracellular biosynthesis of iron oxide nanoparticles by Bacillus subtilis strains isolated from rhizosphere soil.* Biotechnology and Bioprocess Engineering 2012. **17**(4): p. 835-840.

230. Park, J., et al., *One‐nanometer‐scale size‐controlled synthesis of monodisperse magnetic Iron oxide nanoparticles.* Angewandte Chemie, 2005. **117**(19): p. 2932-2937.

231. Brunner, T.J., et al., *In vitro cytotoxicity of oxide nanoparticles: comparison to asbestos, silica, and the effect of particle solubility.* Environmental Science & Technology, 2006. **40**(14): p. 4374-4381.

232. Sies, H., *Oxidative stress: oxidants and antioxidants.* Experimental Physiology, 1997. **82**(2): p. 291-295.

233. Abdal Dayem, A., et al., *The role of reactive oxygen species (ROS) in the biological activities of metallic nanoparticles.* International Journal of Molecular Sciences 2017. **18**(1): p. 120.

234. Wu, H., et al., *Reactive oxygen species-related activities of nano-iron metal and nano-iron oxides.* Journal of food and drug analysis, 2014. **22**(1): p. 86-94.

235. Seifan, M., et al., *Bio-reinforced self-healing concrete using magnetic iron oxide nanoparticles.* Applied Microbiology and Biotechnology, 2018. **102**: p. 2167–2178.

236. Seifan, M., et al., *Mechanical properties of bio self-healing concrete containing immobilized bacteria with iron oxide nanoparticles* Applied Microbiology and Biotechnology, 2018.

237. Dry, C.M., *Three designs for the internal release of sealants, adhesives, and waterproofing chemicals into concrete to reduce permeability.* Cement and Concrete Research, 2000. **30**(12): p. 1969-1977.

238. Hosoda, A., et al. *Self healing of crack and water permeability of expansive concrete*. in *1st International Conference On Self-Healing Materials*. 2007. Noordwijk Aan Zee, The Netherlands.

239. Güneyisi, E., M. Gesoğlu, and K. Mermerdaş, *Improving strength, drying shrinkage, and pore structure of concrete using metakaolin.* Materials and Structures, 2008. **41**(5): p. 937-949.